Nordic nuclear safety research

NKS-409
ISBN 978-87-7893-498-7

COPSAR-NKS Project

Summary report 2017

Markku Puustinen[a]

Timo Pättikangas[b]

Pavel Kudinov[c]

[a] Lappeenranta University of Technology, School of Energy Systems Nuclear Engineering, Finland

[b] VTT Technical Research Centre of Finland Ltd

[c] Royal Institute of Technology (KTH), Division of Nuclear Engineering Stockholm, Sweden

September 2018

Abstract

The COPSAR-NKS project has consisted of the combined effort by LUT, VTT and KTH to implement the ideas outlined in the NORTHNET Roadmap 3 document. To achieve the project objectives, a combined experimental/analytical/computational program has been carried out. LUT has been responsible for developing an experimental database on pool operation related phenomena in the PPOOLEX integral test facility and in the small-scale separate effect test facility. VTT and KTH have used the gathered experimental database for the development, improvement and validation of numerical simulation models. A small-scale separate effect test facility, SEF-POOL, has been designed and constructed at LUT based on a proposal from KTH with the aim to evaluate effective momentum for different condensation regimes. The facility allows the direct measurement of effective momentum induced by steam injection. Analysis of the preliminary steam injection tests by KTH showed that the steam momentum can be roughly predicted by the theoretical estimate and the frequencies obtained with the fast pressure transducer correlate well with the correlations proposed in the literature. Pre-test SEF-T000 performed on the SEF-POOL facility at LUT has been studied with Computational Fluid Dynamics (CFD) calculations at VTT. The simulation produced qualitatively correct description of the chugging oscillation observed in the experiment.

Key words

Steam injection, Direct-contact condensation, Thermal stratification, Mixing, Pressure suppression pool, Containment, Sparger, Spray, Effective momentum, BWR, CFD, GOTHIC

NKS-409
ISBN 978-87-7893-498-7
Electronic report, September 2018
NKS Secretariat
P.O. Box 49
DK - 4000 Roskilde, Denmark
Phone +45 4677 4041
www.nks.org
e-mail nks@nks.org

LUT, VTT, KTH

COPSAR-NKS PROJECT

Summary report 2017

Markku Puustinen, Timo Pättikangas, Pavel Kudinov
9-20-2018

Acknowledgement

NKS conveys its gratitude to all organizations and persons who by means of financial support or contributions in kind have made the work presented in this report possible.

Disclaimer

Contents

1. INTRODUCTION 4
2. DESCRIPTION OF THE ACTIVITY IN 2017 6
   2.1 Activities at LUT 6
   2.2 Activities at VTT 7
   2.3 Activities at KTH 8
   REFERENCES 9

Appendix A Mixing Test in PPOOLEX with Sparger in Centre Position
Appendix B General description of SEF-POOL test rig
Appendix C Characterizing tests in SEF-POOL facility
Appendix D PPOOLEX spray tests on mixing effects in condensation pool
Appendix E CFD simulation of condensation of vapor jets
Appendix F Modelling of a Large Water Pool during Operation of Blowdown Pipes and Spargers

1. INTRODUCTION

The COPSAR-NKS project has consisted of the combined effort by LUT, VTT and KTH to implement the ideas outlined in the NORTHNET Roadmap 3 document. The work at VTT and LUT has been done within the NURESA and INSTAB projects of the national Finnish research programme on nuclear power plant safety (SAFIR2018). The work at KTH has been done in the project “Modelling of Stratification and Mixing Transients in a BWR Pressure Suppression Pool” supported by NORTHNET Roadmap 3 and “Analytical support for the OECD/NEA HYMERES project” supported by SSM. The combined effort has been co-ordinated within the COPSAR-NKS project.

To achieve the project objectives, a combined experimental/analytical/computational program has been carried out. LUT has been responsible for developing an experimental database on pool operation related phenomena in the PPOOLEX integral test facility and in the small-scale separate effect test facility with the help of sophisticated, high frequency measurement instrumentation and high-speed video cameras. VTT and KTH have used the gathered experimental database for the development, improvement and validation of numerical simulation models. In addition, analytical support has been provided for the experimental part by pre- and post-test calculations of the experiments.

There are several scenarios of safety importance where containment pressure suppression function and pressure suppression pool (PSP) operation are affected by (i) stratification and mixing phenomena, (ii) interactions with emergency core cooling systems (ECCS), spray, residual heat removal system (RHR), (iii) overall water balance in the containment compartments, and (iv) interplay between pool behaviour, diagnostics and procedures. Specifically, those scenarios include (i) different LOCAs including scenarios with steam line break inside the radiation shield, broken blowdown pipes, and leaking safety relief valves (SRV); (ii) station blackouts; (iii) severe accidents. There is a need for validated tools for simulation of realistic accident scenarios with interplay between phenomena, safety systems, operational procedures, and overall containment performance.

KTH has developed the Effective Heat Source (EHS) and Effective Momentum Source (EMS) models for steam injection through a vertical pipe submerged in a pool and proposed them to be used for simulation of thermal stratification and mixing during a steam injection into a large pool of water [1]. These models have been implemented in GOTHIC® software and validated against POOLEX and PPOOLEX tests carried out at LUT [2]. Excellent agreement in averaged pool temperature and water level in the pool between the experiment and simulation has been achieved. The development of thermal stratification and mixing of the pool are also well captured in the simulations.

Now KTH is improving the EHS and EMS models for blowdown pipes in order to reduce uncertainties and enhance accuracy in predictions as well as extending the models to SRV spargers [3]. The models have been implemented also in ANSYS Fluent. Later the models will be extended further to other elements of the PSP such as nozzles of the residual heat removal system and strainers in order to be able to carry out comprehensive safety analysis of realistic transients in a BWR containment.

VTT has concentrated on Computational Fluid Dynamics (CFD) simulations with the ANSYS Fluent code of stratification and mixing experiments done in the PPOOLEX facility with the aim to improve currently used calculation models. In particular, the direct-contact condensation models of Fluent have been validated against the experiments performed at LUT.

In chapter 2, the activities related to the COPSAR-NKS project at LUT, VTT and KTH in 2017 are very briefly summarized. The work is described in more detail in the attached research reports from each organization.

2. DESCRIPTION OF THE ACTIVITY IN 2017

2.1 Activities at LUT

Previous experiments and validation of the EHS/EMS models have shown that the phenomena occurring at the thermocline needs to be further analyzed to understand its effects in the erosion of the stratified layer. The sparger test series in PPOOLEX continued in 2017 with the sparger first moved to an alternative position, center of the pool, and the submergence reduced from 1.8 to 1.5 m and then by conducting a test with this new configuration. The test parameters were selected based on a previous stratification/mixing test with the SRV sparger and the objective of the test was to find out how the change in the sparger position affects behaviour during the mixing process. With the help of the experiment results, further development of the EMS model for SRV spargers was pursued to simulate dynamics of the pool mixing and stratification.

The test included a stratification phase and an erosion phase with a moderate steam flow rate and then a final mixing phase with a clearly higher steam flow rate. The general behaviour during the stratification/erosion/mixing phases was almost identical in the new sparger test and in the earlier reference test. The initial uniform temperature profile first changed to a stratified situation and eventually back to an almost uniform and mixed situation at the end of the final mixing phase. During the erosion phase, the thermocline moved slowly downwards and the thickness of the transition region seemed to be almost the same as in the reference test. Moving of the sparger pipe to the centre axis of the pool, however, seems to have a slight effect on the elevation of the thermocline as well as on the temperature profile in the pool. Report in Appendix A summarizes the results from the PPOOLEX test with the sparger in the centre position.

A small-scale separate effect test facility, SEF-POOL, has been designed and constructed at LUT based on a proposal from KTH with the aim to evaluate effective momentum for different condensation regimes. The reference system for the SEF-POOL facility is a SRV sparger pipe of a BWR plant. The facility allows the direct measurement of effective momentum induced by steam injection through 1-3 holes with the help of a force sensor. The facility consists of a small pool with large windows on both sidewalls and of a sparger pipe having its lower end immersed in the pool. High-speed cameras will allow recordings of the condensation regimes and collapsing bubbles. With high frequency pressure measurements, the detachment and collapse frequency of the bubbles will be obtained. Report describing the SEF-POOL facility in more detail can be found in Appendix B.

Preliminary steam/water injection tests have been carried out in the SEF-POOL facility to check the applicability of the measurements, particularly the functioning of the direct force measurement, and to characterize the behavior of the facility. In addition, comparison of the obtained momentum values to the theoretical values have been of interest. Small changes have been made to the facility based on preliminary tests.

Analysis of the steam injection tests by KTH showed that the steam momentum can be roughly predicted by the theoretical estimate and the frequencies obtained with the fast pressure transducer correlate well with the correlations proposed in the literature. A strong temperature dependence, i.e. larger momentum as the pool temperature increases, was noticed. Report on these preliminary tests with the SEF-POOL facility is in Appendix C.

Mixing of a thermally stratified pool with the help of spray injection from above was studied in the PPOOLEX experiments. An additional goal was to obtain data for improving simulation models related to spray operation in CFD and system codes as well as to contribute to the development of the EMS and EHS models for sprays to be implemented in the GOTHIC code by KTH. An effort to measure developing flow fields in the mixing region with the help of the PIV system was made. Four tests were carried out where the location and area of the field-of-view (FOV) of the PIV system was varied. Stratified layers of the pool mixed during the spray operation as a result of internal circulation induced by density difference between the cold spray water and warm pool water. Due to the difficult optical environment, the PIV measurements succeeded only before and after the most intense mixing phase had passed the observation windows. Results from these spray tests are presented in more detail in Appendix D.

2.2 Activities at VTT

Pre-test SEF-T000 performed on direct-contact condensation with the small-scale separate effect facility (SEF-POOL) at LUT has been studied with Computational Fluid Dynamics (CFD) calculations. In the test, steam was injected into water pool. The mass flow rate of steam was small (14.8 g/s) and the temperature of the water was fairly high (67 °C) in the time interval chosen for the simulation. The steam was injected into water horizontally through three orifices having diameter of 16 mm, which corresponds to the mass flux of 24.5 kg/m^{2}s.

The oscillation patterns in direct-contact condensation experiments have previously been classified based on mass flux of steam and water temperature by several authors [4, 5 and 6]. The classification maps suggest that the parameters of the experiment are close to the borderline between condensation oscillation and chugging. Condensation rate and penetration of the vapour jet into the pool have been calculated and compared to the experimental data.

The simulation performed with the ANSYS Fluent version 18.2 contained several simplifying modelling assumptions, which affect the simulation results. Euler-Euler two-phase model was used, where the drag between vapour and water was modelled with “universal” drag model of Fluent. In the calculation, constant bubble diameter of one millimetre was assumed. These modelling choices affect the penetration length of the vapour jet into water.

The condensation was calculated by using the two-resistance model and the evaporation-condensation model of Fluent. In the two-resistance model, the Ranz-Marshall correlation for heat transfer was assumed on the liquid side. On the vapour side, zero resistance was assumed. Interfacial area of the phases was calculated with ia-symmetric model of Fluent. These modeling choices affect the condensation rate, which affects the penetration length of the vapour jet. The condensation rate also affects the growth time and collapse time of vapour bubble during the chugging oscillation.

In the simulation, the chugging oscillation was qualitatively very similar as in the experiment. The period of the oscillation was, however, in the simulation (83 ms) longer than in the experiment (43 ms). In particular, the collapse phase of the bubble was in the simulation (42 ms) considerably longer than in the experiment (11 ms). Visual observation from the high-speed video shows that during the collapse phase of the bubble, the surface of the bubble becomes unstable and the surface area between vapour and liquid-water increases rapidly. This phenomenon is not included in the

CFD model and it leads to much more rapid condensation of the bubbles in the experiment than in the simulation.

The growth phase of the vapour bubbles is also in the simulation (41 ms) somewhat longer than in the experiment (34 ms). The difference is probably due to the heat transfer and interfacial area models used in the simulation. In particular, the assumption of single bubble size with fixed diameter has room for improvement.

The penetration length of the vapour jet into water was larger in the simulation (73 mm) than in the experiment (46 mm). This is consistent with the discussion above, which suggests that the simulation underestimates the heat transfer coefficient and/or the interfacial surface area. The resulting underestimation of the condensation rate leads to too large penetration length of the vapour jet.

The pressure oscillations measured in the experiment (20…50 kPa) are most of the time larger than in the CFD simulation (10…20 kPa). The reason for this lies in the differences in the collapse speeds of the bubbles, which are shorter in the experiment than in the simulation, as was discussed above. The more rapid condensation of the bubbles in the experiments compared to simulation produces higher pressure oscillations.

In conclusion, the present CFD simulation produces qualitatively correct description of the chugging oscillation observed in the experiment. The period of the oscillation, the penetration of the vapour jet and the pressure oscillation are in the simulation reasonably close to the experimental observations. Results that are more accurate could be achieved by improving the description of the interfacial area, in particular, in the collapse phase of the chugging oscillation.

Work done at VTT in 2017 is presented in more detail in Appendix E.

2.3 Activities at KTH

Further development of the Effective Heat Source and Effective Momentum Source models has been pursued by KTH in order to simulate dynamics of suppression pool mixing and stratification. The EHS/EMS models have been implemented in ANSYS Fluent and validated against the PPOOLEX test data on mixing of a stratified pool by steam injection through spargers and water injection through residual heat removal nozzles and against the OECD/HYMERES PANDA tests relevant to PSP. Analysis of the results suggest that modelling of the erosion of a sharp thermocline layer, observed in the experiments, presents a challenge for the contemporary codes. The effect of buoyancy on the turbulence is important for reproducing experimental observed behaviours. A good prediction of the stable stratification and erosion regimes has been achieved with the EHS/EMS models.

A Separate Effect Facility (SEF) has been designed and built in cooperation with LUT to measure the effective momentum induced by the oscillatory bubble regime. KTH has performed pre-test analysis and simulations for the selection of operational parameters to be used in the SEF-POOL tests. Preliminary test results show that the effective momentum is very similar to the steam momentum at the injection holes. The latter was observed to be a function of the cyclic bubble oscillations, and thus to deviate from standard estimations based on a constant steam mass flow rate. Comparison with the effective momentum estimated in the Fluent simulations shows a similar trend with respect to the sub-cooling, but a shift on absolute values. Work continues on the development of the EMS model and quantification of the momentum source for different steam injection conditions with the help of the SEF-POOL test results.

The effect of non-condensable gases on chugging is being analysed by using the data from the clearing phases of the PPOOLEX MIX experiments. Preliminary results show that the volume fraction at which chugging is supressed decreases with the blowdown pipe diameter.

A scaling methodology has been developed and applied to the sparger and mixing nozzle experiments performed in PPOOLEX and PANDA. The goal was to preserve prototypical ranges of injection conditions and pool regimes occurring during prototypical BWR transients. The data obtained with the scaled experiments was used for analysis of the physical phenomena and code validation. Important physical phenomena to be considered in the CFD modelling has been identified: for example, the erosion and mixing mechanisms of the stratified layer, the oscillations at the thermocline, the self-similarity of the liquid jets induced by the sparger, and the downwards inclination of the jets. Codes and EHS/EMS models validated for these conditions can be then used to predict plant behaviour.

Analytical support has been provided to the PPOOLEX, SEF-POOL and PANDA experiments with spargers and mixing nozzles. Pre-test simulations have been run using GOTHIC code. However, limitations of the code, mainly the Cartesian mesh, suggested that ANSYS Fluent, where the radial injection of the sparger can be better represented, would be more adequate for these purposes. Therefore, ANSYS Fluent was selected as the computational platform to validate the EHS/EMS models for spargers against the PPOOLEX and PANDA tests.

Work done at KTH in 2017 is presented in more detail in Appendix F.

REFERENCES

[1] Li, H., Villanueva, W., Kudinov, P., Effective models for simulation of thermal stratification and mixing induced by steam injection into a large pool of water. Division of Nuclear Power Safety, Royal Institute of Technology (KTH), NORTHNET Roadmap 3 Research report, Stockholm, 2014.

[2] Gallego-Marcos, I., Villanueva, W., Kudinov, P., Modelling of pool stratification and mixing induced by steam injection through blowdown pipes, Annals of Nuclear Energy 112 (2018), pp. 624-639.

[3] Gallego-Marcos, I., Kudinov, P., Villanueva, W., Kapulla, R., Paranjape, S., Paladino, D., Laine, J., Puustinen, M., Räsänen, A., Pyy, L., Kotro, E., Pool stratification and mixing induced by steam injection through spargers: analysis of the PPOOLEX and PANDA experiments, Nuclear Engineering and Design 337 (2018), pp. 300-316.

[4] Lahey, R. T., Moody, F. J., 1993. The thermal-hydraulics of a boiling water reactor, Chapter 11. American Nuclear Society, Illinois. Second edition.

[5] Nariai, H., and Aya, I., 1986. Fluid and pressure oscillations occurring at direct contact condensation of steam flow with cold water, Nuclear Engineering and Design 95, pp. 35–45.

[6] Aya, I., and Nariai, H., 1991. Evaluation of heat transfer coefficient at direct-contact condensation of cold water and steam, Nuclear Engineering and Design 131, pp. 17–24.

Appendix A

Mixing Test in PPOOLEX with Sparger in Centre Position

Research Report
Lappeenranta University of Technology
Nuclear Engineering

INSTAB 1/2017

MIXING TEST IN PPOOLEX WITH SPARGER IN CENTRE POSITION

Markku Puustinen, Jani Laine, Antti Räsänen, Eetu Kotro, Kimmo Tielinen

Lappeenranta University of Technology
School of Energy Systems
Nuclear Engineering
P.O. Box 20, FIN-53851 LAPPEENRANTA, FINLAND
Phone +358 5 621 11

Lappeenranta, 15.2.2018

Open your mind. LUT.
Lappeenranta University of Technology

Research organization and address	**Customer**
Lappeenranta University of Technology Nuclear Engineering P.O. Box 20 FIN-53851 LAPPEENRANTA, FINLAND	VYR / SAFIR2018 NKS SSM
Project manager Markku Puustinen	**Contact person** Jari Hämäläinen (SAFIR2018) Christian Linde (NKS), Maria Agrell (NORTHNET)
Diary code 125/322/2015	**Order reference** Drno SAFIR 11/2017
Project title and reference code SAFIR2018-INSTAB NKS-COPSAR	**Report identification & Pages** — **Date** INSTAB 1/2017 — 15.2.2018 17 p. + app. 13 p.

Report title and author(s)

MIXING TEST IN PPOOLEX WITH SPARGER IN CENTRE POSITION

Markku Puustinen, Jani Laine, Antti Räsänen, Eetu Kotro, Kimmo Tielinen

Summary

This report summarizes the results of the sparger pipe test (SPA-CT1) carried out in the PPOOLEX facility at LUT in 2017. The test facility is a closed stainless steel vessel divided into two compartments, drywell and wetwell. In the test, the drywell compartment was bypassed i.e. the sparger pipe in the wetwell was connected directly to the steam line coming from the PACTEL facility which acted as a steam source. Steam was blown through the vertical DN65 sparger pipe to the condensation pool filled with sub-cooled water.

The main objective of the test was to study how the change of the sparger pipe position to the pool centre affects the stratification/erosion/mixing behaviour during steam discharge via the sparger pipe. Particularly, the effect on the elevation and thickness of the thermocline between the cold and warm water volumes and on the temperature profile of the pool were of interest. The SPA-T8R test done earlier with the sparger pipe away from the pool centre acted as a reference case. A secondary goal was to obtain data for the development of the EMS and EHS models to be implemented in GOTHIC code by KTH.

The general behaviour during the stratification/erosion/mixing phases is almost identical in the new sparger test and in the earlier reference test. The initial uniform temperature profile first changes to a stratified situation and eventually back to an almost uniform and mixed situation at the end of the final mixing phase. During the erosion phase the thermocline moves slowly downwards and the thickness of the transition region seems to be almost the same in both tests.

The moving of the sparger pipe to the centre axis of the pool, however, seems to have a slight effect on the elevation of the thermocline as well as on the temperature profile in the pool. The thermocline settles at the end of the stratification phase about 150-250 mm deeper if the sparger pipe is in the centre of the pool compared to the situation where the sparger was about 420 mm away from the centre axis. The temperature profile from the elevations close to the pool bottom reveal that during the final high flow rate mixing phase the internal circulation pattern in the pool could be different in the case where the sparger pipe is at the pool centre compared to the case where it is away from the centre.

Distribution

Members of the SAFIR2018 Reference Group 4

C. Linde (SSM), M. Agrell (SSM), P. Kudinov (KTH), I. G. Marcos (KTH), W. Villanueva (KTH), J. Hämäläinen (VTT), V. Suolanen (VTT), T. Pättikangas (VTT), I. Karppinen (VTT), S. Hillberg (VTT)

Principal author or Project manager	**Reviewed by**
Markku Puustinen, Senior Research Scientist	Vesa Riikonen, Senior Research Scientist
Approved by	**Availability statement**
Heikki Purhonen, Research Director	SAFIR2018 limitations

Open your mind. LUT.
Lappeenranta University of Technology

Acknowledgement

NKS conveys its gratitude to all organizations and persons who by means of financial support or contributions in kind have made the work presented in this report possible.

Disclaimer

Open your mind. LUT.
Lappeenranta University of Technology

CONTENTS

1 INTRODUCTION 6
2 PPOOLEX TEST FACILITY 7
 2.1 TEST VESSEL 7
 2.2 PIPING 8
 2.3 SPARGER PIPE 9
 2.4 AIR REMOVAL SYSTEM 9
 2.5 MEASUREMENT INSTRUMENTATION 9
 2.6 CCTV SYSTEM 10
 2.7 DATA ACQUISITION 10
3 TEST PARAMETERS 10
4 TEST RESULTS 12
 4.1 STRATIFICATION PHASE 12
 4.2 EROSION PHASE 13
 4.3 MIXING PHASE 14
 4.4 COMPARISON OF SPA-CT1 TO SPA-T8R 14
5 SUMMARY AND CONCLUSIONS 15
6 REFERENCES 16

APPENDIXES:
Appendix 1: PPOOLEX drawings
Appendix 2: PPOOLEX instrumentation
Appendix 3: PPOOLEX test facility photographs

NOMENCLATURE

A	Area
D	Pressure difference measurement
F	Flow rate measurement
P	Pressure measurement
S	Strain measurement
T	Temperature measurement

Abbreviations

BWR	Boiling Water Reactor
CCTV	Closed Circuit TeleVision
CFD	Computational Fluid Dynamics
CONDEX	CONdensation EXperiments project
DCC	Direct Contact Condensation
ECCS	Emergency Core Cooling System
EHS	Effective Heat Source
EMS	Effective Momentum Source
EXCOP	EXperimental studies on COntainment Phenomena project
INSTAB	couplings and INSTABilities in reactor systems project
KTH	Kungliga Tekniska Högskolan
LRR	Load Reduction Ring
LOCA	Loss-Of-Coolant Accident
LUT	Lappeenranta University of Technology
MSLB	Main Steam Line Break
NKS	Nordic nuclear safety research
NORTHNET	NORdic nuclear reactor Thermal-Hydraulics NETwork
PACTEL	PArallel Channel TEst Loop
POOLEX	condensation POOL EXperiments project
PSP	Pressure Suppression Pool
RHR	Residual Heat Removal
PPOOLEX	Pressurized condensation POOL EXperiments test facility
SAFIR	SAfety of nuclear power plants - FInnish national Research programme
SG	steam generator
SPA	SPArger experiment series
SRV	Safety/Relief Valve
SSM	Strålsäkerhetsmyndigheten
TC	ThermoCouple
VTT	Technical Research Centre of Finland
VYR	State nuclear waste management fund

1 INTRODUCTION

A pressure suppression pool (PSP) of a BWR reactor containment serves as a heat sink and steam condenser during a postulated main steam line break (MSLB) or loss of coolant accident (LOCA) inside the containment or during safety relief valve (SRV) opening in normal operations. It thus prevents containment pressure build-up when steam released from the reactor vessel is vented through the blowdown pipes (in case of MSLB and LOCA) or through the spargers (in case of SRV operation) to the pool.

Different phenomena inside the drywell and wetwell compartments of BWR containment during steam discharge has been extensively studied in the PPOOLEX test facility at Lappeenranta University of Technology (LUT) and simulated with computer codes during recent years in the framework of the national research programmes on nuclear power plant safety (SAFIR, SAFIR2014) as well as via participation to NORTHNET RM3 and NKS research projects in co-operation with VTT and Kungliga Tekniska Högskolan (KTH). Research topics have included, for example, dynamic loads caused to PSP structures by direct contact condensation (DCC), behaviour of parallel blowdown pipes during the chugging flow mode, effect of blowdown pipe outlet design on structural loads, wall condensation in the drywell and development/break-up of thermal stratification in the PSP [1…10].

The current SAFIR2018/INSTAB project as well as the related NKS and SSM funded research efforts aim to broaden the database to cover experiments with SRV spargers, residual heat removal (RHR) system nozzles, strainers and containment spray systems. Calculation models and numerical methods including CFD and system codes are developed and validated based on the PPOOLEX experiment results at VTT and KTH within the SAFIR2018, NKS, and SSM funded projects. In addition, analytical support is provided for the experimental part by pre- and post-calculations of the experiments.

As a result of steam venting into the suppression pool the coolant temperature in the pool gradually increases. With certain flow modes a thermally stratified condition could develop where the pool's surface temperature is higher than the pool bulk temperature. This leads to a reduction of the pool's pressure suppression capacity because the pool surface temperature determines the steam partial pressure in the wetwell gas space. An increase of the pool's surface temperature due to stratification can therefore lead to a significant increase in containment pressure if mixing of the pool coolant inventory fails [11]. Pool mixing can occur due to steam injection itself if the injection flow mode changes because of increasing or decreasing steam flow rate. Mixing can be achieved also with the help of plant systems designed for that purpose or because of water suction from the pool by the Emergency Core Cooling System (ECCS) pumps.

KTH has developed the Effective Heat Source (EHS) and Effective Momentum Source (EMS) models for steam injection through a vertical pipe submerged in a pool and proposed them to be used for simulation of thermal stratification and mixing during a steam injection into a large pool of water [12]. These models have been implemented in GOTHIC® software and validated against POOLEX and PPOOLEX tests carried out at LUT. Excellent agreement in averaged pool temperature and water level in the pool between the experiment and simulation has been achieved. The development of thermal stratification and mixing of the pool are also well captured in the simulations. The EMS and EHS models will be available to be implemented also in the APROS containment code for the calculation of phenomena related to pool stratification and mixing.

Now KTH is improving the EHS and EMS models for blowdown pipes in order to reduce uncertainties and enhance accuracy in predictions as well as extending the models to SRV spargers. Later the models will be extended further to other elements of the PSP such as nozzles of the residual heat removal system and strainers in order to be able to carry out comprehensive safety analysis of realistic transients in a BWR containment.

Suitable experimental data is limited for validation of the EHS and EMS models. So far, the only available and sufficiently detailed experimental vent pipe data are the POOLEX/PPOOLEX steam discharge experiments with blowdown pipes. The PPOOLEX database was broadened to cover SRV spargers in the SPA test series carried out in 2014, 2015 and 2016 [13, 14, 15]. In 2017, the sparger pipe in the PPOOLEX facility was moved to the centre position in the wetwell pool and a single test was carried out with this new configuration to find out if the stratification/mixing effects differ from those observed in the tests where the sparger pipe was away from the pool centre axis. Chapter two gives a short description of the test facility and its measurements as well as of the data acquisition systems used. The test parameters, initial conditions and test procedure are introduced in chapter three. The test results are presented and discussed in chapter four. Chapter five summarizes the findings of the test series.

2 PPOOLEX TEST FACILITY

The PPOOLEX test facility was taken into use at LUT in the end of 2006. PPOOLEX models the containment of a BWR plant. During the years, the facility has gone through several modifications and enhancements as well as improvements of instrumentation. For example, a model of a SRV sparger was added to the wetwell pool to extend the scope of scenarios, which can be studied with the facility. For the test described in this report the sparger pipe was moved to the centre position in the pool. The PPOOLEX facility is described in more detail in reference [16]. However, the main features of the facility and its instrumentation are introduced below.

2.1 TEST VESSEL

The PPOOLEX facility consists of a wetwell compartment (condensation pool), drywell compartment, inlet plenum and air/steam-line piping. An intermediate floor separates the compartments from each other. Usually a route for gas/steam flow from the drywell to the wetwell is created by a vertical blowdown pipe attached underneath the floor. During the sparger tests the drywell compartment was, however, bypassed i.e. steam was blown directly into the wetwell via the sparger pipe.

The main component of the facility is the ~31 m^3 cylindrical test vessel, 7.45 m in height and 2.4 m in diameter. It is constructed from three plate cylinder segments and two dome segments. The test facility is able to withstand considerable structural loads caused by rapid condensation of steam. The dry and wetwell sections are volumetrically scaled according to the compartment volumes of the Olkiluoto containment (ratio approximately 1:320). There are several windows for visual observation in both compartments. A DN100 (∅ 114.3 x 2.5 mm) drainpipe with a manual valve is connected to the vessel bottom. A relief valve connection is mounted on the vessel head. The removable vessel head and a manhole (DN500) in the wetwell compartment wall provide access to the interior of the vessel for maintenance and modifications of internals and instrumentation. The drywell is thermally insulated.

A sketch of the test vessel is shown in Figure 1. Table 1 lists the main dimensions of the test facility compared to the conditions in the Olkiluoto plant.

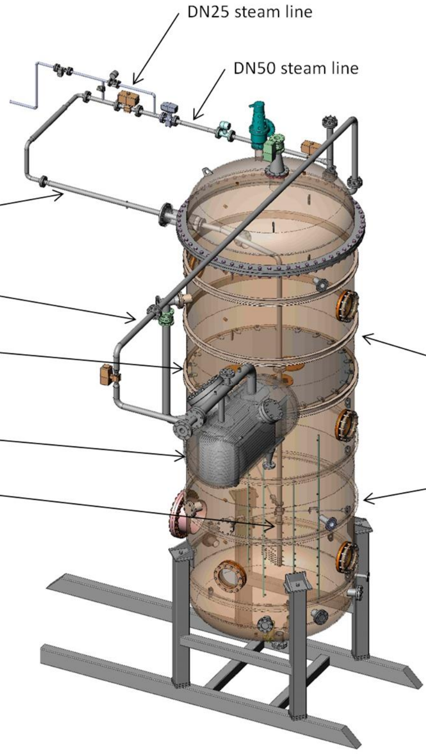

Figure 1. PPOOLEX test vessel.

Table 1. Test facility vs. Olkiluoto 1 and 2 BWRs.

	PPOOLEX test facility	Olkiluoto 1 and 2
Number of blowdown pipes	1-2	16
Inner diameter of the blowdown pipe [mm]	214.1	600
Suppression pool cross-sectional area [m^2]	4.45	287.5
Drywell volume [m^3]	13.3	4350
Wetwell volume [m^3]	17.8	5725
Nominal water volume in the suppression pool [m^3]	8.38*	2700
Nominal water level in the suppression pool [m]	2.14*	9.5
Pipes submerged [m]	1.05	6.5
A_{pipes}/A_{pool}x100%	0.8 / 1.6**	1.6

* Water volume and level can be chosen according to the experiment type in question. The values listed in the table are based on the ratio of nominal water and gas volumes in the plant.
** With one / two blowdown pipes.

2.2 PIPING

Steam needed in the tests is generated with the nearby PACTEL test facility, which has a core section of 1 MW heating power and three horizontal steam generators (SG) [17]. Steam is led through a thermally insulated steam line, made of sections of standard DN80 (Ø88.9x3.2), DN50 (Ø60.3x3.0) and DN65 (Ø76.1x3.0) pipes, from the PACTEL steam generators towards the

PPOOLEX test vessel. The section of the steam piping inside the drywell (bypass) is made of uninsulated DN65 (Ø76.1x3.0) pipe.

2.3 SPARGER PIPE

The DN65 (Ø76.1x4.0) sparger type blowdown pipe was originally positioned vertically inside the pool in a non-axisymmetric location, i.e. the pipe was 420 mm away from the centre of the condensation pool. For the test described in this report the sparger pipe was moved to the centre position of the pool by adding two pipe bends and a short horizontal pipe section above the water level (Figure 2). The total length of the modified sparger pipe is approx. 5.4 m. The pipe is made from austenitic stainless steel EN 1.4571.

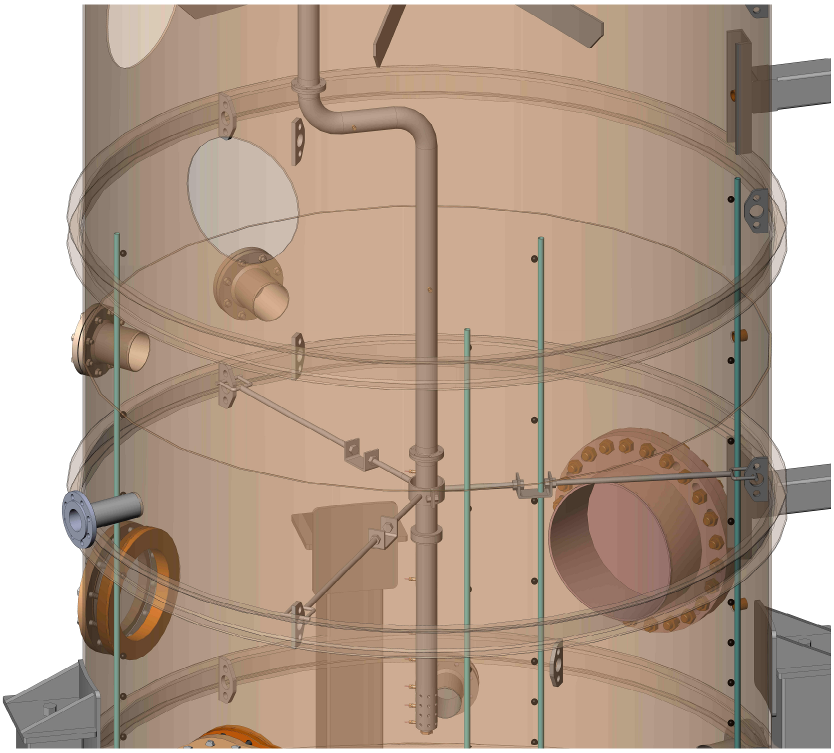

Figure 2. Sparger pipe in centre position in PPOOLEX.

There are 32 Ø8 mm holes drilled radially in the lower part of the pipe (sparger head). These holes are in four rows, eight holes in each row. There is a load reduction ring (LRR) 700 mm above the pipe outlet with 8 axially drilled Ø8 mm holes.

2.4 AIR REMOVAL SYSTEM

For the sparger tests, the PPOOLEX facility was equipped with an air removal system. The system consists of a filter unit and an air removal device. Air is removed in a vacuum chamber by a vacuum pump during the preparation period for the experiments. However, the system is not used in all the experiments.

2.5 MEASUREMENT INSTRUMENTATION

The applied instrumentation depends on the experiments in question. Normally, the test facility is equipped with several thermocouples (TC) for measuring steam, pool water and structure temperatures and with pressure transducers (P) for observing pressures in the drywell, inside the blowdown pipes, at the condensation pool bottom and in the gas space of the wetwell. Steam flow rate is measured with a vortex flow meter (F) in the steam line. Additional instrumentation includes, for example, strain gauges (S) on the pool outer wall and valve position sensors.

For the sparger tests a 6x7 grid of temperature measurements (thermocouples T4000–T4056) was installed in the pool in front of the injection holes of the sparger head. For measuring vertical temperature distribution inside the sparger pipe nine temperature measurements (thermocouples T4070…T4078) were installed with a varying interval. The topmost TC (T4078) was moved to the horizontal section of the piping when the shift to the centre position was done. Four trains of temperature measurements (thermocouples T4100…T4113, T4200…T4219, T4300…T4319 and T4400…T4413) were installed in the pool below the water level for detecting vertical temperature distribution.

Figures in Appendix 2 show the locations of the PPOOLEX measurements during the SPA test series and the table in Appendix 2 lists their identification codes and other details.

2.6 CCTV SYSTEM

Standard video cameras with 25 fps connected to a laptop computer were used for visual observation of the test vessel interior during the test.

2.7 DATA ACQUISITION

National Instruments PXIe PC-driven measurement system was used for data acquisition. The system enables high-speed multi-channel measurements. The maximum number of measurement channels is 64 with additional eight channels for strain gauge measurements. The maximum recording capacity depends on the number of measurements and is in the region of three hundred thousand samples per second. Measurement software was LabView 2015.

Self-made software using the National Instruments FieldPoint measurement system was used for monitoring and recording the essential measurements of the PACTEL facility generating the steam. Both data acquisition systems measure signals as volts. After the tests, the voltage readings are converted to engineering units with conversion software.

The used measurement frequency of LabView was 20 Hz. The rest of the measurements (for example temperature, pressure and flow rate in the steam line) were recorded by the self-made software with the frequency of 0.67 Hz.

3 TEST PARAMETERS

A sparger pipe test labelled as SPA-CT1was carried out in the PPOOLEX facility. The earlier SPA-T8R test done with the sparger pipe away from the pool centre acted as a reference test for this new test. The main purpose of the test was to study how the change of the sparger pipe position to the pool centre affects the stratification/mixing behaviour during steam discharge via the sparger pipe. Particularly, the effect on the elevation and thickness of the thermocline between the cold and warm water volumes and on the temperature profile of the pool were of interest. A secondary goal was to obtain data for the development of the EMS and EHS models to be implemented in GOTHIC code by KTH.

Detailed test specifications were put together based on the reference test SPA-T8R. It had a stratification phase, an erosion phase with slightly increased flow rate and a mixing period with a high flow rate. The same kind of test procedure was followed in the SPA-CT1 test. As in the reference test, all the 32 injection holes of the sparger head were open in SPA-CT1 but the holes of the LRR were blocked.

Before the test, the wetwell pool was filled with ~12 °C isothermal water (in SPA-T8R ~13 °C) to the level of 2.7 m i.e. the sparger pipe outlet was submerged by 1.5 m. In the reference SPA-T8R test the level was 3.0 m and thus the sparger pipe outlet was submerged by 1.8 m. The steam discharge rate into the PPOOLEX vessel was controlled with the help of the pressure level of the steam source (PACTEL steam generator) and a remote-operated control valve (S2002) in the DN50 steam line. In SPA-CT1, only one PACTEL steam generator was used for generating steam. In the reference test, all three SGs were used. This should not have any effect on the test results because one SG is capable of delivering enough saturated steam needed during the test.

The tests were started from atmospheric conditions in PPOOLEX. After the correct initial steam generator pressure (0.6 MPa) had been reached, the remote-controlled cut-off valve (X2100) in the DN50 steam line was opened. To remove air from the steam line and to heat up the piping structures from the PACTEL facility to the PPOOLEX vessel, steam mass flow rate was at first adjusted to a higher level (slightly above 250 g/s) for about 200 seconds. The pool bulk temperature rose approximately 2 °C during this clearing phase.

The stratification process was initiated by reducing the steam flow rate to the level of about 130 g/s. The erosion phase was started after a temperature difference of 20 °C between the bottom and surface layers of the pool had been reached by increasing the steam flow rate into the test vessel to the value of about 140 g/s. The final mixing phase was started once the pool surface temperature had reached 85 °C by further increasing the steam flow rate to about 250 g/s. The test was continued with this flow rate until the pool surface was at 115 °C.

The main parameters of the SPA-CT1 test are listed in Table 2. The path of the SPA-CT1 test as well as the reference SPA-T8R defined by steam mass flux and pool bulk temperature is marked on the condensation mode map for a sparger of Chan and Lee [18] in Figure 4. In the map, steam mass flux is determined as the flow rate through the injection holes of the sparger head divided by the cross-sectional area of the holes.

Table 2. Parameter values of the sparger tests SPA-CT1.

Test	Initial water level [m]	Initial water temperature [°C]	Steam flow rate [g/s]		
			Stratification	Erosion/Mixing phase(s)	Final mixing phase
SPA-CT1	2.7	~12	~127	~138	~248

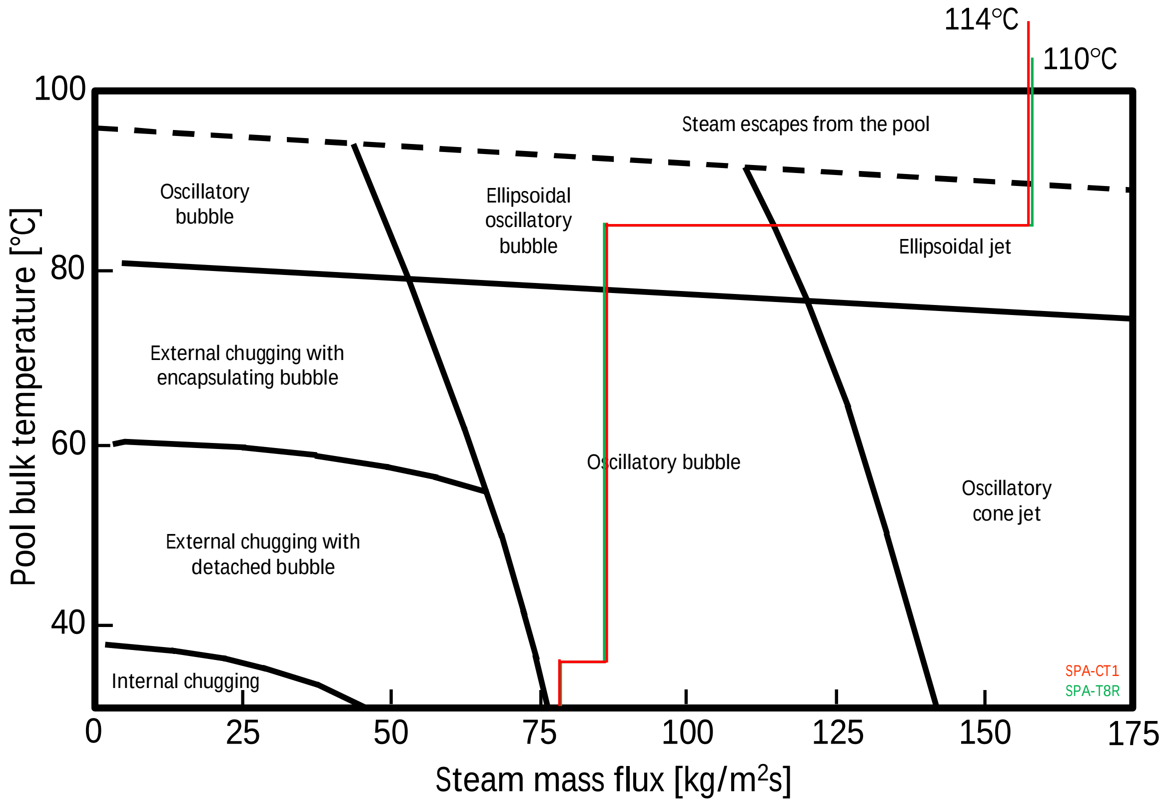

Figure 3. Paths of the SPA-CT1 and SPA-T8R tests marked on the direct condensation mode map for pure steam discharge of Chan and Lee [18].

4 TEST RESULTS

The following chapters give a more detailed description of the SPA-CT1 test, present the observed phenomena and compare the results with the reference test SPA-T8R.

4.1 STRATIFICATION PHASE

Initially, there was water and noncondensible gas (air) inside the sparger pipe. These were expelled out of the pipe during the clearing phase as soon as steam injection was initiated. All the injection holes of the sparger head were open and as a result 32 horizontal and radially directed steam jets developed around the lower end of the sparger after all air had escaped from the pipe. The pipe was practically full of steam during the rest of the test.

The stratification phase with a steam flow rate of ~127 g/s (corresponding to the mass flux of about 79.0 kg/m^{2}s) continued until a 20 °C temperature difference between the pool bottom and surface had developed. According to the direct condensation mode map for pure steam discharge of Chan and Lee, the dominant flow mode is then oscillatory bubble, Figure 3. With this kind of mass flux, steam flows through the injection holes of the sparger as small jets and condenses mainly outside the sparger pipe. Because no chugging kind of phenomenon exists and the steam jets are too weak to create much turbulence in the pool, suitable conditions for thermal stratification to occur prevail.

The stratification phase continued until 3145 seconds into the experiment. Two regions with clearly different water temperatures developed in the pool. Between these regions, there was a transition region (thermocline). The region close to the pool bottom, where the steam jets had no effect, remained at the temperature established after the clearing phase in the beginning of the test. Elevations from about 700 mm to the pool surface heated up instead quite uniformly. The heat-up process was driven by flow of warm condensed water upwards from the sparger outlet as well as by conduction through the pipe wall. In addition, the steam jets created an internal flow pattern that circulated warm water slightly downwards thus heating elevations also quite far below the sparger outlet. The temperature measurements attached to the vertical rods in the pool indicate that the thermocline, where the pool water temperature shifted from cold and warm, was around the 500 mm elevation. The oscillating behaviour of the temperature curves measured by the TCs at the 472 mm and 522 mm elevations confirm the location of this transition region. Compared to the reference test SPA-T8R the thermocline was located somewhat deeper in the pool.

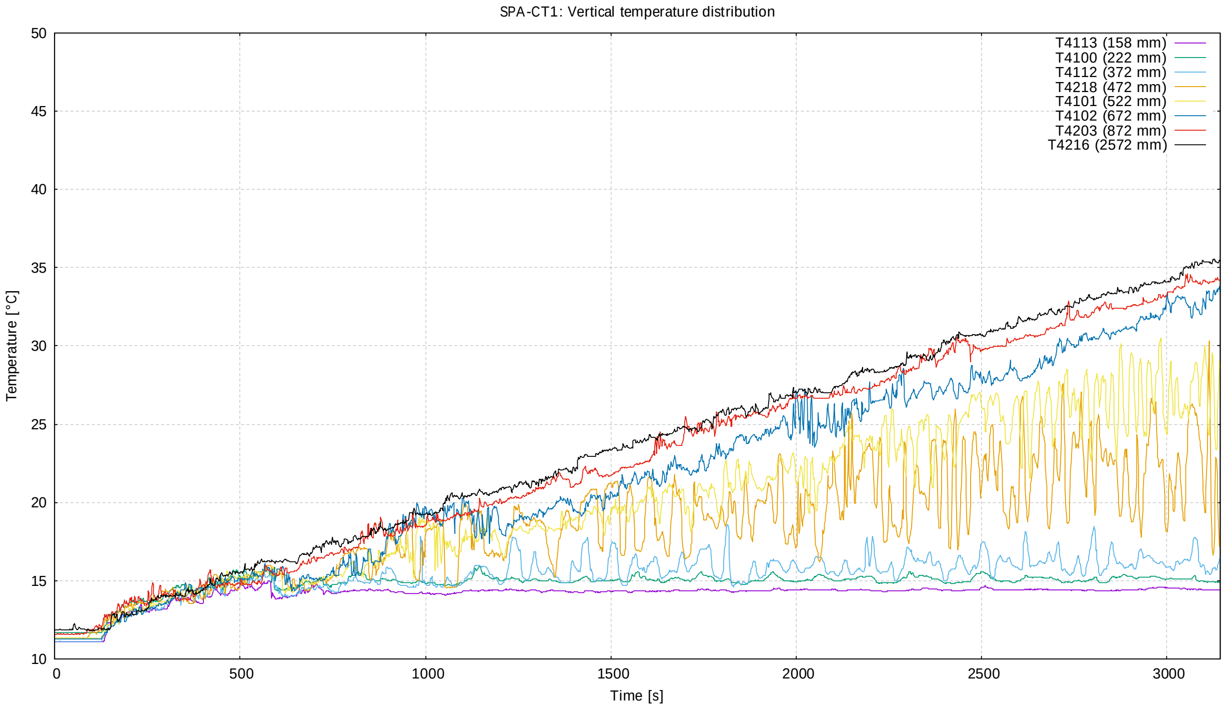

Figure 4. Vertical temperature distribution in wetwell pool during the clearing phase (0-230 s) and stratification phase (230-3145 s) in the SPA-CT1 test.

4.2 EROSION PHASE

On the basis of the pre-test simulations and earlier tests it was known that even a small increase in the steam flow rate could somewhat erode the thermocline and at least partly mix the pool. For the erosion phase in SPA-CT1 the steam flow rate was increased to ~138 g/s (corresponding to the mass flux of about 85.8 kg/m^{2}s). At the end of the erosion phase, the pool water temperature exceeded 80 °C and the flow mode changed from oscillatory bubble to ellipsoidal oscillatory bubble (Figure 3).

Figure 5 shows how the elevation of the thermocline shifts downwards as the TCs in the transition region start to indicate the same readings as all the other TCs above the thermocline. The fact that this happens very slowly verifies that erosion is the prevailing process. At the end of this phase, the thermocline seems to be around the elevations of 372 mm according to the TC measurement T4112. This is slightly deeper than in the reference test SPA-T8R at the end of the erosion phase.

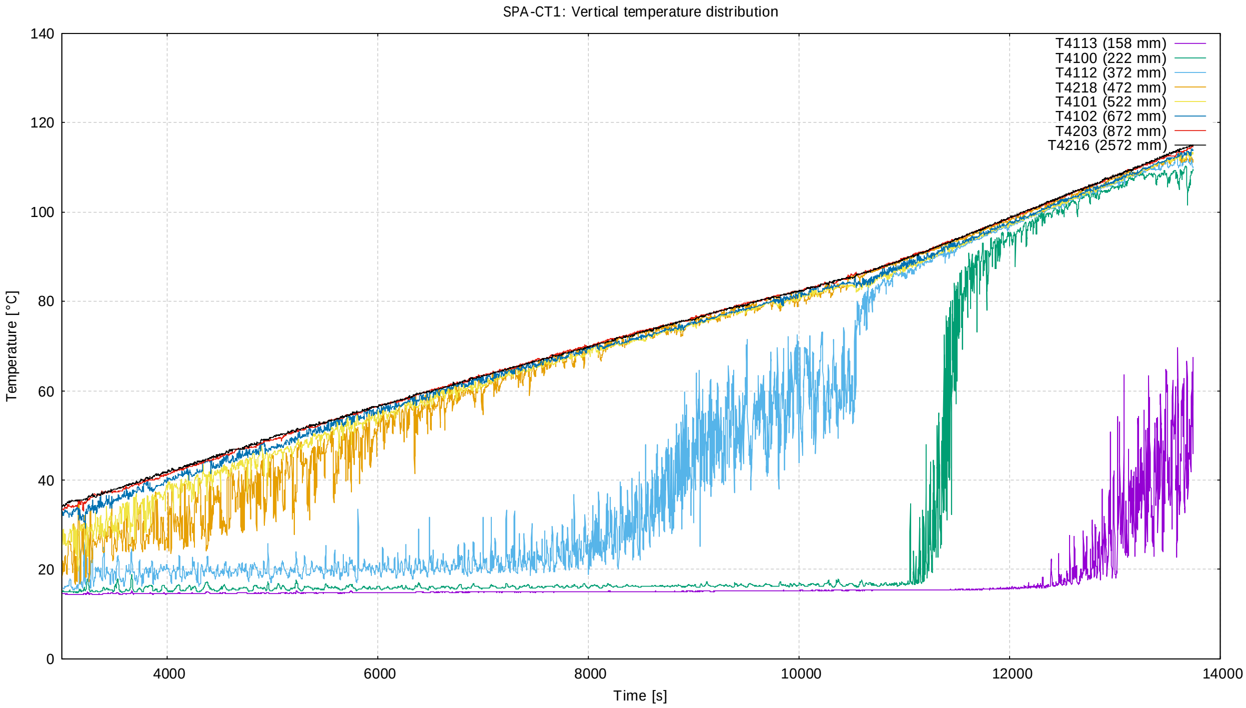

Figure 5. Vertical temperature distribution in wetwell pool during the erosion phase (3145-10480 s) and final mixing phase (10480-13720 s) in the SPA-CT1 test.

4.3 MIXING PHASE

For the final mixing phase, the steam mass flow rate was increased to ~248 g/s (154.2 kg/m^{2}s) at 10480 seconds into the experiment. As a result, the flow mode changed to ellipsoidal jet (Figure 3). The aim was to mix the pool completely and see if the process differs from that of the SPA-T8R test.

The mixing process speeded up considerably compared to the erosion phase but complete mixing was not achieved before the test had to be terminated due to exceeding 115 °C at the top layers of the pool (Figure 5). In this phase, mixing happens via internal circulation induced by horizontal steam jets at the injection holes of the sparger outlet.

4.4 COMPARISON OF SPA-CT1 TO SPA-T8R

The development of the vertical temperature profile of pool water over the whole SPA-CT1 and SPA-T8R tests can be seen from Figure 6 and Figure 7, respectively. The initial uniform temperature profile first changes to a stratified situation and eventually back to an almost uniform and mixed situation at the end of the final mixing phase. At the end of the stratification phase, the temperature curves are almost straight vertical lines outside the transition region indicating rather constant water temperature distribution elsewhere in the pool.

It can be clearly seen from Figure 6 and Figure 7 that in both tests the thermocline moved slowly downwards as the tests proceeded. Furthermore, the thickness of the transition region seems to be almost the same. The comparison of the figures, however, reveals that in SPA-CT1 the thermocline settles at the end of the stratification phase about 150-250 mm deeper than in SPA-T8R.

Another difference in the temperature profile between the two tests can be found from the final mixing phase. Close to the bottom of the pool, the boundary between cold and warm pool water seems to be sharper in the reference SPA-T8R test than in the new test where the sparger pipe had been moved to the centre axis of the pool. The rounded shape of the profile curve close to the bottom in SPA-TC1 indicates that the internal circulation pattern in the pool during the high flow rate phase could be different in the case where the sparger pipe is at the pool centre.

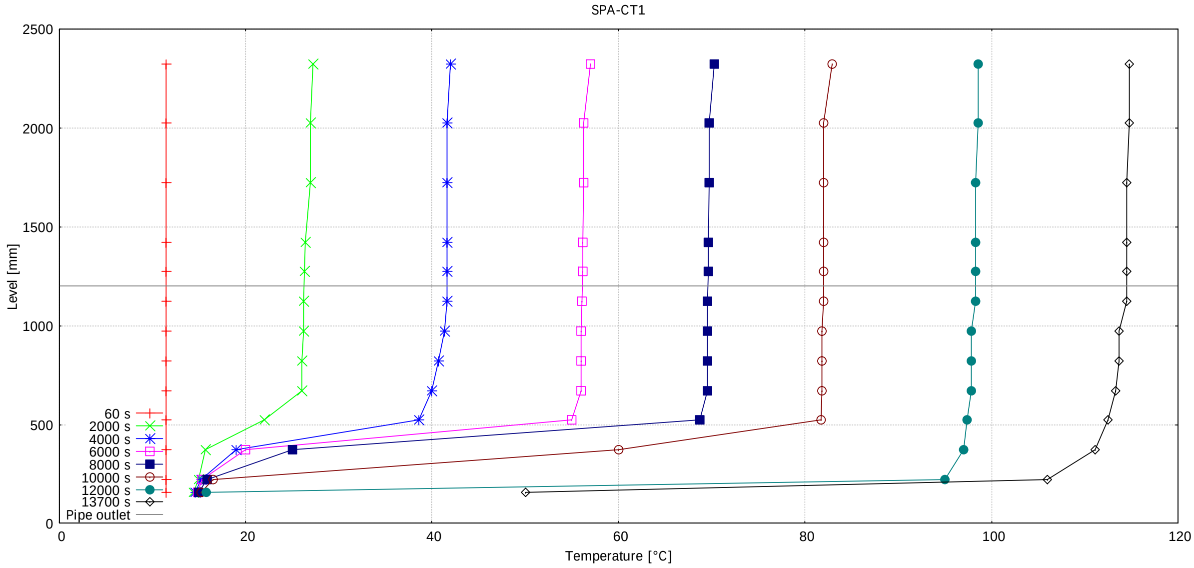

Figure 6. Development of vertical temperature profile of pool water in the SPA-CT1 test.

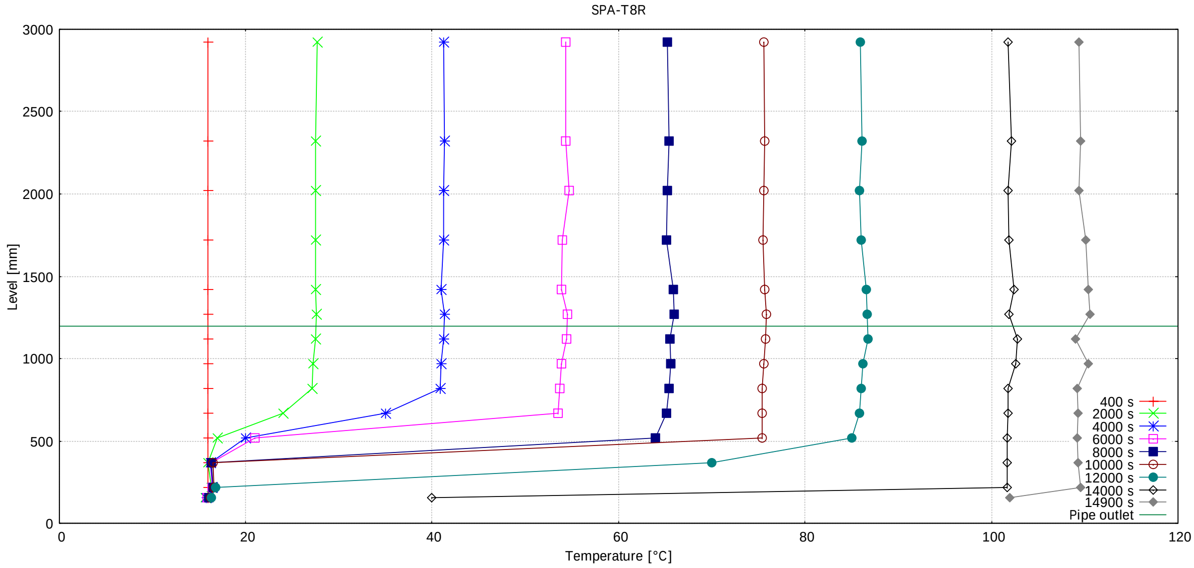

Figure 7. Development of vertical temperature profile of pool water in the reference SPA-T8R test.

5 SUMMARY AND CONCLUSIONS

This report summarizes the results of the sparger pipe test SPA-CT1 carried out in the PPOOLEX facility at LUT in 2017. The test facility is a closed stainless steel vessel divided into two compartments, drywell and wetwell. In the test, the drywell compartment was bypassed i.e. the sparger pipe in the wetwell was connected directly to the steam line coming from the PACTEL facility which acted as a steam source.

The main objective of the test was to study how the change of the sparger pipe position to the pool centre affects the stratification/erosion/mixing behaviour during steam discharge via the sparger pipe. Particularly, the effect on the elevation and thickness of the thermocline between the cold and warm water volumes and on the temperature profile of the pool were of interest. The SPA-T8R test done earlier with the sparger pipe away from the pool centre acted as a reference case. A secondary goal was to obtain data for the development of the EMS and EHS models to be implemented in GOTHIC code by KTH. Originally, the models were developed for straight blowdown pipes but KTH plans to extend the EMS and EHS models to cover also situations where steam injection into the pool is via a sparger pipe.

Steam injection into the pool was only through the holes at the sparger head because the holes of the LRR were blocked. There was a stratification phase and an erosion phase with a moderate steam flow rate and then a final mixing phase with a clearly higher flow rate.

The general behaviour during the stratification/erosion/mixing phases is almost identical in the new sparger test and in the earlier reference test. The initial uniform temperature profile first changes to a stratified situation and eventually back to an almost uniform and mixed situation at the end of the final mixing phase. During the erosion phase the thermocline moves slowly downwards and the thickness of the transition region seems to be almost the same in both tests.

The moving of the sparger pipe to the centre axis of the pool, however, seems to have a slight effect on the elevation of the thermocline as well as on the temperature profile in the pool. The thermocline settles at the end of the stratification phase about 150-250 mm deeper if the sparger pipe is in the centre of the pool compared to the situation where the sparger was about 420 mm away from the centre axis. The temperature profile from the elevations close to the pool bottom reveal that during the final high flow rate mixing phase the internal circulation pattern in the pool could be different in the case where the sparger pipe is at the pool centre compared to the case where it is away from the centre.

This test in PPOOLEX revealed that the change in the radial location of the sparger pipe could have some effect on the pool behaviour during stratification/erosion/mixing processes. Additional tests, however, are needed to verify these effects in more detail.

6 REFERENCES

1. Puustinen, M., Laine, J., Räsänen, A., PPOOLEX Experiments on Thermal Stratification and Mixing. Lappeenranta University of Technology. 2009. Research Report CONDEX 1/2008.
2. Laine, J., Puustinen, M., PPOOLEX Experiments on Wall Condensation. Lappeenranta University of Technology. 2009. Research Report CONDEX 3/2008.
3. Laine, J., Puustinen, M., Räsänen, A., PPOOLEX Experiments with a Modified Blowdown Pipe Outlet. Lappeenranta University of Technology. 2009. Research Report CONDEX 2/2008.
4. Laine, J., Puustinen, M., Räsänen, A., PPOOLEX Experiments with Two Parallel Blowdown Pipes. Lappeenranta University of Technology. 2010. Research Report CONDEX 1/2009.
5. Puustinen, M., Laine, J., Räsänen, A., PPOOLEX Experiments on Dynamic Loading with Pressure Feedback. Lappeenranta University of Technology. 2010. Research Report CONDEX 2/2009.

6. Laine, J., Puustinen, M., Räsänen, A., Tanskanen, V., PPOOLEX Experiments on Stratification and Mixing in the Wet Well Pool. Lappeenranta University of Technology. 2011. Research Report CONDEX 1/2010.
7. Puustinen, M., Laine, J., Räsänen, A., Multiple Blowdown Pipe Experiment with the PPOOLEX Facility. Lappeenranta University of Technology. 2011. Research Report CONDEX 2/2010.
8. Puustinen, M., Laine, J., Räsänen, A., PPOOLEX Experiments with a Blowdown Pipe Collar. Lappeenranta University of Technology. 2012. Research Report EXCOP 1/2011.
9. Laine, J., Puustinen, M., Räsänen, A., PPOOLEX Experiments on the Dynamics of Free Water Surface in the Blowdown Pipe. Lappeenranta University of Technology. 2013. Research Report EXCOP 2/2012.
10. Laine, J., Puustinen, M., Räsänen, A., PPOOLEX Mixing Experiments. Lappeenranta University of Technology. 2014. Research Report EXCOP 1/2013.
11. Gamble, R. E., Nguyen, T. T., Peterson, P. F., Pressure suppression pool mixing in passive advanced BWR plants. Nuclear Engineering and Design, 204, 321-336, 2000.
12. Li, H., Villanueva, W., Kudinov, P., Effective Models for Simulation of Thermal Stratification and Mixing Induced by Steam Injection into a Large Pool of Water. Division of Nuclear Power Safety, Royal Institute of Technology (KTH), NORTHNET Roadmap 3 Research report, Stockholm, 2014.
13. Laine, J. Puustinen, M. Räsänen, A., PPOOLEX Experiments with a Sparger. Lappeenranta University of Technology. 2015. Research Report EXCOP 1/2014.
14. Puustinen, M., Laine, J., Räsänen, A., Additional Sparger Tests in PPOOLEX with Reduced Number of Injection Holes. Lappeenranta University of Technology. 2016. Research Report INSTAB 1/2015.
15. Puustinen, M., Pyy, L., Laine, J., Räsänen, A., Sparger Tests in PPOOLEX on the Behaviour of Thermocline. Lappeenranta University of Technology. 2017. Research Report INSTAB 1/2016.
16. Puustinen, M., Partanen, H., Räsänen, A., Purhonen, H., PPOOLEX Facility Description. Lappeenranta University of Technology. 2007. Technical Report POOLEX 3/2006.
17. Tuunanen, J., Kouhia, J., Purhonen, H., Riikonen, V., Puustinen, M., Semken, R. S., Partanen, H., Saure, I., Pylkkö, H., General Description of the PACTEL Test Facility. Espoo: VTT. 1998. VTT Research Notes 1929. ISBN 951-38-5338-1.
18. Chan, C. K., Lee, C. K. B., A Regime Map for Direct Contact Condensation. Int. J. Multiphase Flow. 1982.

APPENDIX 1: PPOOLEX drawings

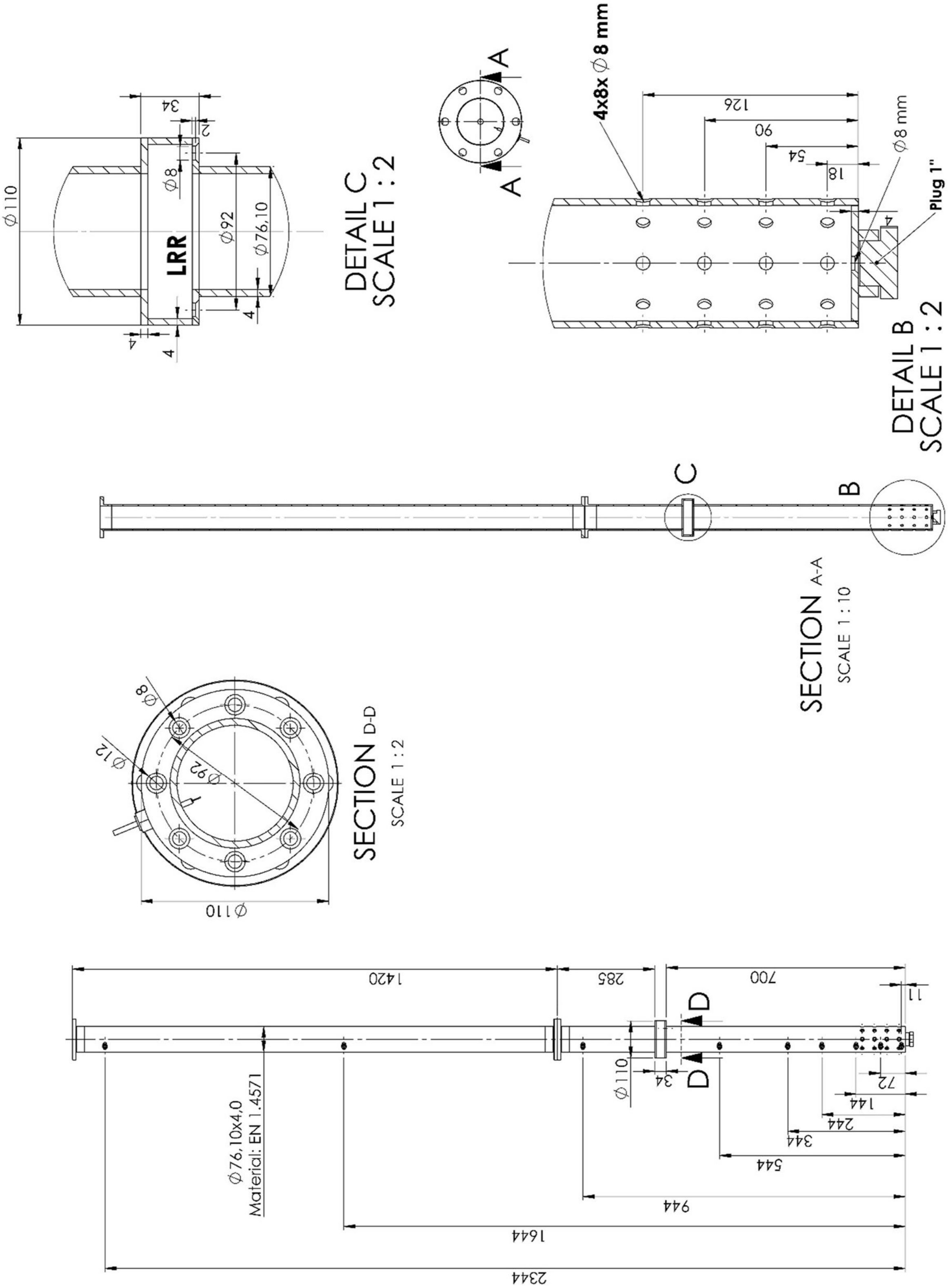

DN65 sparger pipe.

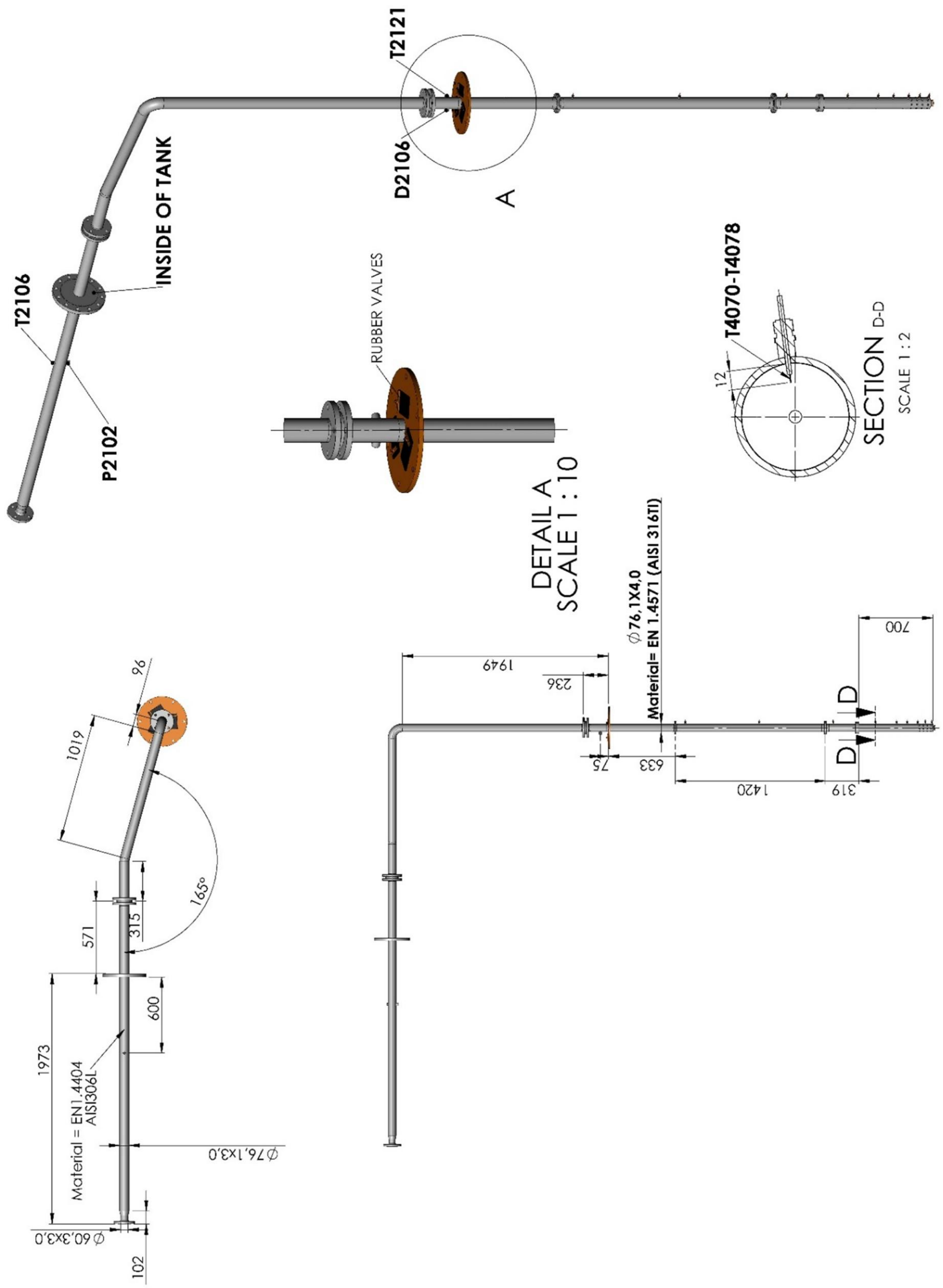

DN65 steam line (The bends made to the piping in the wetwell for the SPA-CT1 test are not shown in the drawing).

Open your mind. LUT.
Lappeenranta University of Technology

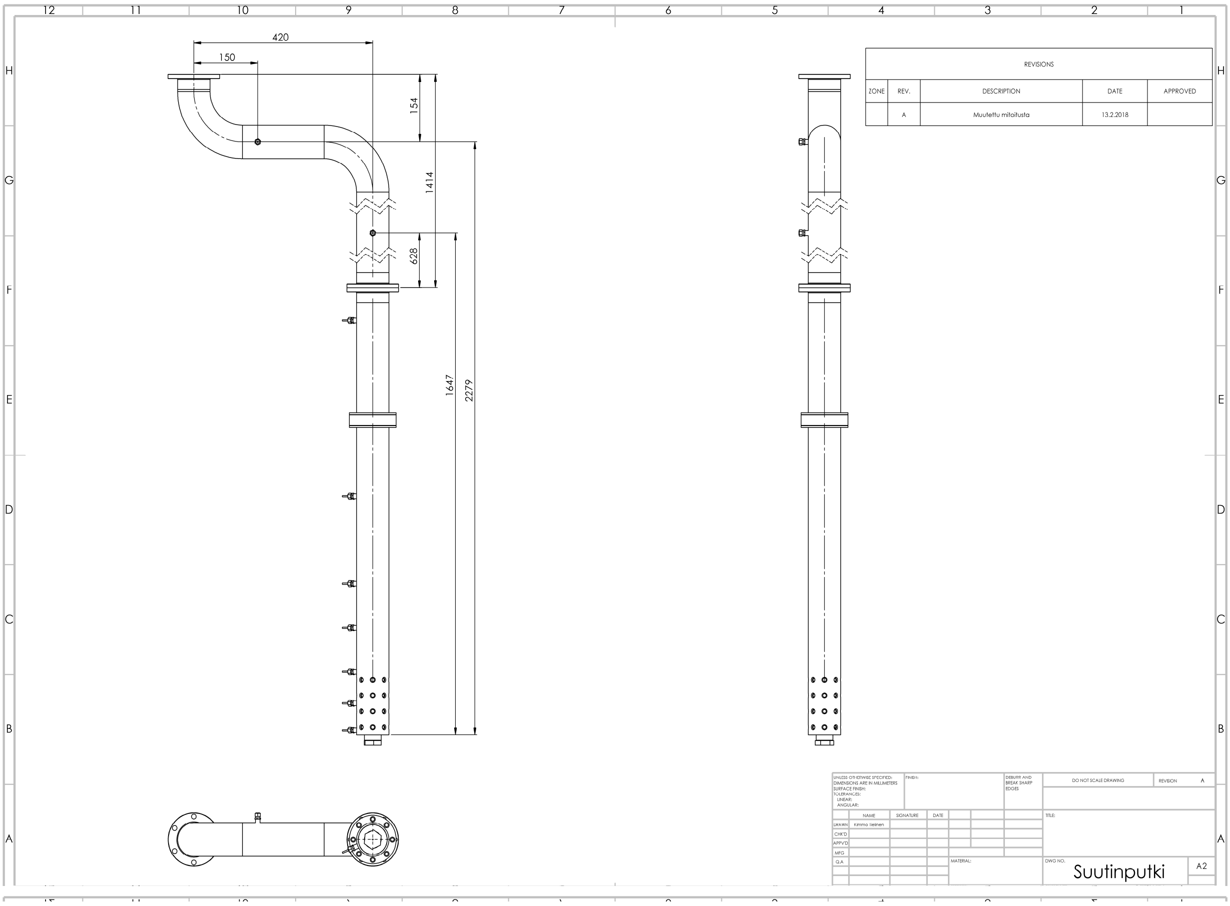

The bends made to the piping to move the sparger to the centre of the pool.

Open your mind. LUT.
Lappeenranta University of Technology

APPENDIX 2: PPOOLEX instrumentation

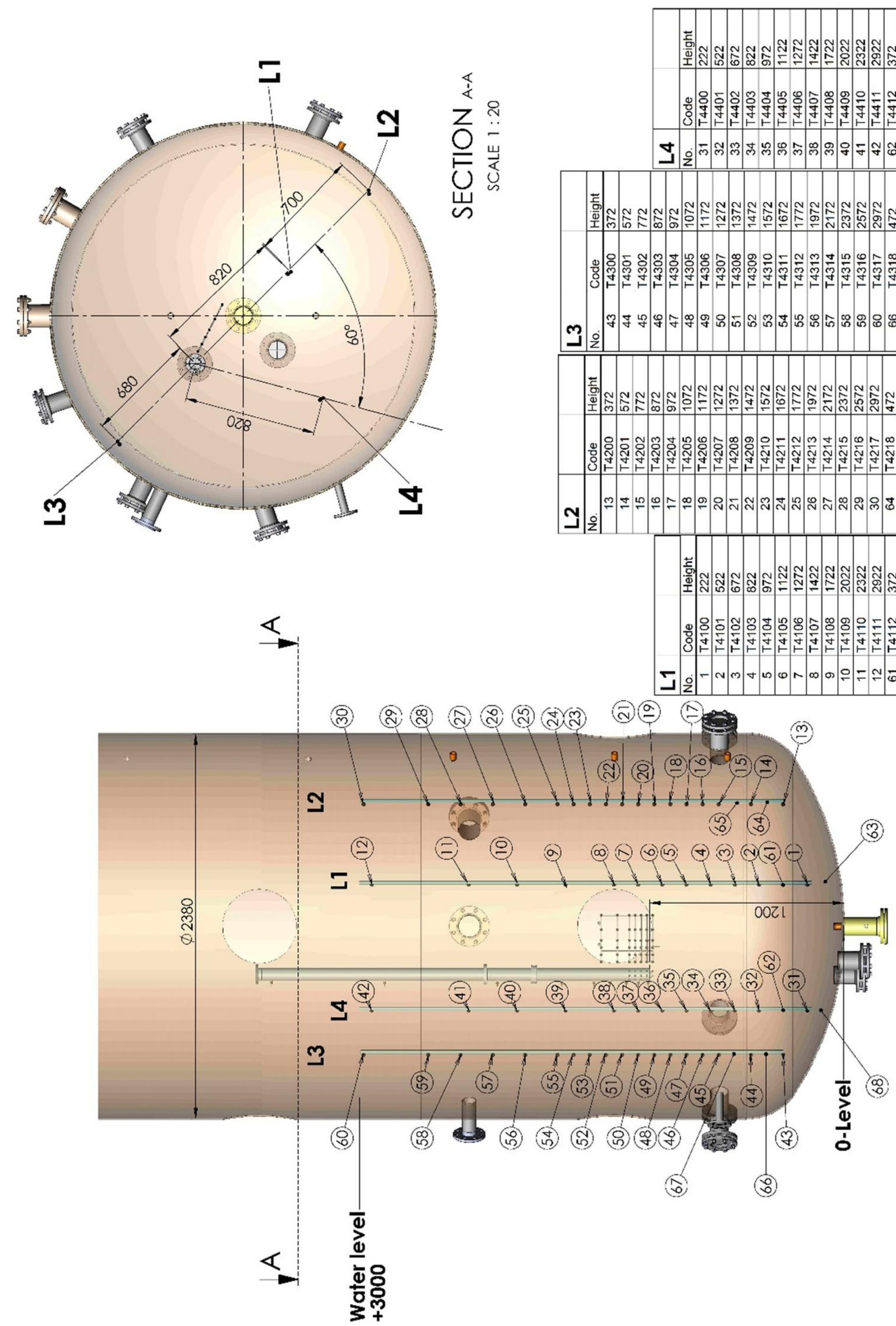

L1

No.	Code	Height
1	T4100	222
2	T4101	522
3	T4102	672
4	T4103	822
5	T4104	972
6	T4105	1122
7	T4106	1272
8	T4107	1422
9	T4108	1722
10	T4109	2022
11	T4110	2322
12	T4111	2922
61	T4112	372
63	T4113	158

L2

No.	Code	Height
13	T4200	372
14	T4201	572
15	T4202	772
16	T4203	872
17	T4204	972
18	T4205	1072
19	T4206	1172
20	T4207	1272
21	T4208	1372
22	T4209	1472
23	T4210	1572
24	T4211	1672
25	T4212	1772
26	T4213	1972
27	T4214	2172
28	T4215	2372
29	T4216	2572
30	T4217	2972
64	T4218	472
65	T4219	672

L3

No.	Code	Height
43	T4300	372
44	T4301	572
45	T4302	772
46	T4303	872
47	T4304	972
48	T4305	1072
49	T4306	1172
50	T4307	1272
51	T4308	1372
52	T4309	1472
53	T4310	1572
54	T4311	1672
55	T4312	1772
56	T4313	1972
57	T4314	2172
58	T4315	2372
59	T4316	2572
60	T4317	2972
66	T4318	472
67	T4319	672

L4

No.	Code	Height
31	T4400	222
32	T4401	522
33	T4402	672
34	T4403	822
35	T4404	972
36	T4405	1122
37	T4406	1272
38	T4407	1422
39	T4408	1722
40	T4409	2022
41	T4410	2322
42	T4411	2922
62	T4412	372
68	T4413	158

Four trains of temperature measurements in the wetwell.

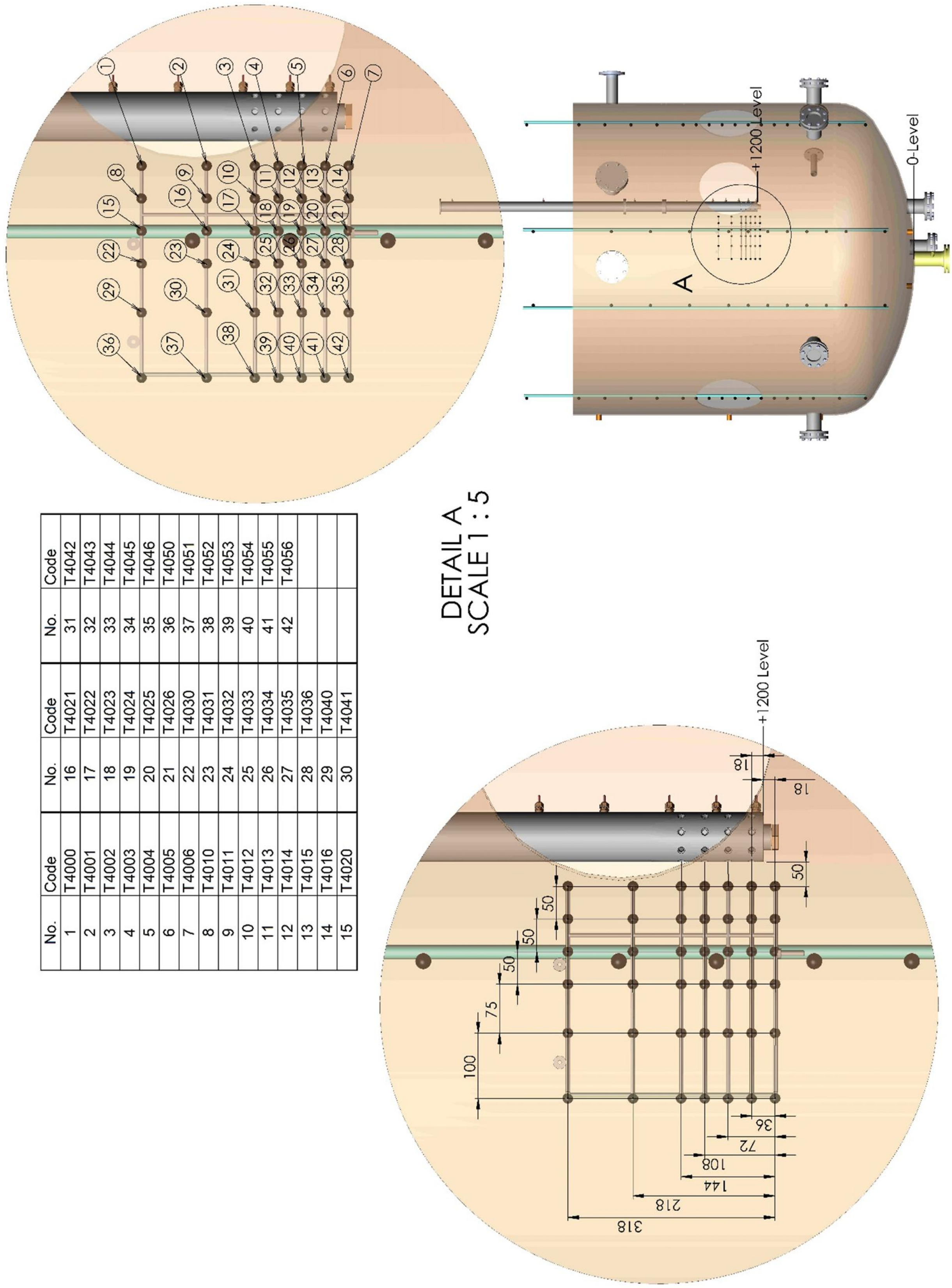

No.	Code	No.	Code	No.	Code
1	T4000	16	T4021	31	T4042
2	T4001	17	T4022	32	T4043
3	T4002	18	T4023	33	T4044
4	T4003	19	T4024	34	T4045
5	T4004	20	T4025	35	T4046
6	T4005	21	T4026	36	T4050
7	T4006	22	T4030	37	T4051
8	T4010	23	T4031	38	T4052
9	T4011	24	T4032	39	T4053
10	T4012	25	T4033	40	T4054
11	T4013	26	T4034	41	T4055
12	T4014	27	T4035	42	T4056
13	T4015	28	T4036		
14	T4016	29	T4040		
15	T4020	30	T4041		

6x7 grid of temperature measurements in the wetwell.

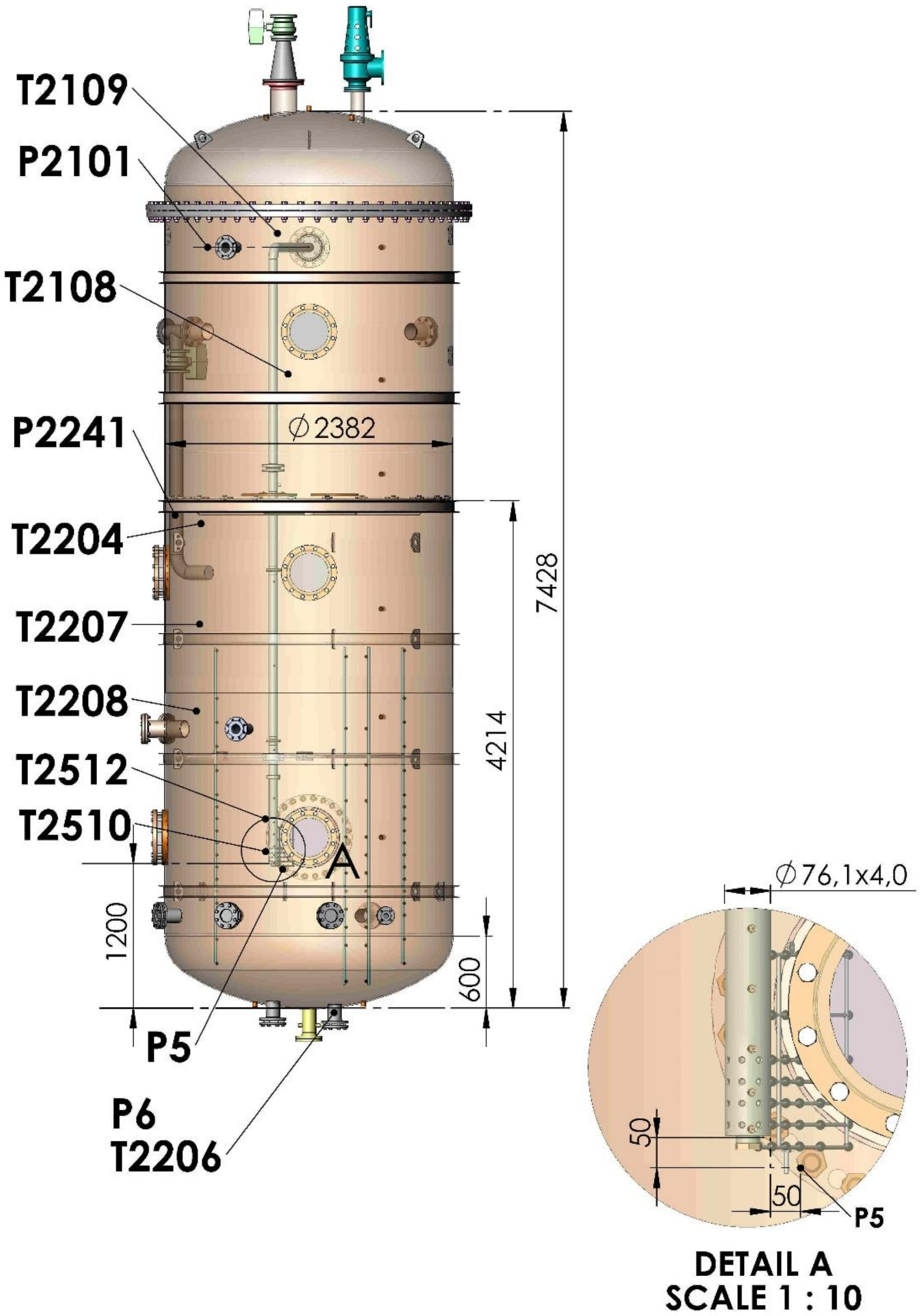

Test vessel measurements.

Open your mind. LUT.
Lappeenranta University of Technology

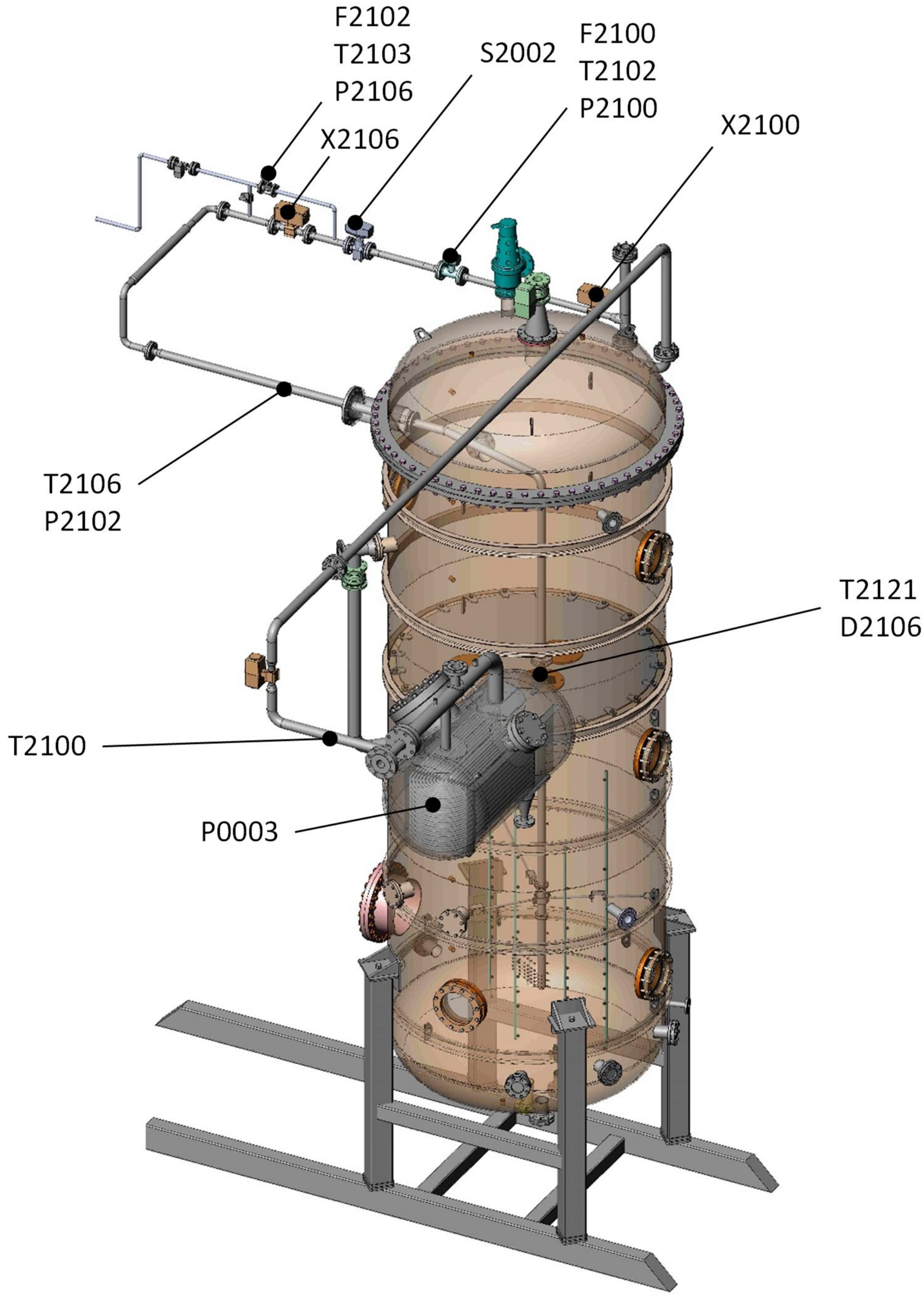

Measurements in the steam line.

Measurement	Code	Elevation	Location	Error estimation	Measurement software
Camera trigger	C1	-	Wetwell	Not defined	LabView
Pressure difference	D2100	700–3300	Wetwell	±0.05 m	FieldPoint
Pressure difference	D2101	3300–4420	Wetwell–drywell	±4 000 Pa	FieldPoint
Pressure difference	D2106	4347	Blowdown pipe–drywell	±3 000 Pa	FieldPoint
Flow rate	F2100	-	DN50 steam line	±5 l/s	FieldPoint
Flow rate	F2102	-	DN25 steam line	±0.7 l/s	FieldPoint
Pressure	P0003	-	Steam generator 1	±0.3 bar	FieldPoint
Pressure	P0004	-	Steam generator 2	±0.3 bar	FieldPoint
Pressure	P0005	-	Steam generator 3	±0.3 bar	FieldPoint
Pressure	P5	1150	Blowdown pipe outlet	±0.7 bar	LabView
Pressure	P6	-15	Wetwell bottom	±0.5 bar	LabView
Pressure	P2100	-	DN50 steam line	±0.2 bar	FieldPoint
Pressure	P2101	6300	Drywell	±0.03 bar	FieldPoint
Pressure	P2102	-	Inlet plenum	±0.03 bar	FieldPoint
Pressure	P2106	-	DN25 steam line	±0.06 bar	FieldPoint
Pressure	P2241	4200	Wetwell gas space	±0.05 bar	FieldPoint
Control valve position	S2002	-	DN50 Steam line	Not defined	FieldPoint
Strain	S1	200	Bottom segment	Not defined	LabView
Strain	S2	200	Bottom segment	Not defined	LabView
Strain	S3	335	Bottom segment	Not defined	LabView
Strain	S4	335	Bottom segment	Not defined	LabView
Temperature	T1279	-3260	Laboratory	±0.1 °C	FieldPoint
Temperature	T1280	-1260	Laboratory	±0.1 °C	FieldPoint
Temperature	T1281	740	Laboratory	±1.8 °C	FieldPoint
Temperature	T1282	2740	Laboratory	±0.1 °C	FieldPoint
Temperature	T1283	4740	Laboratory	±0.1 °C	FieldPoint
Temperature	T1284	6740	Laboratory	±0.1 °C	FieldPoint
Temperature	T1285	8740	Laboratory	±0.1 °C	FieldPoint
Temperature	T2100	-	DN80 steam line	±3 °C	FieldPoint
Temperature	T2102	-	DN50 steam line	±2 °C	FieldPoint
Temperature	T2103	-	DN25 steam line	±2 °C	FieldPoint
Temperature	T2106	-	Inlet plenum	±2 °C	FieldPoint
Temperature	T2108	5200	Drywell	±2 °C	FieldPoint
Temperature	T2109	6390	Drywell	±2 °C	FieldPoint
Temperature	T2121	4347	Blowdown pipe	±2 °C	FieldPoint
Temperature	T2204	4010	Wetwell gas space	±2 °C	FieldPoint
Temperature	T2206	-15	Wetwell bottom	±2 °C	FieldPoint
Temperature	T2207	3185	Wetwell gas space	±2 °C	FieldPoint
Temperature	T2208	2360	Wetwell gas space	±2 °C	FieldPoint
Temperature	T2510	1295	Wetwell	±2 °C	FieldPoint
Temperature	T2512	1565	Wetwell	±2 °C	FieldPoint
Temperature	T4000	1500	Wetwell	±2 °C	FieldPoint
Temperature	T4001	1400	Wetwell	±2 °C	LabView
Temperature	T4002	1326	Wetwell	±2 °C	LabView
Temperature	T4003	1290	Wetwell	±2 °C	LabView
Temperature	T4004	1254	Wetwell	±2 °C	LabView
Temperature	T4005	1218	Wetwell	±2 °C	LabView

Temperature	T4006	1182	Wetwell	±2 °C	LabView
Temperature	T4010	1500	Wetwell	±2 °C	FieldPoint
Temperature	T4011	1400	Wetwell	±2 °C	LabView
Temperature	T4012	1326	Wetwell	±2 °C	LabView
Temperature	T4013	1290	Wetwell	±2 °C	LabView
Temperature	T4014	1254	Wetwell	±2 °C	LabView
Temperature	T4015	1218	Wetwell	±2 °C	LabView
Temperature	T4016	1182	Wetwell	±2 °C	LabView
Temperature	T4020	1500	Wetwell	±2 °C	LabView
Temperature	T4021	1400	Wetwell	±2 °C	LabView
Temperature	T4022	1326	Wetwell	±2 °C	LabView
Temperature	T4023	1290	Wetwell	±2 °C	LabView
Temperature	T4024	1254	Wetwell	±2 °C	LabView
Temperature	T4025	1218	Wetwell	±2 °C	LabView
Temperature	T4026	1182	Wetwell	±2 °C	LabView
Temperature	T4030	1500	Wetwell	±2 °C	LabView
Temperature	T4031	1400	Wetwell	±2 °C	LabView
Temperature	T4032	1326	Wetwell	±2 °C	LabView
Temperature	T4033	1290	Wetwell	±2 °C	LabView
Temperature	T4034	1254	Wetwell	±2 °C	LabView
Temperature	T4035	1218	Wetwell	±2 °C	LabView
Temperature	T4036	1182	Wetwell	±2 °C	LabView
Temperature	T4040	1500	Wetwell	±2 °C	FieldPoint
Temperature	T4041	1400	Wetwell	±2 °C	LabView
Temperature	T4042	1326	Wetwell	±2 °C	LabView
Temperature	T4043	1290	Wetwell	±2 °C	LabView
Temperature	T4044	1254	Wetwell	±2 °C	LabView
Temperature	T4045	1218	Wetwell	±2 °C	LabView
Temperature	T4046	1182	Wetwell	±2 °C	LabView
Temperature	T4050	1500	Wetwell	±2 °C	FieldPoint
Temperature	T4051	1400	Wetwell	±2 °C	FieldPoint
Temperature	T4052	1326	Wetwell	±2 °C	FieldPoint
Temperature	T4053	1290	Wetwell	±2 °C	FieldPoint
Temperature	T4054	1254	Wetwell	±2 °C	FieldPoint
Temperature	T4055	1218	Wetwell	±2 °C	FieldPoint
Temperature	T4056	1182	Wetwell	±2 °C	FieldPoint
Temperature	T4070	1211	Sparger pipe	±2 °C	FieldPoint
Temperature	T4071	1272	Sparger pipe	±2 °C	FieldPoint
Temperature	T4072	1344	Sparger pipe	±2 °C	FieldPoint
Temperature	T4073	1444	Sparger pipe	±2 °C	FieldPoint
Temperature	T4074	1544	Sparger pipe	±2 °C	FieldPoint
Temperature	T4075	1744	Sparger pipe	±2 °C	FieldPoint
Temperature	T4076	2144	Sparger pipe	±2 °C	FieldPoint
Temperature	T4077	2847	Sparger pipe	±2 °C	FieldPoint
Temperature	T4078	3479	Sparger pipe	±2 °C	FieldPoint
Temperature	T4100	222	Wetwell	±2 °C	FieldPoint
Temperature	T4101	522	Wetwell	±2 °C	FieldPoint
Temperature	T4102	672	Wetwell	±2 °C	FieldPoint
Temperature	T4103	822	Wetwell	±2 °C	FieldPoint
Temperature	T4104	972	Wetwell	±2 °C	FieldPoint
Temperature	T4105	1122	Wetwell	±2 °C	FieldPoint
Temperature	T4106	1272	Wetwell	±2 °C	FieldPoint

Temperature	T4107	1422	Wetwell	±2 °C	FieldPoint
Temperature	T4108	1722	Wetwell	±2 °C	FieldPoint
Temperature	T4109	2022	Wetwell	±2 °C	FieldPoint
Temperature	T4110	2322	Wetwell	±2 °C	FieldPoint
Temperature	T4111	2922	Wetwell	±2 °C	FieldPoint
Temperature	T4112	372	Wetwell	±2 °C	FieldPoint
Temperature	T4113	158	Wetwell	±2 °C	FieldPoint
Temperature	T4200	372	Wetwell	±2 °C	FieldPoint
Temperature	T4201	572	Wetwell	±2 °C	FieldPoint
Temperature	T4202	772	Wetwell	±2 °C	FieldPoint
Temperature	T4203	872	Wetwell	±2 °C	FieldPoint
Temperature	T4204	972	Wetwell	±2 °C	FieldPoint
Temperature	T4205	1072	Wetwell	±2 °C	FieldPoint
Temperature	T4206	1172	Wetwell	±2 °C	FieldPoint
Temperature	T4207	1272	Wetwell	±2 °C	FieldPoint
Temperature	T4208	1372	Wetwell	±2 °C	FieldPoint
Temperature	T4210	1572	Wetwell	±2 °C	FieldPoint
Temperature	T4212	1772	Wetwell	±2 °C	FieldPoint
Temperature	T4213	1972	Wetwell	±2 °C	FieldPoint
Temperature	T4214	2172	Wetwell	±2 °C	FieldPoint
Temperature	T4215	2372	Wetwell	±2 °C	FieldPoint
Temperature	T4216	2572	Wetwell	±2 °C	FieldPoint
Temperature	T4217	2972	Wetwell	±2 °C	FieldPoint
Temperature	T4218	472	Wetwell	±2 °C	FieldPoint
Temperature	T4219	672	Wetwell	±2 °C	FieldPoint
Temperature	T4300	372	Wetwell	±2 °C	FieldPoint
Temperature	T4301	572	Wetwell	±2 °C	FieldPoint
Temperature	T4302	772	Wetwell	±2 °C	FieldPoint
Temperature	T4303	872	Wetwell	±2 °C	FieldPoint
Temperature	T4304	972	Wetwell	±2 °C	FieldPoint
Temperature	T4305	1072	Wetwell	±2 °C	FieldPoint
Temperature	T4306	1172	Wetwell	±2 °C	FieldPoint
Temperature	T4307	1272	Wetwell	±2 °C	FieldPoint
Temperature	T4308	1372	Wetwell	±2 °C	FieldPoint
Temperature	T4310	1572	Wetwell	±2 °C	FieldPoint
Temperature	T4312	1772	Wetwell	±2 °C	FieldPoint
Temperature	T4313	1972	Wetwell	±2 °C	FieldPoint
Temperature	T4314	2172	Wetwell	±2 °C	FieldPoint
Temperature	T4315	2372	Wetwell	±2 °C	FieldPoint
Temperature	T4316	2572	Wetwell	±2 °C	FieldPoint
Temperature	T4317	2972	Wetwell	±2 °C	FieldPoint
Temperature	T4318	472	Wetwell	±2 °C	FieldPoint
Temperature	T4319	672	Wetwell	±2 °C	FieldPoint
Temperature	T4400	222	Wetwell	±2 °C	FieldPoint
Temperature	T4401	522	Wetwell	±2 °C	FieldPoint
Temperature	T4402	672	Wetwell	±2 °C	FieldPoint
Temperature	T4403	822	Wetwell	±2 °C	FieldPoint
Temperature	T4404	972	Wetwell	±2 °C	FieldPoint
Temperature	T4405	1122	Wetwell	±2 °C	FieldPoint
Temperature	T4406	1272	Wetwell	±2 °C	FieldPoint
Temperature	T4407	1422	Wetwell	±2 °C	FieldPoint
Temperature	T4408	1722	Wetwell	±2 °C	FieldPoint

Temperature	T4409	2022	Wetwell	±2 °C	FieldPoint
Temperature	T4410	2322	Wetwell	±2 °C	FieldPoint
Temperature	T4411	2922	Wetwell	±2 °C	FieldPoint
Temperature	T4412	372	Wetwell	±2 °C	FieldPoint
Temperature	T4413	158	Wetwell	±2 °C	FieldPoint
Cut-off valve position	V1	-	DN50 Steam line	Not defined	LabView
Cut-off valve position	X2100	-	DN50 Steam line	Not defined	FieldPoint
Steam partial pressure	X2102	5200	Drywell	Not defined	FieldPoint
Cut-off valve position	X2106	-	DN50 Steam line	Not defined	FieldPoint

Measurements of the PPOOLEX facility in the SPA experiment series.

APPENDIX 3: PPOOLEX test facility photographs

Lower part of the sparger pipe.

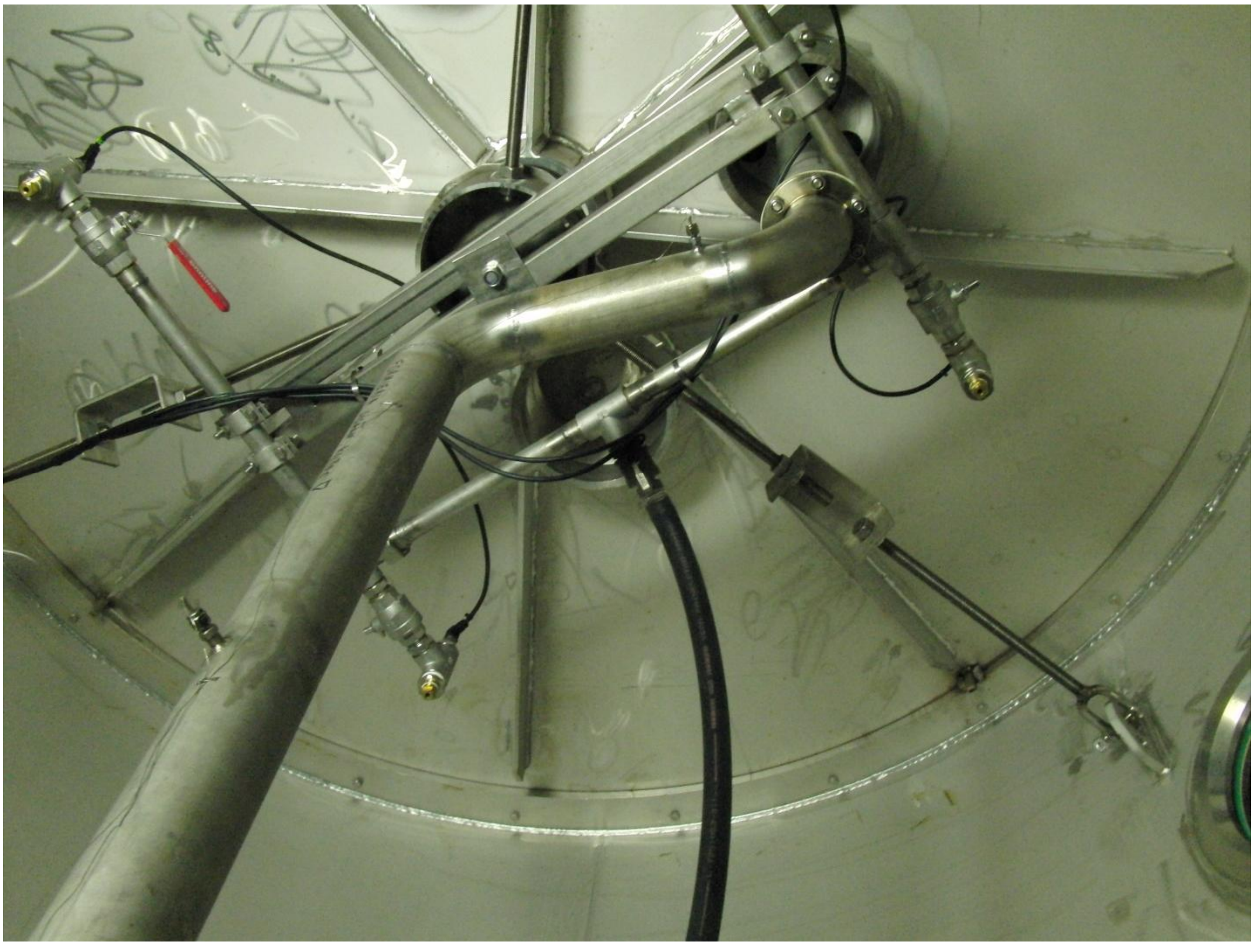

Bend in the sparger pipe to shift the position to the centre of the pool.

Appendix B

General description of SEF-POOL test rig

Technical Report
Lappeenranta University of Technology
Nuclear Engineering

INSTAB 2/2017

General description of SEF-POOL test rig

Kimmo Tielinen, Antti Räsänen, Eetu Kotro, Ilkka Saure

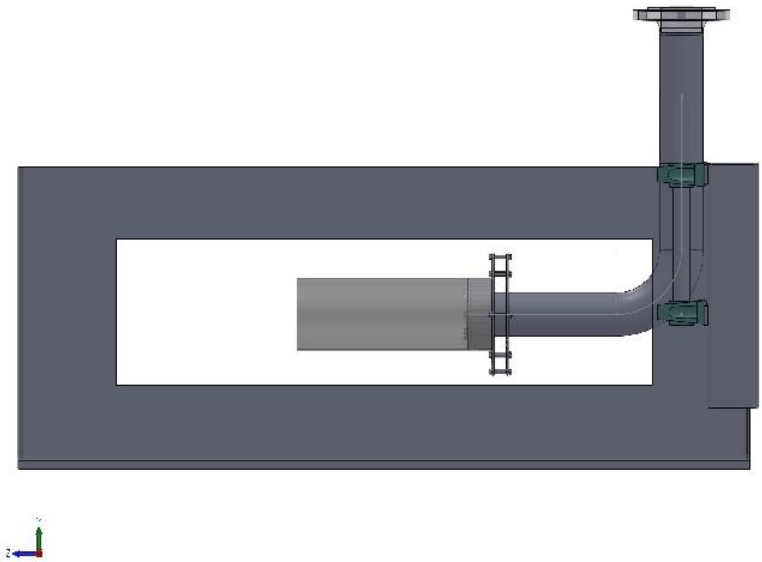

Lappeenranta University of Technology
School of Energy Systems
Nuclear Engineering
P.O. Box 20, FIN-53851 LAPPEENRANTA, FINLAND
Phone +358 294 462 111

Lappeenranta, 9.1.2018

Research organization and address	Customer
Lappeenranta University of Technology School of Energy Systems Nuclear Engineering P.O. Box 20 FIN-53851 LAPPEENRANTA, FINLAND	VYR / SAFIR2018 NKS SSM
Project manager	**Contact person**
Markku Puustinen	Jari Hämäläinen (SAFIR2018) Christian Linde (NKS), Maria Agrell (SSM)
Diary code	**Order reference**
125/322/2015	Drno SAFIR 11/2017
Project title and reference code	**Report identification & Pages** / **Date**
SAFIR2018-INSTAB NKS-COPSAR	INSTAB 2/2017 14 p. + app. 6 p. / 9.1.2018

Report title and author(s)

GENERAL DESCRIPTION OF SEF-POOL TEST RIG

Kimmo Tielinen, Antti Räsänen, Eetu Kotro, Ilkka Saure

Summary

The SEF-POOL test facility has been designed together by KTH and LUT. It has been constructed by the Nuclear Engineering research group at LUT. The work has been part of the SAFIR2018/INSTAB and NKS/COPSAR projects.

The EHS and EMS models have been proposed by KTH for simulation of steam injection into a pool filled with sub-cooled water. The models have been implemented in the GOTHIC code and validated against the PPOOLEX experiments with blowdown pipes.

Now the concepts of the EHS and EMS models are being extended to SRV spargers and validation has been carried out against PANDA and PPOOLEX experiments done with a model of a SRV sparger. This validation effort has shown that the injection angle, total momentum, and momentum profile have a large effect on the pool behaviour. Uncertainty on these parameters exists and therefore the SEF-POOL separate effect test facility has been constructed at LUT in order to measure/define the effective momentum and reduce the uncertainty of the simulations.

This report provides a facility description of the SEF-POOL test rig. The report presents the basic requirements and design principles of the facility. The geometry and the main operational parameters as well as the installed instrumentation are introduced. The appendixes include figures to supplement the SEF-POOL geometry and instrumentation presented in the main text. The flexibility of the facility provides appropriate possibilities to extend the facility set-up according to the future research needs.

Distribution

Members of the SAFIR2018 Reference Group 4

C. Linde (SSM), M. Agrell (SSM), P. Kudinov (KTH), I. G. Marcos (KTH), W. Villanueva (KTH), J. Hämäläinen (VTT), V. Suolanen (VTT), T. Pättikangas (VTT), I. Karppinen (VTT), S. Hillberg (VTT)

Principal author or Project manager	Reviewed by
Kimmo Tielinen Project Researcher	Markku Puustinen Senior Research Scientist
Approved by	**Availability statement**
Heikki Purhonen Research Director	Public

LUT
Lappeenranta
University of Technology

Acknowledgement

NKS conveys its gratitude to all organizations and persons who by means of financial support or contributions in kind have made the work presented in this report possible.

Disclaimer

PREFACE

The SEF-POOL test facility has been designed together by Kungliga Tekniska Högskolan (KTH) and Lappeenranta University of Technology (LUT). It has been constructed by the Nuclear Engineering research group at LUT. The work has been performed under the Finnish Research Programme on Nuclear Power Plant Safety 2015–2018 (SAFIR2018) in the INSTAB project as well as under the NKS-COPSAR project. Financial support for the work has been provided by the National Nuclear Waste Management Fund, NKS, Strålsäkerhetsmyndigheten (SSM) and LUT.

LUT
Lappeenranta
University of Technology

CONTENTS

NOMENCLATURE **6**

1 INTRODUCTION **7**

2 REQUIREMENTS FOR THE TEST FACILITY **7**

3 FACILITY DESCRIPTION **8**

3.1 GENERAL 8

3.2 CONDENSATION POOL 9

3.3 SPARGER SYSTEM 11

3.4 STEAM SUPPLY 11

3.5 FORCE MEASUREMENT 12

3.6 OTHER MEASUREMENTS 13

3.7 DATA ACQUISITION 14

3.8 CAMERA SYSTEM 14

REFERENCES **14**

APPENDIX A: TEST RIG DRAWINGS

APPENDIX B: BASIC INSTRUMENTATION

NOMENCLATURE

Symbols

DP	differential pressure
M_{eff}	effective momentum
M_s	steam momentum
P	pressure
T	temperature

Abbreviations

BWR	boiling water reactor
EHS	effective heat source
EMS	effective momentum source
KTH	Kungliga Tekniska Högskolan
LUT	Lappeenranta University of Technology
PC	polycarbonate
SRV	safety relief valve
SSM	Strålsäkerhetsmyndigheten
TC	thermocouple

1 INTRODUCTION

Effective Heat Source (EHS) and Effective Momentum Source (EMS) models have been proposed by KTH for simulation of steam injection into a pool filled with sub-cooled water [1]. The models have been implemented in the GOTHIC code and validated against PPOOLEX experiments with blowdown pipes done at LUT under the SAFIR2018/INSTAB project [2, 3].

Now the concepts of the EHS/EMS models are being extended to SRV spargers and validation has been carried out against PANDA and PPOOLEX experiments done with a model of a safety relief valve (SRV) sparger [4]. This validation effort has shown that the injection angle, total momentum, and momentum profile have a large effect on the pool behaviour. Due to the uncertainty on these parameters, a separate effect test facility named SEF-POOL, has been designed at LUT in collaboration with KTH to measure/define the effective momentum and reduce the uncertainty of the simulations.

Steam momentum $\boldsymbol{M_S}$ is defined as momentum of the steam right at the injection hole (before condensing). Effective momentum $\boldsymbol{M_{eff}}$ is the amount of momentum transferred from the steam to the liquid. These two momentums are not equal in two phase flow (for example: chugging). Separate-effect tests in the SEF-POOL facility would allow to measure and visualize directly this phenomena.

Focus in the forthcoming test series with the separate effect facility is to determine the effect of the injection hole diameter, number of holes, pool temperature, steam mass flux, etc., on the effective momentum. Furthermore, the detachment and collapse frequencies of the bubbles could be obtained with the help of high frequency measurements and high speed video recordings.

This report provides a facility description of the SEF-POOL test rig. The report presents the basic requirements and design principles of the facility. The geometry and the main operational parameters as well as the installed instrumentation are introduced. Appendix A presents detailed drawings on the facility geometry and Appendix B the locations of the measurements. The flexibility of the facility provides appropriate possibilities to extend the facility set-up according to the future research needs.

2 REQUIREMENTS FOR THE TEST FACILITY

The reference system for the SEF-POOL facility is a SRV sparger pipe of a BWR plant. Hence the SEF-POOL facility should be designed in such a way that discharge of steam through injection holes at the sparger lower end into sub-cooled pool water can be simulated representatively.

The goal is to define the effective momentum for a given steam condensation regime, particularly in the oscillatory bubble and stable jet regimes. For this purpose the design of the test facility should be such that the effective momentum could be directly measured with a force sensor or it could calculated on the basis of measured steam momentum. Alternatively the effective momentum could be evaluated on the basis of velocity field of the water volume developed as a result of steam injection and measured for example with hot-wire measurements. Because the focus is on measuring separate effects of steam injection through the sparger holes and not on stratification/mixing phenomenon, the water pool itself, where the sparger is submerged, can be relatively small in volume.

For helping to recognize different flow regimes and for obtaining the bubble diameter as a function of time the test facility should allow good quality high speed video recordings of the direct contact condensation of steam. Due to the high frequency of the bubble oscillation events, the camera should be able to reach frequencies of at least 600 Hz. The steam-liquid interface should appear as sharp as possible in the recordings. In addition, a high frequency pressure measurement is needed to obtain the detachment and collapse frequency of the bubbles.

Steam is needed in the tests conducted with the SEF-POOL facility. For practical reasons the steam generators of the nearby PACTEL test facility will act as a steam source for the SEF-POOL tests [5].

3 FACILITY DESCRIPTION

3.1 GENERAL

The main parts of the separate effect test rig are the sparger piping and condensation pool. The sparger piping is connected with a pipeline to the PACTEL test facility which supplies steam needed in the tests. The sparger pipe is pivoted on a vertical axis with low friction bearings in order to allow the direct force measurement. The lower end of the sparger pipe mounts a flow plate with injection holes and a polycarbonate (PC) pipe. Steam is discharged through the injection holes and it condenses inside the PC pipe. The purpose of the PC pipe is to create a parallel flow pattern so that the amount of momentum transferred from the steam to the liquid can be estimated at the outlet of the PC pipe for example with hot wire probes. Tests can be conducted also without the PC pipe. Figure 1 presents the SEF-POOL test facility in general.

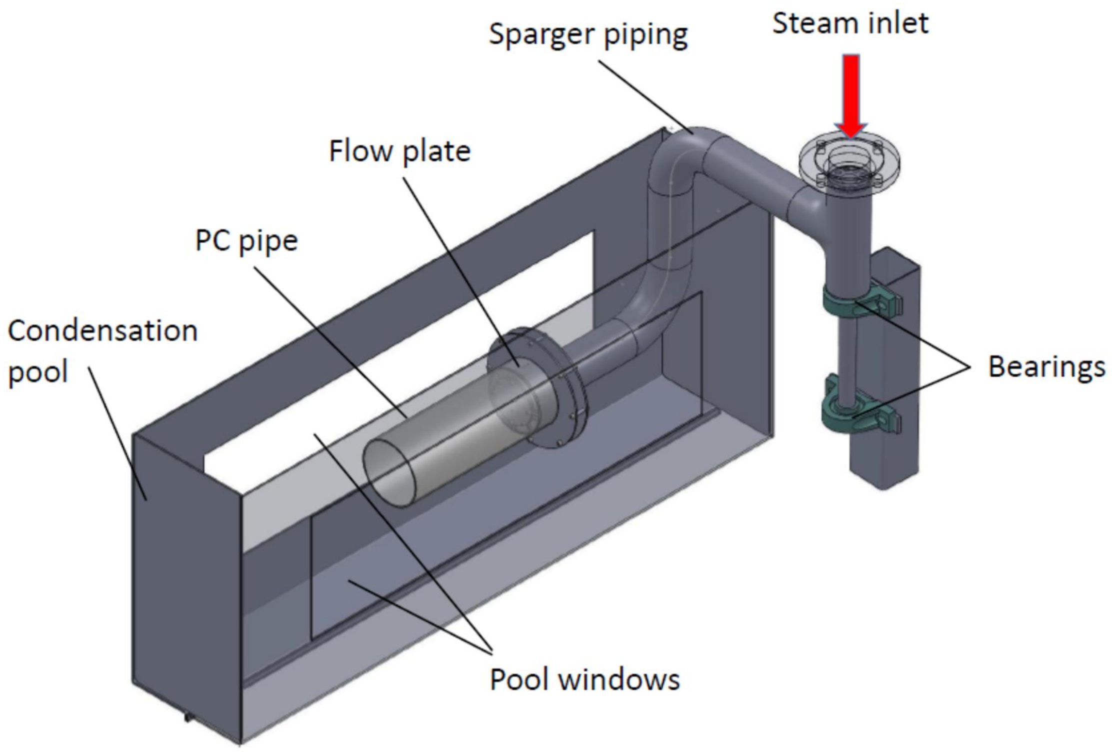

Figure 1. General view of the SEF-POOL test facility.

Temperatures are measured from the sparger pipe and condensation pool. Pressure transducers are used to measure pressure of steam in the sparger piping. The water level in the pool is measured with a differential pressure transducer.

3.2 CONDENSATION POOL

The condensation pool is made of stainless steel. It is 1500 mm long, 300 mm wide and 600 mm tall. The pool is open on top and it is uninsulated. Windows on both sides are 1000 mm wide and 300 mm tall. The pool is mounted on a support made of 50x50 box section. Figures 2 and 3 present the pool and its support structure, respectively.

Filling with water is done with the help of a hose connected to the normal water network of the laboratory although the water is fed through a deaerator to remove soluble gases which might be released from the water when the pool bulk temperature increases during the experiments. Initial pool water temperature can thus range from about 10 °C to about 50 °C depending on the needs of the test in question. Draining of the pool is done via a drainpipe at the bottom. A cover (lid) can be installed to the top to prevent any spill over or splashing of water to the laboratory site during the tests. As the pool is open on top atmospheric pressure will prevail in the pool in all the tests. Figure 1 in Appendix A presents the condensation pool in more detail.

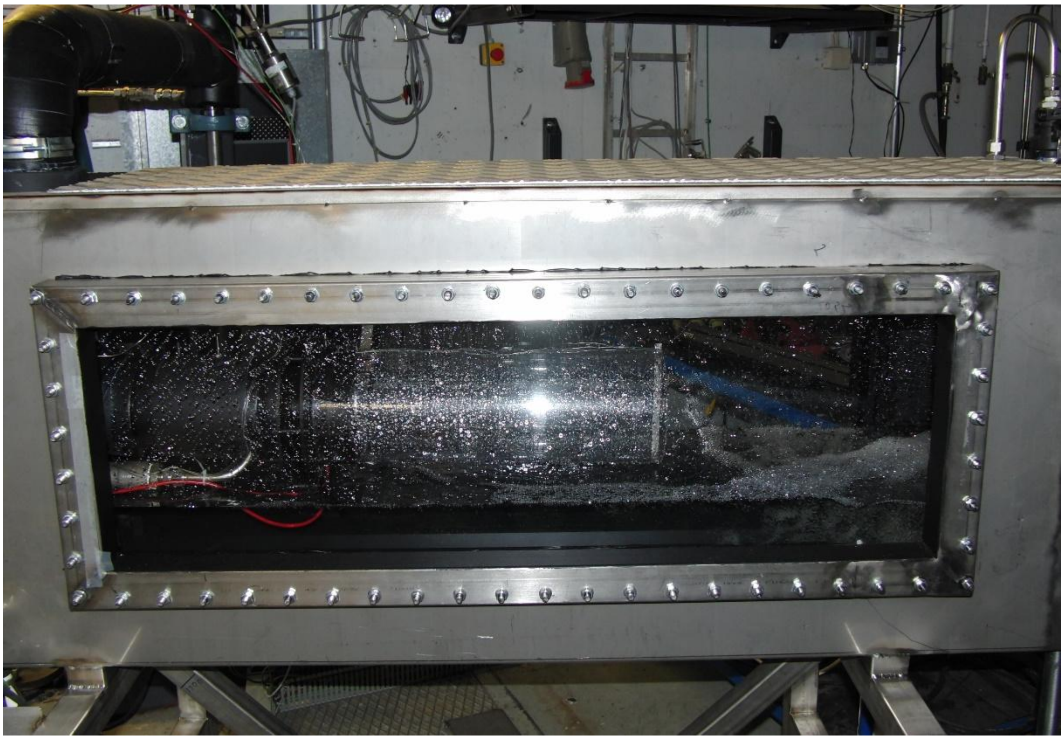

Figure 2. Condensation pool of the SEF-POOL test facility with PC-pipe inside.

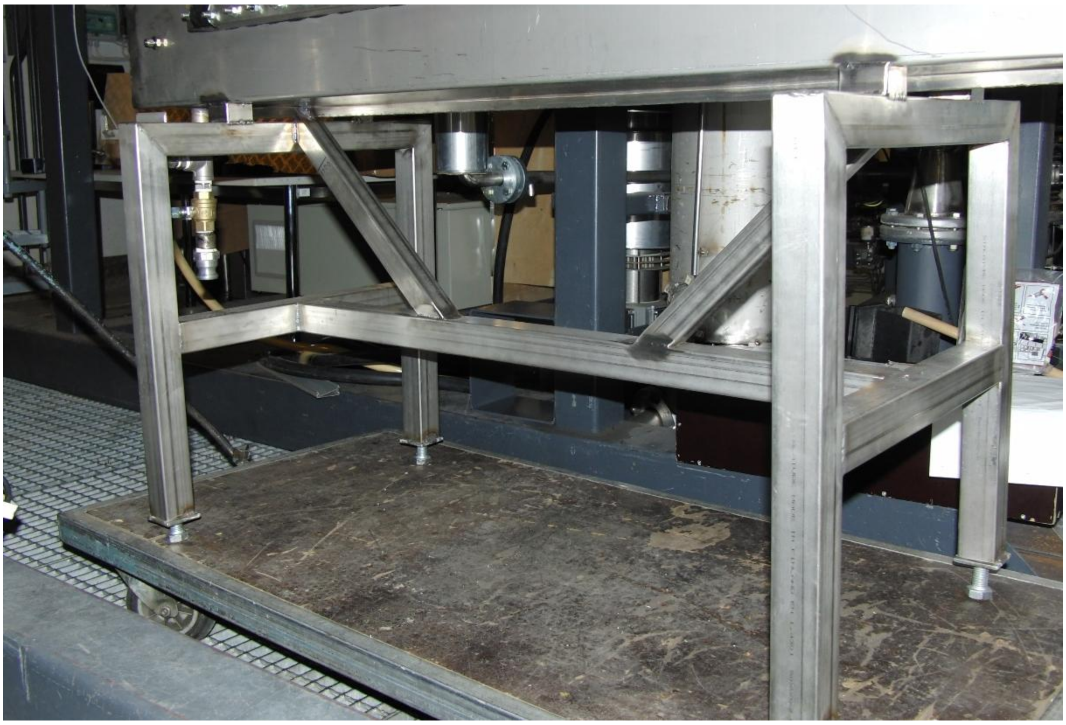

Figure 3. Support structure for the condensation pool of the SEF-POOL test facility.

3.3 SPARGER SYSTEM

The sparger piping is made of sections of DN80 stainless steel pipes and it is insulated with 13 mm thick AP Armaflex® XG flexible elastomeric thermal insulation. Dimensions of the piping are shown in Figure 2 in Appendix A. The piping is connected to the sparger system shown in Figure 3 in Appendix A. The sparger system consists of different kind of stainless steel plates and of a PC pipe. The plates are used for connecting the PC pipe to the sparger piping and for guiding the compensation water flow from the pool into the PC pipe. A perforated flow plate for steam injection is mounted to the end of the sparger pipe. Configuration of the flow plate can be easily changed. Dimensions of different kind of flow plates to be used in the tests are presented in Table 1 in Appendix A. The PC pipe attached to the end of the sparger piping has an inner diameter of 144 mm. Its length is 450 mm, 400 mm of which is downstream from the flow plate. Photo in Figure 4 shows the end section of the sparger piping and the sparger system inside the pool.

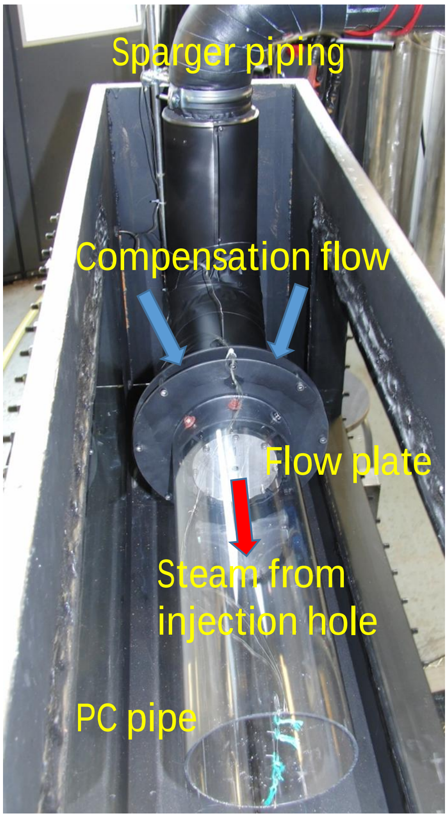

Figure 4. The end of the sparger piping and the sparger system of the SEF-POOL facility.

3.4 STEAM SUPPLY

Steam needed in the tests is generated with the nearby PACTEL test facility, which has a core section of 1 MW heating power and three horizontal steam generators. Pressure and temperature of generated steam can range from 1 bar to 45 bar and from 100 °C to 257 °C, respectively. Steam is led to the test rig through a thermally insulated steam line, made of sections of standard DN50 (Ø60.3x2.0) pipes, a DN50 stainless steel corrugated hose and a 51 mm inner diameter steam rubber hose. Section of the rubber hose is used to prevent torsional forces being generated by the thermal expansion of the steam line. The steam line is connected to the sparger piping with a flange connection. A remote-controlled valve is mounted on the horizontal section of the steam line above the test rig. The opening of this valve activates steam flow from the steam generators into the test rig. Steam flow can be controlled with a high precision Varibell® DN 40 steam valve. The details and dimensions of the steam valve are shown in Figure 4 in Appendix A.

3.5 FORCE MEASUREMENT

The direct force measurement is arranged with a load cell. The load cell is located outside the condensation pool and it is attached to a support pole made of 50x50 box section bolted to the floor of the laboratory. The load cell is at that end of the condensation pool, where the sparger piping is submerged. Force is transmitted from the sparger piping to the sensor via a rod (Figure 5). When steam is injected through the sparger piping and perforated flow plate, momentum is created and as a result the sparger piping tends to rotate around the pivot bearing. This causes compression to the load cell and the generated force can be thus measured. Because the force measurement compression distance is almost non-existent the angle of the sparger piping compared to the condensation pool does not change during the tests.

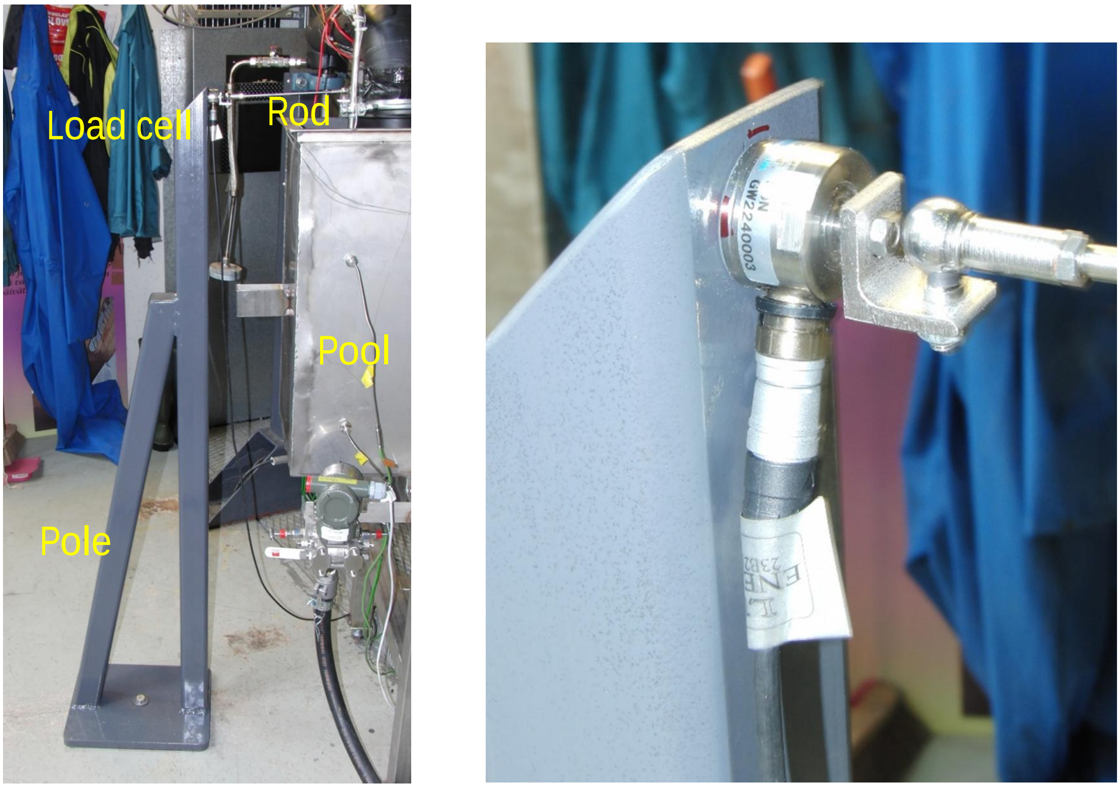

Figure 5. Arrangement for the force measurement (left) and the load cell (right).

3.6 OTHER MEASUREMENTS

Two pressure transducers for steam pressure measurement are mounted in the sparger piping. One is near the steam inlet point and the other one is 140 mm upstream from the perforated flow plate. The measurement range of the both transducer is 0.1-1.0 MPa.

A kHz range pressure sensor is used for capturing the detachment and collapse frequencies of the steam bubbles. It is fixed either to the inner wall of the PC pipe about 100 mm downstream of the perforated flow plate or to a vertical support structure laying at the pool bottom in those tests where the PC pipe is not used. The range of the sensor can be up to 0.2 MPa, 1 MPa or 2 MPa depending on the test in question.

Temperatures are measured with calibrated k-type thermocouples (TC). Temperature of incoming steam is measured with one TC near the inlet point at the same location as the pressure measurement. Steam temperature is also measured in the sparger piping at about 190 mm before the perforated flow plate. Temperatures of water exiting the PC pipe are measured with three vertically positioned TCs (Figure 6). In those tests, where the PC pipe is not used, these three TCs can be attached to the same support structure as the high frequency pressure sensor and positioned in front of the flow plate with a desired distance from the plate.

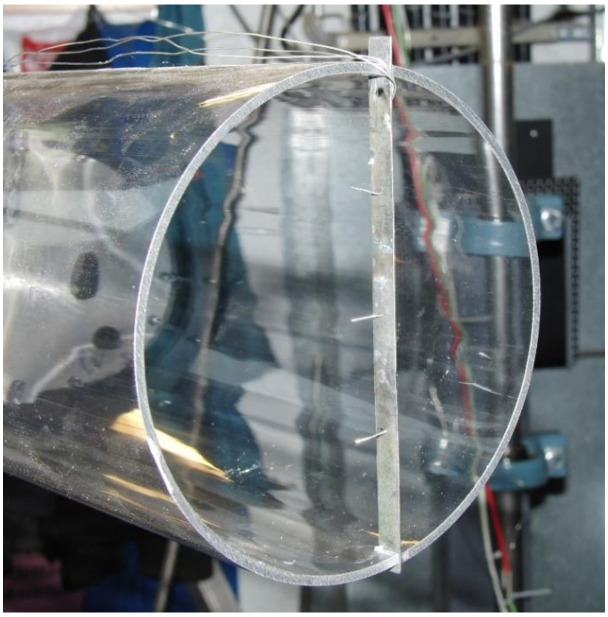

Figure 6. Temperature measurements at the outlet of the PC pipe.

Water level in the condensation pool is measured with a Yokogawa® differential pressure transducer. The transducer is mounted to the base of the pool. Water level is calculated from the differential pressure reading with the help of liquid density. Temperature measurements in the pool are used to define the liquid density.

Steam flow rate is measured with a vortex flow meter in the steam line.

The locations of the thermocouples, pressure transducers and water level measurement are shown in Figures 1-4 in Appendix B. Information on the type/frequency/range of different sensors/instrumentation can be found in Table 1 at the end of Appendix B.

3.7 DATA ACQUISITION

National Instruments PXIe PC-driven measurement system is used for data acquisition. The system enables high-speed multi-channel measurements. The maximum recording capacity depends on the number of measurements and is in the region of mega samples per second. Measurement software is LabView 2015.

3.8 CAMERA SYSTEM

Windows on the both side walls of the condensation pool allow the capture of the direct contact condensation phenomenon of steam with a high speed video system. Different flow regimes could be recognized and bubble diameters obtained with the help of the system.

The high speed camera system consists of a monochromatic Phantom Miro 310 camera. The maximum resolution is 1280x800 px, but in practise the picture area is cropped in order to increase the maximum amount of the images the 12 GB internal memory can hold, thus increasing the total time of the recordings

Optimum conditions for the high speed cameras from the lighting point of view can be arranged by installing light sources both inside and outside of the pool. The window on the opposite side of the camera can be covered with white coloured paper or plastic plate in order to improve the visibility of the steam jets and bubbles.

REFERENCES

[1] Li, H., Villanueva, W., Kudinov, P., Approach and development of effective models for simulation of thermal stratification and mixing induced by steam injection into a large pool of water. Sci. Technol. Nucl. Ins. 2014, http://dx.doi.org/10.1155/2014/108782, (Article ID 108782).

[2] Li, H., Villanueva, W., Puustinen, M., Laine, J., Kudinov, P., Validation of effective models for simulation of thermal stratification and mixing induced by steam injection into a large pool of water. Sci. Technol. Nucl. Ins. 2014, http://dx.doi.org/10.1155/2014/752597, (Article ID752597).

[3] Li, H., Villanueva, W., Puustinen, M., Laine, J., Kudinov, P., Thermal stratification and mixing in a suppression pool induced by direct steam injection. Annals of Nuclear Energy. 2018, 111, https://doi.org/10.1016/j.anucene.2017.09.014.

[4] Gallego-Marcos, I., Villanueva, W., Kapulla, R., Paranjape, S., Paladino, D., Kudinov, P., Modeling of thermal stratification and mixing induced by steam injection through spargers into a large water pool. CDF4NRS-6 Workshop, September 13 - 15, 2016, Massachusetts Institute of Technology.

[5] Tuunanen, J., Kouhia, J., Purhonen, H., Riikonen, V., Puustinen, M., Semken, R. S., Partanen, H., Saure, I., Pylkkö, H., General Description of the PACTEL Test Facility. Espoo: VTT. 1998. VTT Research Notes 1929. ISBN 951-38-5338-1.

Appendix A: Test rig drawings

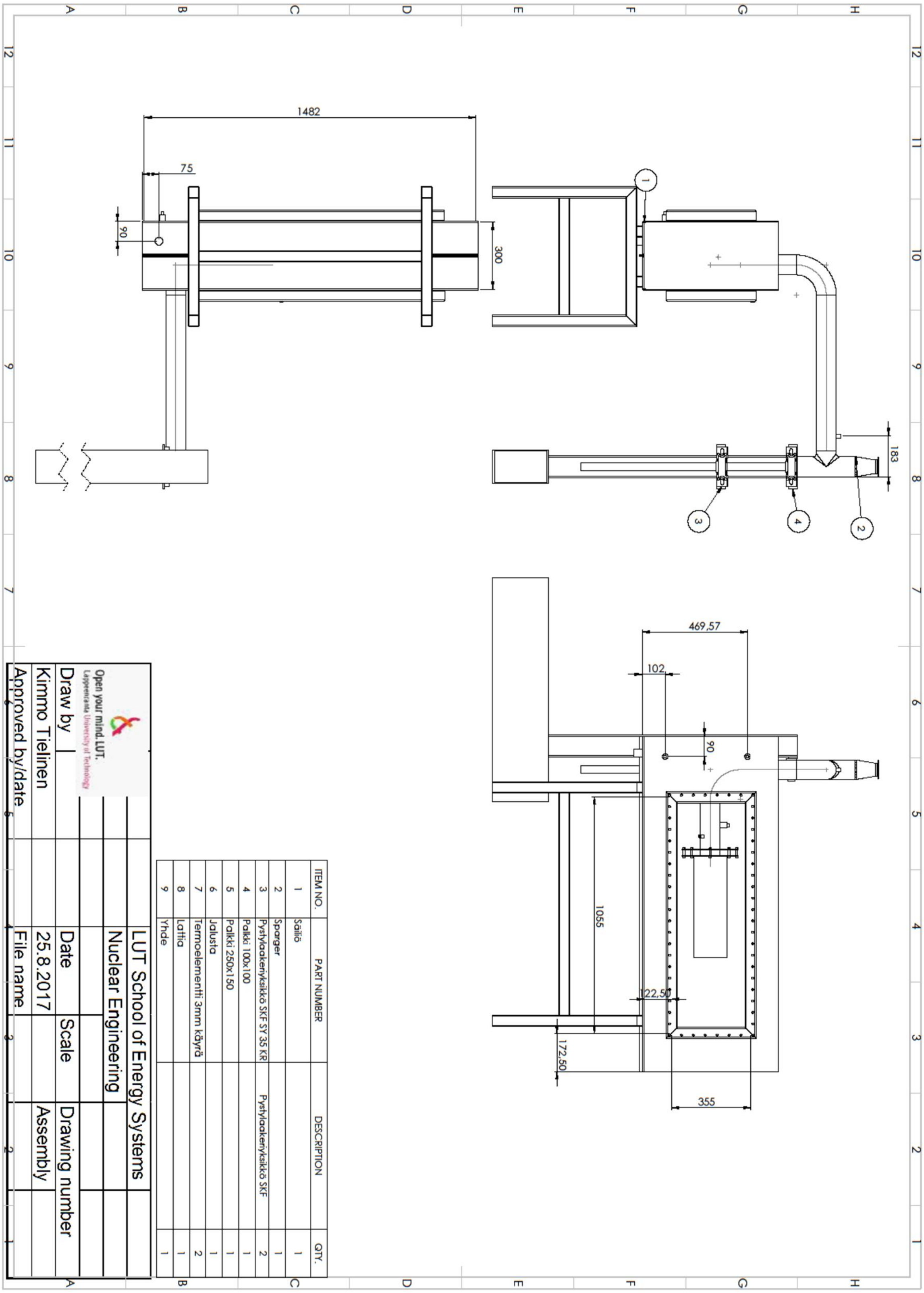

Figure 1. Condensation pool.

Appendix A: Test rig drawings

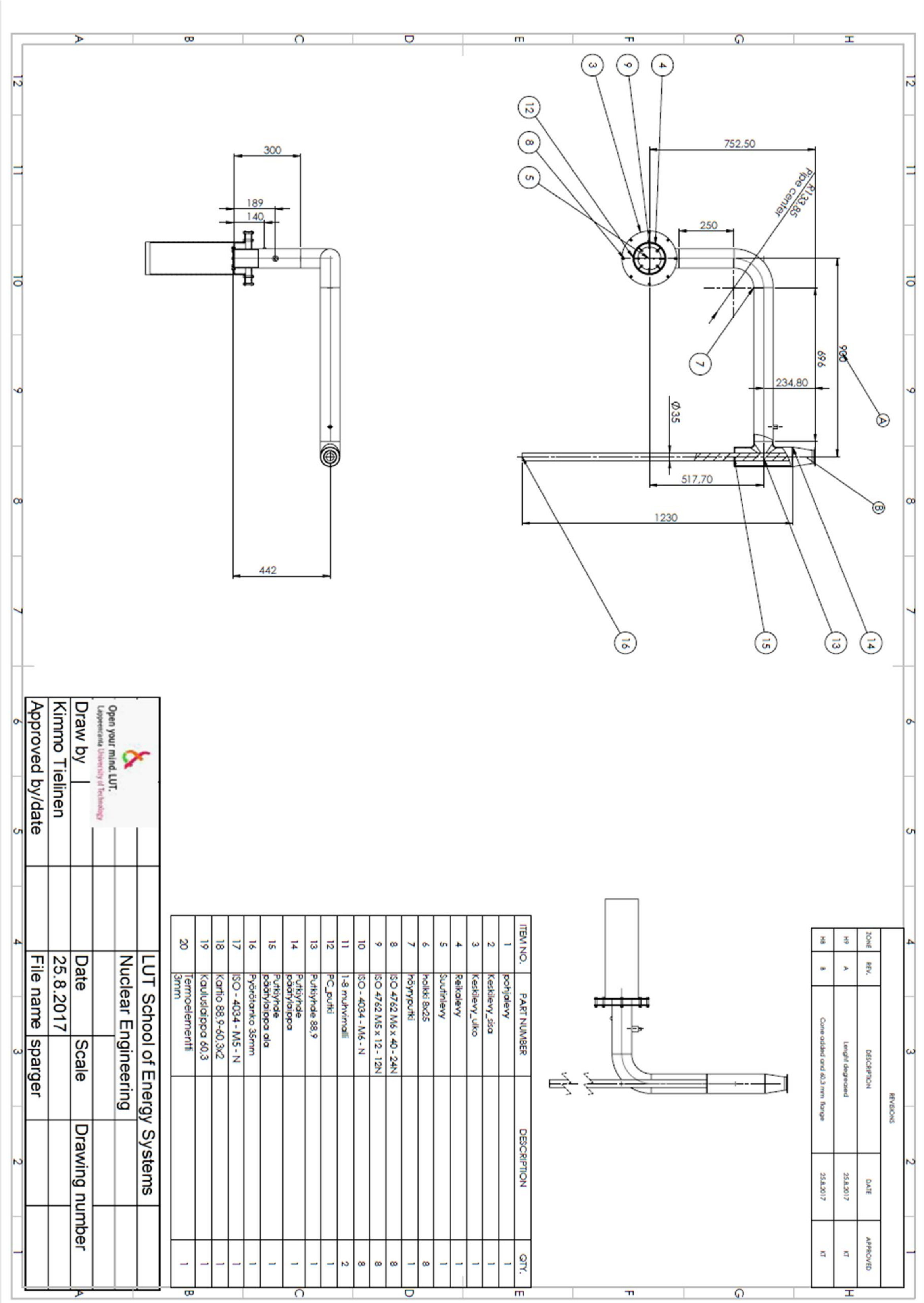

Figure 2. Sparger piping.

Appendix A: Test rig drawings

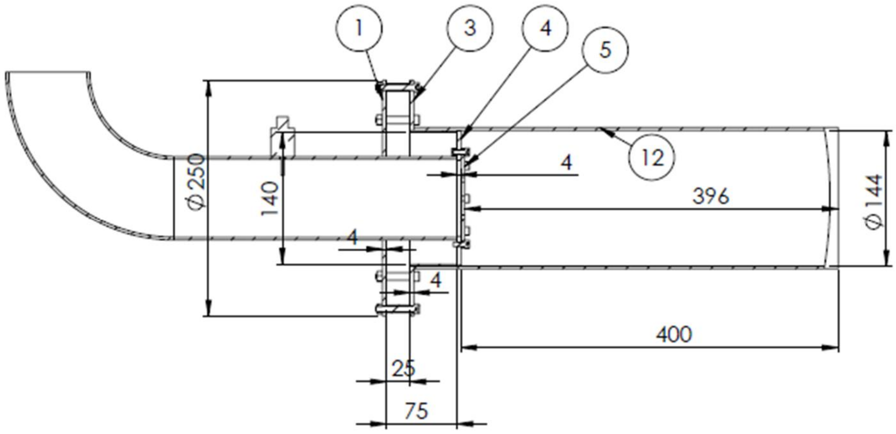

Figure 3. Sparger system.

Table 1. Dimension of the perforated flow plates

	Holes [mm]		Pitch [mm]	Chamfer		Effects
	N	Φ_i [mm]		t [mm]	Φ_o [mm]	
Plate 1	1	8	-	-	-	Base case
Plate 2	1	8	-	2	12	Chamfer
Plate 3	2	8	16	-	-	Number holes + Pitch/diameter
Plate 4	2	8	26	-	-	
Plate 5	2	8	36	-	-	
Plate 6	3	8	26	-	-	
Plate 7	1	16	-	-	-	Hole diameter
Plate 8	1	16	-	2	24	
Plate 9	2	16	32	-	-	
Plate 10	2	16	52	-	-	
Plate 11	3	16	32	-	-	

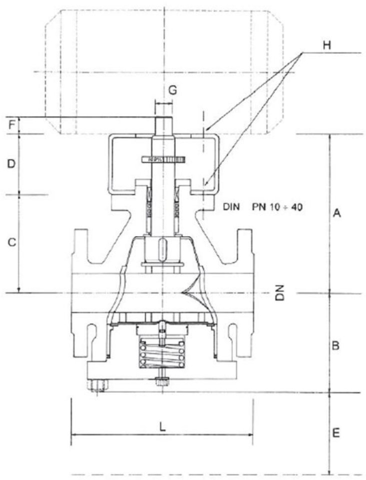

DIN		ANSI		A	B	C	D*)	E	F	G	H	PAINO
DN	L	DN	L									KG
15VE	130			123	73	63	60	80	16	14(10)	F07	5,2
15	130			147	173	86	60	80	16	17	F07	8
25	160	1"	196,9	151	86	91	60	80	16	17	F07	11,5
40	200	1 ½"	235	170	110	110	60	100	16	17	F07	25
50	230	2"	266,7	208	128	128	80	120	22	22	F10	41
80	310	3"	317,5	225	180	150	80	160	25	22(27)	F10	85
100	350	4"	368,3	242	180	162	80	190	37	36	F14	112
150	480			242	180	162	80	190	37	36	F14	130

Figure 4. Dimensions of Varibell® steam valve.

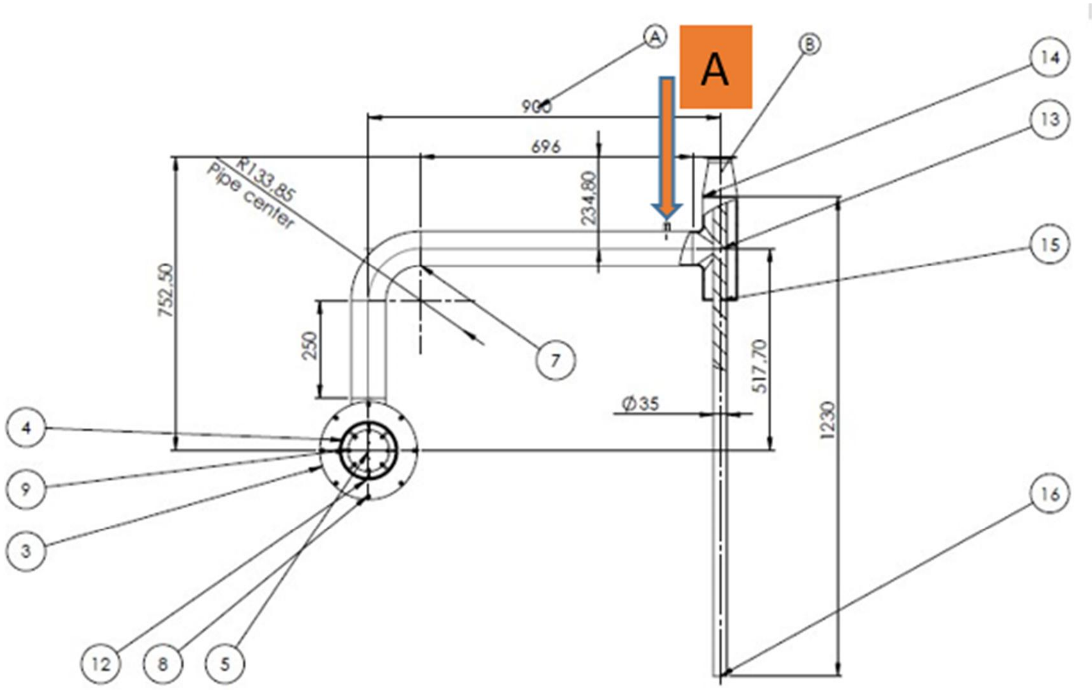

Figure 1. Location (A) for pressure and temperature measurement of incoming steam.

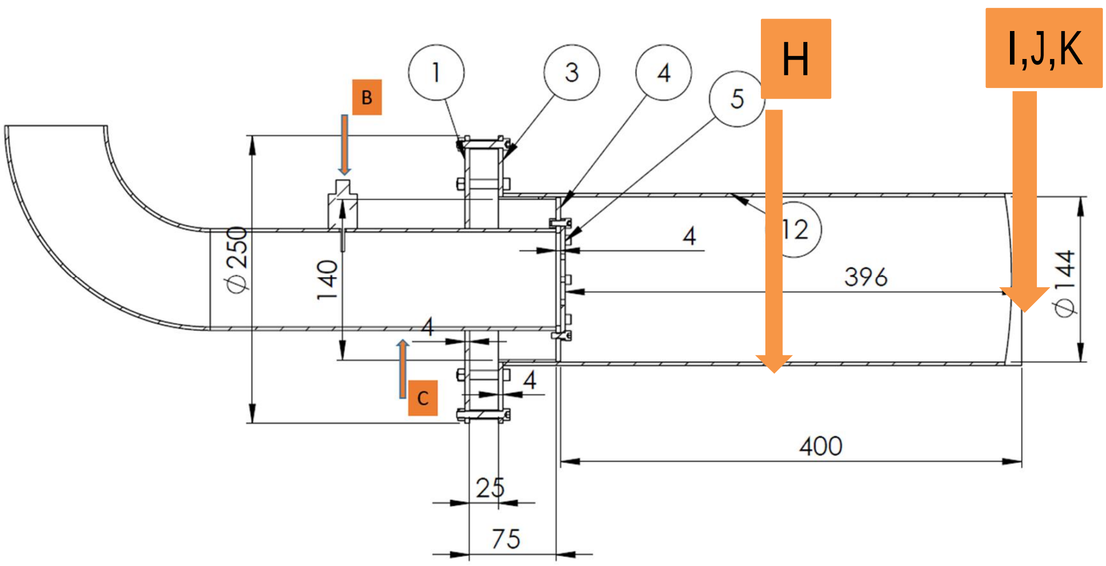

Figure 2. Temperature (B) and pressure (C) measurement of steam before the perforated flow plate, high frequency pressure measurement in the PC pipe (H) and temperature measurements at the outlet of the PC pipe (I, J, K).

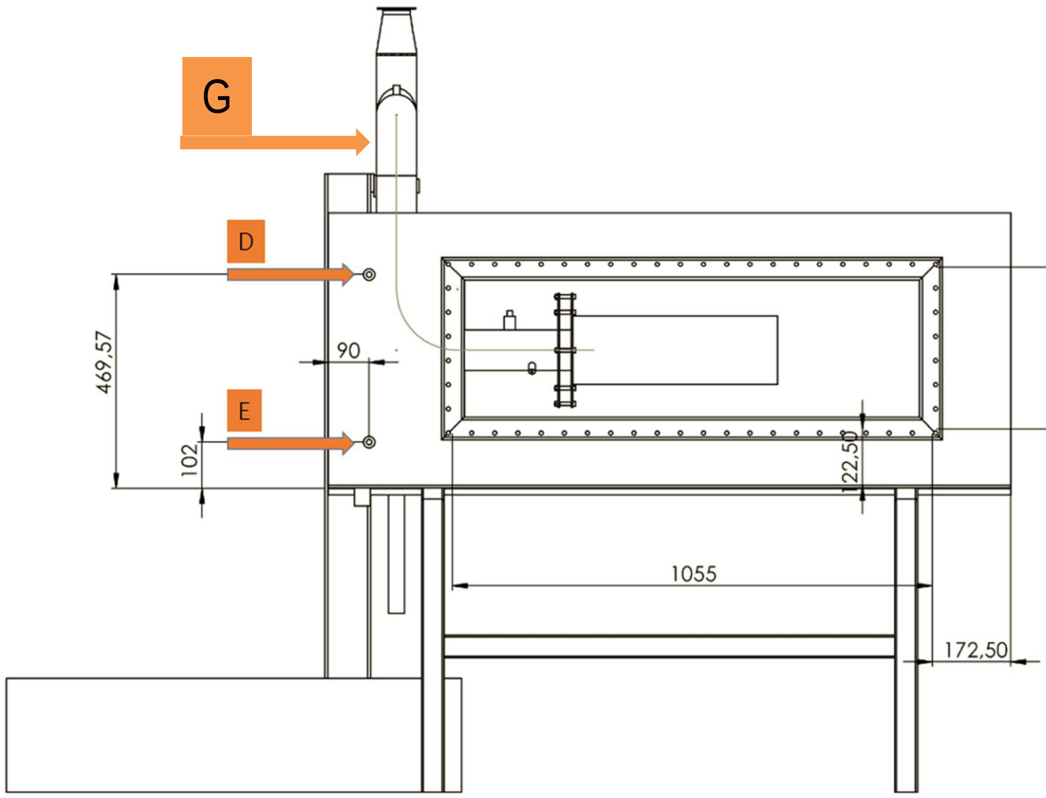

Figure 3. Temperature measurements of condensation pool water (D, E) and force measurement (G).

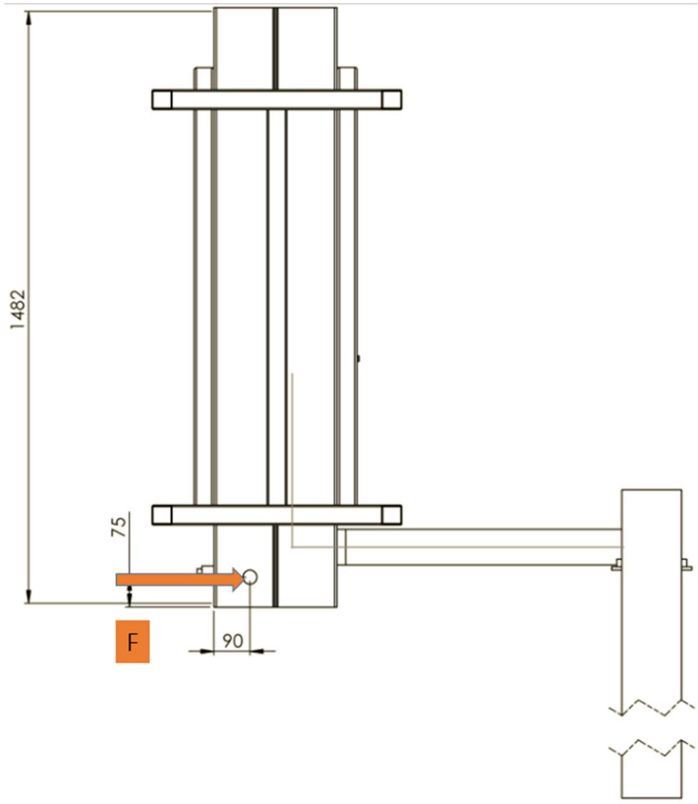

Figure 4. Location (F) of the DP transducer used for water level measurement of condensation pool.

Table 1.Instrumentation of the SEF-POOL facility

Figure code	Data code	Sensor type	Manufacturer/ type	Measurement frequency	Measurement range
A	P2600	Pres. transducer	Wikatronic	2 Hz	0-1 MPa
A	T2600	TC, K- type	Ø3 mm[1]	70 Hz	0-200 °C
B	T2601	TC, K- type	Ø1 mm[1]	70 Hz	0-200 °C
C	P2601	Pressure sensor[2]	Kyowa PHS-B	7 KHz	0-10 bar
D	T2605	TC, K- type	Ø3 mm[1]	2 Hz	0-200 °C
E	T2606	TC, K- type	Ø3 mm[1]	2 Hz	0-200 °C
F	D2600	DP transducer	Yokogawa EAJ110	2 Hz	0-7 kPa
G	X2600	Load sensor[2]	Kyowa LUX-B-50N	7 kHz	±50 N
H	P2602	Pressure sensor[2]	Kyowa PS-2KC[3]	7 kHz	0-0.2 MPa
I	T2602	TC, K- type	Ø 0.5 mm[1]	70 Hz	0-200 °C
J	T2603	TC, K- type	Ø 0.5 mm[1]	70 Hz	0-200 °C
K	T2604	TC, K- type	Ø 0.5 mm[1]	70 Hz	0-200 °C

[1] Diameter of the sensing element
[2] These are used in conjunction with a Strain/Bridge Input Module
[3] Type used depends on the range, the number denotes the measurement range in bars

Appendix C

Characterizing tests in SEF-POOL facility

Technical Report
Lappeenranta University of Technology
Nuclear Engineering

INSTAB 3/2017

Characterizing tests in SEF-POOL facility

Markku Puustinen, Jani Laine, Antti Räsänen,

Eetu Kotro, Kimmo Tielinen

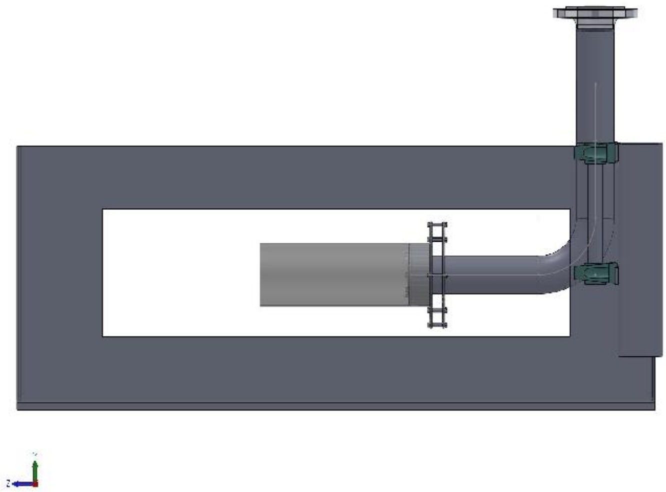

Lappeenranta University of Technology
School of Energy Systems
Nuclear Engineering
P.O. Box 20, FIN-53851 LAPPEENRANTA, FINLAND
Phone +358 294 462 111

Lappeenranta, 27.2.2018

LUT
Lappeenranta
University of Technology

<table>
<tr><td>Research organization and address
Lappeenranta University of Technology
School of Energy Systems
Nuclear Engineering
P.O. Box 20
FIN-53851 LAPPEENRANTA, FINLAND</td><td colspan="2">Customer
VYR / SAFIR2018
NKS
SSM</td></tr>
<tr><td>Project manager
Markku Puustinen</td><td colspan="2">Contact person
Jari Hämäläinen (SAFIR2018)
Christian Linde (NKS), Maria Agrell (SSM)</td></tr>
<tr><td>Diary code
125/322/2015</td><td colspan="2">Order reference
Drno SAFIR 11/2017</td></tr>
<tr><td>Project title and reference code
SAFIR2018-INSTAB
NKS-COPSAR</td><td>Report identification & Pages
INSTAB 3/2017
21 p. + app. 3+3 p.</td><td>Date
27.2.2018</td></tr>
</table>

Report title and author(s)

CHARACTERIZING TESTS IN SEF-POOL FACILITY

Markku Puustinen, Jani Laine, Antti Räsänen, Eetu Kotro, Kimmo Tielinen

Summary

The SEF-POOL test facility has been designed together by KTH and LUT. It has been constructed by the Nuclear Engineering research group at LUT and it will be used for the validation of the EHS and EMS models proposed by KTH for simulation of steam injection into a pool filled with sub-cooled water. The models have been validated against the PPOOLEX experiments with blowdown pipes and are now being extended to SRV spargers.

This report presents the key observations from the preliminary/characterizing tests conducted with the SEF-POOL facility during the latter part of 2017. Steam-to-water and water-to-water injections have been done. One test has been done with water injection into an empty pool. The main goal has been to test different options for the force measurement and to provide data for KTH for preliminary comparison of theoretical effective momentum with values calculated based on directly measured force.

The tests revealed that some modifications to the facility are needed. Most importantly, the arrangement for the direct force measurement was changed.

A quick analysis by KTH showed that the steam momentum can be roughly predicted by the theoretical estimate and the frequencies obtained with the fast pressure transducer correlate well with the correlations proposed in the literature. A strong temperature dependence, i.e. larger momentum as the pool temperature increases, was noticed.

Lower pressure inside the propulsion volume than the ambient pressure in the pool resulted to a lower force measurement than the true jet momentum. LUT and KTH will continue working on the design to solve this issue so that the actual tests to be used for the validation of the EMS model can be carried out in 2018.

Distribution

Members of the SAFIR2018 Reference Group 4

C. Linde (SSM), M. Agrell (SSM), P. Kudinov (KTH), I. G. Marcos (KTH), W. Villanueva (KTH), J. Hämäläinen (VTT), V. Suolanen (VTT), T. Pättikangas (VTT), I. Karppinen (VTT), S. Hillberg (VTT)

Principal author or Project manager	**Reviewed by**
Markku Puustinen Project Researcher	Vesa Riikonen Senior Research Scientist
Approved by	**Availability statement**
Heikki Purhonen Research Director	Public

LUT
Lappeenranta
University of Technology

Acknowledgement

NKS conveys its gratitude to all organizations and persons who by means of financial support or contributions in kind have made the work presented in this report possible.

Disclaimer

LUT
Lappeenranta
University of Technology

PREFACE

Tests done in the SEF-POOL facility have been planned together by Kungliga Tekniska Högskolan (KTH) and the Nuclear Engineering research group at Lappeenranta University of Technology (LUT). The work has been performed under the Finnish Research Programme on Nuclear Power Plant Safety 2015–2018 (SAFIR2018) in the INSTAB project as well as under the NKS-COPSAR project. Financial support for the work has been provided by the National Nuclear Waste Management Fund, NKS, Strålsäkerhetsmyndigheten (SSM) and LUT.

LUT
Lappeenranta
University of Technology

CONTENTS

NOMENCLATURE **6**
1 INTRODUCTION **7**
2 EMS/EHS MODELS AND EFFECTIVE MOMENTUM **7**
3 SEF-POOL TEST FACILITY **8**
3.1 GENERAL 9
3.2 CONDENSATION POOL 9
3.3 SPARGER SYSTEM 9
3.4 FORCE MEASUREMENT 10
3.5 OTHER MEASUREMENTS 10
3.6 DATA ACQUISITION 11
3.7 CAMERA SYSTEM 11
4 PRELIMINARY AND CHARACTERIZING TESTS **11**
4.1 PRELIMINARY TESTS 12
4.2 CHARACTERIZING TESTS WITH WATER INJECTION 15
4.3 CHARACTERIZING TESTS WITH STEAM INJECTION 17
5 CONCLUSIONS **20**
REFERENCES **21**
APPENDIX A: TEST RIG DRAWINGS
APPENDIX B: BASIC INSTRUMENTATION

NOMENCLATURE

Symbols

A	Area
DP	Differential pressure
$\dot{m}$	Mass flow rate
ρ	Density
M_{eff}	Effective momentum
M_s	Steam momentum
P	Pressure
T	Temperature

Abbreviations

BWR	Boiling Water Reactor
DCC	Direct Contact Condensation
EHS	Effective Heat Source
EMS	Effective Momentum Source
INSTAB	Couplings and INSTABilities in Reactor Systems Project
KTH	Kungliga Tekniska Högskolan
LUT	Lappeenranta University of Technology
NKS	Nordic Nuclear Safety Research
PACTEL	PArallel Channel TEst Loop
PC	Polycarbonate
PPOOLEX	Pressurized Condensation POOL EXperiments Test Facility
SAFIR	SAfety of Nuclear Power Plants - FInnish National Research Programme
SEF-POOL	Separate Effect Test Facility
SRV	Safety Relief Valve
SSM	Strålsäkerhetsmyndigheten
TC	ThermoCouple

1 INTRODUCTION

Effective Heat Source (EHS) and Effective Momentum Source (EMS) models have been proposed by KTH for simulation of steam injection into a pool filled with sub-cooled water [1]. The models have been implemented in the GOTHIC code and validated against PPOOLEX experiments with blowdown pipes done at LUT under the SAFIR2018/INSTAB project [2, 3].

Now the concepts of the EHS/EMS models are being extended to the condensation regimes appearing in safety relief valve (SRV) spargers and validation has been carried out against PANDA and PPOOLEX experiments done with a model of a SRV sparger [4]. This validation effort has shown that the injection angle, total momentum, and momentum profile have a large effect on the pool behaviour. Due to the uncertainty on these parameters, a separate effect test facility named SEF-POOL, has been designed at LUT in collaboration with KTH to measure/define the effective momentum and reduce the uncertainty of the simulations.

The SEF-POOL facility was constructed at LUT and a series of preliminary and characterizing tests were conducted with the facility in autumn 2017. The first tests with the facility revealed that some modifications for the design are needed in order to be able to define the effective momentum. After these modifications were implemented more preliminary tests were run at the end of the year. The final design of the facility will be decided during the first quarter of 2018 and after that the actual tests to validate the EMS/EHS models will be conducted.

This report summarizes the characterizing/preliminary tests done in 2017. The concept behind the EMS/EHS models is first shortly discussed in chapter 2. Next, the geometry and installed instrumentation of the SEF-POOL facility are introduced in chapter 3. The main observations from the tests done with the SEF-POOL facility in 2017 and some related preliminary analysis results obtained from KTH are then presented in chapter 4. Some conclusions are drawn in chapter 5.

2 EMS/EHS MODELS AND EFFECTIVE MOMENTUM

The general idea behind the EMS/EHS models is that, to predict the global pool behaviour, the small scale phenomena occurring at the level of direct contact condensation does not need to be resolved [1]. Instead, it is the time averaged heat and momentum transferred from the steam to the large scale pool circulation that needs to be provided. With this approach computational efficiency can be improved considerably, when large domains such as pressure suppression pools of BWRs and long term transients, are modelled. Particularly the modelling of steam jets at the injection holes of a sparger requires very fine meshes and small time steps. Furthermore, instability issues will arise if we attempt to resolve the direct contact condensation of such jets.

In the EMS/EHS model approach, simplified conservation equations of mass, momentum, and energy in a control volume, where the steam jets are expected to condense completely, are solved and a mean (time-averaged) condensate flow at the control volume boundary is defined. Steam momentum $\boldsymbol{M_S}$ is defined as momentum of the steam right at the injection hole (before condensing) and can be expressed by $\dot{m}^2/(\rho A)$, where $\dot{m}$ is steam mass flow rate, ρ steam density and A cross sectional flow area. Effective momentum $\boldsymbol{M_{eff}}$ is the amount of momentum transferred from the steam to the liquid. These two momentums are not equal in two phase flow (for example: chugging). It is the $\boldsymbol{M_{eff}}$ term that needs to be known in the EMS model approach. Separate-effect tests in the SEF-POOL facility would allow to measure and visualize directly the difference between $\boldsymbol{M_S}$ and $\boldsymbol{M_{eff}}$. The tests will help to map the effective momentum of different condensation regimes and will thus provide closures for the EMS model development for spargers by KTH.

Focus in the forthcoming test series with the SEF-POOL facility in 2018 is to determine the effect of the injection hole diameter, number of holes, pool temperature, steam mass flux, etc., on the effective momentum. Furthermore, the detachment and collapse frequencies of the bubbles could be obtained with the help of high frequency measurements and high-speed video recordings.

3 SEF-POOL TEST FACILITY

The reference system for the SEF-POOL facility is a SRV sparger pipe of a BWR plant. Hence the SEF-POOL facility is designed in such a way that discharge of steam through injection holes at the sparger lower end into sub-cooled pool water can be simulated representatively.

The goal in the tests with the facility is to define the effective momentum for a given steam condensation regime, particularly in the oscillatory bubble and stable jet regimes. For this purpose the design of the test facility is such that the effective momentum can be directly measured with a force sensor or it can calculated on the basis of measured steam momentum. Alternatively the effective momentum could be evaluated on the basis of velocity field of the water volume developed as a result of steam injection and measured for example with hot-wire measurements. Because the focus is on measuring separate effects of steam injection through the sparger holes and not on stratification/mixing phenomenon, the water pool itself, where the sparger is submerged, is relatively small in volume.

For helping to recognize different flow regimes and for obtaining the bubble diameter as a function of time the test facility allows high-speed video recordings of the direct contact condensation (DCC) of steam. In addition, a high frequency pressure measurement helps to obtain the detachment and collapse frequency of the bubbles. Steam needed in the tests is generated with the nearby PACTEL test facility [5]. The design principles and the geometry and installed instrumentation of the facility are presented in more detail in reference [6]. Appendix A presents some drawings on the facility geometry and Appendix B the locations of the measurements. The flexibility of the facility provides appropriate possibilities to extend the facility set-up according to the future research needs.

3.1 GENERAL

The main parts of the separate effect test rig are the sparger piping and condensation pool. The sparger piping is connected with a pipeline to the PACTEL test facility which supplies steam needed in the tests. The sparger pipe is pivoted on a vertical axis with low friction bearings in order to allow the direct force measurement. The lower end of the sparger pipe mounts a flow plate with injection holes and a polycarbonate (PC) pipe. Steam is discharged through the injection holes and it condenses inside the PC pipe. The purpose of the PC pipe is to act as a propulsion volume and to create a parallel flow pattern so that the amount of momentum transferred from the steam to the liquid at the outlet of the PC pipe can be estimated. Tests can be conducted also without the PC pipe. Figure 1 presents the SEF-POOL test facility in general.

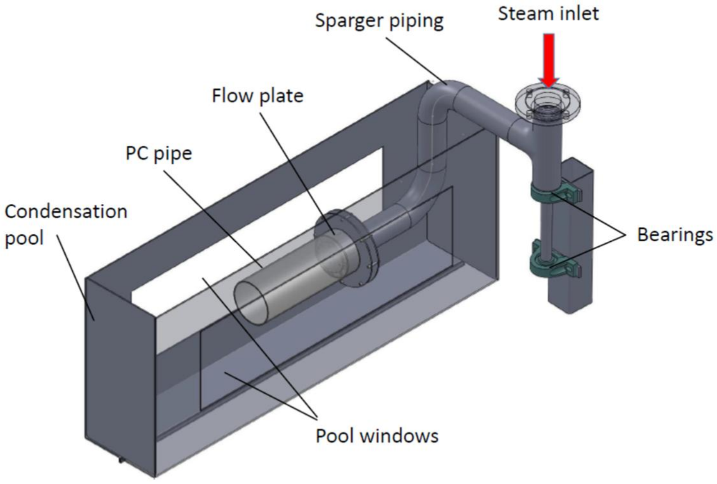

Figure 1. General view of the SEF-POOL test facility.

3.2 CONDENSATION POOL

The condensation pool is made of stainless steel. It is 1500 mm long, 300 mm wide and 600 mm tall. The pool is open on top and it is uninsulated. Windows on both sides are 1000 mm wide and 300 mm tall. The pool is mounted on a support made of 50x50 box section. A cover (lid) can be installed to the top to prevent any spill over or splashing of water to the laboratory site during the tests. As the pool is open on top atmospheric pressure will prevail in the pool in all the tests. Figure 1 in Appendix A presents the condensation pool in more detail.

3.3 SPARGER SYSTEM

The sparger piping is made of sections of DN80 stainless steel pipes and it is insulated with 13 mm thick AP Armaflex® XG flexible elastomeric thermal insulation. Dimensions of the piping are shown in Figure 2 in Appendix A. The piping is connected to the sparger system shown in Figure 3 in Appendix A. The sparger system consists of different kind of stainless steel plates and of a PC pipe. The plates are used for connecting the PC pipe to the sparger piping and for guiding the compensation water flow from the pool into the

PC pipe. A perforated flow plate for steam injection is mounted to the end of the sparger pipe. Configuration of the flow plate can be easily changed. Dimensions of different kind of flow plates to be used in the tests are presented in Table 1 in Appendix A. The PC pipe attached to the end of the sparger piping has an inner diameter of 144 mm. Its length is 450 mm, 400 mm of which is downstream from the flow plate. Photo in Figure 2 shows the end section of the sparger piping and the sparger system inside the pool.

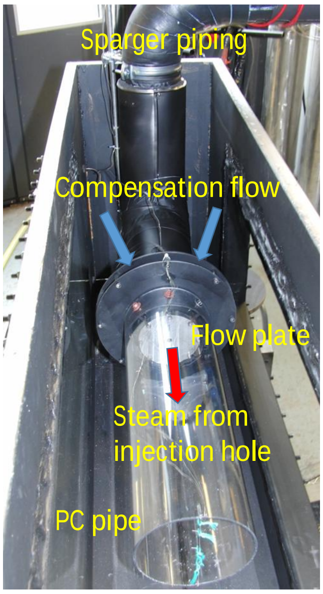

Figure 2. The end of the sparger piping and the sparger system of the SEF-POOL facility.

3.4 FORCE MEASUREMENT

The direct force measurement is arranged with a load cell. The load cell is located outside the condensation pool and it is attached to a support pole made of 50x50 box section bolted to the floor of the laboratory. The load cell is at that end of the condensation pool, where the sparger piping is submerged. Force is transmitted from the sparger piping to the sensor via a rod. When steam is injected through the sparger piping and perforated flow plate, momentum is created and as a result the sparger piping tends to rotate around the pivot bearing. This causes compression to the load cell and the generated force can be thus measured. Because the force measurement compression distance is almost non-existent the angle of the sparger piping compared to the condensation pool does not change during the tests.

3.5 OTHER MEASUREMENTS

Two pressure transducers for steam pressure measurement are mounted in the sparger piping. One is near the steam inlet point and the other one is 140 mm upstream from the perforated flow plate. The measurement range of the both transducer is 0.1-1.0 MPa.

A kHz range pressure sensor is used for capturing the detachment and collapse frequencies of the steam bubbles. It is fixed either to the inner wall of the PC pipe about

100 mm downstream of the perforated flow plate or to a vertical support structure laying at the pool bottom in those tests where the PC pipe is not used. The range of the sensor can be up to 0.2 MPa, 1 MPa or 2 MPa depending on the test in question.

Temperatures are measured with calibrated k-type thermocouples (TC). Temperature of incoming steam is measured with one TC near the inlet point at the same location as the pressure. Steam temperature is also measured in the sparger piping at about 190 mm before the perforated flow plate. Temperatures of water exiting the PC pipe are measured with three vertically positioned TCs. In those tests, where the PC pipe is not used, these three TCs can be attached to the same support structure as the high frequency pressure sensor and positioned in front of the flow plate with a desired distance from the plate.

Water level in the condensation pool is measured with a Yokogawa® differential pressure transducer. The transducer is mounted to the base of the pool. Water level is calculated from the differential pressure reading with the help of liquid density. Temperature measurements in the pool are used to define the liquid density.

Steam flow rate is measured with a vortex flow meter in the steam line.

The locations of the thermocouples, pressure transducers and water level measurement are shown in Figures 1-4 in Appendix B. Information on the type/frequency/range of different sensors/instrumentation can be found in Table 1 at the end of Appendix B.

3.6 DATA ACQUISITION

National Instruments PXIe PC-driven measurement system is used for data acquisition. The system enables high-speed multi-channel measurements. The maximum recording capacity depends on the number of measurements and is in the region of mega samples per second. Measurement software is LabView 2015.

3.7 CAMERA SYSTEM

Windows on the both side walls of the condensation pool allow the capture of the DCC phenomenon of steam with a high-speed video system. Different flow regimes could be recognized and bubble diameters obtained with the help of the system.

The high-speed camera system consists of a monochromatic Phantom Miro 310 camera. The maximum resolution is 1280x800 px, but in practise the picture area is cropped in order to increase the maximum amount of the images the 12 GB internal memory can hold, thus increasing the total time of the recordings.

4 PRELIMINARY AND CHARACTERIZING TESTS

Several preliminary/characterizing tests have been conducted with the SEF-POOL facility during the latter part of 2017. Steam-to-water and water-to-water injections have been done. One test has been done with water injection into an empty pool. Test parameters and procedures were obtained from KTH.

The main goal has been to test different options for the force measurement and to provide data for KTH for preliminary comparison of theoretical effective momentum with values calculated based on directly measured force. In addition, high-speed video clips of the direct contact condensation phenomenon of steam have been recorded. Table 1 lists the main parameters of the tests.

Table 1. Preliminary/characterizing tests in the SEF-POOL facility in 2017

Test	PC tube yes/no	Force sensor attached to	Injected substance	Flow rate steam [g/s] water [l/min]	Initial pool water level/temp [m/°C]	Flow plate	High speed video (700 fps)
SEF-T0	yes	pool wall	steam	~50-90	0.54/25	3x8 mm	yes
SEF-T00	yes	pool wall	steam	~8-110	0.59/20	3x8 mm	yes
SEF-T000	yes	pool wall	steam	~15-100	0.51/19	3x16 mm	yes
SEF-W1	yes	pool wall	water	~15-69	0.44/15	1x8 mm	no
SEF-W2	no	pole in floor	water	~15-69	0.49/18	1x8 mm	no
SEF-A1	yes	pole in floor	water	~15-69	empty	1x8 mm	yes
SEF-W3	yes	pole in floor	water	~9-69	0.51/17	1x8 mm	100 fps
SEF-S1	no	pole in floor	steam	~12-44	0.49/23	3x8 mm	yes
SEF-S2	no	pole in floor	steam	~12-51	0.49/23	3x8 mm	yes
SEF-S3	no	pole in floor	steam	~19	0.49/14	3x8 mm	yes
SEF-S4	no	pole in floor	steam	~50	0.48/18	3x8 mm	yes
SEF-S5	no	pole in floor	steam	~64	0.49/15	1x16 mm	yes
SEF-S6	no	pole in floor	steam	~26	0.48/17	1x16 mm	yes
SEF-S7	no	pole in floor	steam	~43	0.48/14	1x16 mm	yes

It is typical for the first tests with a new facility that problems can be encountered. Either some systems or parts of the facility don’t fulfill design specifications, leak tightness is not 100%, instrumentation is not functioning properly or the used test procedure needs to be changed. Different kind of problems related to facility structures and measurement sensors were encountered also with the SEF-POOL facility during the preliminary/characterizing tests listed in the table above. Therefore the following chapters present only selected results from the most successful tests and discuss some key observations based on those results. Evolution of the facility design as a result of the analysis of the test results can also be tracked from the following chapters.

4.1 PRELIMINARY TESTS

Three preliminary steam-to-water injection tests were carried out to check the functioning of instrumentation and to learn general behaviour of the facility. Flow plates with 3x8 mm and 3x16 mm injection holes were used. Steam flow rate was varied from the minimum measurable ~8 g/s to ~110 g/s. Different flow steps were used to see how the force sensor reacts and to find out if the same flow rates give similar force values repeatedly. Figure 3 shows the flow rate of steam injection and the related force in the same graph from the SEF-T000 test. The force sensor was connected in these first tests in such a way that thrust force was indicated as a negative value.

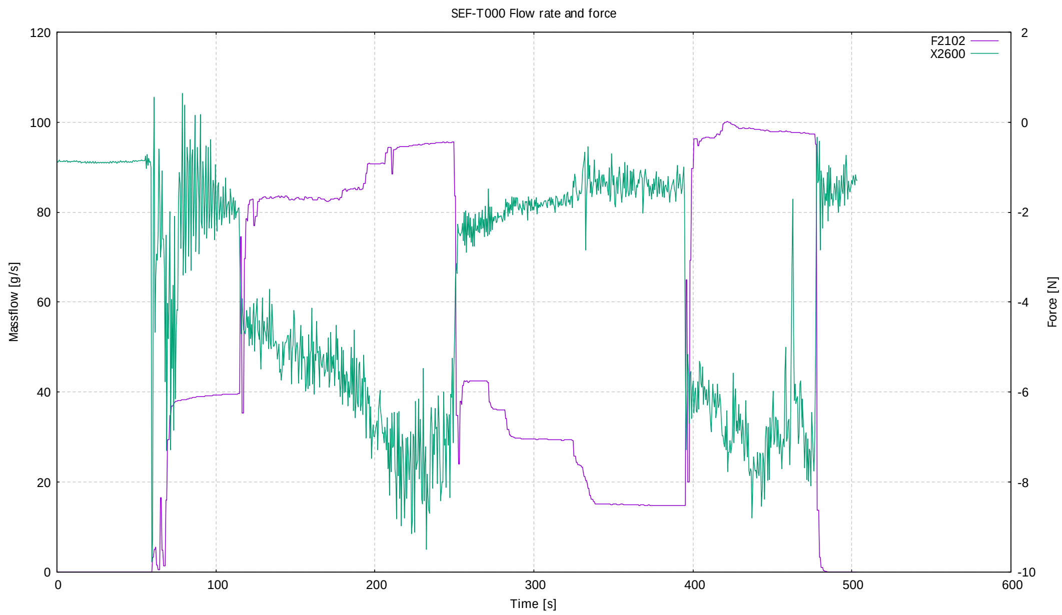

Figure 3. Steam flow rate (F2102) and corresponding force (X2600) in SEF-T000.

It can be seen that the measured force values are quite well in line with changes in the flow rate. However, large oscillations in the force measurement signal even during constant flow rate periods are present. A post-processing of the results by KTH showed that the oscillations of force measurement have a well-defined leading frequency at about 6 Hz. This suggests that the system is exited to its resonant mode. The fast pressure transducer shows that the frequency of the collapsing steam bubbles is about 20-400 times larger than the 6 Hz. It is believed that such high values are not able to excite the system to a low 6 Hz frequency and therefore the resonance might be due to the steam flowing through the sparger pipe (flow-induced vibration) or due to vibrations of the pool caused by water movement.

One preliminary water-to water injection test was carried out in order to further calibrate the force measurement. Unlike in steam, the water momentum can be easily computed and compared to the force measurement. Figure 4 presents how the force measurement reacts during different water injection flow steps.

Again the response of the force sensor is logical. Measured force increases with increasing injection flow rate. Vibrations are smaller than in the steam-to-water injection case but as the water injection rate is raised waving in the pool increases causing larger vibrations of the pool registered by the sensor.

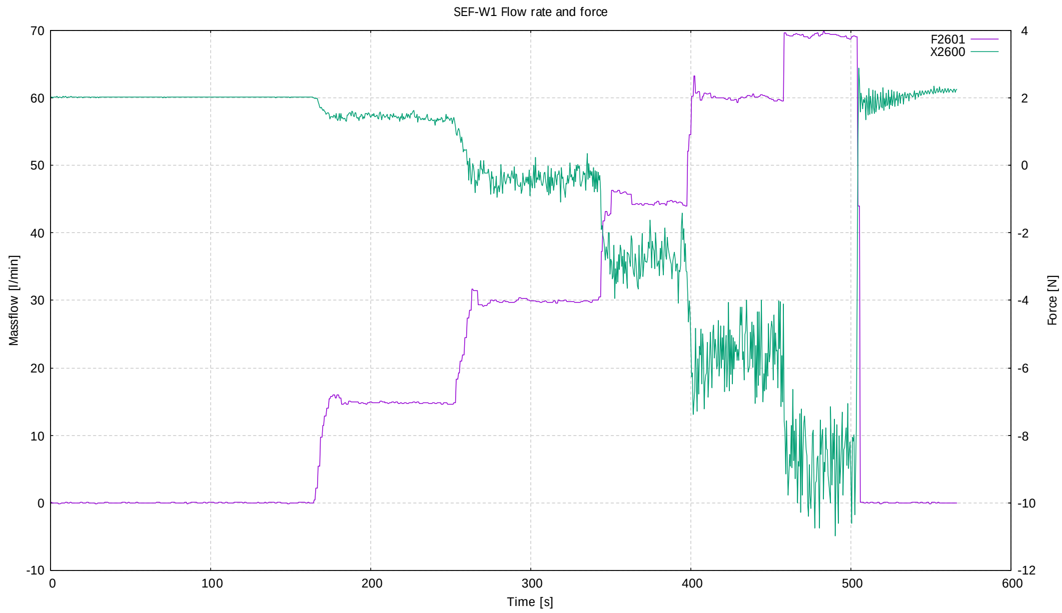

Figure 4. Water flow rate (F2601) and corresponding force (X2600) in SEF-W1.

However, post-processing of the water-to-water test by KTH showed that there seems to be a major deviation between the force measurement and the theoretical estimate (Figure 5).

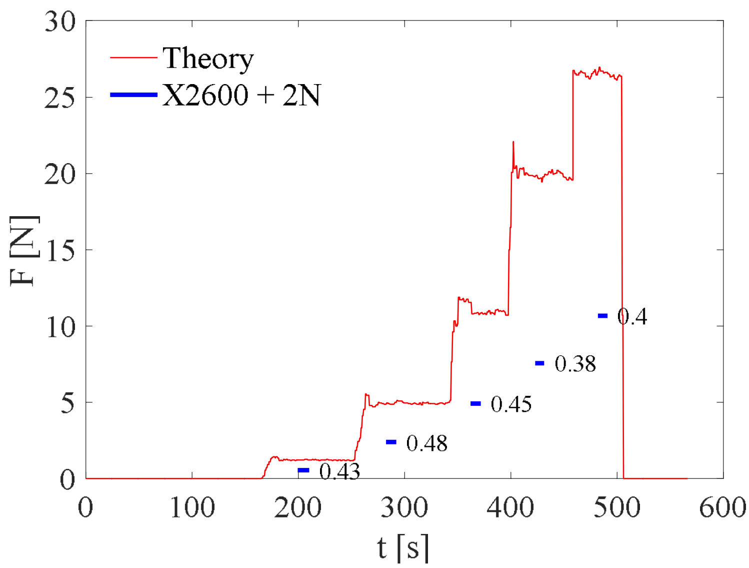

Figure 5. Measured and theoretical force value with water injection. The +2N is added to the measured value to compensate the offset of the zero point. Comparison done by KTH.

To reduce the oscillations registered by the force sensor and to make sure that correct force for finally obtaining $\boldsymbol{M_{eff}}$ is measured, it was decided that before further tests the arrangement for the force measurement is changed so that the sensor is attached to a structure which is not connected with the pool itself. Thus, after four preliminary tests the force sensor was removed from the pool wall and attached to a vertical pole which is bolted to the floor. The pole is positioned to that end of the pool where the sparger piping is and the sensor and the pole are connected with a horizontal rod above the edge of the pool wall.

4.2 CHARACTERIZING TESTS WITH WATER INJECTION

Entrainment (compensation) flow at the annular plate between the sparger piping and the PC pipe is believed to have a large effect on the results. If the entrainment area at the annular plate is not large enough a significant pressure drop inside the PC pipe might develop which in turn could affect the measured force. The relevance of this explanation was checked by removing the PC pipe completely and by performing a water injection test (SEF-W2) otherwise with almost identical parameters as the previous SEF-W1 test. Figure 6 presents the measured water flow rate and corresponding force value in SEF-W2. In this test as well as in the following tests the force sensor was connected in such a way that thrust force is indicated as a positive value.

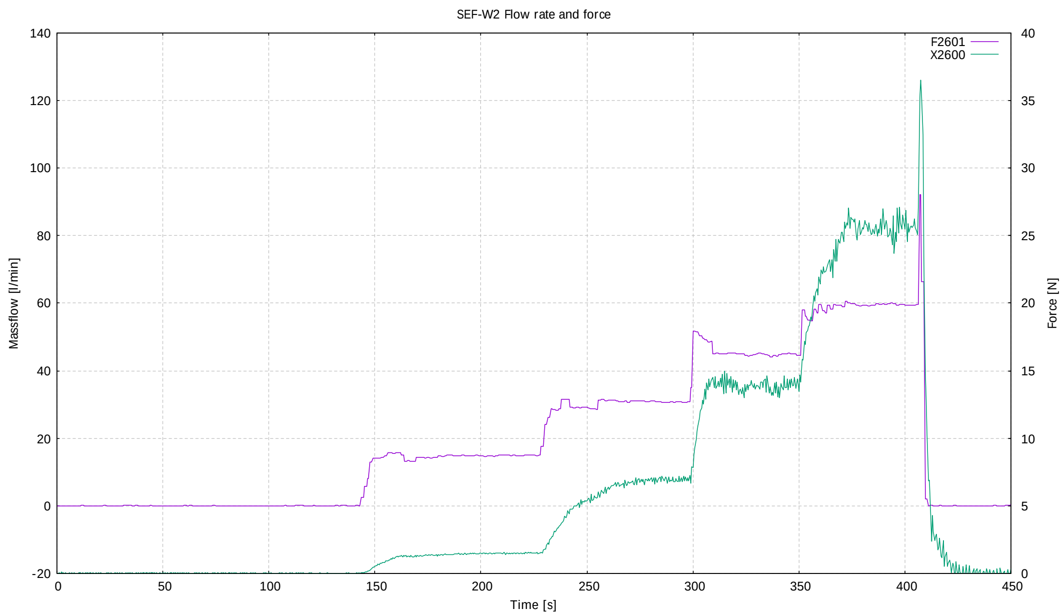

Figure 6. Water flow rate (F2601) and corresponding force (X2600) in SEF-W2.

It looks like the setup, where the PC pipe is removed, is over-estimating the water momentum. The previous setup (including the PC pipe) had the opposite effect i.e. under-predicting the momentum. Thus, it seems that the entrainment flow pattern has a large effect on the results.

It was decided that to clarify this effect a test with no water in the pool, i.e. injecting water into air, is performed. An additional goal of this SEF-A1 test was to see whether the water jet is contracting at the outlet or not. This is an effect which should be considered in the theoretical estimate of the water momentum. Figure 7 presents the measured water flow rate and corresponding force value in SEF-A1.

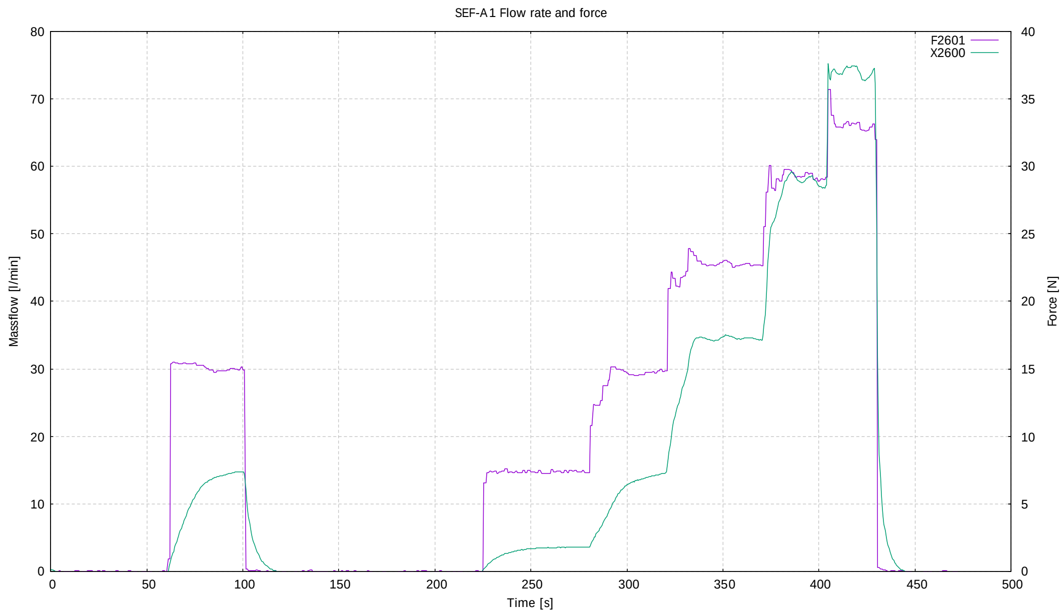

Figure 7. Water flow rate (F2601) and corresponding force (X2600) in SEF-A1.

Analysis of video clips from the test with injection of water into an empty pool revealed that the water jet seems to have a smaller diameter than the injection hole. Having a contraction means that, to compute the water momentum, the jet cross section area rather than the injection hole area should be used. This improves the results considerably. Figure 8 compares the force measurement and the theoretical estimate from the water-to-air injection test when the contraction of the jet is taken into account. The previous water injection test SEF-W2 also shows that the force measurement is in good agreement with the theory when using the jet diameter to estimate the momentum.

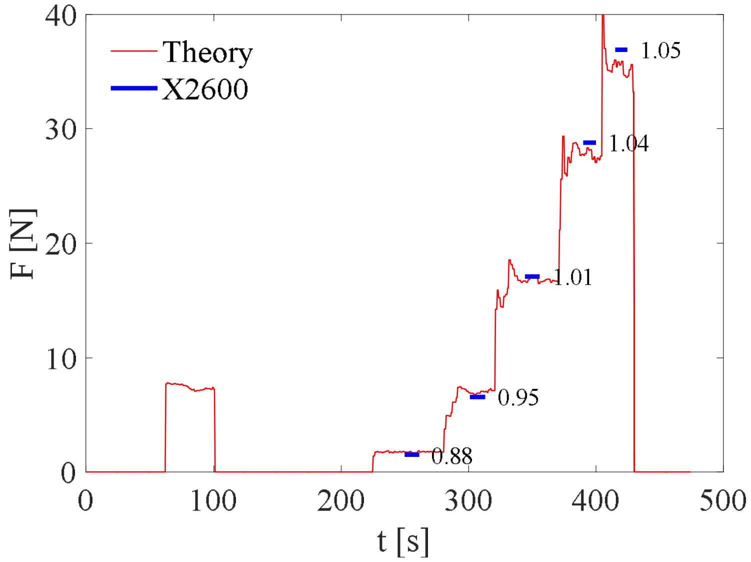

Figure 8. Measured and theoretical force value with water injection into an empty pool (SEF-A1). Comparison done by KTH.

In the next step, the effect of the propulsion volume (PC pipe) was studied. The water injection test SEF-W1 (with the PC pipe) showed that the momentum is substantially under-predicted. However, the force measurement in SEF-W1 was attached to the pool wall, and it was not clear whether it was this arrangement or the propulsion volume what caused the under-prediction. To clarify this another water-to-water test with the new force measurement arrangement and including the PC pipe was carried out. However, the PC pipe was used together with an annular plate at the outlet to reduce the exit flow area.

The force measurements were about 60% lower than the theoretically calculated water momentum (Figure 9). This shows that the PC pipe has a large effect on the results. The force measurement is only dependent on the mass flow and injection hole diameter at the outlet. CFD simulations by KTH show that the under-estimation of the momentum observed in the previous tests with the PC pipe was due to a low pressure region downstream of the flow plate. Lower pressure than the ambient pool pressure results to a lower force measurement than the true jet momentum. To preserve the momentum, the pressure on the sparger pipe walls and at the PC pipe outlet should be similar to the ambient pressure. The gap between the sparger and the PC pipe should therefore be made larger so that entrainment (compensation flow) into the PC pipe increases and the pressure levels in the PC pipe and pool are thus closer to each other. This kind of changes would be radical and would result in a "no return" situation regarding the structure, where the sparger and PC pipe are connected. Therefore KTH will continue working on the design while the experimental campaign was continued with steam-to-water tests.

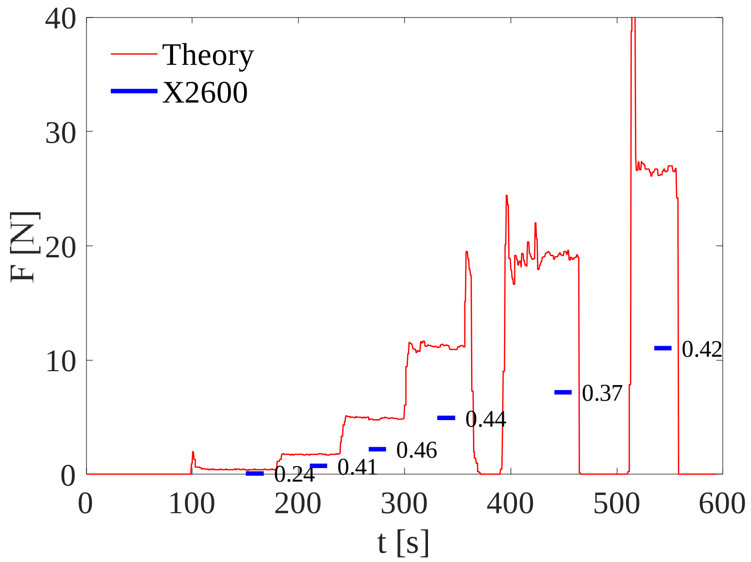

Figure 9. Measured and theoretical force values with water injection in the SEF-W3 test done with the PC pipe having a reduced exit area. Comparison done by KTH.

4.3 CHARACTERIZING TESTS WITH STEAM INJECTION

The first characterizing steam-to-water test SEF-S1 was done using the current setup, but just removing the PC pipe. This kind of test would give the steam momentum at the orifice, which, according to the previous water-to-water experiments, deviates from the standard theoretical estimation due to the contraction of the steam jet at the exit. In addition, the goal would be to map the steam mass fluxes (75-300 kg/m^{2}s) and pool temperatures (15-90 °C) developed in the earlier PPOOLEX tests with spargers.

A flow plate with 3x8 mm injection holes was used. Steam flow rate varied from ~12 g/s to ~44 g/s. Difficulties with steam flow control and the long time needed to move recorded video clips from the memory of the high-speed camera to flash memory in the middle of the test made SEF-S1 more or less a rehearsal test. Analysis by KTH showed, however, that for the unstable regimes, the measured force was quite different from the theoretical estimates. As the steam mass flux increased, the measured and theoretical values showed a better agreement.

For the SEF-S2 test, the test procedure was slightly modified to allow a better regulation of the steam flow rate and to have more time to move the video clips from the camera to the flash memory. The test parameters were otherwise practically the same with SEF-S1. Still, the test couldn't be done as fluently as desired and the recorded data should be considered only indicative.

For the next test, SEF-S3, the test procedure was changed so that after initial adjustment a constant steam flow rate (~19 g/s) was maintained throughout the test to avoid compilations induced by flow control manoeuvres. The idea was to detect the momentum change due to the increase in pool bulk temperature, not due to change in flow rate. Figure 10 shows the constant steam flow rate, increasing pool temperature and corresponding force value in the SEF-S3 test.

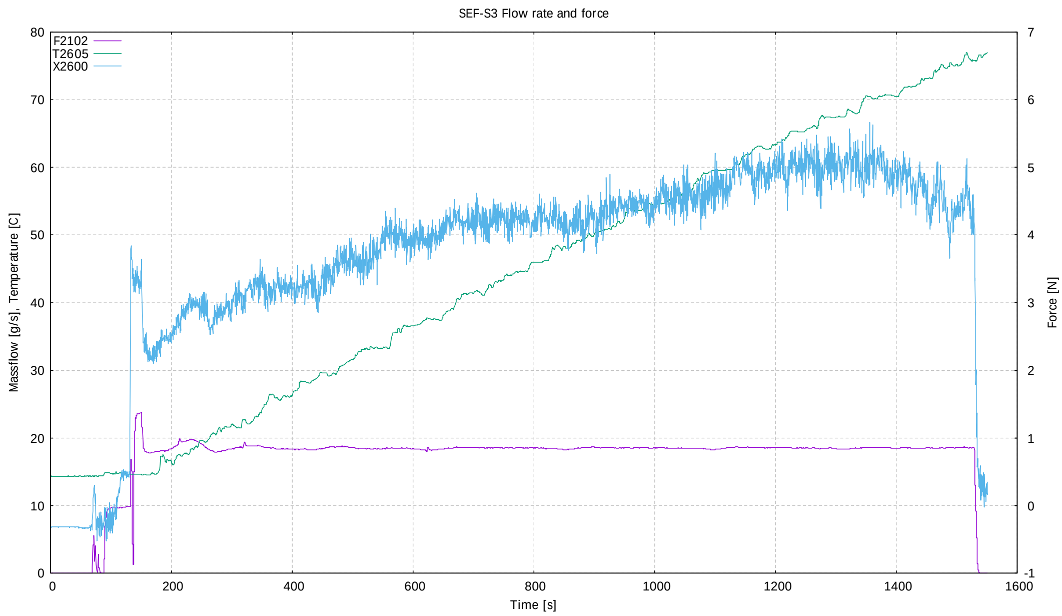

Figure 10. Steam flow (F2102), pool temperature (T2605) and corresponding force (X2600) in SEF-S3.

Analysis by KTH showed that the steam momentum can be roughly predicted by the theoretical estimate of $\dot{m}^2/(\rho A)$ and the frequencies obtained with the fast pressure transducer correlate well with the correlations proposed in the literature. However, the apparent temperature dependence is not captured with the theory.

The constant steam flow rate procedure was used also in the two next tests, SEF-S4 and SEF-S5. The steam flow rate was maintained at ~50 g/s in SEF-S4 and at ~64 g/s in SEF-S5 throughout the test. The 3x8 mm flow plate was in use in SEF-S4. It was replaced with 1x16 mm flow plate for the SEF-S5 test.

KTH concluded that the deviations between the experiment and theory in the force value seem to be due to the uncertainty of the steam density at the injection holes. In the analysis this density needs to be estimated based on the measured pressures and temperatures. Despite this uncertainty, the estimated momentum agrees well with the experiment. However, the deviation is not consistent between the multi and single-hole experiments. Peak frequencies correlated well with values found in the literature but a small over-prediction can be observed.

Two more steam injection tests (SEF-S6 and SEF-S7) were done to address the deviation between single and multi-hole results at low steam mass fluxes. The same fluxes (125 kg/m^2s and 215 kg/m^2s) as the ones generated during the multi-hole SEF-S2, SEF-S3, and SEF-S4 tests were used. With the 1x16 mm flow plate these fluxes correspond to steam flow rates of ~26 g/s and ~43 g/s, respectively. Constant flow rate was maintained for the whole duration of the test. After SEF-S6, it was noticed that the zero point of the force sensor had shifted about 6 N. This happened most probably in the beginning of the test when the steam flow rate was adjusted. A strong flow peak appeared and it could have affected the delicate sensor. This shift complicates the analysis somewhat.

Analysis by KTH indicates that there is a strong temperature dependence in SEF-S6 and SEF-S7, i.e. larger momentum as the pool temperature increases. There is some deviation between the SEF-S6 test and the SEF-S5/SEF-S7 tests. If the above mentioned shift of the zero-point of the force measurement is taken into account a better agreement between the experiment and theory is achieved. Figure 11 presents the dependence between the pool temperature and measured force from all the characterizing steam injection tests (ΔT is the difference to saturation conditions).

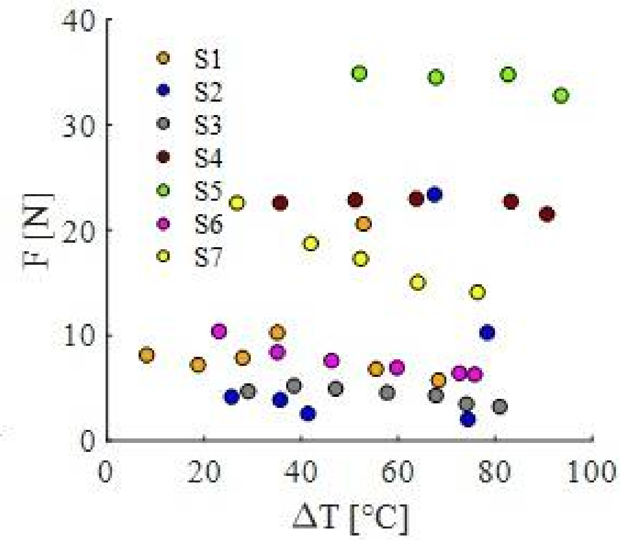

Figure 11. Measured force as a function of pool temperature from steam injection tests SEF-S1…SEF-S7. Analysis done by KTH.

5 CONCLUSIONS

The SEF-POOL test facility has been designed together by KTH and LUT. It has been constructed by the Nuclear Engineering research group at LUT. The facility will be used for the validation of EHS and EMS models proposed by KTH for simulation of steam injection into a pool filled with sub-cooled water. The models have been implemented in the GOTHIC code and validated against the PPOOLEX experiments with blowdown pipes. Now the concepts of the EHS and EMS models are being extended to SRV spargers.

The reference system for the SEF-POOL facility is a SRV sparger pipe of a BWR plant. Hence the SEF-POOL facility is designed in such a way that discharge of steam through injection holes at the sparger lower end into sub-cooled pool water can be simulated representatively. The goal in the tests with the facility is to define the effective momentum for a given steam condensation regime, particularly in the oscillatory bubble and stable jet regimes.

Several preliminary/characterizing tests have been conducted with the SEF-POOL facility during the latter part of 2017. Steam-to-water and water-to-water injections have been done. One test has been done with water injection into an empty pool. The main goal has been to test different options for the force measurement and to provide data for KTH for preliminary comparison of theoretical effective momentum with values calculated based on directly measured force.

During the preliminary/characterizing test series it was noticed that some modifications to the facility are needed. Most importantly, the arrangement for the direct force measurement was changed. Part of the tests were done without the propulsion volume (PC pipe) to see if this has an effect on the momentum value derived from the test results. Also the test procedure was changed from the initial version with several flow steps to a constant flow rate version in order avoid complications caused by a coarse flow control system.

Analysis of the steam injection tests by KTH showed that the steam momentum can be roughly predicted by the theoretical estimate and the frequencies obtained with the fast pressure transducer correlate well with the correlations proposed in the literature. A strong temperature dependence, i.e. larger momentum as the pool temperature increases, was noticed. This temperature dependence is not captured with the theory.

Analysis of video clips from the test with injection of water into an empty pool revealed that the water jet seems to have a smaller diameter than the injection hole. Having a contraction means that the jet cross section area rather than the injection hole area should be used in the computation of momentum. If this contraction effect is taken into account also in the steam injection tests an even better agreement with the theory in the estimation of the momentum is achieved.

It was also found out that if the entrainment (compensation) flow into the propulsion volume is too small a significant pressure drop inside the PC pipe might develop which in turn could affect the measured force. The force measurement is only dependent on the mass flow and injection hole diameter at the outlet. Lower pressure inside the PC pipe than the ambient pressure in the pool results to a lower force measurement than the true jet momentum. To get rid of this distortion, entrainment into the PC pipe should be somehow increased so that the pressure levels in the PC pipe and in the pool are closer to each other. LUT and KTH will continue working on the design to solve this issue so that the actual tests to be used for the validation of the EMS model can be carried out in 2018.

REFERENCES

[1] Li, H., Villanueva, W., Kudinov, P., Approach and development of effective models for simulation of thermal stratification and mixing induced by steam injection into a large pool of water. Sci. Technol. Nucl. Ins. 2014, http://dx.doi.org/10.1155/2014/108782, (Article ID 108782).

[2] Li, H., Villanueva, W., Puustinen, M., Laine, J., Kudinov, P., Validation of effective models for simulation of thermal stratification and mixing induced by steam injection into a large pool of water. Sci. Technol. Nucl. Ins. 2014, http://dx.doi.org/10.1155/2014/752597, (Article ID752597).

[3] Li, H., Villanueva, W., Puustinen, M., Laine, J., Kudinov, P., Thermal stratification and mixing in a suppression pool induced by direct steam injection. Annals of Nuclear Energy. 2018, 111, https://doi.org/10.1016/j.anucene.2017.09.014.

[4] Gallego-Marcos, I., Villanueva, W., Kapulla, R., Paranjape, S., Paladino, D., Kudinov, P., Modeling of thermal stratification and mixing induced by steam injection through spargers into a large water pool. CDF4NRS-6 Workshop, September 13 - 15, 2016, Massachusetts Institute of Technology.

[5] Tuunanen, J., Kouhia, J., Purhonen, H., Riikonen, V., Puustinen, M., Semken, R. S., Partanen, H., Saure, I., Pylkkö, H., General Description of the PACTEL Test Facility. Espoo: VTT. 1998. VTT Research Notes 1929. ISBN 951-38-5338-1.

[6] Tielinen, K., Räsänen, A., Kotro, E., Saure, I., General description of SEF-POOL test rig. Lappeenranta University of Technology, School of Energy Systems, Nuclear Engineering, Research Report INSTAB 2/2017. Lappeenranta 2018.

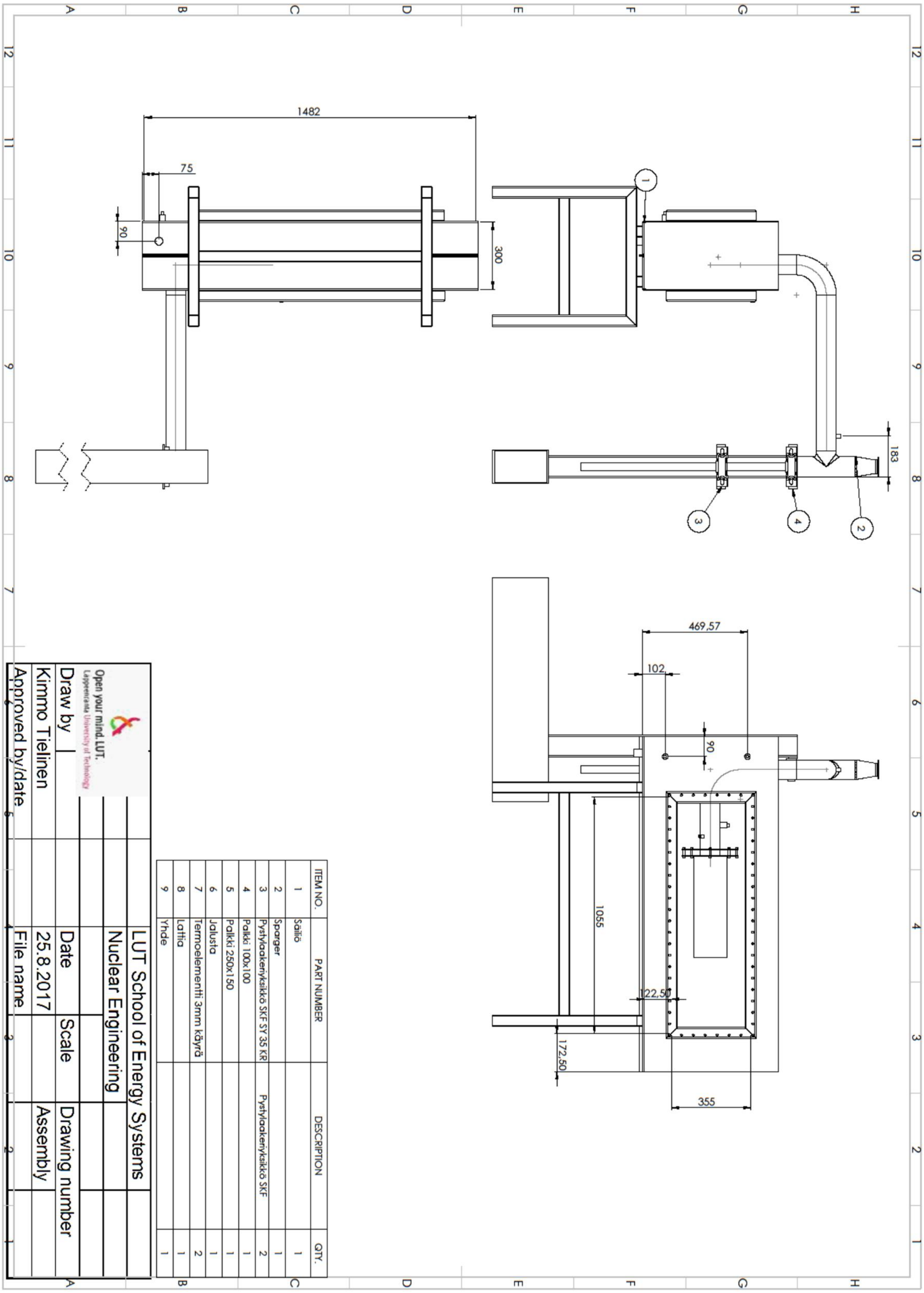

Figure 1. Condensation pool.

Appendix A: Test rig drawings

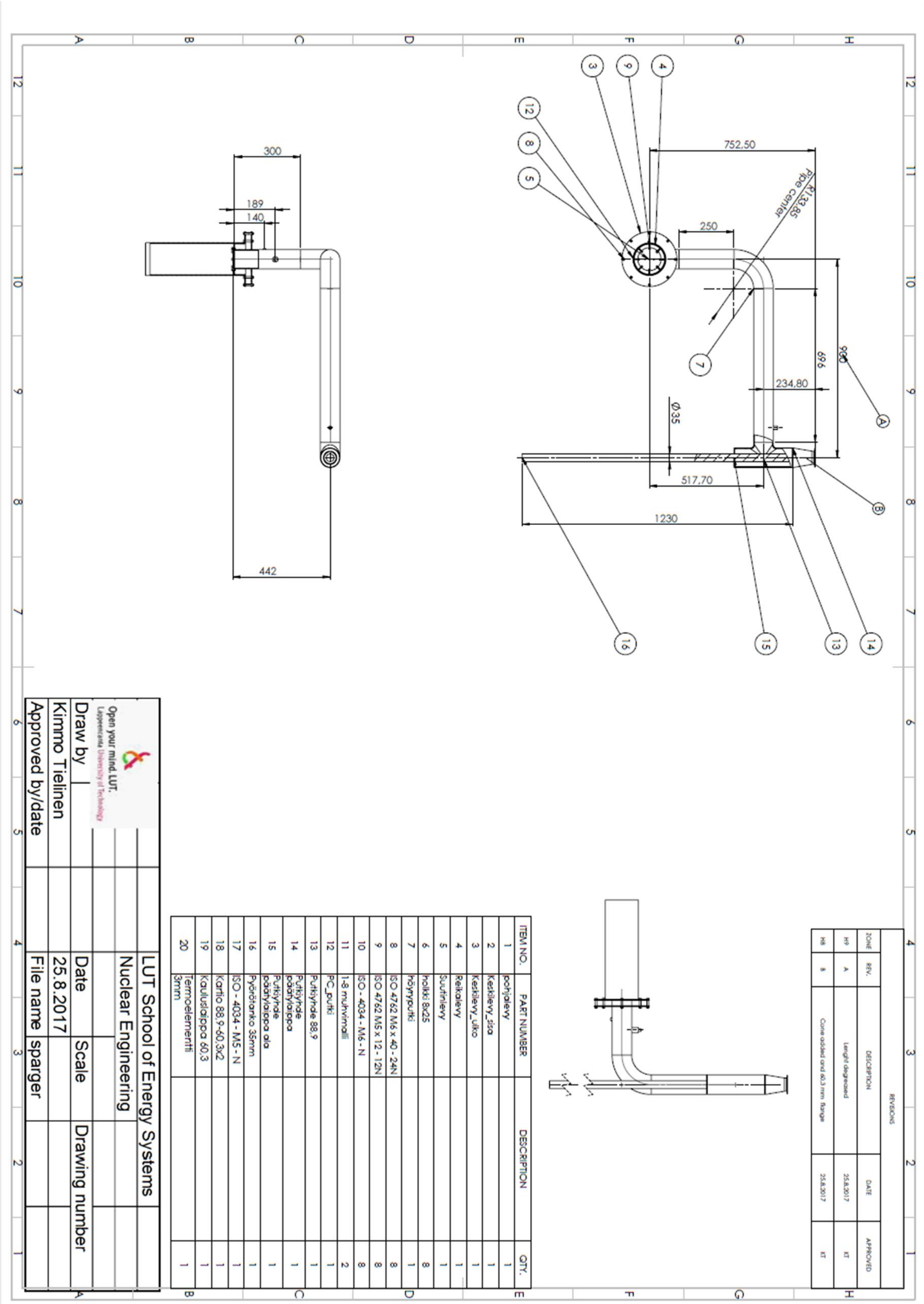

Figure 2. Sparger piping.

Appendix A: Test rig drawings

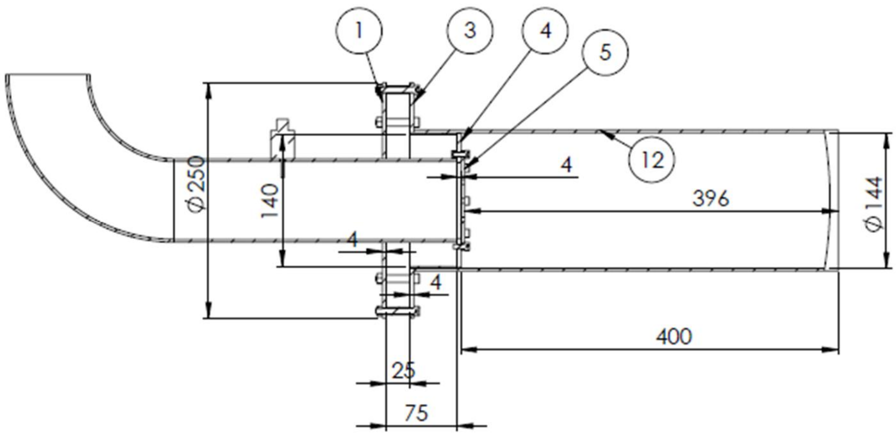

Figure 3. Sparger system.

Table 1. Dimensions of perforated flow plates

	Holes [mm]		Pitch [mm]	Chamfer		Effects
	N	Φ_i [mm]		t [mm]	Φ_o [mm]	
Plate 1	1	8	-	-	-	Base case
Plate 2	1	8	-	2	12	Chamfer
Plate 3	2	8	16	-	-	Number holes + Pitch/diameter
Plate 4	2	8	26	-	-	
Plate 5	2	8	36	-	-	
Plate 6	3	8	26	-	-	
Plate 7	1	16	-	-	-	Hole diameter
Plate 8	1	16	-	2	24	
Plate 9	2	16	32	-	-	
Plate 10	2	16	52	-	-	
Plate 11	3	16	32	-	-	

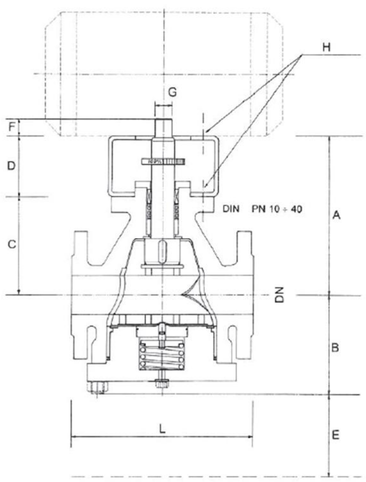

DIN		ANSI		A	B	C	D*)	E	F	G	H	PAINO
DN	L	DN	L									KG
15VE	130			123	73	63	60	80	16	14(10)	F07	5,2
15	130			147	173	86	60	80	16	17	F07	8
25	160	1"	196,9	151	86	91	60	80	16	17	F07	11,5
40	200	1 ½"	235	170	110	110	60	100	16	17	F07	25
50	230	2"	266,7	208	128	128	80	120	22	22	F10	41
80	310	3"	317,5	225	180	150	80	160	25	22(27)	F10	85
100	350	4"	368,3	242	180	162	80	190	37	36	F14	112
150	480			242	180	162	80	190	37	36	F14	130

Figure 4. Dimensions of Varibell® steam valve.

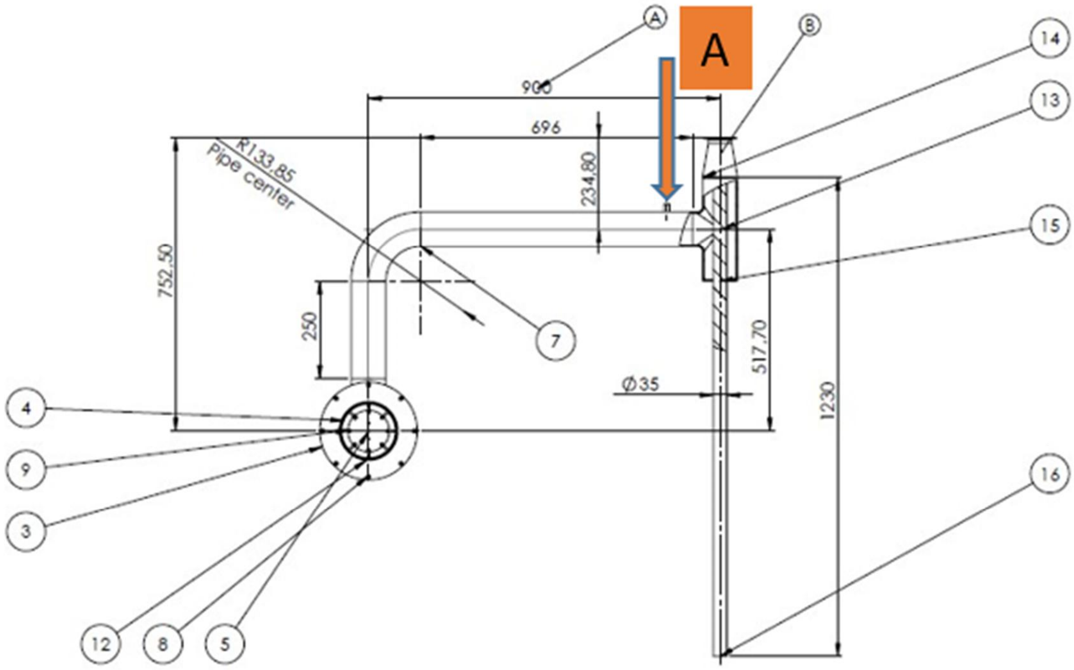

Figure 1. Location (A) for pressure and temperature measurement of incoming steam.

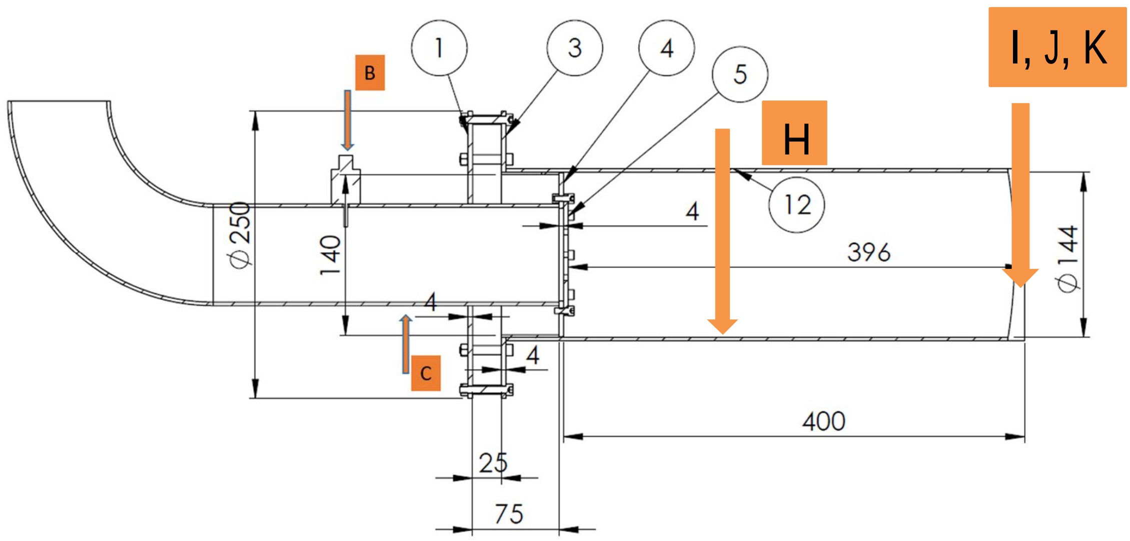

Figure 2. Temperature (B) and pressure (C) measurement of steam before the perforated flow plate, high frequency pressure measurement in the PC pipe (H) and temperature measurements at the outlet of the PC pipe (I, J, K).

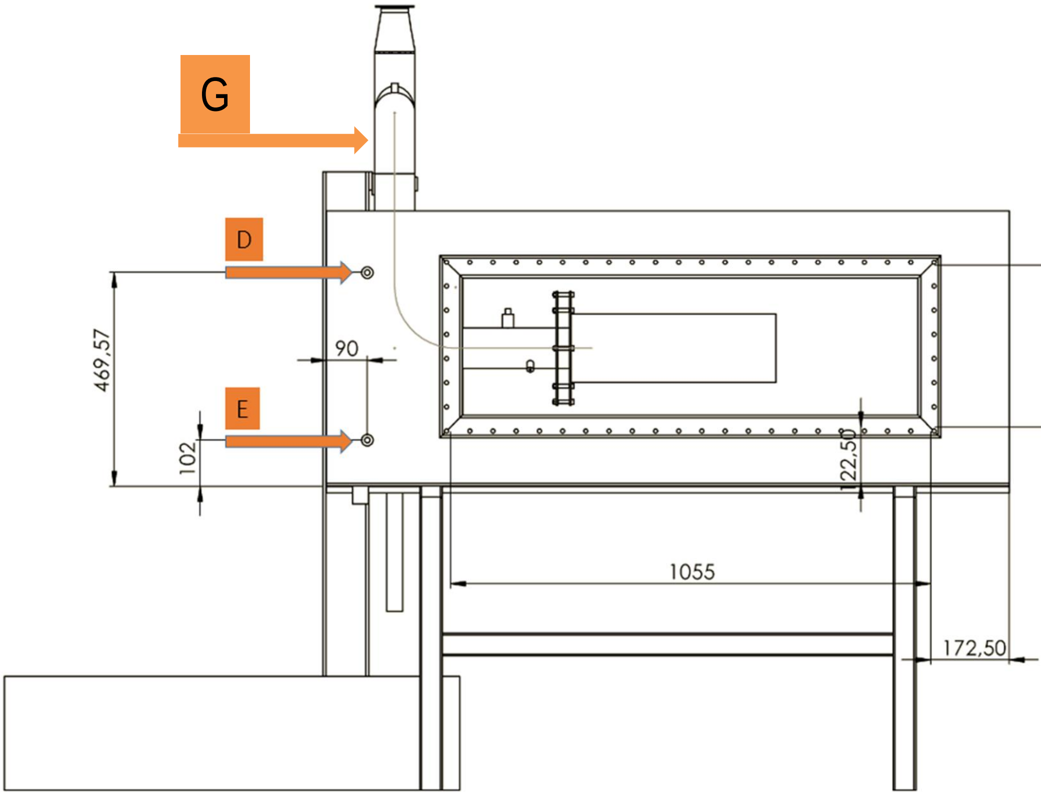

Figure 3. Temperature measurements of condensation pool water (D, E) and force measurement (G).

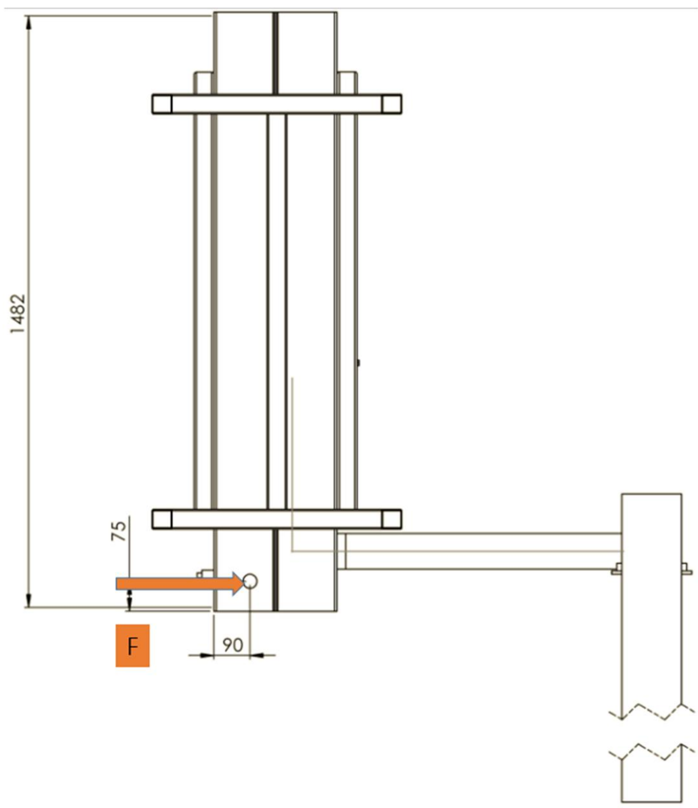

Figure 4. Location (F) of the DP transducer used for water level measurement of condensation pool.

Table 1. Instrumentation of the SEF-POOL facility

Figure code	Data code	Sensor type	Manufacturer/ type	Measurement frequency	Measurement range
A	P2600	Pres. transducer	Wikatronic	2 Hz	0-1 MPa
A	T2600	TC, K- type	Ø3 mm¹	70 Hz	0-200 °C
B	T2601	TC, K- type	Ø1 mm¹	70 Hz	0-200 °C
C	P2601	Pressure sensor²	Kyowa PHS-B	7 KHz	0-10 bar
D	T2605	TC, K- type	Ø3 mm¹	2 Hz	0-200 °C
E	T2606	TC, K- type	Ø3 mm¹	2 Hz	0-200 °C
F	D2600	DP transducer	Yokogawa EAJ110	2 Hz	0-7 kPa
G	X2600	Load sensor²	Kyowa LUX-B-50N	7 kHz	±50 N
H	P2602	Pressure sensor²	Kyowa PS-2KC³	7 kHz	0-0.2 MPa
I	T2602	TC, K- type	Ø 0.5 mm¹	70 Hz	0-200 °C
J	T2603	TC, K- type	Ø 0.5 mm¹	70 Hz	0-200 °C
K	T2604	TC, K- type	Ø 0.5 mm¹	70 Hz	0-200 °C

¹ Diameter of the sensing element
² These are used in conjunction with a Strain/Bridge Input Module
³ Type used depends on the range, the number denotes the measurement range in bars

Appendix D

PPOOLEX spray tests on mixing effects in condensation pool

Research Report
Lappeenranta University of Technology
Nuclear Engineering

INSTAB 4/2017

PPOOLEX spray tests on mixing effects in condensation pool

Lauri Pyy, Tatu Hovi, Markku Puustinen, Antti Räsänen, Eetu Kotro

Lappeenranta University of Technology
School of Energy Systems
Nuclear Engineering
P.O. Box 20, FIN-53851 LAPPEENRANTA, FINLAND
Phone +358 5 621 11

Lappeenranta, 30.1.2018

Open your mind. LUT.
Lappeenranta University of Technology

Research organization and address	Customer	
Lappeenranta University of Technology Nuclear Engineering P.O. Box 20 FIN-53851 LAPPEENRANTA, FINLAND	VYR / SAFIR2018 NKS SSM	
Project manager Markku Puustinen	**Contact person** Jari Hämäläinen (SAFIR2018) Christian Linde (NKS), Maria Agrell (NORTHNET)	
Diary code 125/322/2015	**Order reference** Drno SAFIR 11/2017	
Project title and reference code	**Report identification & Pages**	**Date**
SAFIR2018-INSTAB NKS-COPSAR	INSTAB 4/2014 33 p. + app. 9 p.	30.1.2018

Report title and author(s)

PPOOLEX SPRAY TESTS ON MIXING EFFECTS IN CONDENSATION POOL

Lauri Pyy, Tatu Hovi, Markku Puustinen, Antti Räsänen, Eetu Kotro

Summary

This report summarizes the results of the spray tests carried out in the PPOOLEX facility at LUT. The test facility is a closed stainless steel vessel divided into two compartments, drywell and wetwell. For the spray tests, the facility was equipped with a model of a spray injection system with four nozzles.

The main purpose of the tests was to study mixing of a thermally stratified pool with the help of spray injection from above. An additional goal was to obtain data, particularly PIV measurement data, for improving simulation models related to spray operation in CFD and system codes as well as to contribute to the development of the EMS and EHS models for sprays to be implemented in the GOTHIC code by KTH.

The initial thermally stratified situation was created in all the tests by injecting first warm and then cold water from the tap into the wetwell of the PPOOLEX facility. The thickness of the layer of warm water floating above a volume of cold water was about 200 mm. The temperature difference between the bottom and the top layer of the pool before the initiation of spray injection varied from 29 °C to 32 °C.

First, the cold spray water penetrated the water surface causing mixing in the top layers. Then an internal circulation process took place in the pool at the elevation of the thermocline between the cold and warm water as the cold and therefore more dense sprayed water pushed its way downwards. Most of the pool water volume mixed during the tests as the downwards penetrating mixing process continued. However, the tests were terminated before complete mixing of the pool was achieved.

For the analysis of the PIV results all the tests could be separated to three phases. In first phase, the movement of the particles is minor and thus the velocities are very small. The whole particle ensemble moves in unison and there are indications that there is no mixing involved. The second phase covers the time period when the optical environment does not suit to PIV measurement at all. The last phase starts after the mixing has occurred in the PIV measurement area and the optical environment enables PIV to be executed to some extent in a normal manner by averaging velocity fields. However, the dynamical characteristics of the flow makes the analysis of the results difficult and ambiguous.

Distribution

Members of the SAFIR2018 Reference Group 4

C. Linde (SSM), M. Agrell (SSM), P. Kudinov (KTH), I. G. Marcos (KTH), W. Villanueva (KTH), J. Hämäläinen (VTT), V. Suolanen (VTT), T. Pättikangas (VTT), I. Karppinen (VTT), S. Hillberg (VTT)

Principal author or Project manager	Reviewed by
Lauri Pyy, Research Scientist	Jani Laine, Research Scientist
Approved by	**Availability statement**
Heikki Purhonen, Research Director	SAFIR2018 limitations

Open your mind. LUT.
Lappeenranta University of Technology

Acknowledgement

NKS conveys its gratitude to all organizations and persons who by means of financial support or contributions in kind have made the work presented in this report possible.

Disclaimer

Open your mind. LUT.
Lappeenranta University of Technology

CONTENTS

1 INTRODUCTION 6
2 PPOOLEX TEST FACILITY 7
2.1 TEST VESSEL 7
2.2 WETWELL SPRAY SYSTEM 9
2.3 MEASUREMENT INSTRUMENTATION 10
2.4 DATA ACQUISITION 10
2.5 PIV MEASUREMENT SET-UP 10
3 TEST PROGRAM 12
4 TEST RESULTS 13
4.1 MIXING EFFECTS 13
4.2 PIV MEASUREMENTS 17
4.2.1 Detailed descriptions of test series 17
4.2.2 Results 20
5 SUMMARY AND CONCLUSIONS 31
6 REFERENCES 32

APPENDIX 1: PPOOLEX instrumentation
APPENDIX 2: Turbulence intensity calculation method

NOMENCLATURE

Symbols

A	Area
D	Pressure difference measurement
dt	time delay
F	Flow rate measurement
N	number of image pairs
P	Pressure measurement
S	Strain measurement
T	Temperature measurement
TI	Turbulence intensity
u	velocity
u_{rms}	turbulence strength
$\bar{u}$	mean velocity

Abbreviations

BWR	Boiling Water Reactor
CCD	Charge-Coupled Devices
CFD	Computational Fluid Dynamics
CONDEX	CONdensation EXperiments project
DCC	Direct Contact Condensation
ECCS	Emergency Core Cooling System
EHS	Effective Heat Source
EMS	Effective Momentum Source
EXCOP	EXperimental studies on COntainment Phenomena project
INSTAB	couplings and INSTABilities in reactor systems project
KTH	Kungliga Tekniska Högskolan
LOCA	Loss-Of-Coolant Accident
LUT	Lappeenranta University of Technology
MSLB	Main Steam Line Break
NKS	Nordic nuclear safety research
NORTHNET	NORdic nuclear reactor Thermal-Hydraulics NETwork
PACTEL	PArallel Channel TEst Loop
PIV	Particle Image Velocimetry
POOLEX	condensation POOL EXperiments project
PPOOLEX	Pressurized condensation POOL EXperiments test facility
PSP	Pressure Suppression Pool
RHR	Residual Heat Removal
SAFIR	SAfety of nuclear power plants - FInnish national Research programme
SRV	Safety/Relief Valve
SSM	Strålsäkerhetsmyndigheten
TC	ThermoCouple
VTT	Technical Research Centre of Finland
VYR	State nuclear waste management fund

1 INTRODUCTION

A pressure suppression pool (PSP) of a BWR reactor containment serves as a heat sink and steam condenser during a postulated main steam line break (MSLB) or loss of coolant accident (LOCA) inside the containment or during safety relief valve (SRV) opening in normal operations. It thus prevents containment pressure build-up when steam released from the reactor vessel is vented through the blowdown pipes (in case of MSLB and LOCA) or through the spargers (in case of SRV operation) to the pool. Furthermore, spray systems in the containment are designed to reduce pressure build-up in such accident scenarios, where steam is present in the gas space of the wetwell and/or in the drywell.

Different phenomena inside the drywell and wetwell compartments of BWR containment during steam discharge has been extensively studied in the PPOOLEX test facility at LUT and simulated with computer codes during recent years in the framework of the national research programmes on nuclear power plant safety (SAFIR, SAFIR2014) as well as via participation to NORTHNET RM3 and NKS research projects in co-operation with VTT and Kungliga Tekniska Högskolan (KTH). Research topics have included, for example, dynamic loads caused to PSP structures by direct contact condensation (DCC), behaviour of parallel blowdown pipes during the chugging flow mode, effect of blowdown pipe outlet design on structural loads, wall condensation in the drywell and development/break-up of thermal stratification in the PSP [1…10].

The current SAFIR2018/INSTAB project as well as the related NKS and SSM funded research efforts aim to broaden the database to cover experiments with SRV spargers, residual heat removal (RHR) system nozzles, strainers and containment spray systems. Calculation models and numerical methods including CFD and system codes are developed and validated on the basis of the PPOOLEX experiment results at VTT and KTH within the SAFIR2018, NKS, and SSM funded projects. Also analytical support is provided for the experimental part by pre- and post-calculations of the experiments.

As a result of steam venting into the suppression pool the coolant temperature in the pool gradually increases. With certain flow modes a thermally stratified condition could develop where the pool's surface temperature is higher than the pool bulk temperature. This leads to a reduction of the pool's pressure suppression capacity because the pool surface temperature determines the steam partial pressure in the wetwell gas space. An increase of the pool's surface temperature due to stratification can therefore lead to a significant increase in containment pressure if mixing of the pool coolant inventory fails [11]. Pool mixing can occur due to steam injection itself if the injection flow mode changes as a result of increasing or decreasing steam flow rate. Mixing can be achieved also with the help of plant systems designed for that purpose or as a result of water suction from the pool by the Emergency Core Cooling System (ECCS) pumps or water injection into the pool via the RHR system nozzles. Operation of spray system in the wetwell could also have an effect on the behaviour of a thermally stratified suppression pool. It has been suggested that mixing induced by spray had a role in the pressure drop in Fukushima Unit 3 where pressure build-up in the containment during the first 20 hours after station blackout was attributed to stratification in the pool.

KTH has developed the Effective Heat Source (EHS) and Effective Momentum Source (EMS) models for steam injection through a vertical pipe submerged in a pool and proposed them to be used for simulation of thermal stratification and mixing during a steam injection into a large pool of water [12]. These models have been implemented in GOTHIC® software and validated against

POOLEX and PPOOLEX tests carried out at LUT. Excellent agreement in averaged pool temperature and water level in the pool between the experiment and simulation has been achieved. The development of thermal stratification and mixing of the pool are also well captured in the simulations. The EMS and EHS models will be available to be implemented also in the APROS containment code for the calculation of phenomena related to pool stratification and mixing. At the moment KTH is improving the EHS and EMS models for blowdown pipes in order to reduce uncertainties and enhance accuracy in predictions as well as extending the models to SRV spargers and RHR system nozzles in order to be able to carry out comprehensive safety analysis of realistic transients in a BWR containment. In future the EMS/EHS models will be developed and validated also for a spray system operation in the wetwell.

Suitable experimental data is limited for validation of the EHS and EMS models. So far, the only available and sufficiently detailed experimental vent pipe data are the POOLEX/PPOOLEX steam discharge experiments with blowdown pipes. The PPOOLEX database was broadened to cover SRV spargers and RHR system nozzles in the test series carried out in 2014, 2015 and 2016 [13, 14, 15 and 16]. A spray injection system was constructed and installed to the wetwell compartment of the PPOOLEX facility at the end of 2016 and preliminary wetwell spray tests were carried out in January 2017. Mixing of a thermally stratified pool with the help of spray injection from above was of interest [17]. In addition, verification data for improving simulation models in CFD and system codes at VTT and KTH was provided.

Studies on the mixing effects of spray injection in condensation pool was continued in the spring/summer of 2017 by conducting a series of spray tests in PPOOLEX. The goal was to obtain verification data to be used in the development work of the EHS/EMS models. For this purpose, the PIV measurement system was used to help define flow fields in the mixing region. In this report these spray tests in PPOOLEX are described. Chapter two gives a short description of the test facility and its measurements. The test parameters, initial conditions and test procedure are introduced in chapter three. The test results are presented and discussed in chapter four with the help the traditional measurements as well as with the help of the PIV measurements. Chapter five summarizes the findings of the test series.

2 PPOOLEX TEST FACILITY

The PPOOLEX test facility was taken into use at LUT in the end of 2006. PPOOLEX models the containment of a BWR plant. During the years, the facility has gone through several modifications and enhancements as well as improvements of instrumentation. For the spray tests described in this report, the facility was equipped with a model of a wetwell spray system with four nozzles. The PPOOLEX facility is described in more detail in reference [18]. However, the main features of the facility and its instrumentation are introduced below.

2.1 TEST VESSEL

The PPOOLEX facility consists of a wetwell compartment (condensation pool), drywell compartment, inlet plenum and air/steam-line piping. An intermediate floor separates the compartments from each other. Usually a route for gas/steam flow from the drywell to the wetwell is created by a vertical blowdown pipe attached underneath the floor. During the sparger and spray tests the drywell compartment was, however, bypassed i.e. steam was blown directly into the wetwell via the sparger pipe.

The main component of the facility is the ~ 31-m3 cylindrical test vessel, 7.45 m in height and 2.4 m in diameter. It is constructed from three plate cylinder segments and two dome segments. The test facility is able to withstand considerable structural loads caused by rapid condensation of steam. The dry and wetwell sections are volumetrically scaled according to the compartment volumes of the Olkiluoto containment (ratio approximately1:320). There are several windows for visual observation in both compartments. A DN100 (∅ 114.3 x 2.5 mm) drainpipe with a manual valve is connected to the vessel bottom. A relief valve connection is mounted on the vessel head. The removable vessel head and a manhole (DN500) in the wetwell compartment wall provide access to the interior of the vessel for maintenance and modifications of internals and instrumentation. The drywell is thermally insulated.

A sketch of the test vessel is shown in Figure 1. Table 1 lists the main dimensions of the test facility compared to the conditions in the Olkiluoto plant.

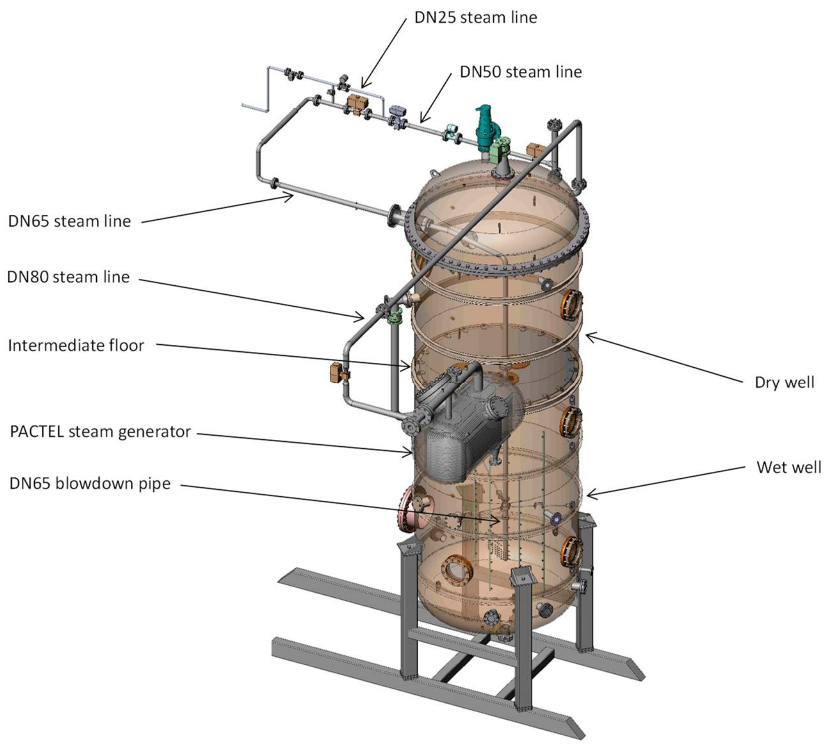

Figure 1. PPOOLEX test vessel.

Table 1. Test facility vs. Olkiluoto 1 and 2 BWRs

	PPOOLEX test facility	Olkiluoto 1 and 2
Number of blowdown pipes	1-2	16
Inner diameter of the blowdown pipe [mm]	214.1	600
Suppression pool cross-sectional area [m^2]	4.45	287.5
Drywell volume [m^3]	13.3	4350
Wetwell volume [m^3]	17.8	5725
Nominal water volume in the suppression pool [m^3]	8.38*	2700
Nominal water level in the suppression pool [m]	2.14*	9.5
Pipes submerged [m]	1.05	6.5
A_{pipes}/A_{pool}x100%	0.8 / 1.6**	1.6

* Water volume and level can be chosen according to the experiment type in question. The values listed in the table are based on the ratio of nominal water and gas volumes in the plant.
** With one / two blowdown pipes.

2.2 WETWELL SPRAY SYSTEM

For the spray tests, the PPOOLEX facility was equipped with a model of a wetwell spray system. (Figure 2). It consists of four spray nozzles, an injection pipeline and supporting structures. Each spray nozzle is at a 0.6 m distance from the vessel wall. The nozzles are in a square lattice and about 0.85 m from each other.

Figure 2. Spray system with four nozzles in PPOOLEX wetwell.

In 2015, single spray nozzle tests with different capacity full cone nozzles were carried out in an open test environment in order to develop a measurement procedure for determining droplet size and velocity distributions of the spray jets [19]. The shadowgraphy application of the PIV measurement system was used. The model of the spray nozzles installed to PPOOLEX in 2016 is B1/2HH-40 FULLJET. A similar nozzle was tested also in the single spray nozzle tests in 2015.

The orifice diameter of the nozzle is 6.2 mm. The nozzle properties provided by the manufacturer are presented in Table 2 and Table 3 [20].

Table 2. Capacity of the spray nozzle used in the tests with different pressure values

Pressure over nozzle [bar]	0.4	0.5	0.7	1.5	3.0	6.0	7.0	10.0
Capacity [l/min]	11.9	13.1	15.2	21.0	29.0	39.0	44.0	52.0

Table 3. Spray angle of the nozzle used in the tests with different pressure values

Pressure over nozzle [bar]	0.5	1.5	6.0
Spray angle [deg]	88	91	83

Water for the PPOOLEX spray system is taken from the water-supply pipe of the laboratory and led via a pipeline and flexible hose, connected to a lead-in close to the pool bottom, to the spray header. In the header, water is divided to the four nozzles. Each nozzle has its own manual shut-off valve. Injection flow through the nozzles was balanced with those valves before the system was lifted up and attached with supporting rods to the wall of the wetwell compartment. Spray water flow and temperature are measured in the injection pipeline outside the pool.

2.3 MEASUREMENT INSTRUMENTATION

The applied instrumentation depends on the experiments in question. Normally, the test facility is equipped with several thermocouples (T) for measuring steam, pool water and structure temperatures and with pressure transducers (P) for observing pressures in the drywell, inside the blowdown pipes, at the condensation pool bottom and in the gas space of the wetwell. Steam flow rate is measured with a vortex flow meter (F) in the steam line. Flow rate of the spray water is measured with magnetic flow meter installed to the injection pipeline. Additional instrumentation includes, for example, strain gauges (S) on the pool outer wall and valve position sensors.

Four trains of temperature measurements (thermocouples T4100…T4113, T4200…T4219, T4300…T4319 and T4400…T4413) were installed in the pool below the water level to be used for detecting vertical temperature distribution in the thermal stratification/mixing tests with the sparger pipe. Since these vertical trains with TCs suit well for detecting the behaviour of the pool also in the spray tests, no extra temperature measurements were added to PPOOLEX at this time except the one used for measuring spray injection water temperature. In addition, the 6x7 grid of temperature measurements (thermocouples T4000–T4056) in front of the injection holes of the sparger head can be used for determining mixing effects also during the spray tests.

Figures in Appendix 1 show the locations of the PPOOLEX measurements during the spray test series and the table in Appendix 1 lists their identification codes and other details.

2.4 DATA ACQUISITION

National Instruments PXIe PC-driven measurement system was used for data acquisition. The system enables high-speed multi-channel measurements. The maximum number of measurement channels is 64 with additional eight channels for strain gauge measurements. The maximum recording capacity depends on the number of measurements and is in the region of three hundred thousand samples per second. Measurement software was LabView 2015. The data acquisition systems measure signals as volts. After the tests, the voltage readings are converted to engineering units with conversion software. The used measurement frequency of LabView was 20 Hz. The data acquisition system is discussed in more detail in reference.

2.5 PIV MEASUREMENT SET-UP

PIV measurements were conducted in the spray tests in order to produce velocity field data. The PIV system's laser is a Neodym-YAG double-cavity laser. The two-pulsed lasers emit the beam in infrared range at 1064 nm and they are polarization combined. A second harmonic generator is used to convert the beam to visible range at 532 nm. The appropriate thickness of the light sheet is achieved with the two spherical lenses. The system's cameras are Imager Pro X 4M CCD cameras having progressive-scan technology with a dual frame-technique for cross correlation. The CCD sensors are cooled with Peltier element to +10°C to reduce background noise. With remote controlled focus rings, the focus and aperture of the camera lenses can be controlled with computer software. The system has also a remote controlled Scheimpflug mount, which allows all areas of the image plane to be in focus. For collecting PIV recording and other data the equipment has a system computer. The system utilizes DaVis software solution for image acquisition and analysis of flow fields in both 2D and 3D cases.

Setting up the PIV system inside the PPOOLEX test facility is challenging in many ways, not least due to the small size of the viewing windows originally reserved for the PIV laser and cameras. For the spray tests presented in this report, the test arrangement was changed so that the larger viewing windows of the wetwell could be utilized in the PIV measurements. This was achieved by slightly increasing the amount of pool water from the previous tests and thus positioning the transition region between cold and hot water on an optimal elevation in the pool from the PIV measurement point of view. This means that the middle point in vertical direction of the PIV measurement was at about 1455 mm elevation in SPR-T4, SPR-T5 and SPR-T6. And at about 1440 mm elevation in SPR-T7. Due to the support structures of the pool internals, the calibration process was challenging but could be conducted successfully and the laser sheet could be lined up to the measurement plane.

In first three tests, the measurement plane was about 0.5 m away from the pool centre axis and the field-of-view (FOV) area was about 95x95 mm. In the fourth test, the measurement plane was in the pool centre and the FOV area was about 151x151 mm. Two-camera stereo PIV measurements were conducted in the first test and single-camera planar measurements in the three remaining tests. A horizontal cross section view of the measurement set-up scheme for the three first test cases, SPR-T4, SPR-T5 and SPR-T6, is presented in Figure 3.

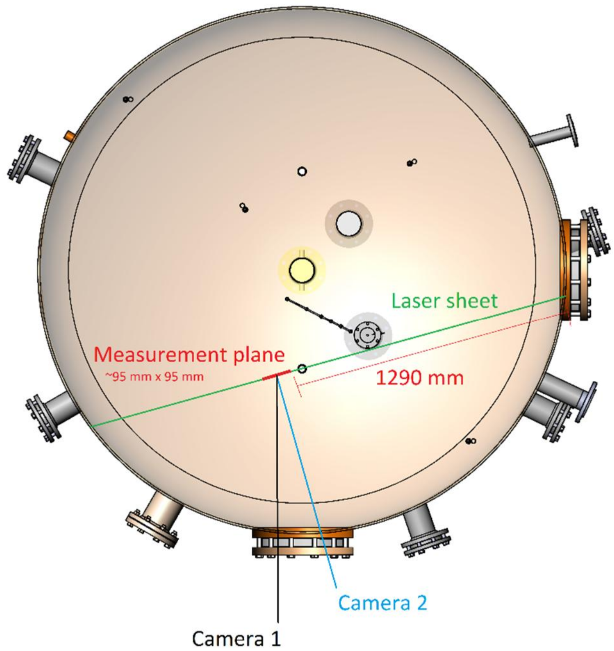

Figure 3. A schematic presentation of the PIV measurement set-up in SPR-T4, SPR-T5 and SPR-T6.

Vertically the measurement plane located from 1410 mm to 1500 mm from the vessel bottom. The front end of the measurement plane was approximately 1290 mm from the laser window. The camera setup was chosen in a way that camera 2 could be used individually in planar mode as the measurement plane could only be placed in one position within the PPOOLEX due to the inner structures. Camera 1 viewing axel was nearly perpendicular to the observation window but at an angle towards the laser sheet.

Based on gathered experience from the SPR-T4, SPR-T5 and SPR-T6 tests it was decided that the measurement set-up is changed for the last test by moving some of the inner structures so that the measurement plane can be positioned to the center of the pool. The measurement set-up for the SPR-T7 test is presented in the Figure 4.

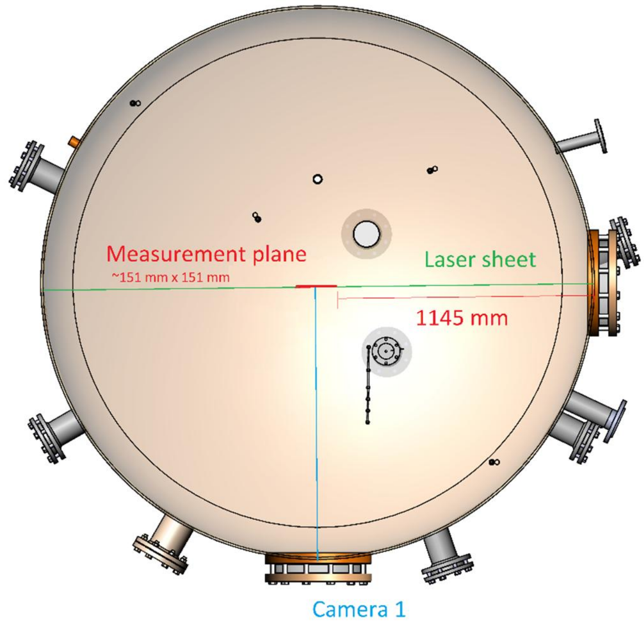

Figure 4. A schematic presentation of the PIV measurement set-up in SPR-T7.

3 TEST PROGRAM

Four spray tests labelled as SPR-T4, SPR-T5, SPR-T6 and SPR-T7 were carried out in the PPOOLEX facility in June 2018. Interplay between suppression pool behaviour and the spray system was of interest. The main purpose of the tests was to further study mixing of a thermally stratified pool with the help of spray injection from above. An additional goal was to obtain data, particularly PIV measurement data, for improving simulation models related to spray operation in CFD and system codes as well as to contribute to the development of the EMS and EHS models for sprays to be implemented in the GOTHIC code by KTH.

The initial thermally stratified situation was created in all the tests by injecting first warm and then cold water from the tap into the wetwell of the PPOOLEX facility. The injection of cold water was done cautiously to prevent the warm and cold water from mixing. The aim was to create about 200 mm thick layer of warm water, which floats above a volume of cold water.

In SPR-T4, SPR-T5 and SPR-T7, an initial water level of about 1.8 m was used but in SPR-T6, the water level was reduced to about 1.5 m. This means that in SPR-T6 the thermocline between the hot and cold water was around the 1.3 m elevation and in the other tests at about 1.6 m elevation. The temperature difference between the bottom and the top layer of the pool before the initiation of spray injection varied between 29-32 °C depending on the test in question (pool bottom temperature 13-14 °C and surface temperature 42-45 °C).

The same spray nozzles were used throughout the test series. In all four tests, the flow rate of spray injection was the maximum available from the water supply system of the laboratory i.e. about 122-128 l/min. When divided equally to the four spray nozzles it gives 30.5-32.0 l/min per nozzle. That is a few l/min under the theoretical capacity with the 0.55 MPa pressure difference over the nozzle that prevailed in these PPOOLEX spray tests. In SPR-T4, SPR-T5, SPR-T6 and SPR-T7 the spray injection continued for about 1315 s, 2163 s, 1379 s and 1915 s and during the spray operation, the pool water level increased about 610 mm, 1050 mm, 600 mm and 880 mm, respectively. Water as cold as possible was taken from the tap for the spray in all the tests. At the initialization of the spray injection, the water temperature was about 21-24 °C but dropped very soon to about 12 °C and remained there for the rest of the injection.

The tests were started from atmospheric pressure conditions in PPOOLEX. There was no pressure increase during the tests because the valve in the pressure balancing line between the drywell and wetwell as well as the valve to atmosphere on top of the drywell were open.

The main parameters of the SPR-T4, SPR-T5, SPR-T6 and SPR-T7 tests are listed in Table 4.

Table 4. Parameter values of the spray tests SPR-T4, SPR-T5, SPR-T6 and SPR-T7 in PPOOLEX

Test	Initial pool water level [m]	Initial pool water temperature bottom/surface [°C]	Spray start time [s]	Spray injection flow rate [l/min]	Spray water temperature [°C]	Final pool water level [m]
SPR-T4	1.87	~13/42	230	~128…125	~12…11	2.48
SPR-T5	1.80	~13/44	115	~128…127	~12…11	2.85
SPR-T6	1.48	~13/45	43	~125…122	~13…12	2.08
SPR-T7	1.78	~14/45	913	~124	~15…12	2.66

4 TEST RESULTS

The following chapters give a more detailed description of the SPR-T4, SPR-T5, SPR-T6 and SPR-T7 tests and present the observations. The main interest was in trying to get useful PIV measurement data and therefore the test parameters were varied very little. As a result, thermal hydraulic behaviour in the tests was much alike. First, the general behaviour in the tests, particularly the mixing efficiency due to spray injection, is presented with the help of the traditional measurements and then the findings from the PIV measurements are introduced in the following chapters.

Both the four vertical trains of temperature measurements and the grid of TCs in front of the sparger head can be used for evaluating how deep the mixing effect of spray injection penetrates. The exact locations of the TCs in the trains and grid can be found from the drawings presenting PPOOLEX instrumentation in Appendix 1.

4.1 MIXING EFFECTS

In the tests, the initial stratified condition was artificially created by injecting first warm and then cold water from the tap into the wetwell of the PPOOLEX facility. As a result, there was a layer of warm water with the thickness of about 200 mm on top of the volume of cold water before the spray injection was started. Figure 5 shows the spray injection volumetric flow rate and spray water temperature in the SPR-T5 test. It can be seen that the temperature of spray injection water (T3611) is initially about 24 °C because it warms up to the temperature of the surroundings while stagnant in the pipeline but drops fast to about 12 °C as the spray injection is started.

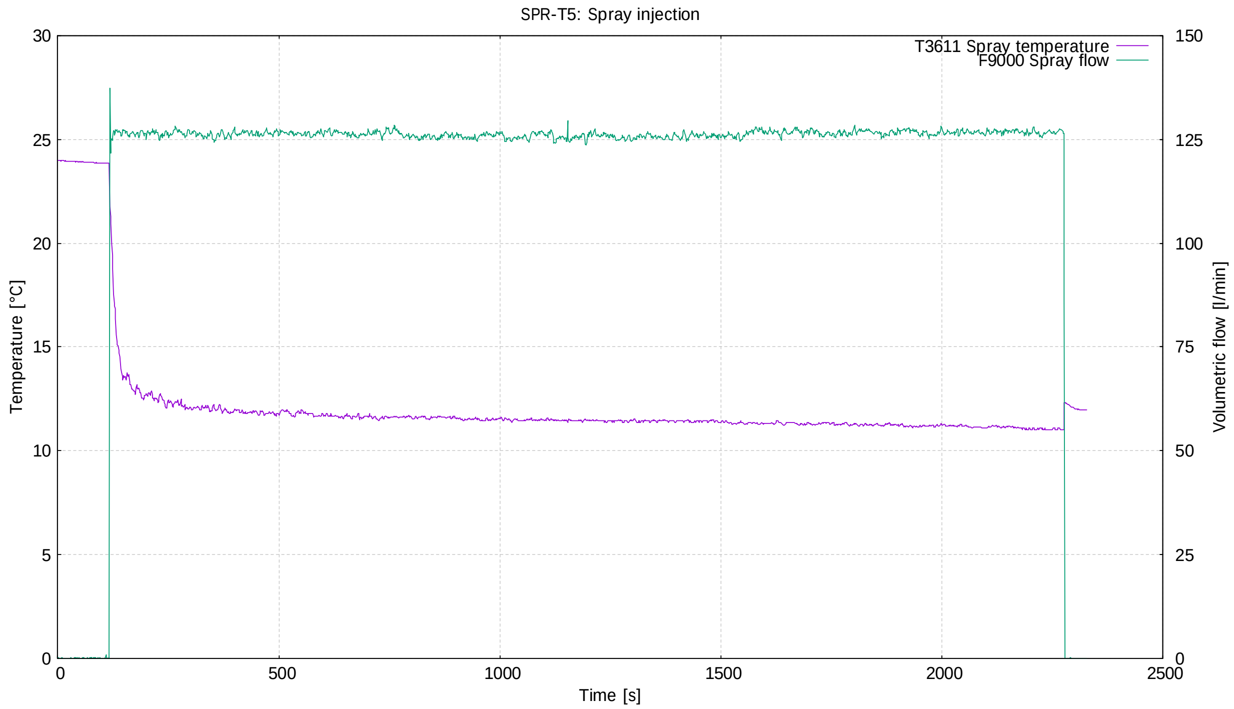

Figure 5. Spray water volumetric flow rate and temperature in SPR-T5.

Figure 6 presents the development of temperature distribution of pool water in SPR-T5 as measured by the TCs in the grid in front of the sparger head. The measurements are from the vertical line farthest away of the sparger head. The elevation of each measurement is expressed as a distance from the bottom horizontal rod of the grid; see Appendix 1 for more details.

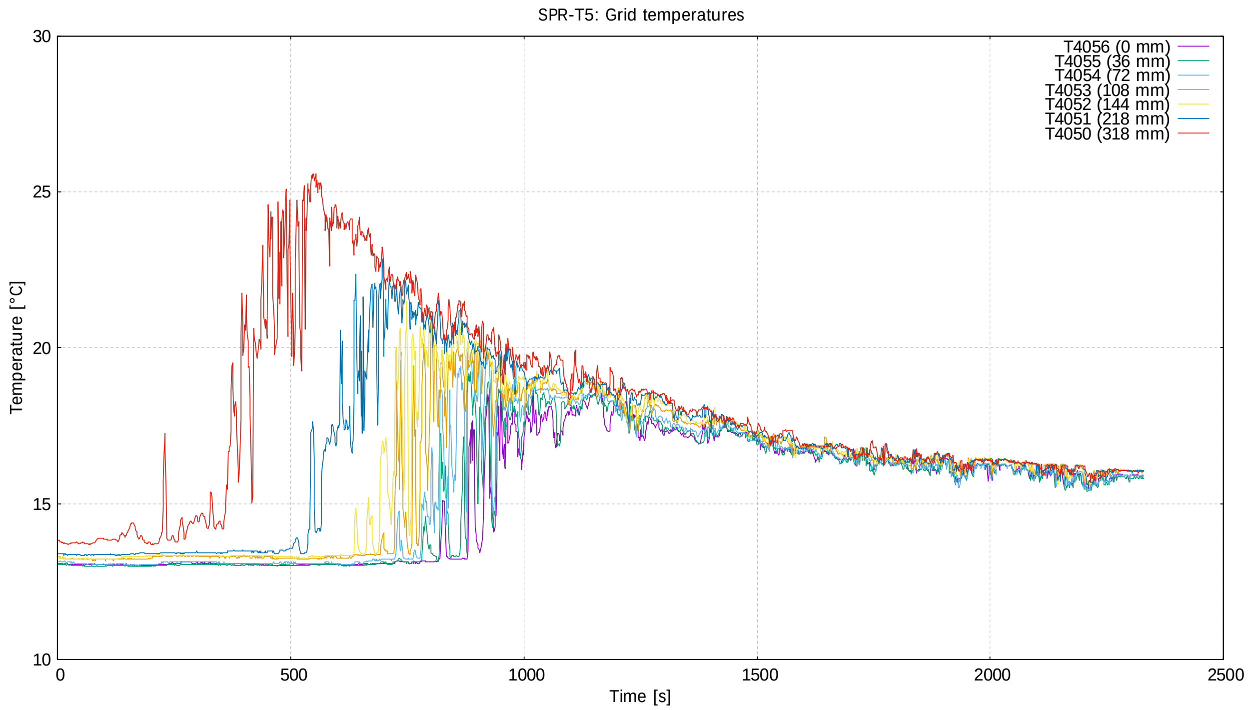

Figure 6. Temperature distribution across the TC grid in the SPR-T5 test.

Before the spray injection was started (at 115 s) all the TCs in the grid indicated cold temperatures because the volume of warm water was located above the grid. Only the topmost T4050 at the elevation of 318 mm had a slightly higher temperature.

When the spray injection started, the top TC (T4050) soon started to show increasing temperatures. This indicates that the thermocline between the cold and warm water started to disappear as a result some kind of internal circulation process in the pool. However, this behaviour was oscillating in nature and it took sometime before the peak temperature value was reached. As the test progressed, also the other TCs in the grid started to indicate increasing temperatures. At the same time, the topmost TC had already a decreasing trend. After about 1200-1300 seconds of spray injection, the curves of all the TCs had practically united indicating a mixed condition at the elevations covered by the TC grid. For the rest of the test the decreasing trend of these temperature curves continued. The behaviour of the measurements of the TC grid in the SPR-T4 and SPR-T7 tests was similar to the behaviour described above with the exception of slightly different timing of the events.

In the SPR-T6 test, the behaviour of the TCs in the grid differ from that in the SPR-T4, SPR-T5 and SPR-T7 because the initial pool water level was lower (1.48 m). Figure 7 shows the grid measurements in SPR-T6. Now the volume of warm water was mostly at the elevation of the grid. The different initial temperatures of the TCs in the grid reveal that there was not a sharp thermocline between the cold and warm water volumes, where the water temperature would have abruptly changed from cold to warm, but instead the shift was more or less continuous in nature.

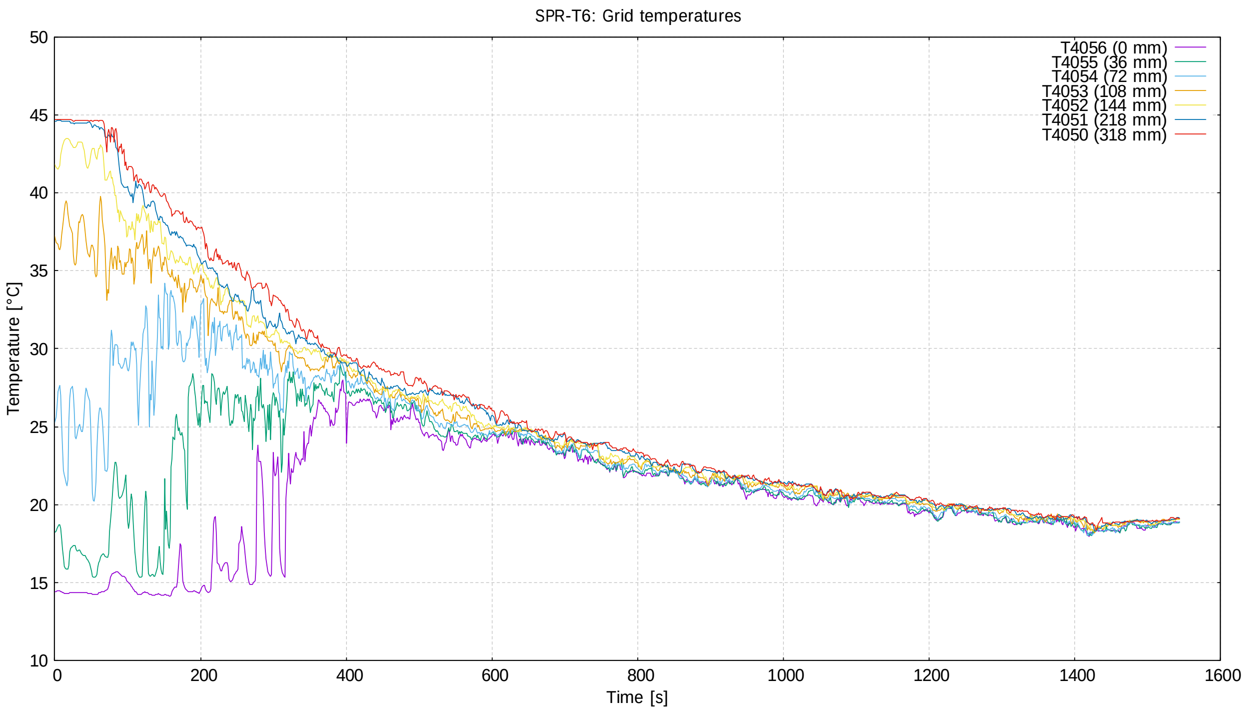

Figure 7. Temperature distribution across the TC grid in the SPR-T5 test.

When the spray injection started (at 43 s), the four top measurements started to indicate decreasing temperatures as the cold spray water penetrated the surface as well as caused some mixing circulations in the top layers. The rest three TCs showed an increasing trend accompanied with oscillations. Thus, an internal circulation process took place in the pool at the elevation of the thermocline between the cold and warm water when cold and therefore more dense sprayed water pushed its way downwards. The curves with decreasing and increasing trends practically united after 400 seconds into the test indicating a mixed condition at the elevations covered by the TC grid and then started a common decreasing trend until the end of the test.

All the tests continued for some time after the grid temperature measurements indicated a mixed situation. However, the whole pool was not mixed at the end of the tests. This can be seen from the temperature curves of a vertical TC measurement train presented in Figure 8. The elevation of each TC is from the pool bottom.

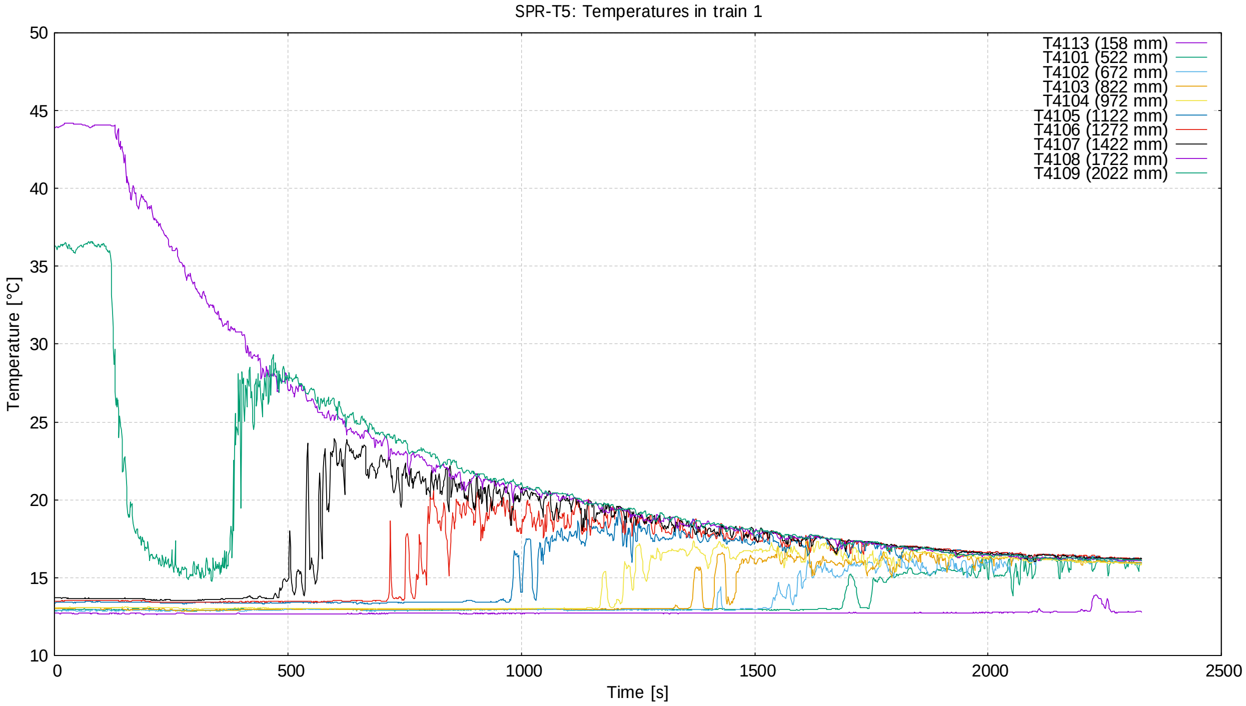

Figure 8. Temperature distribution over the pool water volume in the SPR-T5 test.

The topmost measurement (T4109) at the elevation of 2022 mm was above the water surface in the beginning of the test. As soon as the spray injection started, it indicated a sharp drop in temperature because the spray cooled down the gas space of the wetwell effectively. Also the measurement just below the pool surface (T4108) and thus initially in the warm water region indicated cool down as soon as the spray injection was started. When the water level rose above the T4109 measurement, it showed an increase in temperature and united with the T4108 curve.

The rest of the TCs plotted in Figure 8 were initially in the cold water region. They indicate the same kind of downwards penetrating mixing process as the TCs in the grid presented earlier with the exception of the TC at the lowest elevation. First, they show an increasing trend with oscillations one after another and then a decreasing trend after they join the decreasing curve of the T4108 measurement. The TC close to the pool bottom (T4113) remains at its original temperature thus verifying that complete mixing was not achieved during the test. However, it can be speculated that the whole water volume could have been mixed if the tests had been continued for a longer period of time. In these tests, the aim was to study the behaviour in the top layers as well as at the elevation of the thermocline with PIV and therefore the tests were not continued to full mixing.

Figure 9 presents the vertical temperature profile of the pool at certain points of time from the initiation of spray injection at 115 s onward in the SPR-T5 test. It can be seen that the temperatures even out i.e. temperatures at the top layers decrease while temperatures elsewhere in the pool, with the exception of the very bottom, increase. At the end of the test (2270 s) the vertical temperature profile is practically a straight line apart from the bottom measurement elevation. Figure 9 also shows how the cold spray water first cools the topmost layers and how the internal circulation induced by density differences then starts to mix the pool deeper and deeper.

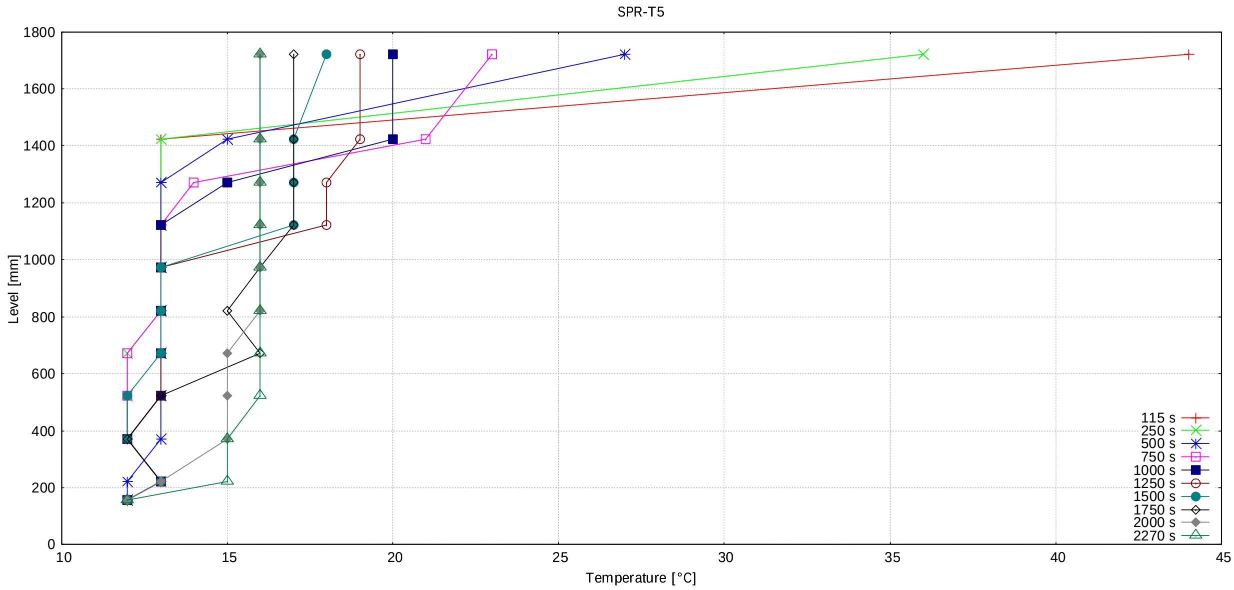

Figure 9. Vertical temperature profile in the pool in the SPR-T5 test.

In all the tests, the behaviour shown by the TC trains is almost identical. In SPR-T6, the lower initial water level means that the measurement T4108 also is first above the water level but otherwise the behaviour over the whole water volume matches that of the other tests.

4.2 PIV MEASUREMENTS

In Chapter 2.5 the two different measurement set-ups for the test series are presented. The first set-up (Figure 3) was initially planned to serve as a hybrid set-up that would allow stereo-PIV and planar-PIV measurements to be executed. The SPR-T4 test was performed in stereo-PIV and the latter SPR-T5 and SPR-T6 tests in planar mode.

Seeding particles were fed into the wetwell water by using two routes. In SPR-T4, the seeding was spread to the pool water when the filling of the pool from bottom up was done. In SPR-T5, the seeding was spread via the spray nozzles only. There were also remnants from the previous test in the pool water but with very low seeding density. In SPR-T6 and later in SPR-T7, both methods of seeding were used but most of the seeding particles were spread to pool water during the fill-up process and a smaller amount through the spray nozzles during spray injection.

4.2.1 Detailed descriptions of test series

4.2.1.1 SPR-T4

In SPR-T4, five individual PIV measurements were conducted. The main parameters for the test series are presented in Table 5.

Table 5. Main PIV measurement parameters of SPR-T4

Test series name	dt [µs]	N [-]
SPR-T4-1	60000	350
SPR-T4-2	60000	350
SPR-T4-3	60000	350
SPR-T4-4	60000	350
SPR-T4-5	20000	350

Measuring frequency was 7 Hz for the whole series. When using stereo-PIV arrangement the system computer can only capture roughly 350 image pairs before RAM gets full and the future image pairs are taken when memory is available. The time delay, dt, is changed according to movement of the particles but cannot be adjusted within the measurement.

In stereo-PIV arrangement, the particle images are not similar due to the camera placement. Camera 2 with perpendicular angle to the laser sheet had slightly bigger particles in size. Camera 1 with perpendicular angle to the observation window but an angle towards the light sheet had sharper but elongated particles. As stated before, the optical environment was not optimal for PIV.

4.2.1.2 SPR-T5

In SPR-T5, four individual PIV measurements were conducted and the main parameters are presented below in Table 6.

Table 6. Main PIV measurement parameters of SPR-T5

Test series name	dt [µs]	N [-]
SPR-T5-1	60000	1000
SPR-T5-2	25000	1000
SPR-T5-3	30000	1000
SPR-T5-4	20000	1000

In SPR-T5, camera 1 was shut off and the system was used in planar-PIV arrangement. 1000 image pairs were captured. The particles were injected through the spray nozzles for comparison.

4.2.1.3 SPR-T6

In SPR-T6, only two individual PIV measurements were conducted and the main parameters are presented in Table 7.

Table 7. Main PIV measurement parameters of SPR-T6

Test series name	dt [µs]	N [-]
SPR-T6-1	60000	1000
SPR-T6-2	20000	1000

The main difference to SPR-T5 was that the water surface and thus also the top of the hot water layer was ca. at 1500 mm measured from the bottom of the vessel. This means that the whole PIV measurement area was also situated vertically at the hot water region in the beginning of the test. The test was also shorter in length, approximately 1422 s.

4.2.1.4 SPR-T7

In SPR-T7, five individual PIV measurements were conducted and the main parameters are presented in Table 8.

Table 8. Main PIV measurement parameters of SPR-T7

Test series name	dt [μs]	N [-]
SPR-T7-1	65000	1000
SPR-T7-2	65000	1000
SPR-T7-3	35000	1000
SPR-T7-4	40000	1000
SPR-T7-5	20000	1000

As the previous stereo and planar-PIV setups were not considered ideal for PIV measurements in conditions prevailing during the spray tests, the thermocouple grid in the pool was turned to another position in order to allow the PIV measurement plane to be located in the pool center and thus achieve perpendicular angle for the laser sheet and the observation window. This enhanced the quality of the particle images.

In Figure 10, a "road map" of all the PIV test series indicating how they were placed time wise after the activation of spray nozzles is presented.

time since the starting of sprays in wet well										
0 s ->	100 s ->	300 s ->	400 s ->	500 s ->	800 s ->	1100 s ->	1400 s ->	1500 s ->	1700 s ->	1800 s ->
T4-1 20 s - 70 s		**T4-2** 312 s - 362 s		**T4-3** 570 s - 620 s	**T4-4** 845 s - 895 s	**T4-5** 1158 s - 1208 s				
T5-1 3 s - 146 s						**T5-2** 1184 s - 1327 s		**T5-3** 1510 s - 1654 s		**T5-4** 1808 s - 1951 s
	T7-1 167 s - 310 s		**T7-2** 467 s - 610 s			**T7-3** 1114 s - 1257 s	**T7-4** 1447 s - 1590 s		**T7-5** 1739 s - 1882 s	
T6-1 1 s - 144 s					**T6-2** 889 s - 1032 s					

Figure 10. A timeline of all conducted PIV measurement sequences in the spray tests.

In Table 9 below, a detailed description of the quality of the particle images within the individual test sequences is given.

Table 9. A quick overall analysis of the particle images

Test series name	Time since spray start	Description
T6-1	1 s – 144 s	*Note 1
T5-1	3 s – 146 s	Ok after 591 image pairs (~87,4 s)
T4-1	20 s – 70 s	Ok
T7-1	167 s – 310 s	Ok up to initial 300 image pairs (167 s – 217 s), after that aberrations (~217 s – 310 s)
T4-2	312 s – 362 s	Very poor
T7-2	467 s – 610 s	Very poor
T4-3	570 s – 620 s	Very poor
T4-4	845 s – 895 s	Poor, aberrations
T6-2	889 s - 1032 s	Poor, aberrations
T7-3	1114 s – 1257 s	Poor, aberrations
T4-5	1158 s – 1208 s	Poor, aberrations
T5-2	1184 s – 1327 s	Poor, aberrations
T7-4	1447 – 1590 s	**Note 2
T5-3	1510 s – 1654 s	Ok, bit blurry
T7-5	1739 s – 1882 s	Ok
T5-4	1808 s – 1951 s	Ok, bit blurry

**Note 1: Laser is lost after 22 images due to the system failure*
***Note 2: Wrong dt as it cannot be adjusted during the test*

In all the spray tests, there was a time period in the middle when the optical environment was very poor for the PIV measurements to succeed. Results were only obtained from the beginning and at the end of the tests. In T5-3 and T5-4, using the camera in an angle towards the window made the particle images bit more blurry. In the following analysis of the PIV results those measurement sequences, where the optical environment was poor, are omitted.

4.2.2 Results

In SPR-T4-1, SPR-T5-1 and SPR-T7-1, the measured velocities from the measurement area were in the range of mm/s. An example of an averaged velocity field from sequence SPR-T7-1 of the first 300 image pairs before optical aberrations is presented in the Figure 11.

As it can be seen from Figure 11, the velocities are ranging from 3 mm/s to almost 0 mm/s. When inspecting the instantaneous vector field it can be noticed that velocities are in the same range and they are randomly spread to all directions. After initial presentation of the results in the SAFIR RG4 meeting and discussion based on them it was decided that it is more beneficial to focus on turbulence intensity than on averaged velocity fields. For this reason, a script in Python was written and it is presented more in detail in Appendix 2.

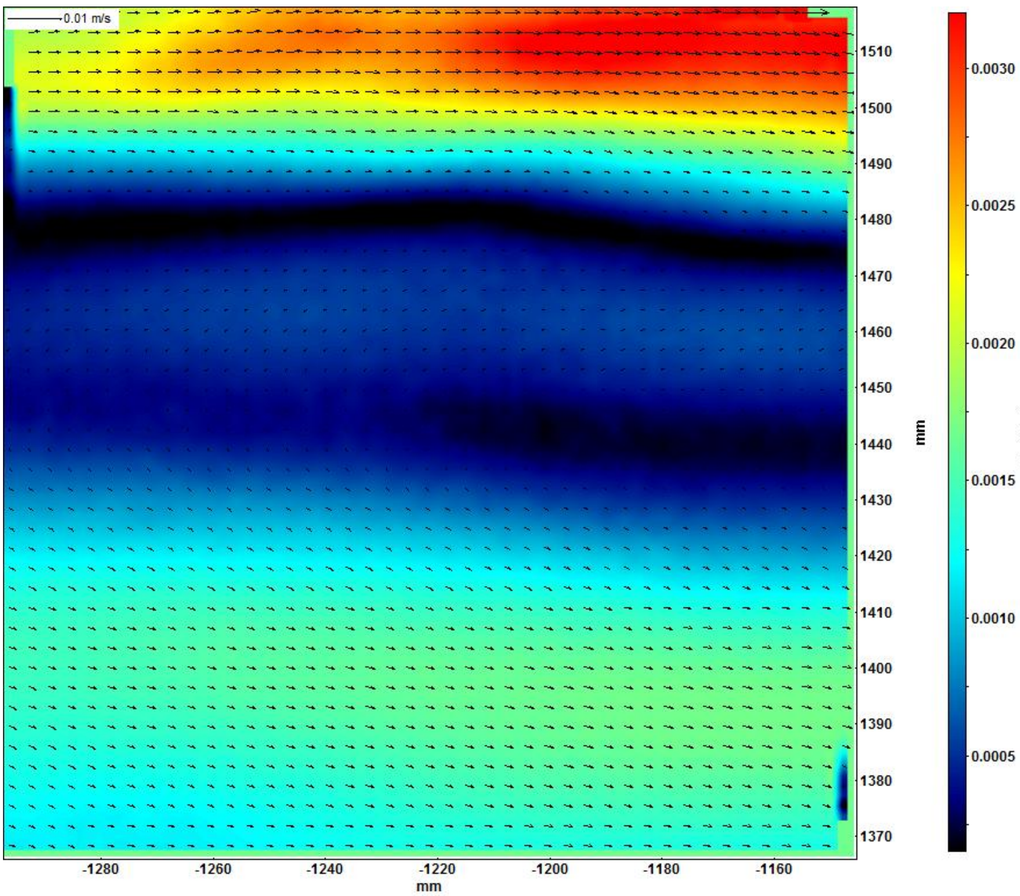

Figure 11. Averaged velocity field of PIV measurement sequence SPR-T7-1, 1-300.

After finishing the script and analysing the results with it, it was found that turbulence intensities were enormous in the beginning of SPR-T4-1, SPR-T5-1 and SPR-T7-1. The corresponding turbulence intensity field is presented in Figure 12.

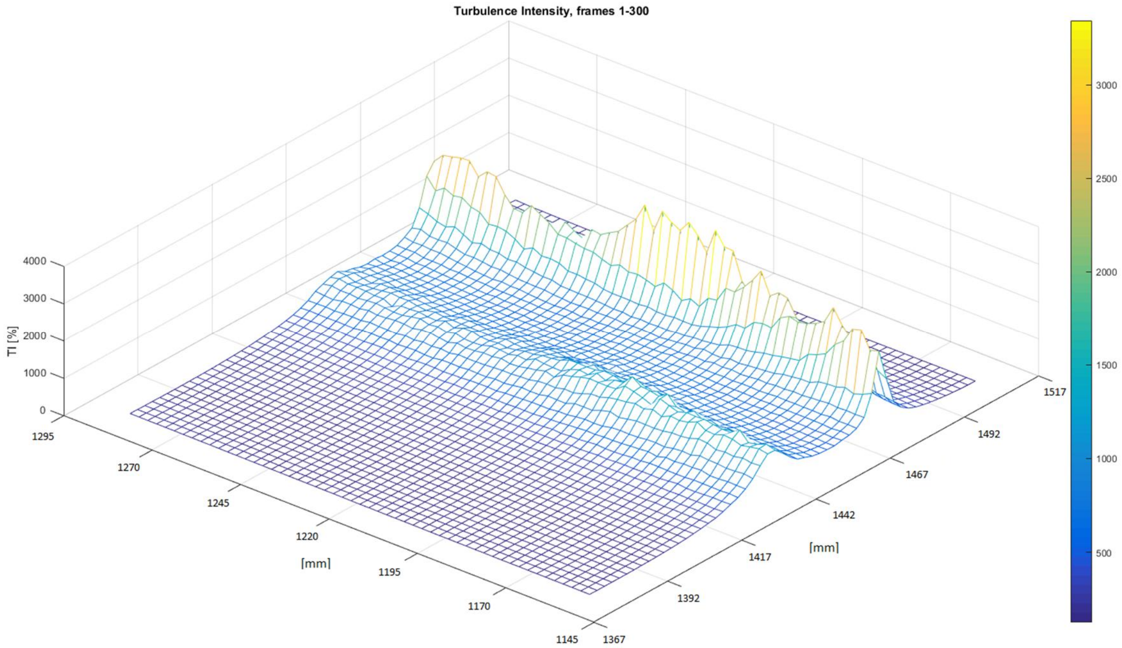

Figure 12. Turbulence intensity field of PIV measurement sequence SPR-T7-1, 1-300.

From Figure 12 it can be seen that even if the average velocity closes to zero, standard deviation of the velocities can be many magnitudes higher at the same time. Sequences SPR-T4-1 and SPR-T5-1 had a similar outcome. This fact creates difficulties in interpreting the results for the tests mentioned. The particle images were inspected visually for this reason and in the chapter below the key findings from the particle images are presented.

4.2.2.1 Visual analysis of the particle images

As stated in chapter 4.2.2 the results after usual analysis were indistinct. By visually inspecting the particle images some conclusions can be made.

In SPR-T4-1, particle images were captured from 20 s to 70 s after the spray start. It can be noticed that between individual frames the particle movement is very random and movement is almost non-existent. This finding was also backed by instantaneous vector fields. There were no visual indications of mixing of any sort in any region. The whole particle ensemble in the measurement area seems to move more or less in unison and there are no indicative downward flow motion or any mixing areas during the measurement sequence.

In SPR-T5-1, particle images were captured from 3 s to 146 s after the spray start. In SPR-T5-1, the seeding method was changed so that the particles were seeded from the spray nozzles to the wetwell. In the beginning there are some leftover particles in the measurement area from the previous measurement in the pool water before the start of spray injection. As the seeding density was too low in the beginning there were a lot of spurious vectors in the instantaneous vector fields. This resulted in making 591 image pairs not suitable for proper cross correlation. Visual inspection of particle images with different seeding densities gave a better opportunity to see how the spray water with the seeding particles mixed in the measurement area. The actual particle movement between individual frames is easier to perceive with low seeding density. The movement of the particle ensemble is analogous to SPR-T4-1 i.e. the seeding particle ensemble moves in unison with a very low velocity in random direction. As the particles are injected from the spray nozzles the more seeded phase appears to penetrate the top of the measurement area after 245 images which corresponds approximately to 38.43 s after the spray start. After additional 78 images or 11.14 seconds the more seeded phase has moved approximately 20 mm from the top downwards which is relative to few mm/s velocities measured in SPR-T4-1 and later in SPR-T7-1. Even after 1000 images or 146 s from the spray start the more seeded phase has not mixed with the low seeded water in the bottom.

In SPR-T7-1, particle images were captured from 167 s to 310 s from the spray start. Seeding is layered in the beginning indicating that mixing is non-existent before 167 s. Similarly to SPR-T4-1 and SPR-T5-1 the particle ensemble is moving really slowly and in random direction. First indication of hotter water entering the measurement area is approximately after 163 images or 190.29 s after the spray start. The optical aberrations in the top part of the measurement area points to this finding. The aberrations are very visible after 350 images or 217 s after the spray start. One major visual clue indicating that there are no mixing involved is the layer of water with lower seeding density which is distinctive up to 713 images or 268.86 s after the spray start. This indicates that even to this point there is no mixing. The layer with lower seeding density in the first captured image and after 713 images is presented in Figure 13.

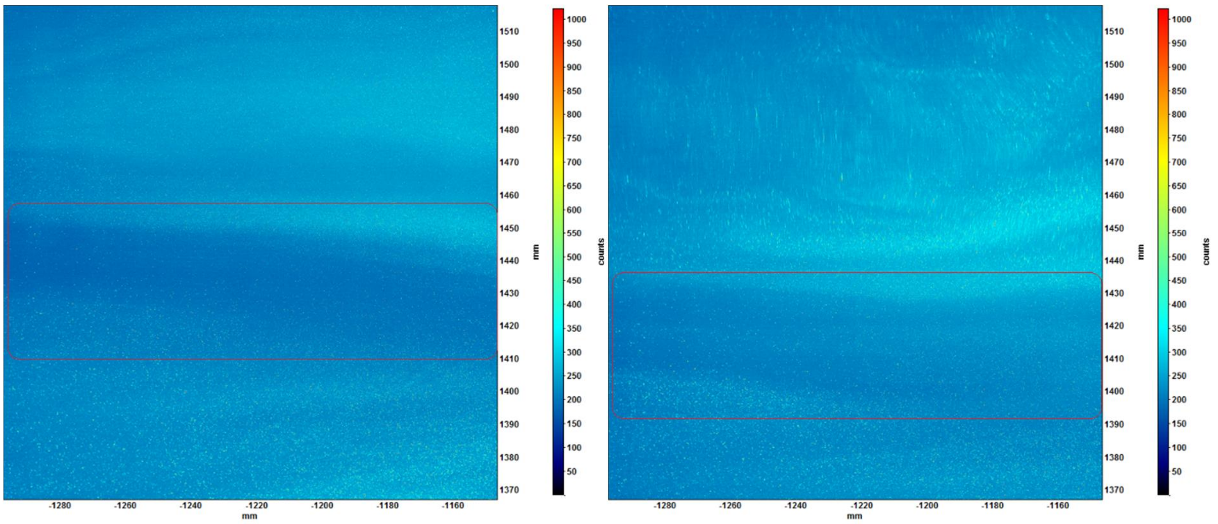

Figure 13. Highlighted lower seeding density zone that remains unmixed 268.86 s after the spray start, N=1 on the left, N=713 on the right.

The lower seeding zone, which is highlighted in Figure 13, is distinguishable in every particle image. After 900 images or 295.57 s after the spray start the whole measurement area is completely fuzzy due to the aberrations. Similar aberration can be seen in Figure 13 on the right side image on the top part of the measurement area.

All in all, the visual inspections indicated that at the start the particle movement is very small and random in all the cases above. There are also indications that there are no mixing involved at least in the first 217 s from starting the sprays. The optical environment gets very poor after 217 s and continues until 1510 s meaning that during the major part of the spray time the information is completely lost. After 1510 s more stable flow patterns with less turbulence intensity can be seen and the results are presented in the following chapter.

4.2.2.2 Results from SPR-T5-3, SPR-T5-4 and SPR-T7-5

For the test series in question the flow environment was more stable with higher velocities compared to the first phase of the measurement. Optical quality of the particle images was good especially in SPR-T7-5. The seeding density in all tests in question suggests that complete mixing has occurred. Also the optical stableness of the particle images points to same conclusion.

By inspecting the instantaneous vector fields it can be concluded that a general flow direction was upwards in SPR-T5-3, SPR-T5-4 and SPR-T7-5. The averaged velocity vector field and corresponding turbulence intensity field from SPR-T5-3 for the first 500 image pairs are presented in Figure 14 and 15.

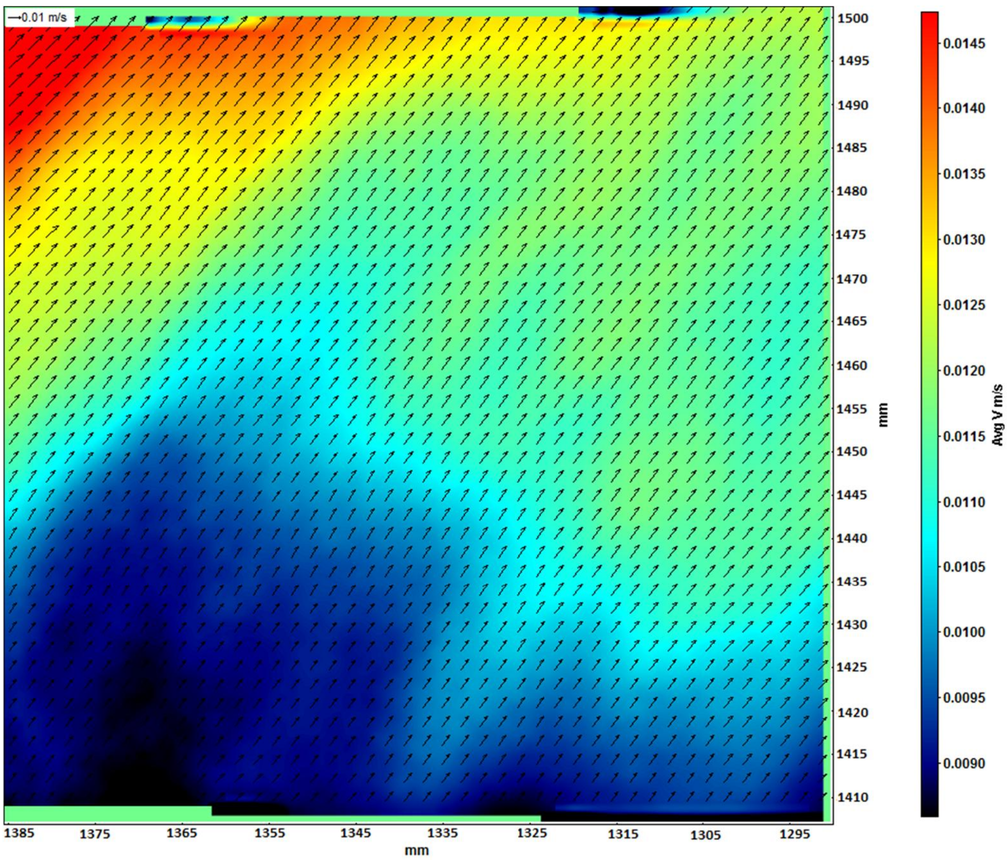

Figure 14. Averaged velocity vector field of PIV measurement sequence SPR-T5-3, N=1-500.

From Figure 14 it can be seen that the average velocities are ranging approximately from 0.9 cm/s to 1.45 cm/s. Turbulence intensity stays below 75%. Figure 16 and 17 present same fields for the last 500 image pairs.

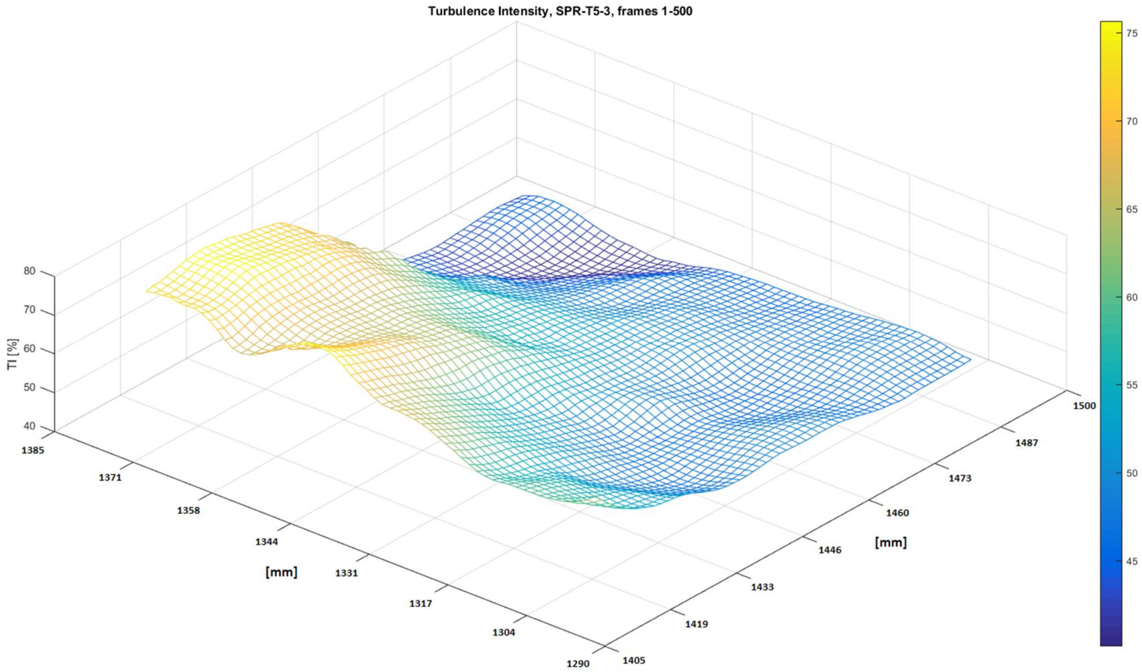

Figure 15. The turbulence intensity field of PIV measurement sequence SPR-T5-3, N=1-500.

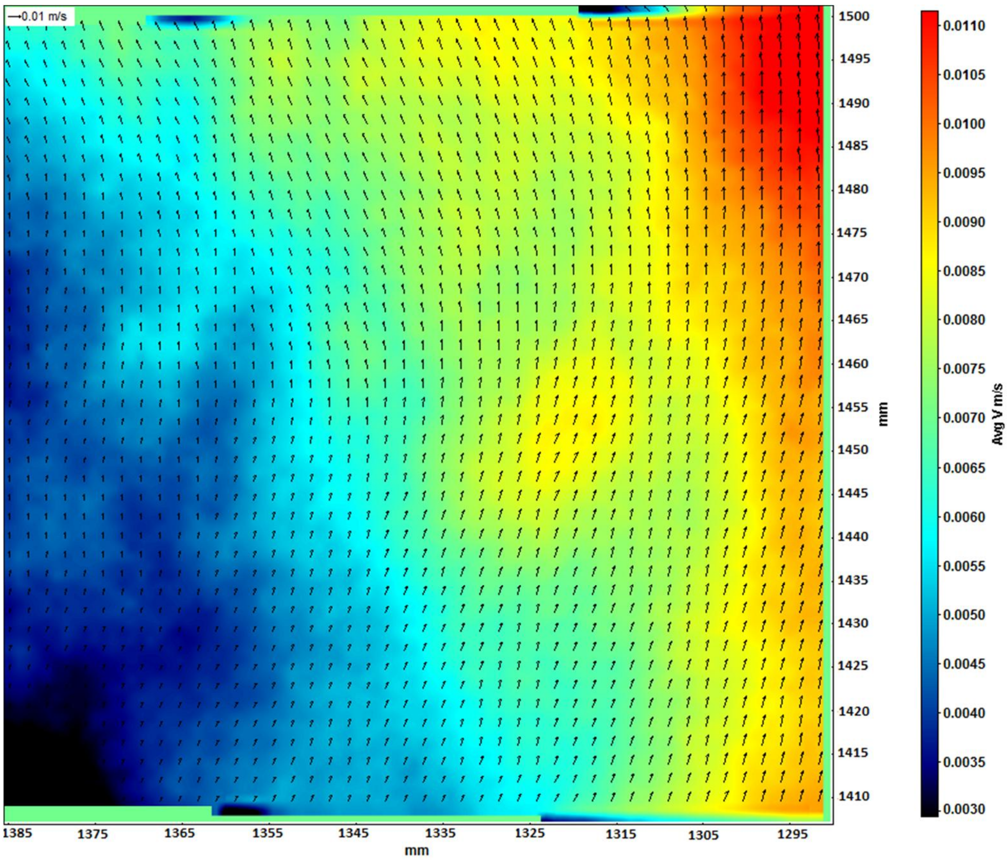

Figure 16. The averaged velocity vector field of PIV measurement sequence SPR-T5-3, N=501-1000.

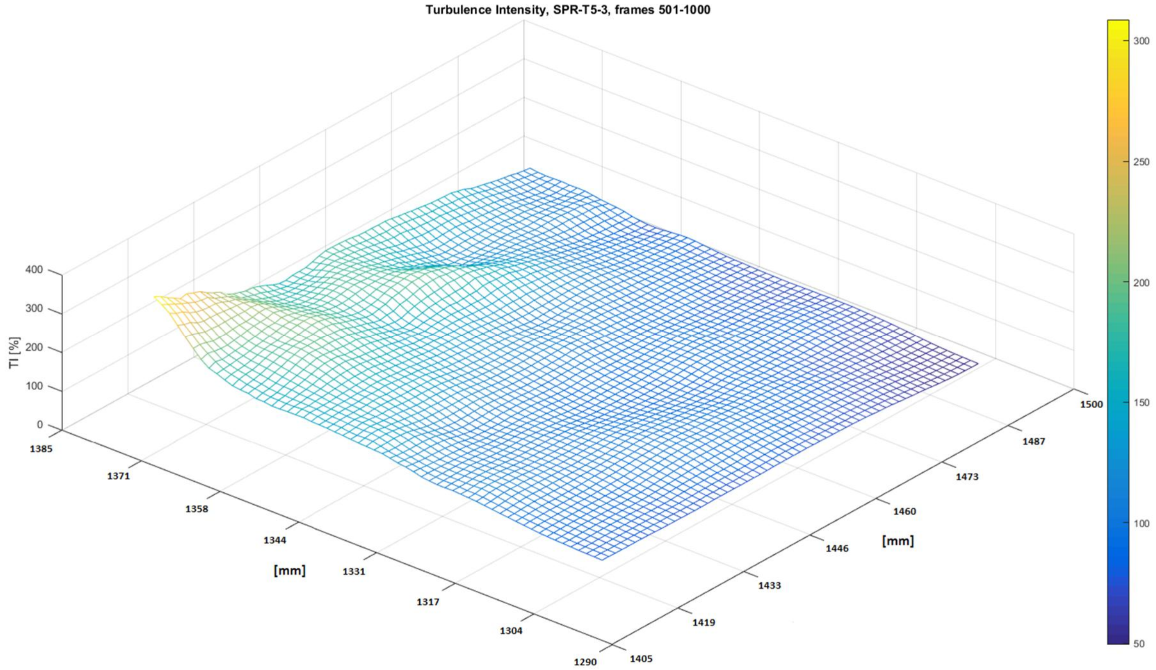

Figure 17. The turbulence intensity field of PIV measurement sequence SPR-T5-3, N=501-1000.

For the latter 500 image pairs the average velocity on the bottom left part of the measurement field has lower velocities and higher turbulence intensity. Inspection of instantaneous velocity fields reveals that the flow direction trend between images 750-850 is downwards making the average velocity smaller and turbulence intensity higher in that area. This is one example of the difficulty of interpreting the results. It would require huge work load to inspect thousands of particle and vector images separately. And even after this one would end up with an ensemble of different possible flow patterns with different sample sizes from the measurement area. But still one can conclude that in SPR-T5-3 the general flow trend is upwards from the bottom of the vessel to the water surface in the measurement area.

When comparing SPR-T5-3 and SPR-T5-4 the time difference between the end of SPR-T5-3 and the beginning of SPR-T5-4 is 154 seconds. In Figure 18, the averaged velocity vector field from the first 500 image pairs from SPR-T5-4 is presented.

The velocities are higher than in the same image pairs from SPR-T5-3 which indicates that the internal circulation process strengthens during the end of the cycle. This is logical. When inspecting the instantaneous velocity vector fields it was found out that there are no frames with downward vectors throughout the whole measurement series. The corresponding turbulence intensity field is presented in Figure 19.

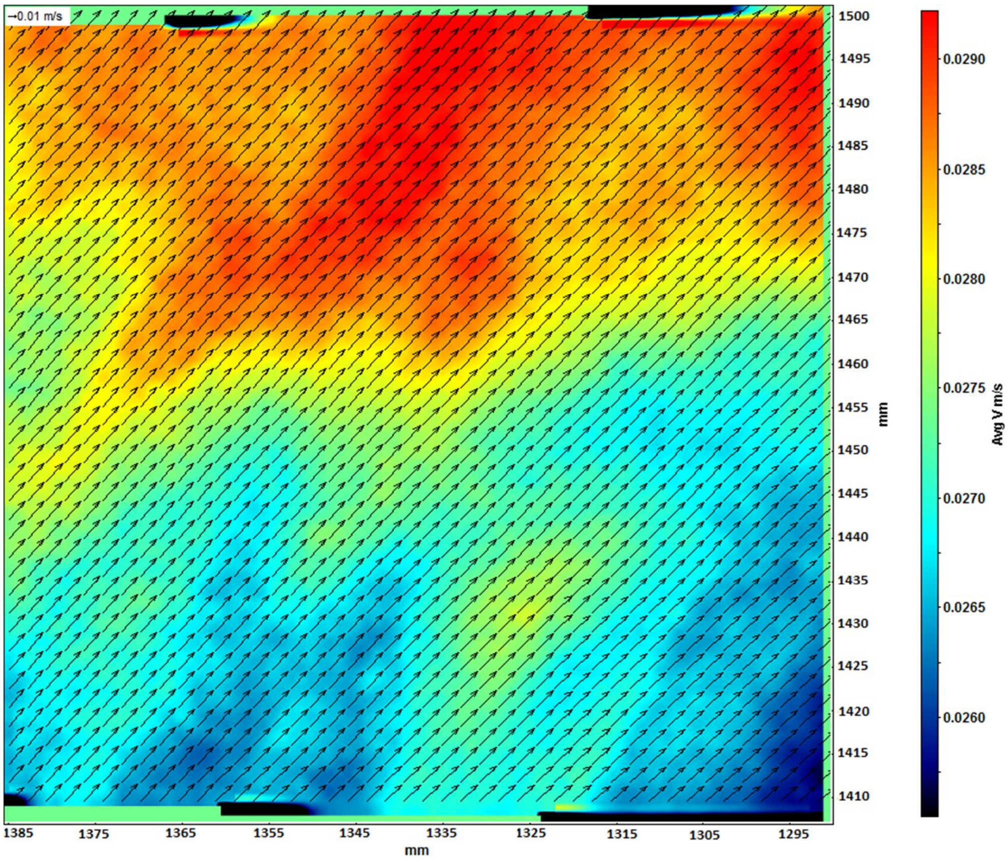

Figure 18. The averaged velocity vector field of PIV measurement sequence SPR-T5-4, N=1-500.

As it was foreseeable from the averaged velocity field, the turbulence intensity field is more stable compared to the earlier SPR-T5-3 case. The averaged vector velocity fields from SPR-T5-4 from the last 500 image pairs are presented in Figure 20.

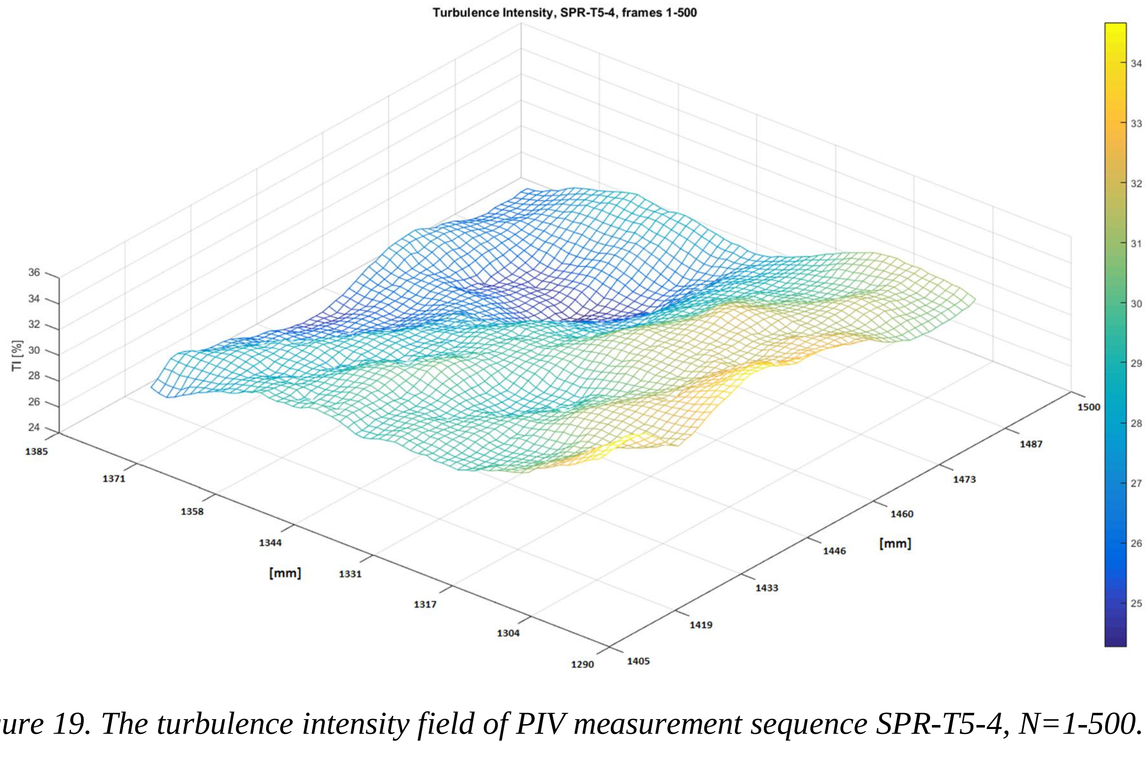

Figure 19. The turbulence intensity field of PIV measurement sequence SPR-T5-4, N=1-500.

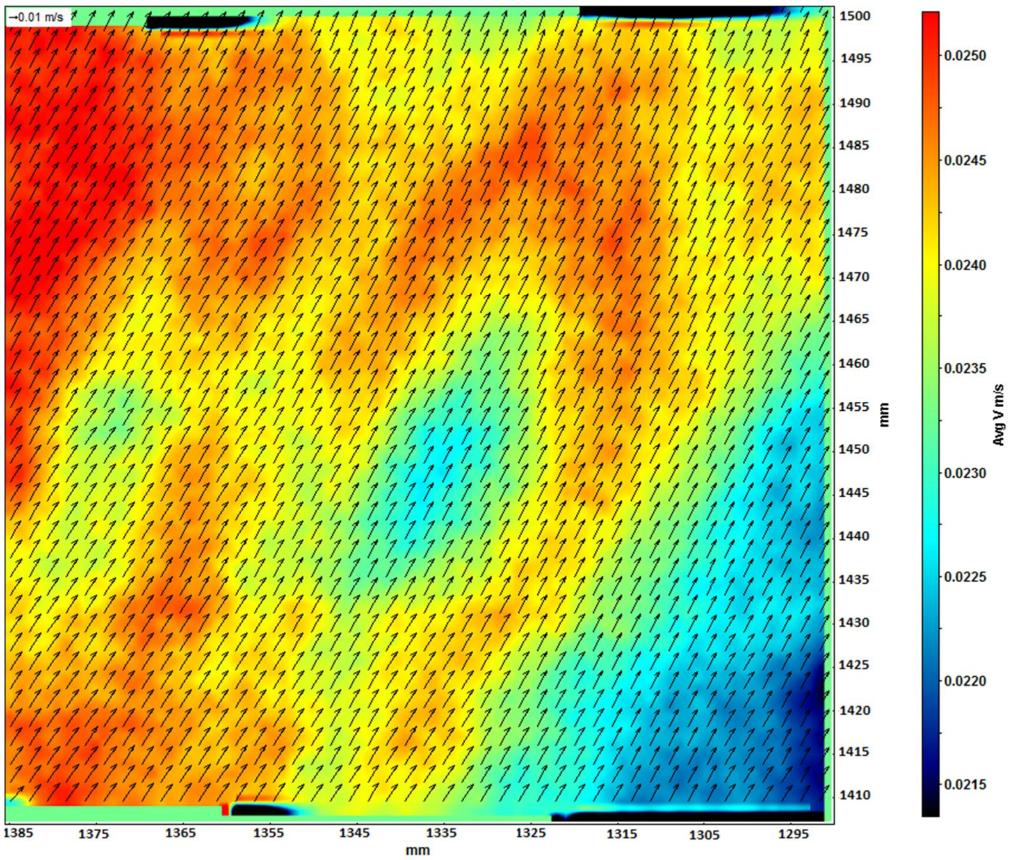

Figure 20. The averaged velocity vector field of PIV measurement sequence SPR-T5-4, N=501-1000.

The averaged velocity vector field from the latter part of the series is very similar to the one obtained on the basis of the first 500 image pairs in Figure 18. In the top part of the measurement area the average velocity is slightly smaller which might indicate that the internal circulation process is diminishing. This finding could only be verified by having a longer spray time or making measurements after the sprays are turned off. The SPR-T5 test was ended 70 seconds after the capturing of images. The corresponding turbulence intensity field is presented in Figure 21. The magnitude of turbulence intensity is similar to the one calculated from the first 500 image pairs of the SPR-T5-4 sequence.

When the instantaneous velocity vector fields from SPR-T7-5 were inspected visually it was found out that there were no single instantaneous velocity vector field with downward flow which might indicate that the internal circulation process has begun. The averaged velocity vector fields for the first 500 image pairs are presented in Figure 22.

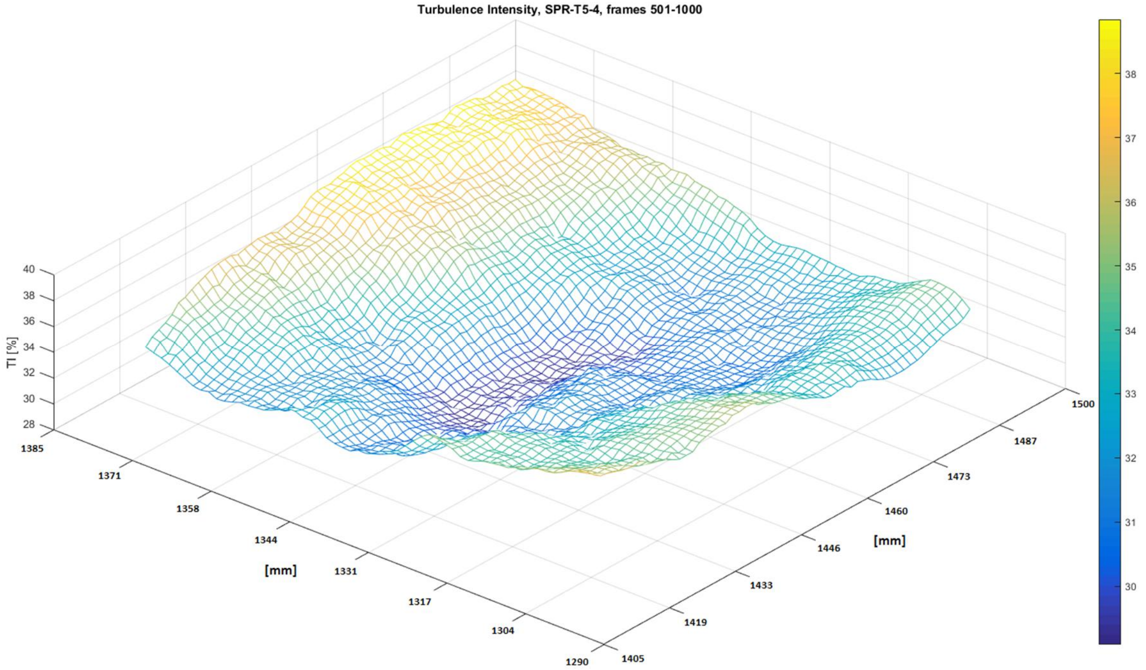

Figure 21. The turbulence intensity field of PIV measurement sequence SPR-T5-4, N=501-1000.

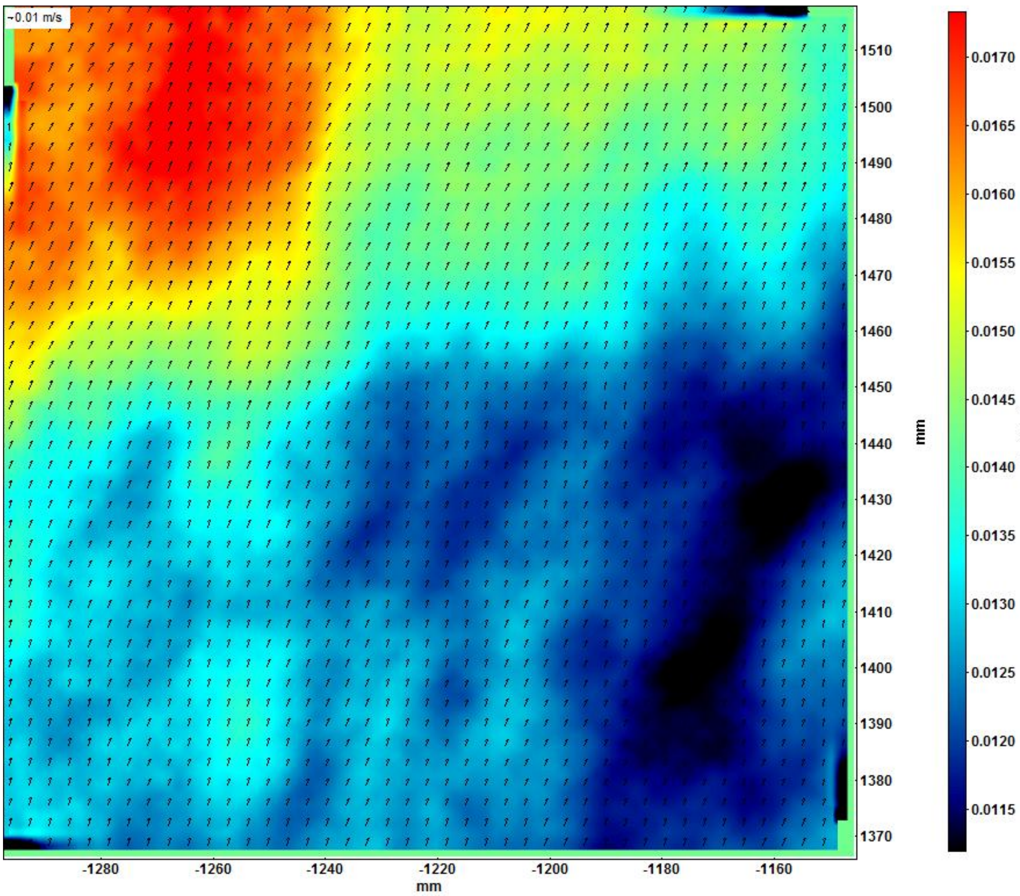

Figure 22. The averaged velocity vector field of PIV measurement sequence SPR-T7-5, N=1-500.

The averaged velocity has grown compared to SPR-T5-3, which is the previous test in the timeline. When comparing the results between SPR-T7 and SPR-T5 it must be remembered that the measurement areas are not in the same location. Vertically they are located on the same plane and SPR-T7 covers the whole SPR-T5 measurement area. The corresponding turbulence intensity field is presented in Figure 23.

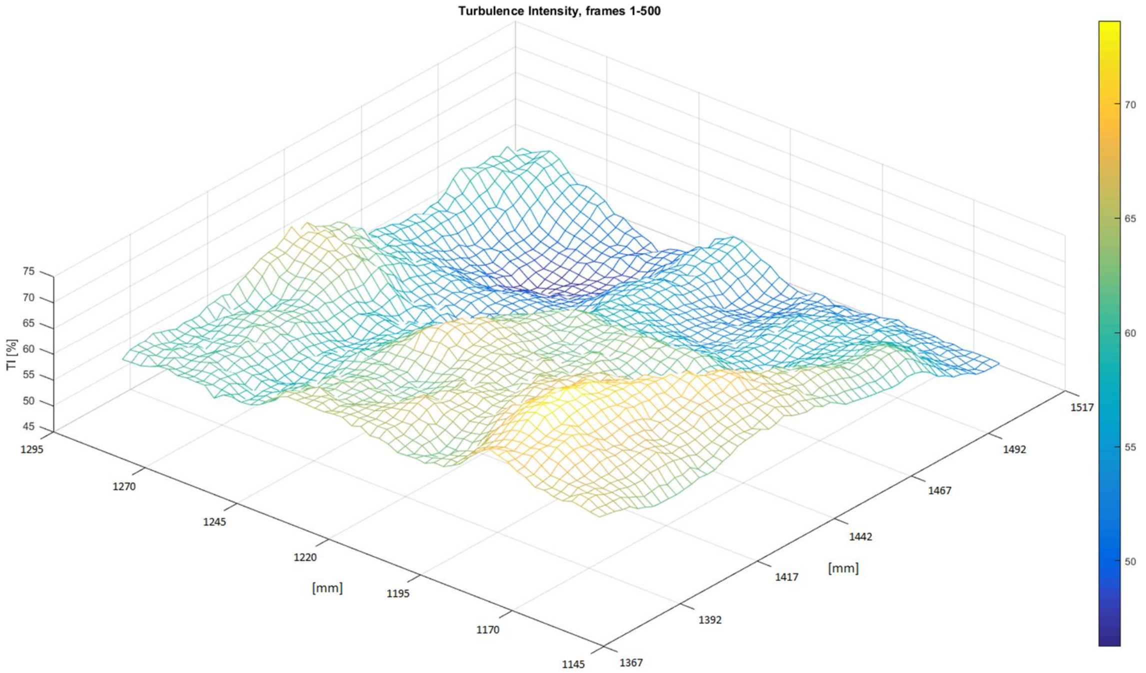

Figure 23. The turbulence intensity field of PIV measurement sequence SPR-T7-5, N=1-500.

It can be seen that the turbulence intensity level is higher than in SPR-T5-4.

There is overlapping in the timeline between SPR-T7-5 and SPR-T5-4. In SPR-T7-5, the capturing of images started at 1739 s and ended at 1882 s after the spray start whereas in SPR-T5-4, the capturing started at 1808 s and ended at 1951 s after spray start. The latter 500 image pairs of SPR-T7-5 and the first 500 image pairs of SPR-T5-4 are captured almost from the same time window after the spray start (~1810 s – 1882 s for SPR-T7-5 and ~1808 s – 1879 s). The averaged velocity vector field for the latter 500 image pairs of SPR-T7-5 is presented in Figure 24.

The average velocities have grown in the latter part of SPR-T7-5 but differ from those in SPR-T5-4. Because there are no additional measurements after SPR-T7-5, the dissipation of internal cycling process, that was a possible finding of SPR-T5-4, cannot be confirmed. Similarly to SPR-T5-4, the highest average velocities were measured ~1810 s after the spray start although they were smaller in the whole measurement area. The corresponding turbulence intensity field is presented in Figure 25.

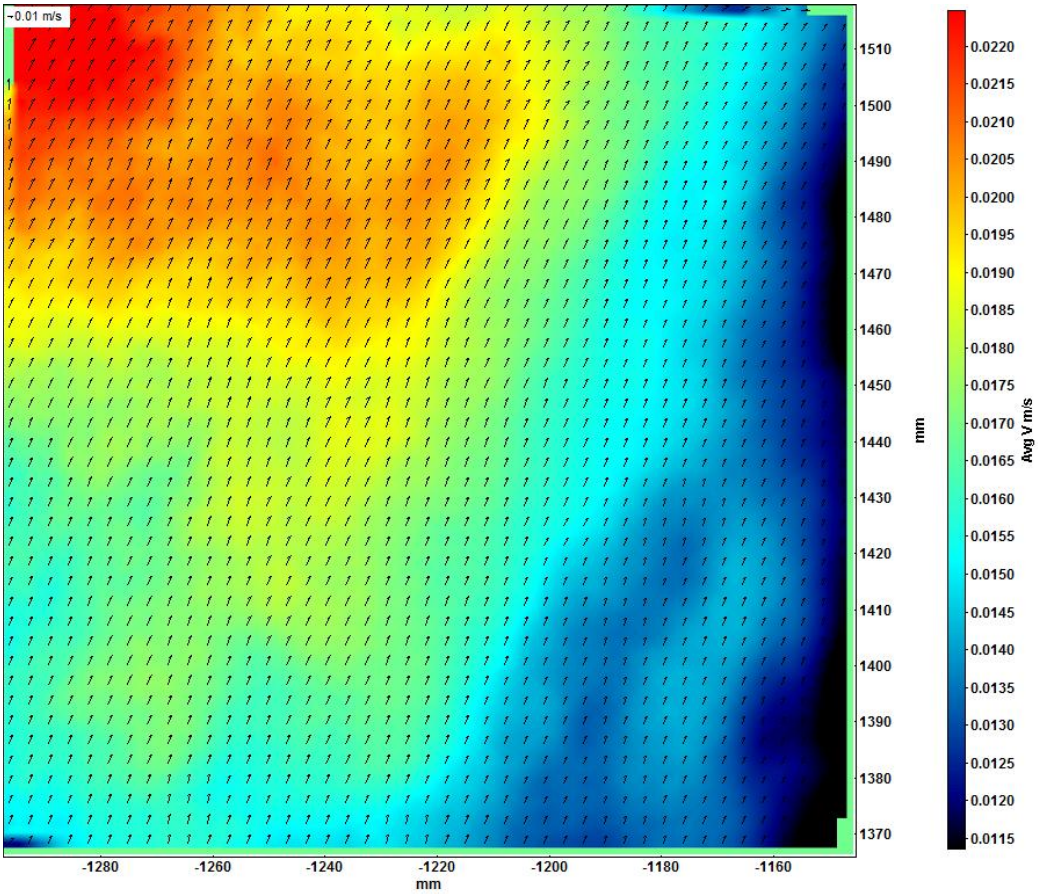

Figure 24. The averaged velocity vector field of PIV measurement sequence SPR-T7-5, N=501-1000.

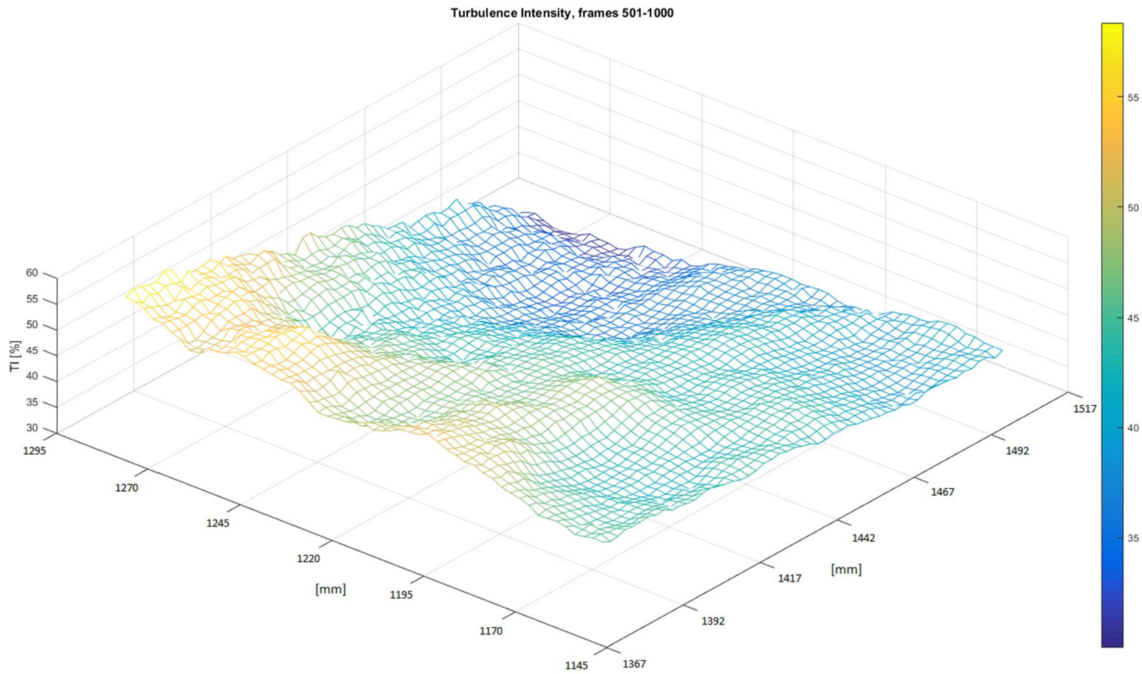

Figure 25. The turbulence intensity field of PIV measurement sequence SPR-T7-5, N=501-1000.

As the velocities on the plane grow the turbulence intensity gets smaller. All in all, the turbulence intensity fields are not the most effective way to describe the flow in the measured cases. Only when the turbulence intensity gets high, to the level of hundreds of percent, there are most likely some reversed flow periods compared to the main flow motion.

Continuing the SPR-T7 experiment longer and having more PIV measurement sequences in the end, the development of the internal cycling process could have been followed better. Results obtained from SPR-T5 and SPR-T7 indicate that it takes up to ~1739 s before the circulation starts.

5 SUMMARY AND CONCLUSIONS

This report summarizes the results of the spray tests (SPR-T4, SPR-T5, SPR-T6 and SPR-T7) carried out in the PPOOLEX facility at LUT. The test facility is a closed stainless steel vessel divided into two compartments, drywell and wetwell. For the spray tests, the PPOOLEX facility was equipped with a model of a spray injection system with four nozzles and an associated water injection line.

The main purpose of the tests was to study mixing of a thermally stratified pool with the help of spray injection from above. An additional goal was to obtain data, particularly PIV measurement data, for improving simulation models related to spray operation in CFD and system codes as well as to contribute to the development of the EMS and EHS models for sprays to be implemented in the GOTHIC code by KTH.

The initial thermally stratified situation was created in all the tests by injecting first warm and then cold water from the tap into the wetwell of the PPOOLEX facility. The thickness of the layer of warm water floating above a volume of cold water was about 200 mm. An initial water level of about 1.8 m was used in three tests and 1.5 m in one test. The temperature difference between the bottom and the top layer of the pool before the initiation of spray injection varied between 29-32 °C. In all four tests, the flow rate of spray injection was between 30.5-32.0 l/min per nozzle. Water as cold as possible was taken from the tap for the spray. At the initialization of the spray, the water temperature was about 21-24 °C but dropped very soon to about 12 °C.

The test arrangement was such that the larger viewing windows of the wetwell could be utilized in the PIV measurements instead of the small size viewing windows originally reserved for the PIV laser and cameras. This was achieved by slightly increasing the amount of pool water from the previous tests and thus positioning the transition region between cold and hot water on an optimal elevation in the pool from the PIV measurement point of view. This means that the middle point in vertical direction of the PIV measurement was at about 1455 mm elevation in SPR-T4, SPR-T5 and SPR-T6. In SPR-T7 it was at about 1440 mm elevation. In the first three tests, the measurement plane was about 0.5 m away from the pool centre axis and the FOV area was 95x95 mm. In the fourth test, the measurement plane was in the pool centre and the FOV area was 151x151 mm. Two-camera stereo PIV measurements were conducted in the first test and single-camera planar measurements in the three remaining tests.

First, the cold spray water penetrated the water surface causing mixing in the top layers. Then an internal circulation process took place in the pool at the elevation of the thermocline between the cold and warm water as the cold and therefore more dense sprayed water pushed its way downwards. Most of the pool water volume mixed during the tests as the downwards penetrating mixing process continued. However, the tests were terminated before complete mixing of the pool was achieved.

For the analysis of the PIV results all the tests could be separated to three phases. In first phase, the movement of the particles is minor and thus the velocities are very small. The whole particle ensemble moves in unison and there are indications that there is no mixing involved. The second phase covers the time period when the optical environment does not suit the PIV measurement at all. The last phase starts after the mixing has occurred in the PIV measurement area and the optical environment enables PIV to be executed to some extent in a normal manner by averaging velocity fields. The dynamic characteristics of the flow makes the analysis of the results difficult and ambiguous. It would also be very beneficial to have a method for validating the PIV results at least to a point where it can be reliably stated that the velocities are in the correct range, particularly in the beginning of the tests when the velocities are only in the range of mm/s. It must be also remembered that the PIV measurement plane is small in size compared to the PPOOLEX wetwell pool and therefore development of large internal circulations in the pool cannot be captured by the PIV measurement system. Only local flow fields can be measured if the optical environment is optimal.

The PIV measurement setup used in the SPR-T7 test was found to be the most suitable for the conditions prevailing in the PPOOLEX wetwell during the spray tests. It is suggested that this arrangement is used in the possible future spray tests. Based on the experience gained from these spray tests it could be worth the effort to investigate the internal circulation process and how it dissipates by measuring with PIV after the sprays have been stopped or when spraying is continued longer. Seeding could be executed in a way where seeding particles are spread to the pool only through the spray nozzles. That would give visible indications on how much time it takes for the water spray, or the mixed spray and hot water layer, to enter the PIV measurement area as the current velocity information is ambiguous. Some indications of the hot layer of water entering the measurement area can be seen from the optical aberrations but big uncertainty in this finding is the fact that the hot water might be circulating more on the vessel wall side and thus the optical aberration might be in the water volume penetrated by the laser sheet and not in the measurement area that is filmed.

6 REFERENCES

1. Puustinen, M., Laine, J., Räsänen, A., PPOOLEX Experiments on Thermal Stratification and Mixing. Lappeenranta University of Technology. 2009. Research Report CONDEX 1/2008.
2. Laine, J., Puustinen, M., PPOOLEX Experiments on Wall Condensation. Lappeenranta University of Technology. 2009. Research Report CONDEX 3/2008.
3. Laine, J., Puustinen, M., Räsänen, A., PPOOLEX Experiments with a Modified Blowdown Pipe Outlet. Lappeenranta University of Technology. 2009. Research Report CONDEX 2/2008.
4. Laine, J., Puustinen, M., Räsänen, A., PPOOLEX Experiments with Two Parallel Blowdown Pipes. Lappeenranta University of Technology. 2010. Research Report CONDEX 1/2009.
5. Puustinen, M., Laine, J., Räsänen, A., PPOOLEX Experiments on Dynamic Loading with Pressure Feedback. Lappeenranta University of Technology. 2010. Research Report CONDEX 2/2009.

6. Laine, J., Puustinen, M., Räsänen, A., Tanskanen, V., PPOOLEX Experiments on Stratification and Mixing in the Wet Well Pool. Lappeenranta University of Technology. 2011. Research Report CONDEX 1/2010.
7. Puustinen, M., Laine, J., Räsänen, A., Multiple Blowdown Pipe Experiment with the PPOOLEX Facility. Lappeenranta University of Technology. 2011. Research Report CONDEX 2/2010.
8. Puustinen, M., Laine, J., Räsänen, A., PPOOLEX Experiments with a Blowdown Pipe Collar. Lappeenranta University of Technology. 2012. Research Report EXCOP 1/2011.
9. Laine, J., Puustinen, M., Räsänen, A., PPOOLEX Experiments on the Dynamics of Free Water Surface in the Blowdown Pipe. Lappeenranta University of Technology. 2013. Research Report EXCOP 2/2012.
10. Laine, J., Puustinen, M., Räsänen, A., PPOOLEX Mixing Experiments. Lappeenranta University of Technology. 2014. Research Report EXCOP 1/2013.
11. Gamble, R. E., Nguyen, T. T., Peterson, P. F., Pressure suppression pool mixing in passive advanced BWR plants. Nuclear Engineering and Design, 204, 321-336, 2000.
12. Li, H., Villanueva, W., Kudinov, P., Effective Models for Simulation of Thermal Stratification and Mixing Induced by Steam Injection into a Large Pool of Water. Division of Nuclear Power Safety, Royal Institute of Technology (KTH), NORTHNET Roadmap 3 Research report, Stockholm, 2014.
13. Laine, J. Puustinen, M. Räsänen, A., PPOOLEX Experiments with a Sparger. Lappeenranta University of Technology. 2015. Research Report EXCOP 1/2014.
14. Puustinen, M., Laine, J., Räsänen, A., Additional Sparger Tests in PPOOLEX with Reduced Number of Injection Holes. Lappeenranta University of Technology. 2016. Research Report INSTAB 1/2015.
15. Puustinen, M., Pyy, L., Laine, J., Räsänen, A., Sparger Tests in PPOOLEX on the Behaviour of Thermocline. Lappeenranta University of Technology. 2017. Research Report INSTAB 1/2016.
16. Puustinen M., Laine J., Räsänen A., Kotro E., Mixing tests with an RHR nozzle in PPOOLEX. Lappeenranta University of Technology. 2017. Research Report INSTAB 2/2016.
17. Puustinen M., Räsänen A., Kotro E., Preliminary spray tests in PPOOLEX. Lappeenranta University of Technology. 2017. Research Report INSTAB 3/2016.
18. Puustinen, M., Partanen, H., Räsänen, A., Purhonen, H., PPOOLEX Facility Description. Lappeenranta University of Technology. 2007. Technical Report POOLEX 3/2006.
19. Pyy, L., Single Spray Nozzle Tests. Lappeenranta University of Technology. 2016. Research Report INSTAB 2/2015.
20. http://www.spray.com/cat75/hydraulic-m/index.html

Open your mind. LUT.
Lappeenranta University of Technology

APPENDIX 1: PPOOLEX instrumentation

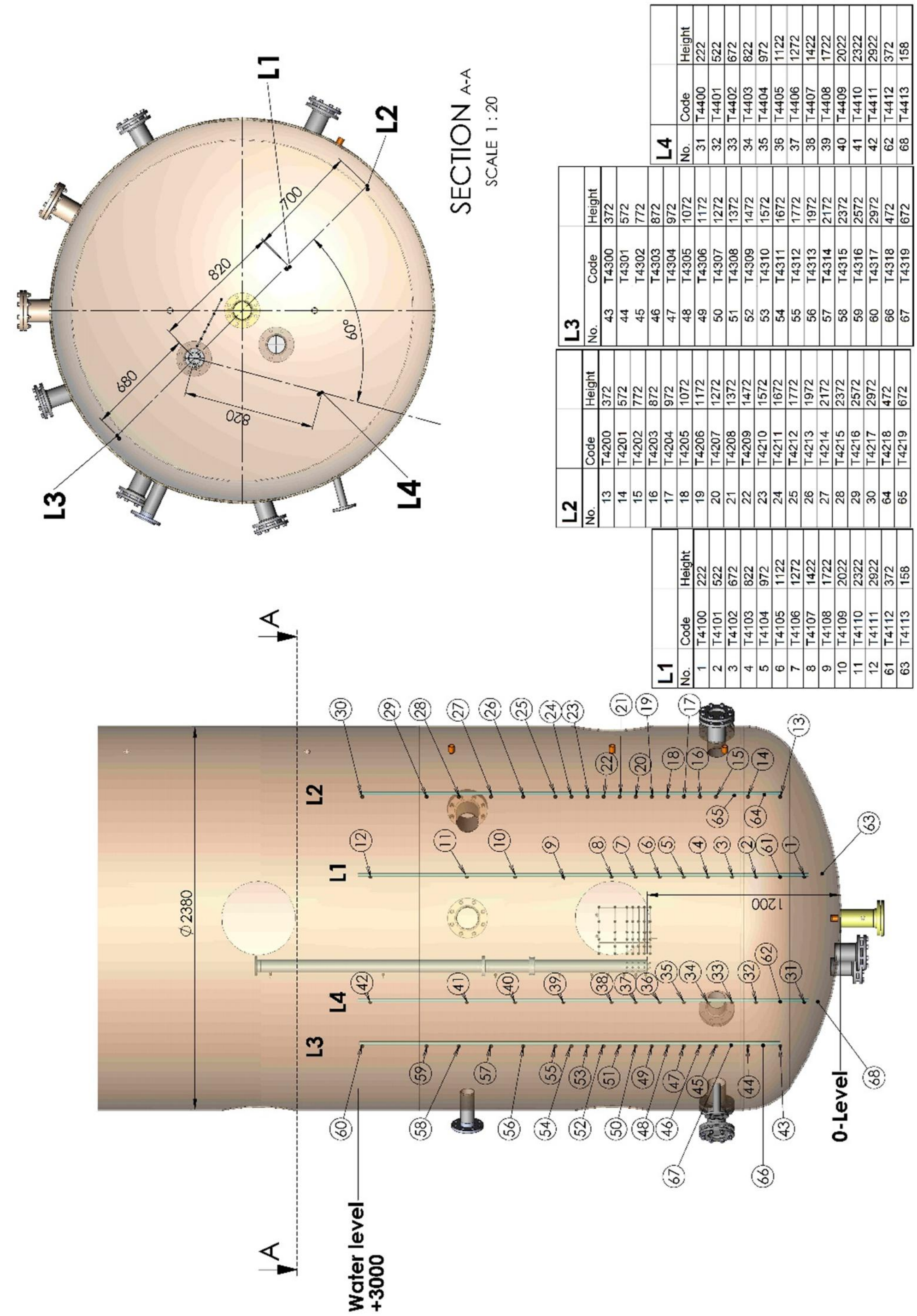

L1		
No.	Code	Height
1	T4100	222
2	T4101	522
3	T4102	672
4	T4103	822
5	T4104	972
6	T4105	1122
7	T4106	1272
8	T4107	1422
9	T4108	1722
10	T4109	2022
11	T4110	2322
12	T4111	2922
61	T4112	372
63	T4113	158

L2		
No.	Code	Height
13	T4200	372
14	T4201	572
15	T4202	772
16	T4203	872
17	T4204	972
18	T4205	1072
19	T4206	1172
20	T4207	1272
21	T4208	1372
22	T4209	1472
23	T4210	1572
24	T4211	1672
25	T4212	1772
26	T4213	1972
27	T4214	2172
28	T4215	2372
29	T4216	2572
30	T4217	2972
64	T4218	472
65	T4219	672

L3		
No.	Code	Height
43	T4300	372
44	T4301	572
45	T4302	772
46	T4303	872
47	T4304	972
48	T4305	1072
49	T4306	1172
50	T4307	1272
51	T4308	1372
52	T4309	1472
53	T4310	1572
54	T4311	1672
55	T4312	1772
56	T4313	1972
57	T4314	2172
58	T4315	2372
59	T4316	2572
60	T4317	2972
66	T4318	472
67	T4319	672

L4		
No.	Code	Height
31	T4400	222
32	T4401	522
33	T4402	672
34	T4403	822
35	T4404	972
36	T4405	1122
37	T4406	1272
38	T4407	1422
39	T4408	1722
40	T4409	2022
41	T4410	2322
42	T4411	2922
62	T4412	372
68	T4413	158

Four trains of temperature measurements in the wetwell.

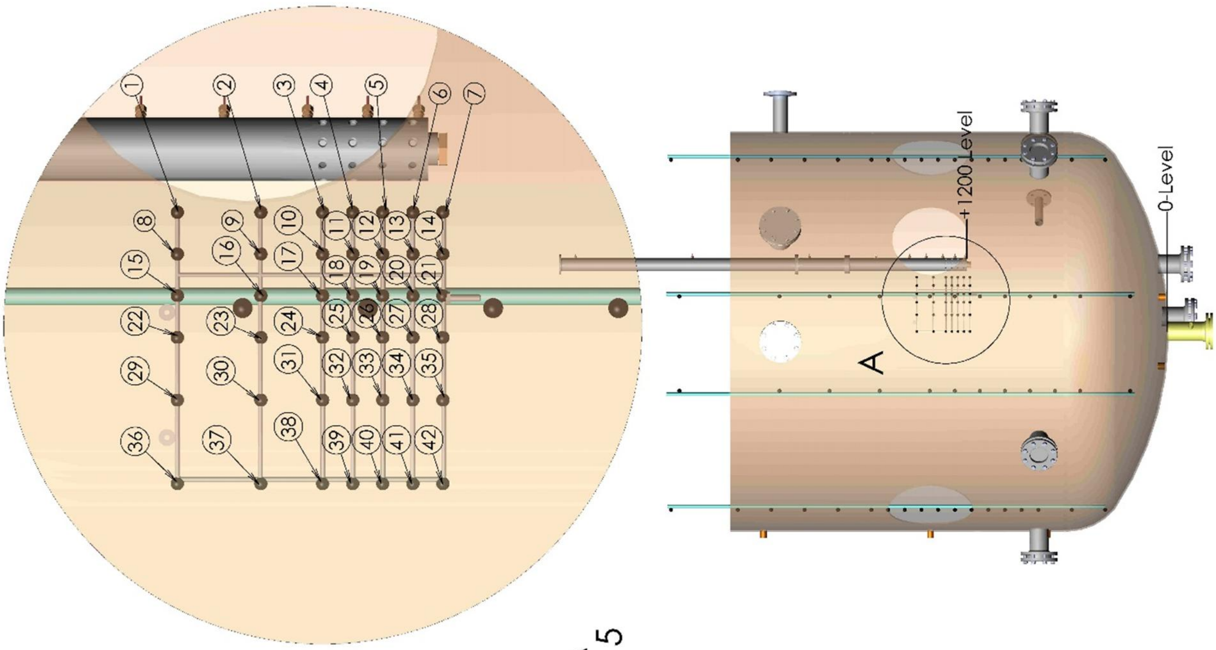

DETAIL A
SCALE 1 : 5

No.	Code	No.	Code	No.	Code
1	T4000	16	T4021	31	T4042
2	T4001	17	T4022	32	T4043
3	T4002	18	T4023	33	T4044
4	T4003	19	T4024	34	T4045
5	T4004	20	T4025	35	T4046
6	T4005	21	T4026	36	T4050
7	T4006	22	T4030	37	T4051
8	T4010	23	T4031	38	T4052
9	T4011	24	T4032	39	T4053
10	T4012	25	T4033	40	T4054
11	T4013	26	T4034	41	T4055
12	T4014	27	T4035	42	T4056
13	T4015	28	T4036		
14	T4016	29	T4040		
15	T4020	30	T4041		

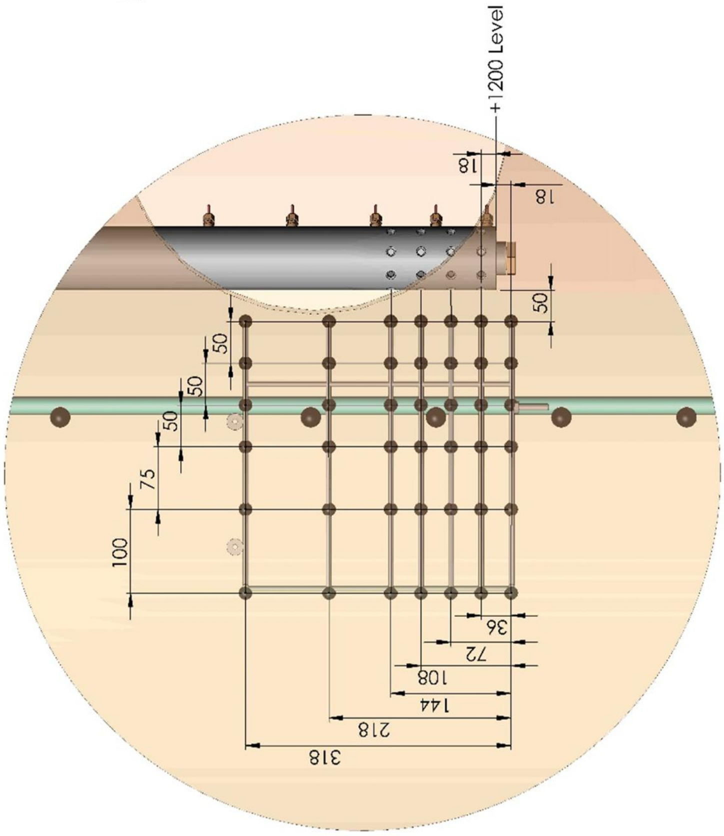

6x7 grid of temperature measurements in the wetwell.

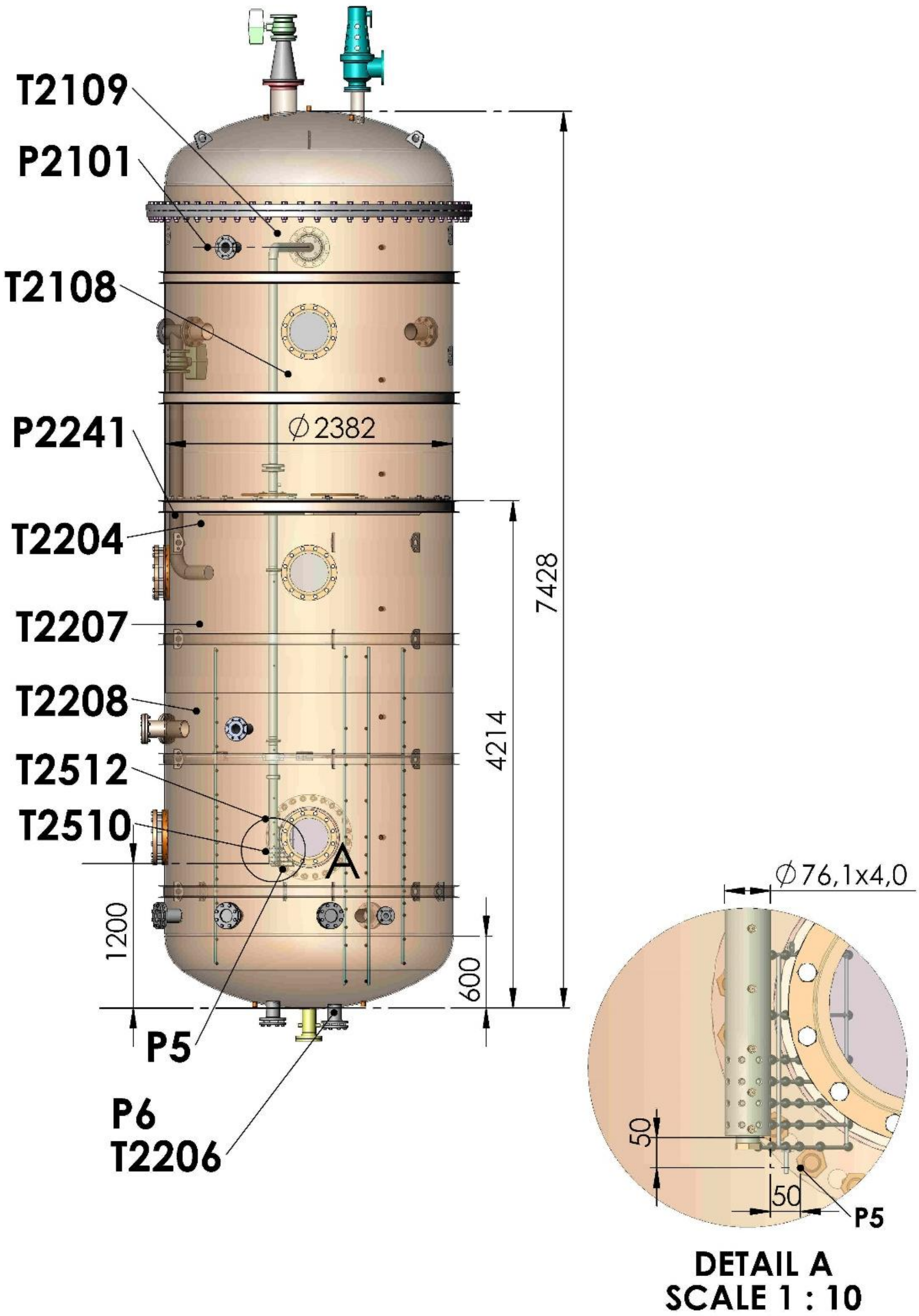

Test vessel measurements.

Measurement	Code	Elevation	Location	Error estimation	Measurement software
Camera trigger	C1	-	Wetwell	Not defined	LabView
Pressure difference	D2100	700–3300	Wetwell	±0.05 m	FieldPoint
Pressure difference	D2101	3300–4420	Wetwell–drywell	±4 000 Pa	FieldPoint
Pressure difference	D2106	4347	Blowdown pipe–drywell	±3 000 Pa	FieldPoint
Pressure difference	D9000	-130-5800	Wetwell	±0.1 m	FieldPoint
Flow rate	F2100	-	DN50 steam line	±5 l/s	FieldPoint
Flow rate	F2102	-	DN25 steam line	±0.7 l/s	FieldPoint
Flow rate	F9000	-	Spray line	±0.007 kg/s	FieldPoint
Pressure	P0003	-	Steam generator 1	±0.3 bar	FieldPoint
Pressure	P0004	-	Steam generator 2	±0.3 bar	FieldPoint
Pressure	P0005	-	Steam generator 3	±0.3 bar	FieldPoint
Pressure	P5	1150	Blowdown pipe outlet	±0.7 bar	LabView
Pressure	P6	-15	Wetwell bottom	±0.5 bar	LabView
Pressure	P2100	-	DN50 steam line	±0.2 bar	FieldPoint
Pressure	P2101	6300	Drywell	±0.03 bar	FieldPoint
Pressure	P2102	-	Inlet plenum	±0.03 bar	FieldPoint
Pressure	P2106	-	DN25 steam line	±0.06 bar	FieldPoint
Pressure	P2241	4200	Wetwell gas space	±0.05 bar	FieldPoint
Control valve position	S2002	-	DN50 Steam line	Not defined	FieldPoint
Strain	S1	200	Bottom segment	Not defined	LabView
Strain	S2	200	Bottom segment	Not defined	LabView
Strain	S3	335	Bottom segment	Not defined	LabView
Strain	S4	335	Bottom segment	Not defined	LabView
Temperature	T1279	-3260	Laboratory	±0.1 °C	FieldPoint
Temperature	T1280	-1260	Laboratory	±0.1 °C	FieldPoint
Temperature	T1281	740	Laboratory	±1.8 °C	FieldPoint
Temperature	T1282	2740	Laboratory	±0.1 °C	FieldPoint
Temperature	T1283	4740	Laboratory	±0.1 °C	FieldPoint
Temperature	T1284	6740	Laboratory	±0.1 °C	FieldPoint
Temperature	T1285	8740	Laboratory	±0.1 °C	FieldPoint
Temperature	T2100	-	DN80 steam line	±3 °C	FieldPoint
Temperature	T2102	-	DN50 steam line	±2 °C	FieldPoint
Temperature	T2103	-	DN25 steam line	±2 °C	FieldPoint
Temperature	T2106	-	Inlet plenum	±2 °C	FieldPoint
Temperature	T2108	5200	Drywell	±2 °C	FieldPoint
Temperature	T2109	6390	Drywell	±2 °C	FieldPoint
Temperature	T2121	4347	Blowdown pipe	±2 °C	FieldPoint
Temperature	T2204	4010	Wetwell gas space	±2 °C	FieldPoint
Temperature	T2206	-15	Wetwell bottom	±2 °C	FieldPoint
Temperature	T2207	3185	Wetwell gas space	±2 °C	FieldPoint
Temperature	T2208	2360	Wetwell gas space	±2 °C	FieldPoint
Temperature	T2510	1295	Wetwell	±2 °C	FieldPoint
Temperature	T2512	1565	Wetwell	±2 °C	FieldPoint
Temperature	T3611	1565	Spray line	±2 °C	FieldPoint
Temperature	T4000	1500	Wetwell	±2 °C	FieldPoint
Temperature	T4001	1400	Wetwell	±2 °C	LabView

Temperature	T4002	1326	Wetwell	±2 °C	LabView
Temperature	T4003	1290	Wetwell	±2 °C	LabView
Temperature	T4004	1254	Wetwell	±2 °C	LabView
Temperature	T4005	1218	Wetwell	±2 °C	LabView
Temperature	T4006	1182	Wetwell	±2 °C	LabView
Temperature	T4010	1500	Wetwell	±2 °C	FieldPoint
Temperature	T4011	1400	Wetwell	±2 °C	LabView
Temperature	T4012	1326	Wetwell	±2 °C	LabView
Temperature	T4013	1290	Wetwell	±2 °C	LabView
Temperature	T4014	1254	Wetwell	±2 °C	LabView
Temperature	T4015	1218	Wetwell	±2 °C	LabView
Temperature	T4016	1182	Wetwell	±2 °C	LabView
Temperature	T4020	1500	Wetwell	±2 °C	LabView
Temperature	T4021	1400	Wetwell	±2 °C	LabView
Temperature	T4022	1326	Wetwell	±2 °C	LabView
Temperature	T4023	1290	Wetwell	±2 °C	LabView
Temperature	T4024	1254	Wetwell	±2 °C	LabView
Temperature	T4025	1218	Wetwell	±2 °C	LabView
Temperature	T4026	1182	Wetwell	±2 °C	LabView
Temperature	T4030	1500	Wetwell	±2 °C	LabView
Temperature	T4031	1400	Wetwell	±2 °C	LabView
Temperature	T4032	1326	Wetwell	±2 °C	LabView
Temperature	T4033	1290	Wetwell	±2 °C	LabView
Temperature	T4034	1254	Wetwell	±2 °C	LabView
Temperature	T4035	1218	Wetwell	±2 °C	LabView
Temperature	T4036	1182	Wetwell	±2 °C	LabView
Temperature	T4040	1500	Wetwell	±2 °C	FieldPoint
Temperature	T4041	1400	Wetwell	±2 °C	LabView
Temperature	T4042	1326	Wetwell	±2 °C	LabView
Temperature	T4043	1290	Wetwell	±2 °C	LabView
Temperature	T4044	1254	Wetwell	±2 °C	LabView
Temperature	T4045	1218	Wetwell	±2 °C	LabView
Temperature	T4046	1182	Wetwell	±2 °C	LabView
Temperature	T4050	1500	Wetwell	±2 °C	FieldPoint
Temperature	T4051	1400	Wetwell	±2 °C	FieldPoint
Temperature	T4052	1326	Wetwell	±2 °C	FieldPoint
Temperature	T4053	1290	Wetwell	±2 °C	FieldPoint
Temperature	T4054	1254	Wetwell	±2 °C	FieldPoint
Temperature	T4055	1218	Wetwell	±2 °C	FieldPoint
Temperature	T4056	1182	Wetwell	±2 °C	FieldPoint
Temperature	T4070	1211	Blowdown pipe	±2 °C	FieldPoint
Temperature	T4071	1272	Blowdown pipe	±2 °C	FieldPoint
Temperature	T4072	1344	Blowdown pipe	±2 °C	FieldPoint
Temperature	T4073	1444	Blowdown pipe	±2 °C	FieldPoint
Temperature	T4074	1544	Blowdown pipe	±2 °C	FieldPoint
Temperature	T4075	1744	Blowdown pipe	±2 °C	FieldPoint
Temperature	T4076	2144	Blowdown pipe	±2 °C	FieldPoint
Temperature	T4077	2844	Blowdown pipe	±2 °C	FieldPoint
Temperature	T4078	3544	Blowdown pipe	±2 °C	FieldPoint
Temperature	T4100	222	Wetwell	±2 °C	FieldPoint
Temperature	T4101	522	Wetwell	±2 °C	FieldPoint
Temperature	T4102	672	Wetwell	±2 °C	FieldPoint

Open your mind. LUT.
Lappeenranta University of Technology

Temperature	T4103	822	Wetwell	±2 °C	FieldPoint
Temperature	T4104	972	Wetwell	±2 °C	FieldPoint
Temperature	T4105	1122	Wetwell	±2 °C	FieldPoint
Temperature	T4106	1272	Wetwell	±2 °C	FieldPoint
Temperature	T4107	1422	Wetwell	±2 °C	FieldPoint
Temperature	T4108	1722	Wetwell	±2 °C	FieldPoint
Temperature	T4109	2022	Wetwell	±2 °C	FieldPoint
Temperature	T4110	2322	Wetwell	±2 °C	FieldPoint
Temperature	T4111	2922	Wetwell	±2 °C	FieldPoint
Temperature	T4112	372	Wetwell	±2 °C	FieldPoint
Temperature	T4113	158	Wetwell	±2 °C	FieldPoint
Temperature	T4200	372	Wetwell	±2 °C	FieldPoint
Temperature	T4201	572	Wetwell	±2 °C	FieldPoint
Temperature	T4202	772	Wetwell	±2 °C	FieldPoint
Temperature	T4203	872	Wetwell	±2 °C	FieldPoint
Temperature	T4204	972	Wetwell	±2 °C	FieldPoint
Temperature	T4205	1072	Wetwell	±2 °C	FieldPoint
Temperature	T4206	1172	Wetwell	±2 °C	FieldPoint
Temperature	T4207	1272	Wetwell	±2 °C	FieldPoint
Temperature	T4208	1372	Wetwell	±2 °C	FieldPoint
Temperature	T4210	1572	Wetwell	±2 °C	FieldPoint
Temperature	T4212	1772	Wetwell	±2 °C	FieldPoint
Temperature	T4213	1972	Wetwell	±2 °C	FieldPoint
Temperature	T4214	2172	Wetwell	±2 °C	FieldPoint
Temperature	T4215	2372	Wetwell	±2 °C	FieldPoint
Temperature	T4216	2572	Wetwell	±2 °C	FieldPoint
Temperature	T4217	2972	Wetwell	±2 °C	FieldPoint
Temperature	T4218	472	Wetwell	±2 °C	FieldPoint
Temperature	T4219	672	Wetwell	±2 °C	FieldPoint
Temperature	T4300	372	Wetwell	±2 °C	FieldPoint
Temperature	T4301	572	Wetwell	±2 °C	FieldPoint
Temperature	T4302	772	Wetwell	±2 °C	FieldPoint
Temperature	T4303	872	Wetwell	±2 °C	FieldPoint
Temperature	T4304	972	Wetwell	±2 °C	FieldPoint
Temperature	T4305	1072	Wetwell	±2 °C	FieldPoint
Temperature	T4306	1172	Wetwell	±2 °C	FieldPoint
Temperature	T4307	1272	Wetwell	±2 °C	FieldPoint
Temperature	T4308	1372	Wetwell	±2 °C	FieldPoint
Temperature	T4310	1572	Wetwell	±2 °C	FieldPoint
Temperature	T4312	1772	Wetwell	±2 °C	FieldPoint
Temperature	T4313	1972	Wetwell	±2 °C	FieldPoint
Temperature	T4314	2172	Wetwell	±2 °C	FieldPoint
Temperature	T4315	2372	Wetwell	±2 °C	FieldPoint
Temperature	T4316	2572	Wetwell	±2 °C	FieldPoint
Temperature	T4317	2972	Wetwell	±2 °C	FieldPoint
Temperature	T4318	472	Wetwell	±2 °C	FieldPoint
Temperature	T4319	672	Wetwell	±2 °C	FieldPoint
Temperature	T4400	222	Wetwell	±2 °C	FieldPoint
Temperature	T4401	522	Wetwell	±2 °C	FieldPoint
Temperature	T4402	672	Wetwell	±2 °C	FieldPoint
Temperature	T4403	822	Wetwell	±2 °C	FieldPoint
Temperature	T4404	972	Wetwell	±2 °C	FieldPoint

Temperature	T4405	1122	Wetwell	±2 °C	FieldPoint
Temperature	T4406	1272	Wetwell	±2 °C	FieldPoint
Temperature	T4407	1422	Wetwell	±2 °C	FieldPoint
Temperature	T4408	1722	Wetwell	±2 °C	FieldPoint
Temperature	T4409	2022	Wetwell	±2 °C	FieldPoint
Temperature	T4410	2322	Wetwell	±2 °C	FieldPoint
Temperature	T4411	2922	Wetwell	±2 °C	FieldPoint
Temperature	T4412	372	Wetwell	±2 °C	FieldPoint
Temperature	T4413	158	Wetwell	±2 °C	FieldPoint
Temperature	T4501	-	RHR nozzle injection line	±2 °C	FieldPoint
Cut-off valve position	V1	-	DN50 Steam line	Not defined	LabView
Cut-off valve position	X2100	-	DN50 Steam line	Not defined	FieldPoint
Steam partial pressure	X2102	5200	Drywell	Not defined	FieldPoint
Cut-off valve position	X2106	-	DN50 Steam line	Not defined	FieldPoint

Measurements of the PPOOLEX facility in the spray tests.

APPENDIX 2: Turbulence intensity calculation method

Turbulence intensity

Turbulence intensity is the ratio of the root-mean-square of turbulent velocity fluctuations and the mean velocity. Estimated velocity vectors gained from PIV measurements are in series of discrete points. Turbulence intensity varies depending on how many of these discrete points are taken into consideration. In general, when turbulence intensity is calculated by using only a few discrete points the results are considered to be unreliable. The time period should be longer and thus the amount of discrete points larger than the longest fluctuation of the turbulence. The required equations for calculating the turbulence intensity are presented next.
Mean velocity is defined as:

$$\bar{u} = \frac{1}{N}\sum_{i=1}^{N} u_i \qquad (1)$$

Where N is the amount of discrete points or in other words, the number of different PIV frames and u_i is the estimated velocity at the discrete point i. The turbulent fluctuation can be calculated by using mean velocity as follows:

$$u_i' = u_i - \bar{u} \qquad (2)$$

The figure below illustrates the velocity at different discrete points, mean velocity and the turbulence fluctuation.

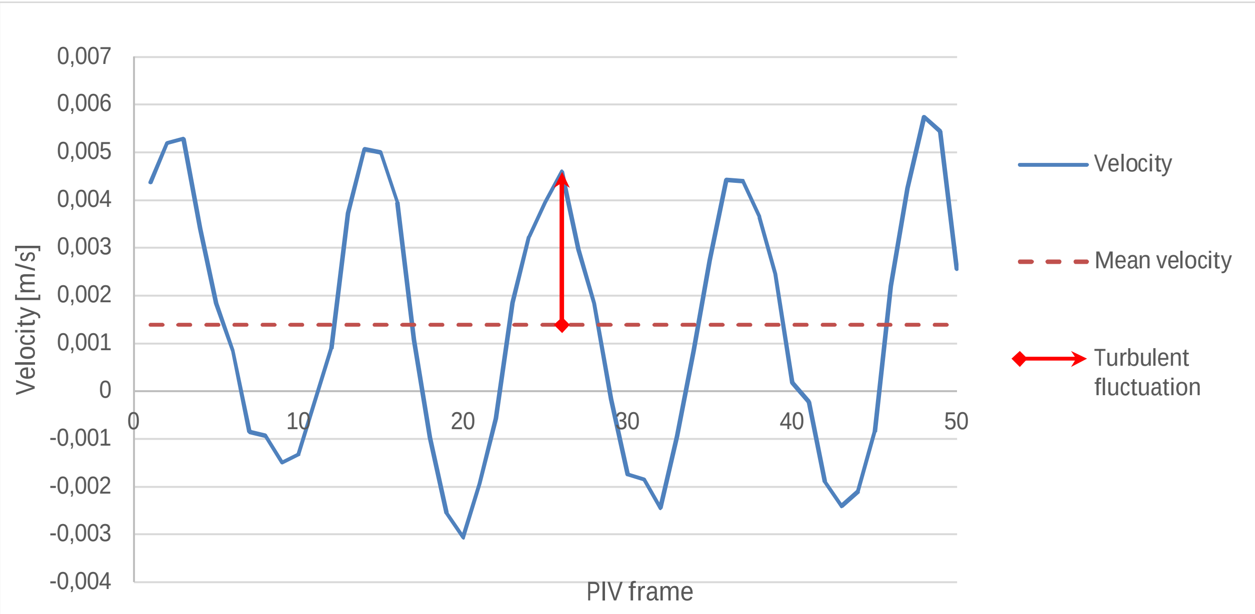

Recorded velocity, mean velocity for 50 PIV frames and turbulent fluctuation for the PIV frame number 26.

Turbulence strength is the root-mean-square of turbulent fluctuation and it is defined as:

$$u_{rms} = \sqrt{\frac{1}{N}\sum_{i=1}^{N} (u_i')^2} \qquad (3)$$

Finally, the turbulence intensity can be calculated as follows:

$$TI = \frac{u_{rms}}{\bar{u}} \tag{4}$$

The former example is for one velocity and the velocity u can be longitudinal, vertical or lateral. In case where there are three velocity components, the turbulence strength is computed as:

$$u_{rms} = \sqrt{\frac{1}{3}\left(u_{rms,x}^2 + u_{rms,y}^2 + u_{rms,z}^2\right)} \tag{5}$$

And the mean velocity:

$$\bar{u} = \sqrt{\bar{u}_x^2 + \bar{u}_y^2 + \bar{u}_z^2} \tag{6}$$

Python script and the estimation of turbulence intensity for SPR-T7-5

A python script was developed for calculating the turbulence intensity. The script takes PIV vector frame data as input values. All input vectors from PIV are not valid and these are displayed in input as zero vectors. Currently, in addition to calculating the turbulence intensity, the script can attempt to fix some of these faulty zero vectors by interpolating values from the neighboring vectors. The script does not take faulty vectors into account when calculating the turbulence intensity.

In PIV input values, the velocity vectors are divided into calculation windows with the area of 64 by 64. This area had to be reduced to the area of 58 by 58 because the upper parts of the calculation windows had too many faulty vectors for estimating turbulence intensity. An example of a turbulence intensity field is presented in the figure below.

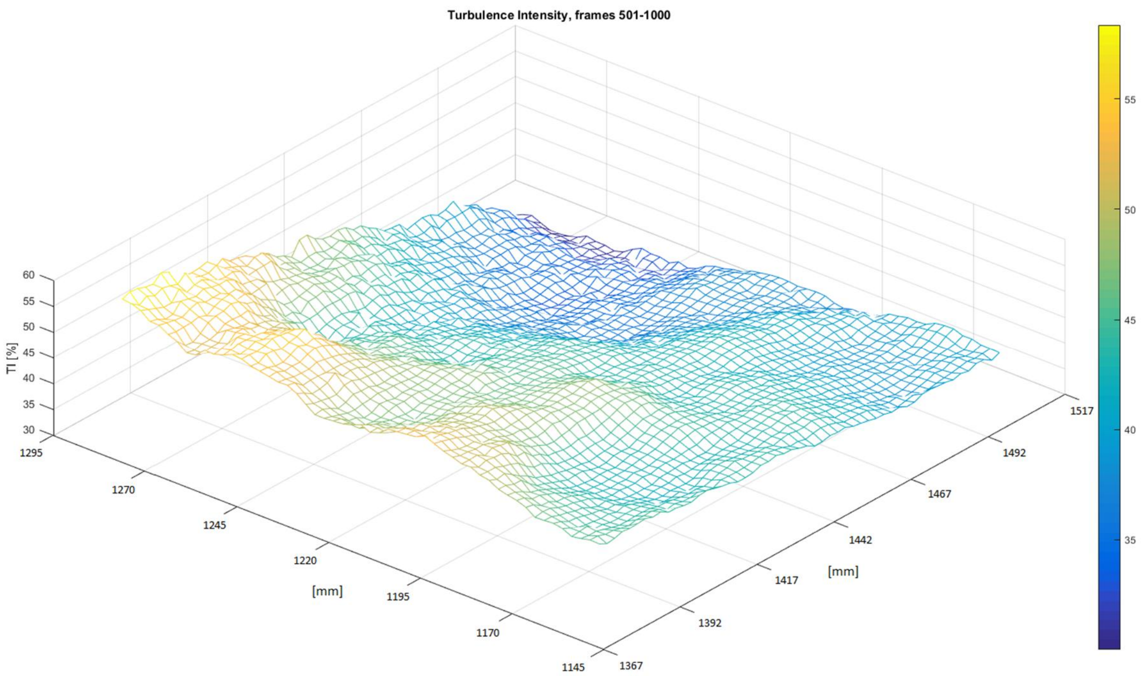

An example turbulence intensity field from PIV measurement sequence SPR-T7-5, N=501-1000.

Appendix E

CFD simulation of condensation of vapor jets

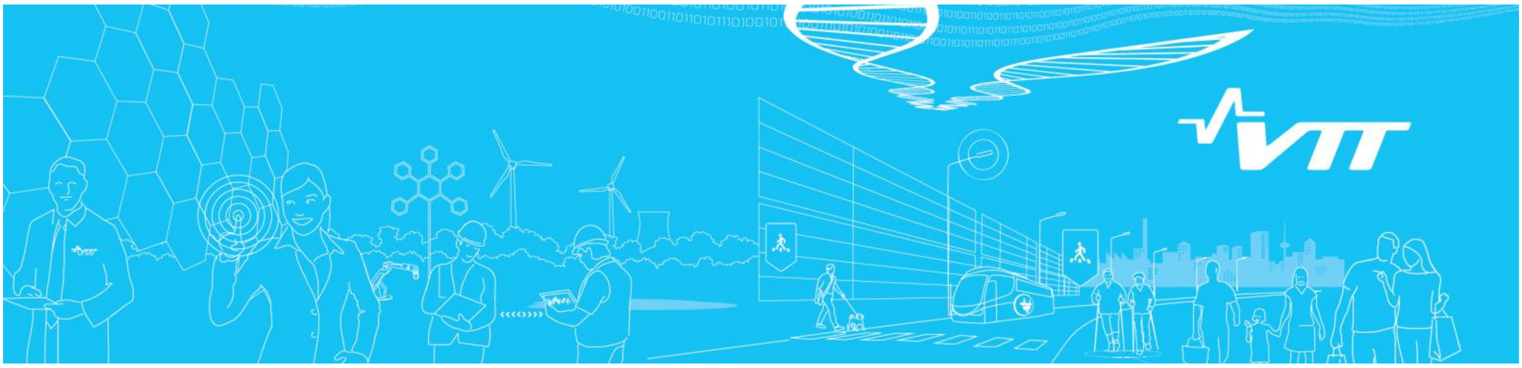

RESEARCH REPORT

VTT-R-00993-18

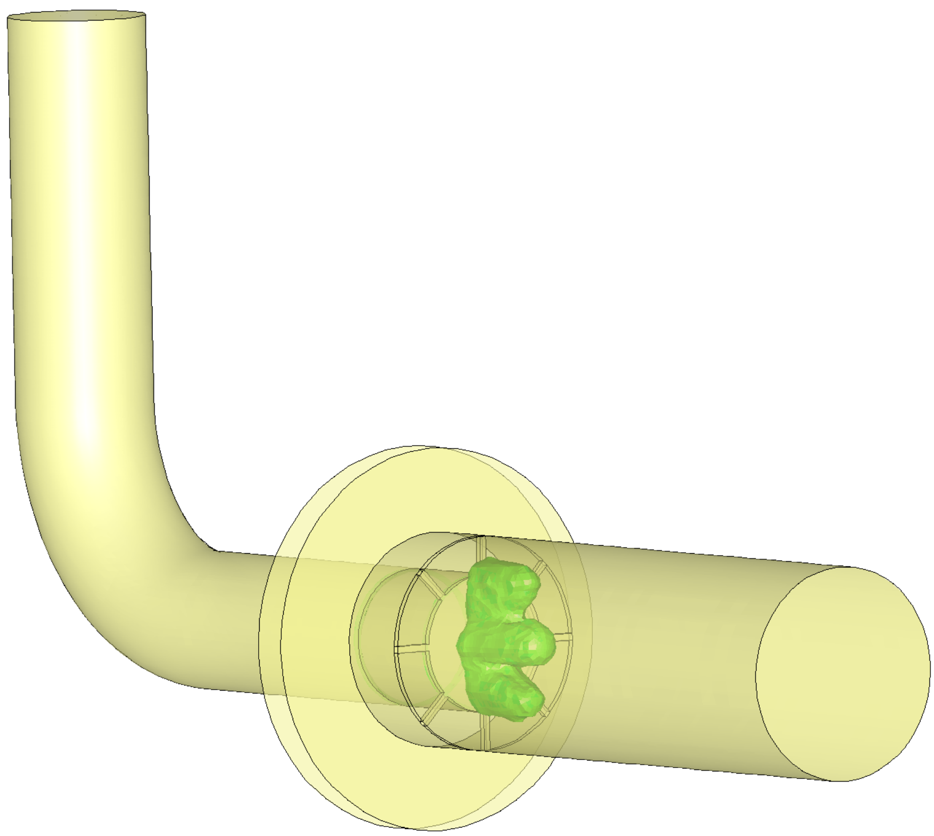

CFD simulation of condensation of vapor jets

Authors: Timo Pättikangas and Ville Hovi

Confidentiality: Public

Report's title	
CFD simulation of condensation of vapor jets	
Customer, contact person, address 1. Yli-insinööri Jorma Aurela, Valtion ydinjätehuoltorahasto, PL 32, 00023 Valtioneuvosto 2. Cristian Linde, Programme Manager NKS-R, Strålsäkerhetsmyndigheten, SE-171 16 Stockholm, Sweden	**Order reference** Dnro SAFIR 15/2017 AFT/NKS-R(17)114/3
Project name Development and Validation of CFD Methods for Nuclear Reactor Safety Assessment (NURESA)	**Project number/Short name** 113373 / SAFIR_2018_NURESA_2017
Author(s) Timo Pättikangas and Ville Hovi	**Pages** 26
Keywords Direct-contact condensation, sparger, stratification, BWR, pressure suppression pool, CFD, computational fluid dynamics	**Report identification code** VTT-R-00993-18

Summary

Pre-test SEF-T000 performed on direct-contact condensation in the INSTAB project at LUT has been studied with Computational Fluid Dynamics (CFD) calculations. The pre-test was performed with the newly constructed separate effect test facility, where steam was injected into water pool. The mass flow rate of steam was small (14.8 g/s) and the temperature of the water was fairly high (67 °C) in the time interval chosen for the simulation. The steam was injected into water horizontally through three orifices having diameters of 16 mm, which corresponds to the mass flux of 24.5 kg/m^{2}s.

The oscillation patterns in direct-contact condensation experiments have previously been classified based on mass flux of steam and water temperature by several authors. The classification maps suggested that the parameters of the experiment are in the transition region between condensation oscillation and chugging.

The CFD simulation was performed with the Euler-Euler two-phase model of ANSYS Fluent. Two-resistance heat transfer model of Fluent was used, where the Ranz-Marshall correlation for heat transfer was assumed on the liquid side and zero resistance the gas side.

The CFD simulation was found to produce qualitatively correct description of the chugging oscillation observed in the experiment. The period of the oscillation, the penetration of the vapor jet and the pressure oscillation were reasonably close to the experimental observations.

Confidentiality	Public

Espoo, 28.2.2018

Written by	Reviewed by	Accepted by
Timo Pättikangas	Risto Huhtanen	Lars Kjäldman
Timo Pättikangas, Principal Scientist	Risto Huhtanen, Senior Scientist	Lars Kjäldman, Research Team Leader

VTT's contact address

P.O.Box 1000, FI-02044 VTT, Finland

Distribution (customer and VTT)

Vesa Suolanen, SAFIR2018 Reference Group 4, Programme Manager NKS-R

Preface

This work has been carried out in the Work Package 2 of the NURESA project of the SAFIR2018 programme (The Finnish Research Programme on Nuclear Power Plant Safety). The project has been funded by Valtion ydinjätehuoltorahasto, VTT and NKS (Nordic nuclear safety research). The authors are grateful for comments obtained from the members of the SAFIR2018 Reference Group 4.

Espoo, 28 February 2018

Authors

Contents

Preface....3

Contents....4

1. Introduction....5

2. Separate effect test facility....6

3. CFD model of the test facility....7

4. CFD simulation of chugging....10

5. Comparison with the pre-test SEF-T000....20

6. Summary and conclusions....24

References....25

1. Introduction

In 2011, earthquake and large tsunami occurred near eastern Japan, which caused accidents in the Fukushima Daiichi nuclear power plants. During the subsequent station blackout, the reactor core isolation cooling (RCIC) systems of Units 2 and 3 provided cooling water into the reactor vessels. In Unit 3, the RCIC system had only single steam injection sparger, which means that the thermal energy was transferred in localized region near the sparger. In addition, in Unit 3 the pressure in the primary containment vessel increased drastically during the RCIC operation. Therefore, it is suspected that thermal stratification occurred in the pressure suppression pool of Unit 3. (Jo et al., 2016)

In boiling water reactors (BWR), the analysis of thermal stratification of the pressure suppression pool is important, when hypothetical accident scenarios are investigated. At KTH, Gallego-Marcos et al. (2017) have formulated and implemented Effective Mass Source and Effective Heat Source (EMS/EHS) method for the studies of thermal stratification in water pools. The method has been validated against PPOOLEX and PANDA experiments and implemented in the GOTHIC and ANSYS Fluent codes (Gallego-Marcos et al., 2016, 2017).

At LUT, separate effect test facility has been constructed for detailed direct-contact condensation studies of spargers. The test facility has been designed in co-operation with KTH by Puustinen and Kudinov (2017). In the test facility, vapor is injected horizontally into water pool through small orifices. Either one or three orifices are used in the experiments.

The condensation regime maps for the injection of vapor into water pools has previously been presented by several authors, for instance, Nariai and Aya (1966), Aya and Nariai (1991), Lahey and Moody (1993), Gulawani et al. (2006) and Gallego-Marcos et al. (2017). In Figure 1, one of these maps has been reproduced. The behavior of condensation has been found to depend on the mass flux of vapor and on the temperature of the water of the pool. At high mass flux condensation oscillations occur, where the condensation occurs outside the sparger that is used for steam injection. At low mass fluxes, chugging occurs, where water penetrates into the sparger pipe and condensation also occurs inside the pipe. Between these two regions is the transition regime.

Landram et al. (1982) presented one of the earliest CFD calculation of chugging in BWR pressure suppression pool. They used free surface model with a simple model for the condensation rate, which was calculated by comparing the vapor pressure to the saturation pressure. More recently, Gulawani et al. (2006), studied condensation vertical vapor plumes with CFD calculations and developed models for the interfacial area in direct-contact condensation. Timperi et al. (2013) studied pressure loads during chugging in the PPOOLEX test facility. Patel et al. (2017) studied chugging by implementing the Rayleigh-Taylor interface instability model in the NEPTUNE_CFD and OpenFOAM codes.

In the present work, the pre-test SEF-T000 performed by Puustinen et al. (2017) at the Lappeenranta University of Technology is studied with CFD simulations. In the experiment, the mass flux of steam was 24.5 kg/m^{2}s and the temperature of the water pool was 67 °C. According to the regime map of Aya and Nariai (1991), this experiment is in the transition regime between condensation oscillations and chugging. The goal of the simulations is to obtain insight into the mechanisms of the condensation oscillation and chugging

Two-phase Euler-Euler simulations are performed with the ANSYS Fluent CFD code, where two-resistance model is used for the heat transfer and the condensation-evaporation model of Fluent for the phase change. The simulation results are compared to pressure measurements and to the high-speed video from the experiment. At a later stage, the CFD results can also be compared against the EMS/EHS models.

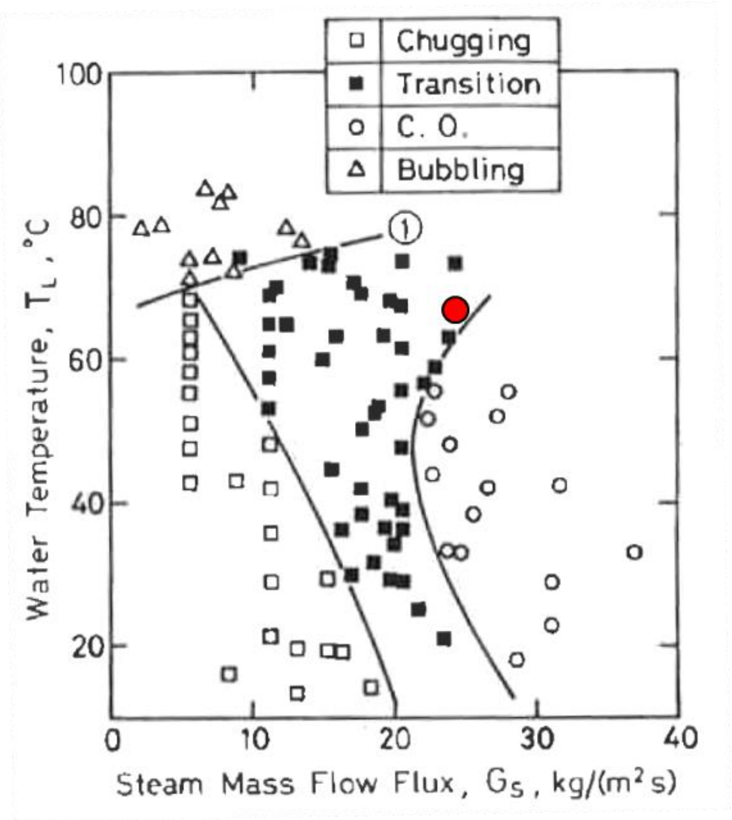

Figure 1. Regime map of steam condensation in water pool (Aya and Nariai, 1991). The experiment SEF-T000 has been marked with a red dot.

2. Separate effect test facility

The separate effect test facility of LUT is shown in Figure 2. The test facility is located in a rectangular box that is filled with water. Steam line runs downwards from the top of the box and bends to horizontal direction. At the end of the steam line, steel plate with one or three orifices is installed. The steam is injected through the orifice(s) into transparent plexiglass tube, where the condensation occurs.

The diameter of the plexiglass tube is somewhat larger than that of the steam line. The steel plate at the end of the steam line is surrounded by an annular channel, where liquid water can flow into the plexiglass tube from the water pool. The flow path is through the flange connecting the steam line to the plexiglass tube.

The condensation of vapor is monitored with high-speed camera through the window on one side of the box. The collapse frequencies of the vapor bubbles are monitored with high-frequency pressure measurements. The temperature of water is measured with three sensors located at the end of the plexiglass tube. The momentum transferred from the vapor jet to liquid-water is determined by force measurement on the steam line.

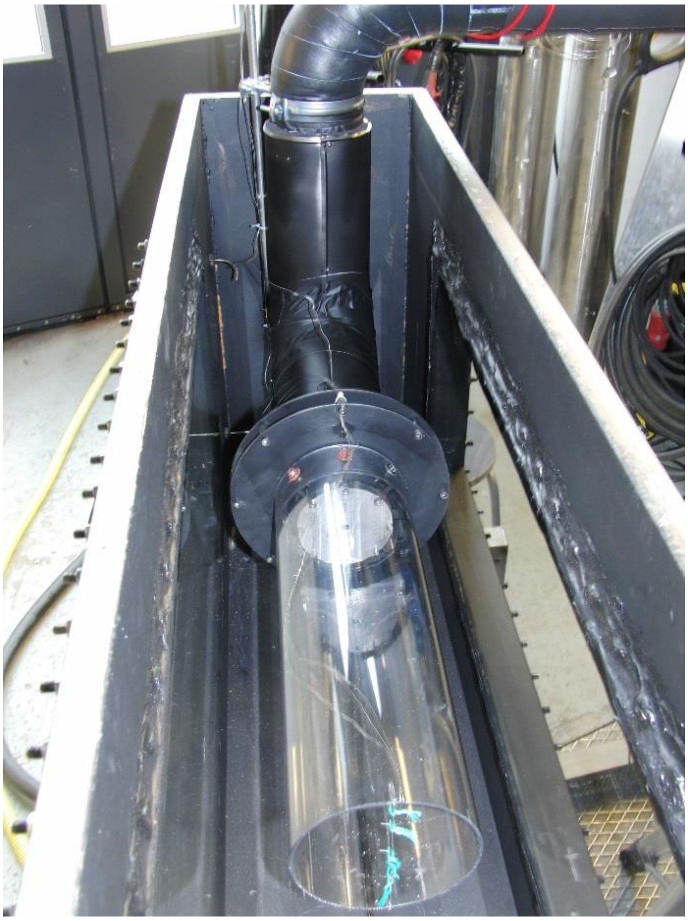

Figure 2. Separate effect test facility of LUT for the direct-contact condensation experiments (Puustinen et al., 2017).

The goal of the experiments is to determine effective heat and momentum sources from the vapor jet to the liquid water in the pool. The effective sources can then be used in coarse grained modelling of stratification in pressure suppression pools of BWRs, where steam is injected through SRV spargers (Kudinov, 2016). Such coarse grained models can be implemented, for instance, in the GOTHIC code for analysis of the pressure suppression pools of BWR plants.

3. CFD model of the test facility

The geometry model of the separate effect test facility is shown in Figure 3. In the model, steam is injected downwards into the vertical pipe, which bends to horizontal direction. A steel plate with three orifices (∅16mm) is located at the end of the horizontal section. Steam flows through the orifices into the plexiglass tube. The tube is submerged in a box filled with water. Some water can also flow from the box into the plexiglass tube through the flange connecting the steam line to the plexiglass tube.

The hexahedral CFD mesh is shown in Figure 4. The mass flow inlet for the steam injection is in the beginning of the vertical tube. A small amount of water is injected through the second mass flow inlet of the flange. The injected water flows into the plexiglass tube through the flow path surrounding the steel plate with three orifices. The flow path and the orifices are shown in green color in Figure 4. Pressure outlet is located at the end of the plexiglass tube. The hexahedral mesh has about 140 000 control volumes.

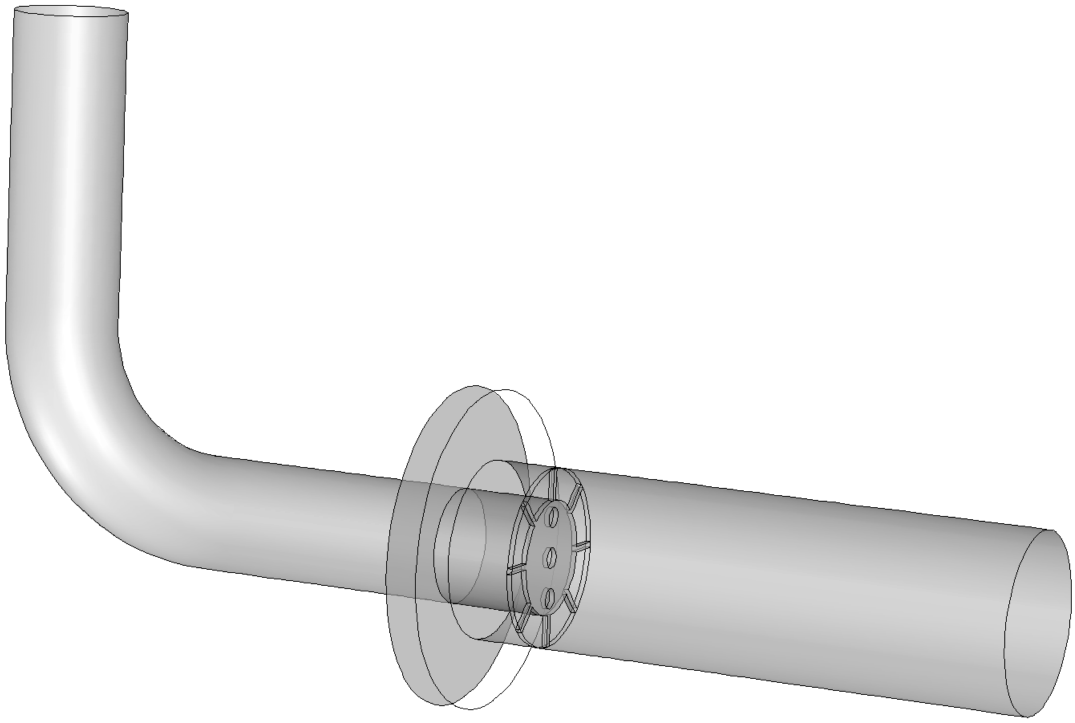

Figure 3. Geometry model of the separate effect test facility. The tube is inserted into box filled with water as is shown in Figure 2.

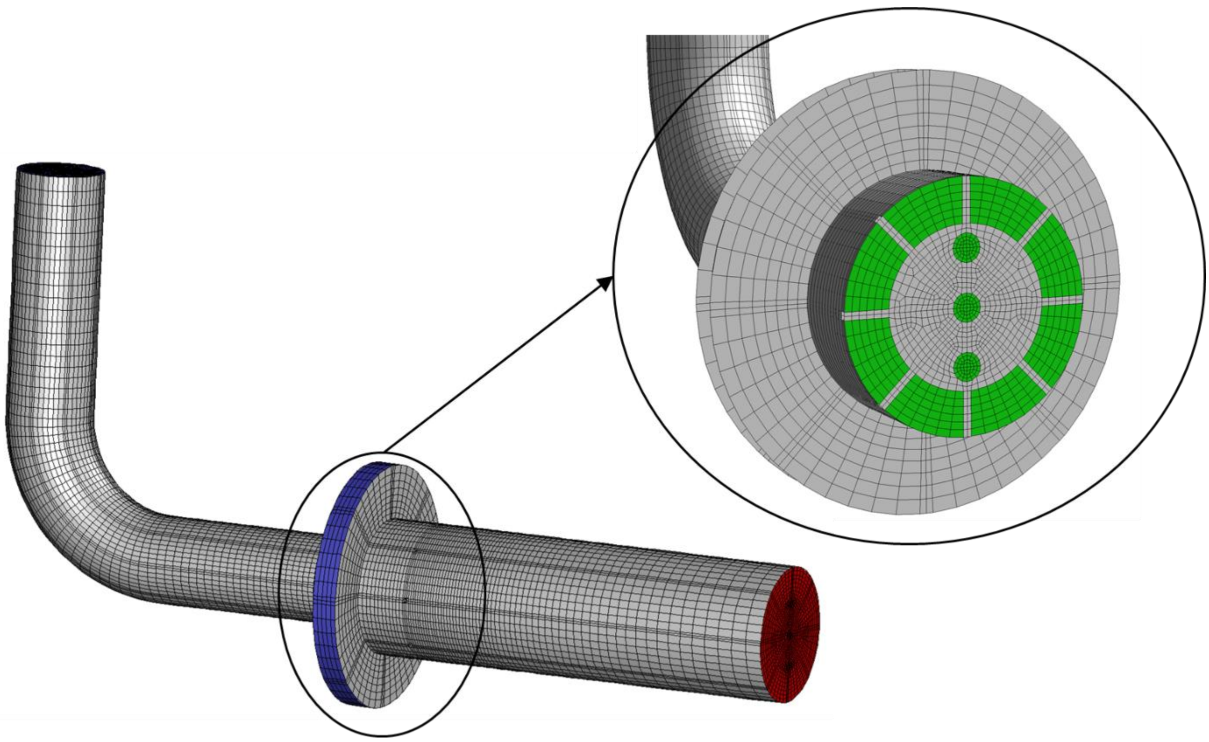

Figure 4. Surface mesh of the CFD model.

In the following, the pre-test SEF-T000 is studied. The simulation parameters are chosen to correspond time t = 353 s of the experiment. The mass flow rate of saturated vapor was 14.8 g/s, which corresponds to mass flux of 24.5 kg/m^{2}s. The vapor was modelled as condensing ideal gas. The temperature of water in the pool was about 67 °C.

The calculations were performed by using the Euler-Euler two-phase model of ANSYS Fluent version 18.2, which was found to be more stable than the previous versions. The condensation was calculated by using the two-resistance model, where the Ranz-Marshall model for heat transfer was assumed on the liquid side. On the vapor side, zero resistance was assumed. Evaporation-condensation model of Fluent was used.

“Universal” drag model was applied for the momentum transfer between vapor and liquid-waver. Interfacial area of the phases was calculated with ia-symmetric model of Fluent. In the calculation, constant bubble diameter of one millimeter was assumed. Turbulence was described with mixture k-ε model, where Lopez de Bertodano model was used for the turbulent dispersion.

The saturated vapor injected into the plexiglass tube may contain small amount of water droplets. The amount of water in the present experiment is not known. In the simulation, volume fraction of 0.001 of water was assumed. Since the density of the water is much higher than that of vapor, the mass fraction of water is significant and affects the simulation results.

4. CFD simulation of chugging

CFD simulation of a short period around time t = 353 s of the SEF-T000 pre-test was performed. The simulation was initialized so that the plexiglass tube contained water with a temperature of 67 °C. The steam line was full of saturated vapor, which contained a small volume fraction of saturated water. When more steam was flowing into the steam line, the pressure on the orifice plate increased and vapor started flowing into the plexiglass tube.

In Figure 5, the time evolution of the void fraction near the orifice plate is shown. The periodic condensation of the vapor in the plexiglass tube lead to an oscillatory behavior of the vapor jets. The first maximum of the volume fraction occurs at time t = 0.05 s, which is followed by rapid condensation of vapor and minimum of the void fraction at time t = 0.082 s. The following maxima of the void fraction occur at the instants of time t = 0.120 s, 0.200 s, 0.286 s, 0.358 s, 0.453 s, 0.548 s, and 0.623 s. The period of the chugging is approximately Δt = 83 ms, which corresponds to a frequency of 12 Hz. The growth phase of the bubbles last on average approximately 41 ms and the collapse lasts 42 ms.

In Figure 5, four frames are shown for each period of the chugging. When rapid condensation occurs, for instance at time t = 0.498 s, some liquid water penetrates behind the orifice plate. The water is mixed into the vapor flow, which carries the water droplets through the orifices back to the plexiglass tube. Therefore, the vapor flowing into the plexiglass tube unavoidably contains some amount of liquid water.

In Figure 6, condensation rate of vapor is shown at a few instants of time. The frames shown correspond to middle part of the time series shown in Figure 5. Four frames are again shown for each period of the chugging. The maximum condensation rates of about 600 kg/m^3s occur, when the collapse of the steam jets starts. The rapid condensation leads to the penetration of liquid water behind the orifice plate, which can be clearly seen in the condensation rate at time t = 0.498 s.

In Figure 7, the velocity magnitude of vapor is shown. Note that the velocity scale is logarithmic and the velocities above the scale are shown in red. The frames correspond to one period of chugging starting at time t = 0.413 s, when previous vapor bubbles have collapsed. New vapor bubbles reach their maximum size at time t = 0.453 s and are fully condensed at time t = 0.498 s. The maximum vapor velocities occur in the orifices and are about 100 m/s.

In Figure 8, the relative static pressure during the same period of chugging is shown. The relative pressure in the steam line has its maximum value of 9 kPa, when the formation of new bubbles is beginning at time t = 0.413 s. The increasing vapor pressure pushes liquid water from the orifices and forms vapor bubbles in the plexiglass tube. At time t = 0.453 s, the rapid condensation of the bubbles has already started and the relative pressure has its minimum value of –7 kPa. At time t = 0.498 s, the increase of pressure has started, which leads to new period of chugging. The total amplitude of the pressure oscillation is approximately 16 kPa.

In Figure 9, time evolution of the temperature of the liquid water is shown. In the beginning of the simulation, the temperature of water is 67 °C. The condensation of vapor gradually increases the temperature the liquid water. In the end of the simulation at time t = 1.064 s, the temperature of the liquid near the orifice plate is about 80 °C. At the outlet of the plexiglass tube, the temperature does not change much during the short simulation.

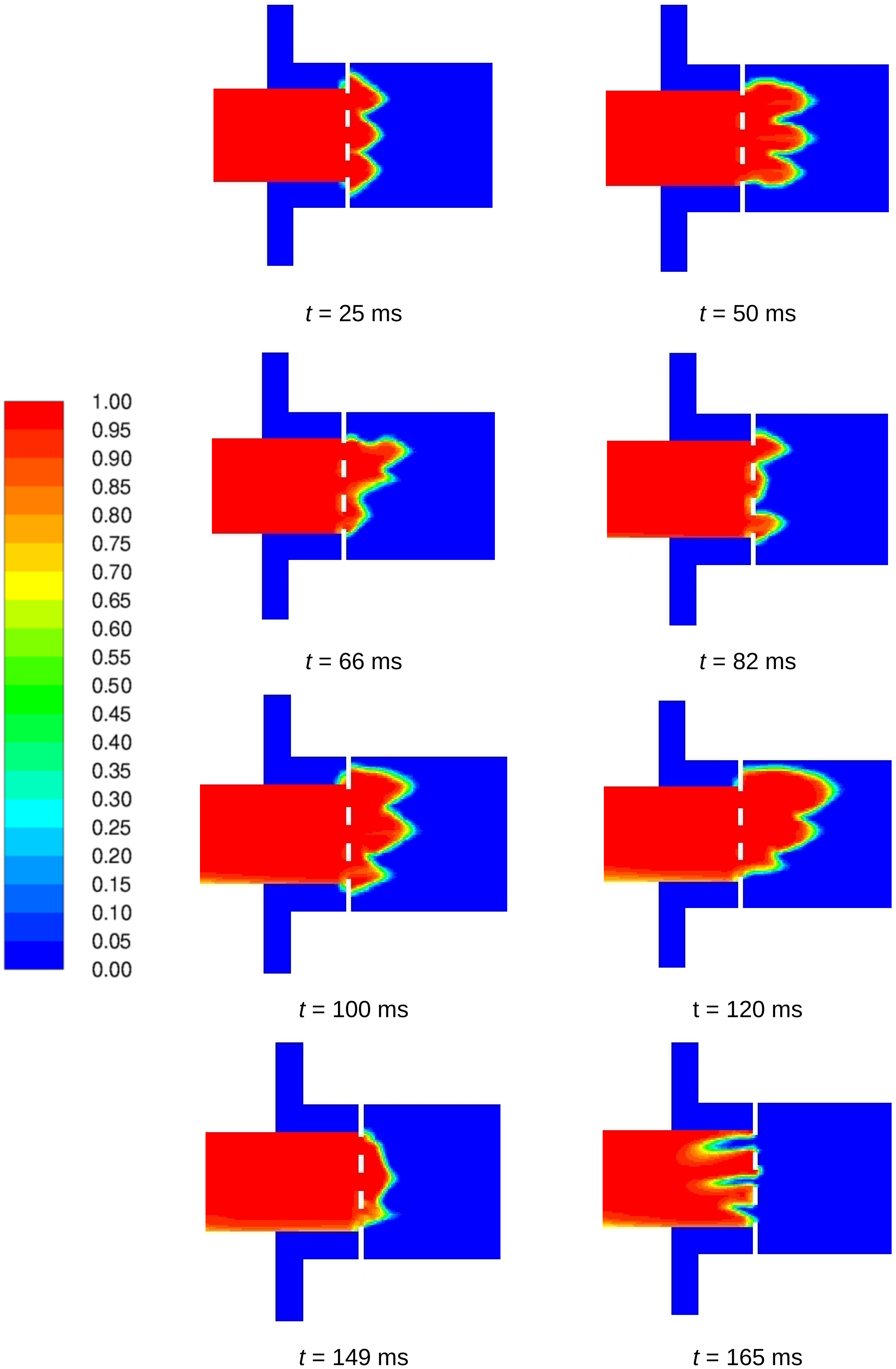

Figure 5. Void fraction in the vertical center plane of the test facility. Void fractions are shown at the instants of time, when the vapor bubbles have the maximum size, are contracting, have minimum size and are growing (continues on the following pages).

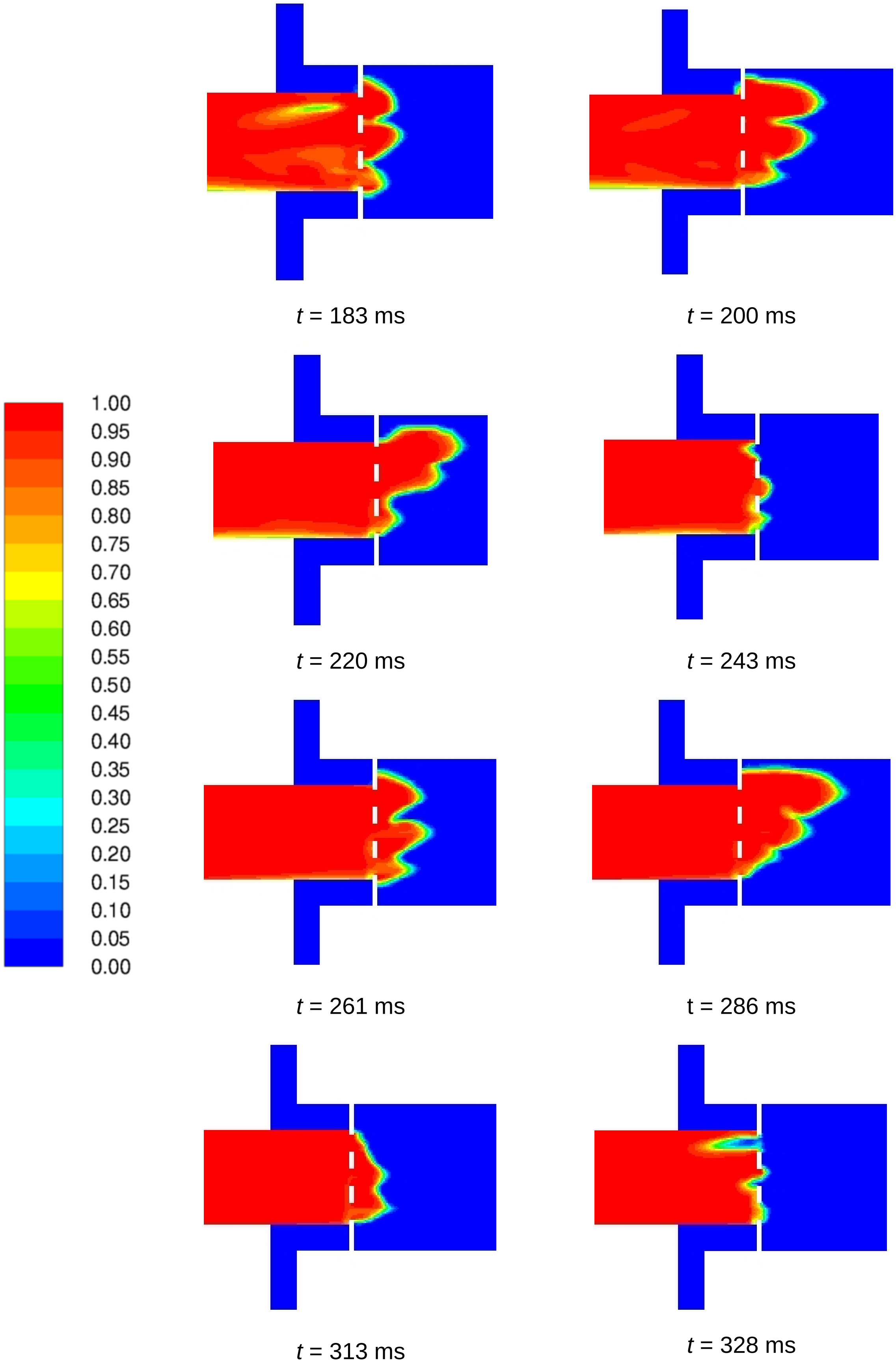

Figure 5. Void fraction in the vertical center plane of the separate effect test facility (continuation from the previous page).

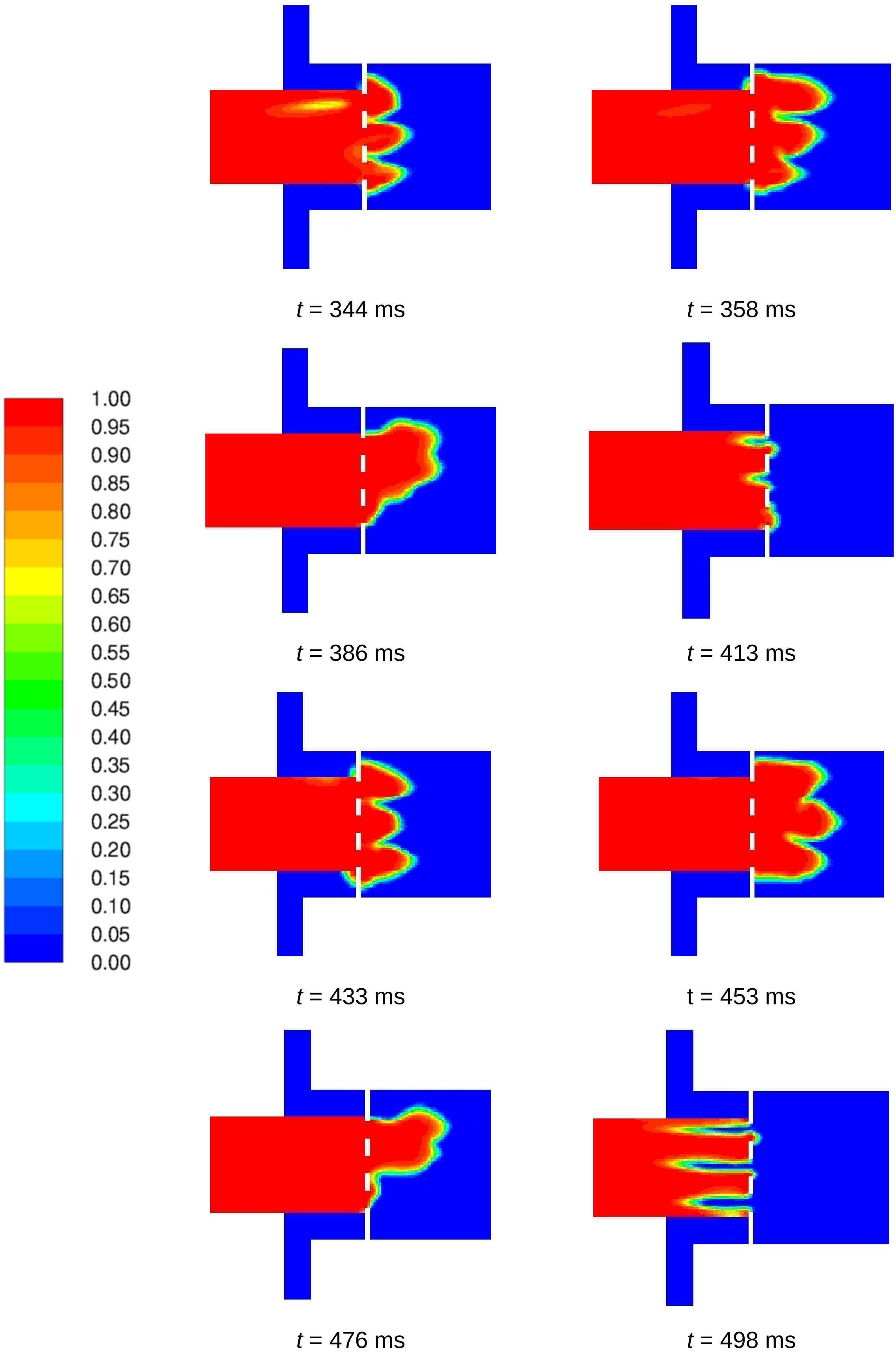

Figure 5. Void fraction in the vertical center plane of the separate effect test facility (continuation from the previous pages).

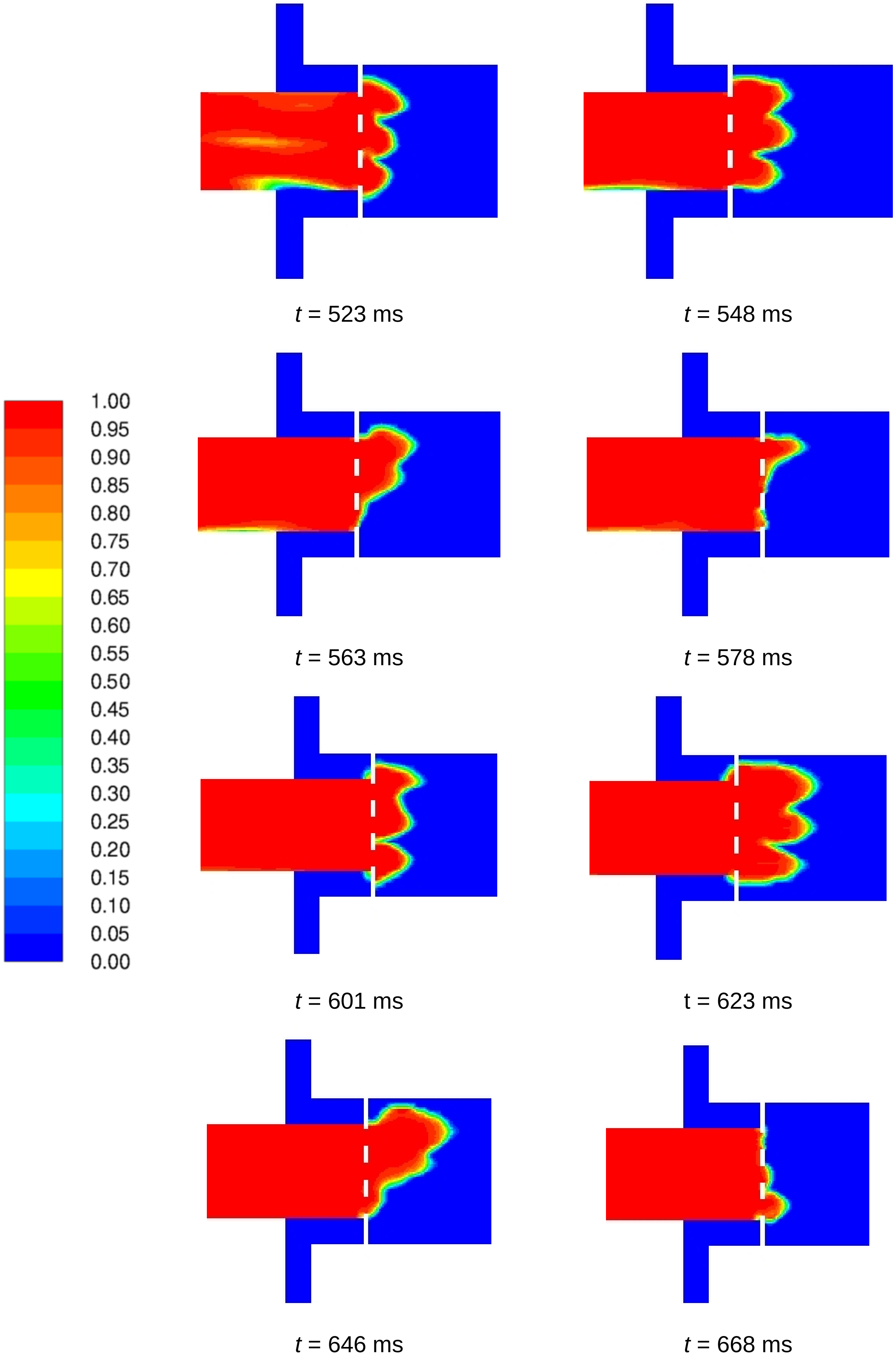

Figure 5. Void fraction in the vertical center plane of the separate effect test facility (continuation from the previous pages).

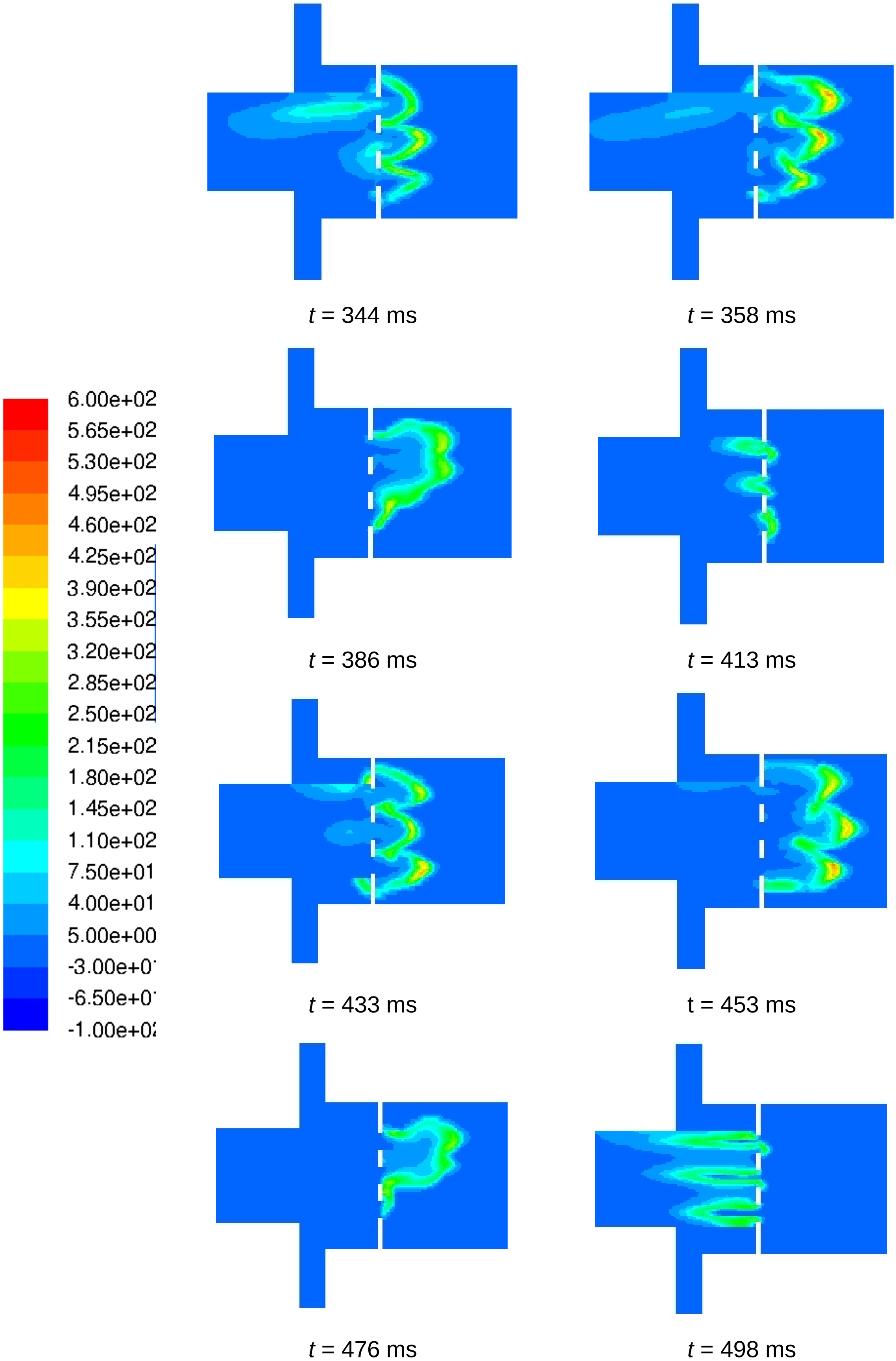

Figure 6. Condensation rate of vapor (kg/m^{3}s) in the vertical center plane of the test facility.

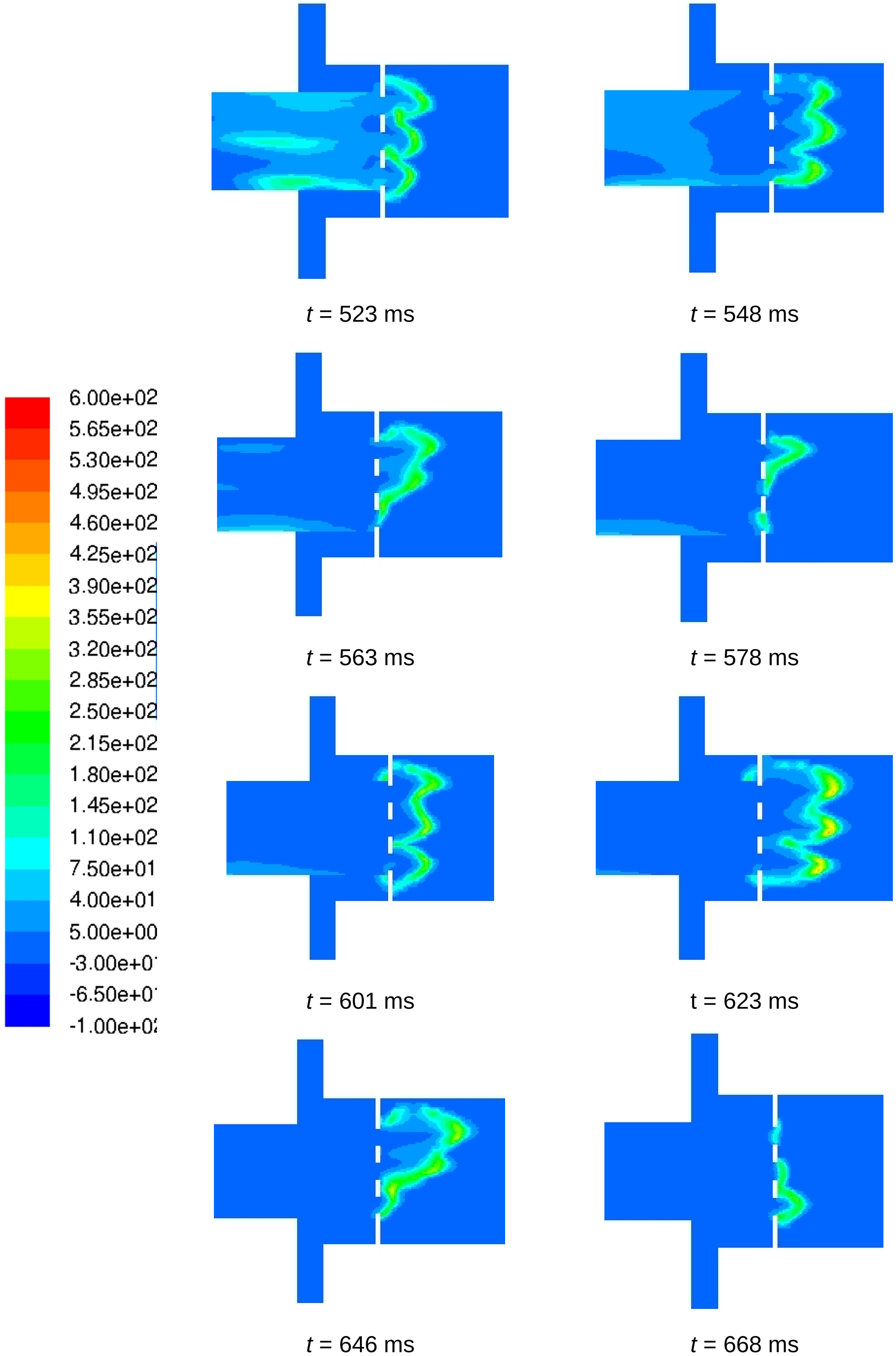

Figure 6. Condensation rate of vapor (kg/m^{3}s) in the vertical center plane of the test facility (continuation from the previous page).

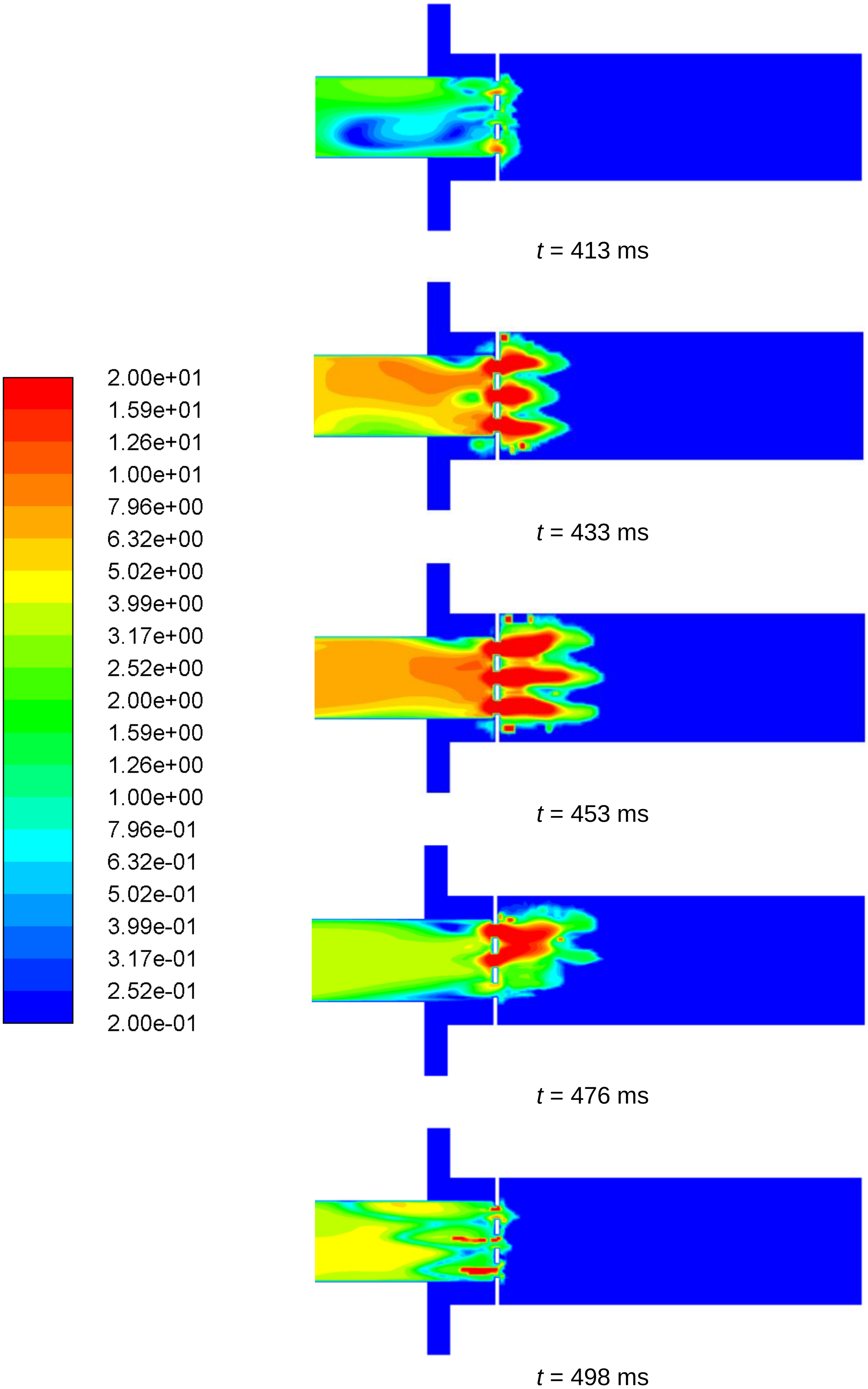

Figure 7. Velocity magnitude (m/s) of vapor at different instants of time. Note that the scale is logarithmic and the values below the scale are shown in blue and the values above the scale are shown in red.

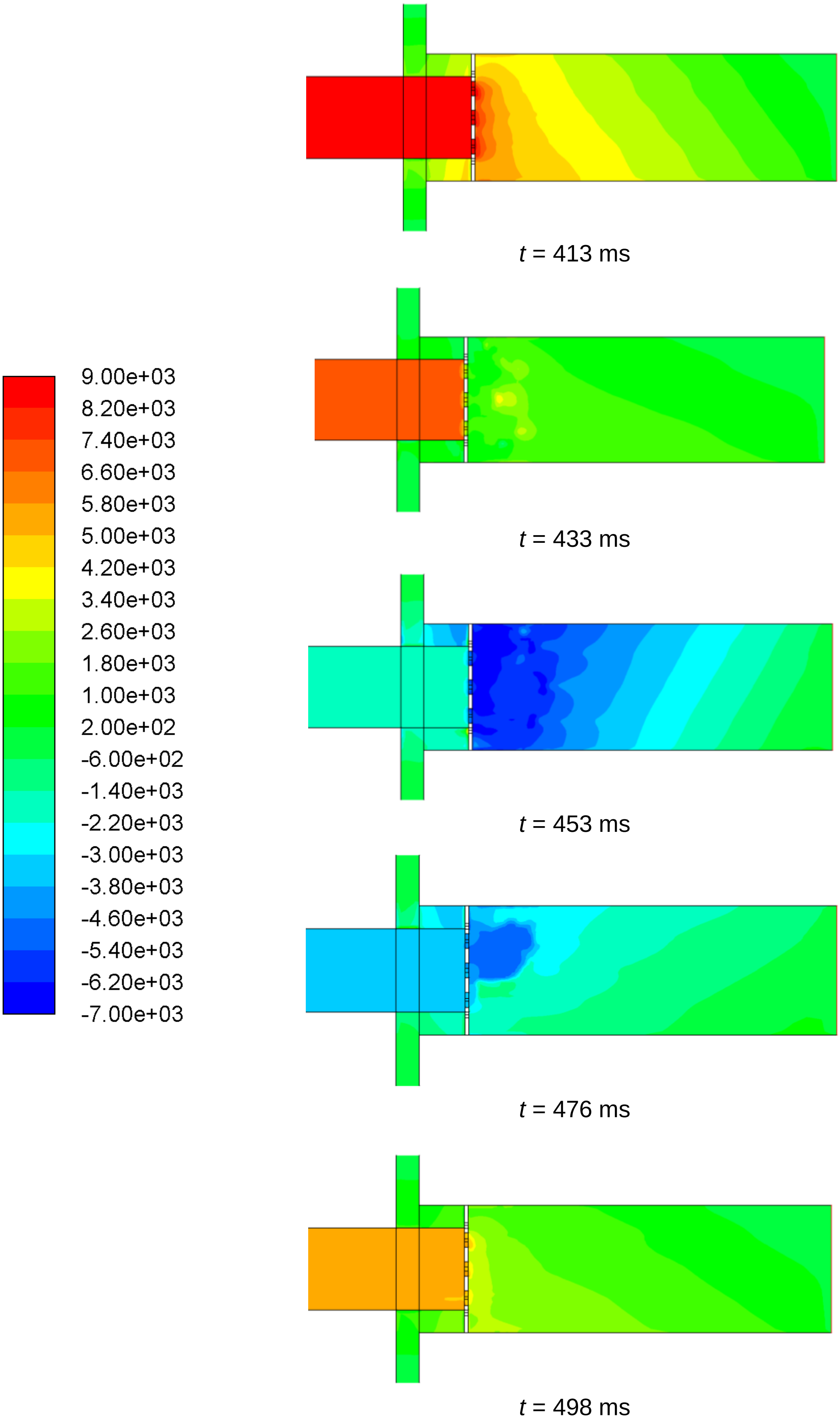

Figure 8. Relative static pressure (Pa) at different instants of time.

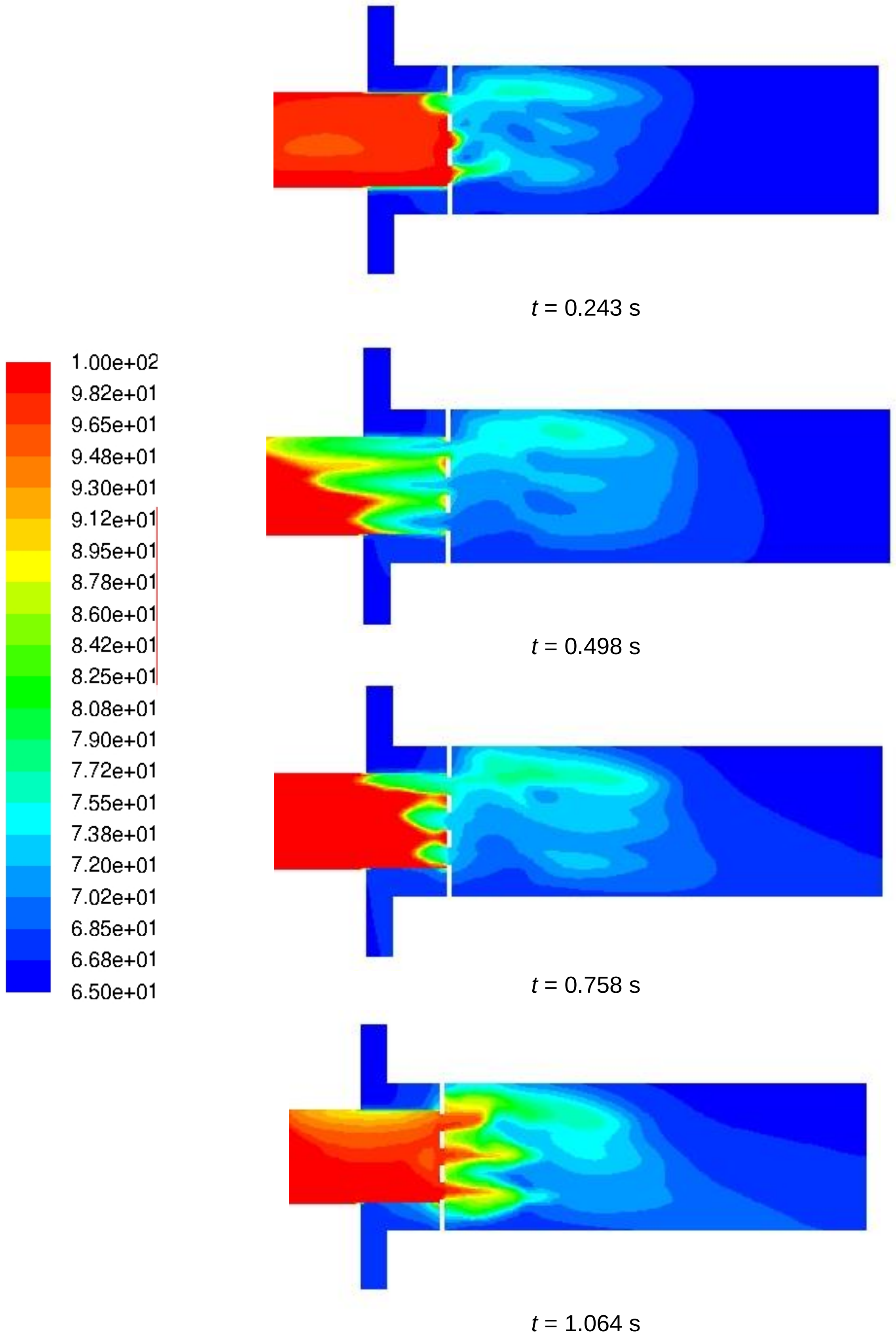

Figure 9. Temperature (°C) of liquid-water at different instants of time.

5. Comparison with the pre-test SEF-T000

The simulation results can be compared with the pre-test SEF-T000 at time t = 353 s, where high-speed video and high-frequency pressure measurements are available. In Figure 10, frames from the high-speed video of Puustinen et al. (2017) have been chosen by using the same method as was used for the CFD simulation in Figure 5. Four frames has been chosen for each period of the chugging: (i) the vapor bubbles have the minimum size, (ii) bubbles are growing, (iii) bubbles have maximum size, and (iv) bubbles are contracting.

In Figure 10, the vapor bubbles have their maximum sizes at time t = 221, 270, 311 and 357 ms. Calculation of the average period of the chugging from the high-speed video images give the results Δt = 0.45 ms, which is shorter than the period of Δt = 82 ms found in the simulation. In the experiment, the collapse of vapor bubble occurs faster than the growth of the bubble. In the experiment, the average collapse lasts 11 ms, but in the CFD simulation the collapse time was 42 ms. In the experiment, the growth of the bubble lasted 34 ms and in the simulation 42 ms. Thus, the difference between the simulation and the experiment is largest in the collapse phase, which is too slow in the simulation.

During the chugging, the penetration of the vapor jets into the liquid-water can only be roughly estimated from the high-speed video images. In the experiment, the average maximum penetration of the vapor jet is approximately 46 mm, i.e., roughly three diameters of the orifice. In the simulation, the maximum penetration was about 73 mm, which is clearly longer than the observation from the high-speed video. This is consistent with the longer period of the chugging in the simulation compared to the experiment.

In Figure 11, the pressure oscillation is shown that was measured in front of the orifice plate in the plexiglass tube by Puustinen et al. (2017). The top and center frames shows clearly low-frequency oscillation of the pressure superposed with high-frequency oscillations. The amplitude spectrum of the bottom frame shows that the low-frequency oscillation occurs at the frequency of 23.5 Hz, which corresponds to period of Δt = 43 ms. This is very close to the value obtained by visual observation of high-speed videos and corresponds to the period of chugging.

In Figure 11, the amplitude of the pressure oscillation from minimum to maximum value varies between 20…50 kPa. In the example shown in Figure 8, the corresponding variation of pressure was 16 kPa. This is a typical value for the present simulation, where the pressure variations in most chugging periods were 10…20 kPa. The values are lower than in the experiment, where the rapid collapses of vapor bubbles produced higher variations of pressure.

In the simulation, a few collapses of the vapor bubbles produced much larger pressures than the typical values discussed above. The largest pressure variations were even about 100 kPa. This can be attributed to incompressibility of water in the simulation, which may lead to high pressure during rapid condensation of a bubble. In addition, the water in the experiment contained a small amount of non-condensable gas, which can be seen in the frames of Figure 10. The non-condensable gas makes the water more “soft” and reduces the pressure variations.

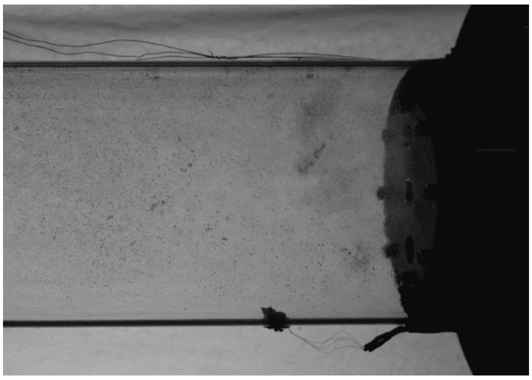

t = 186 ms

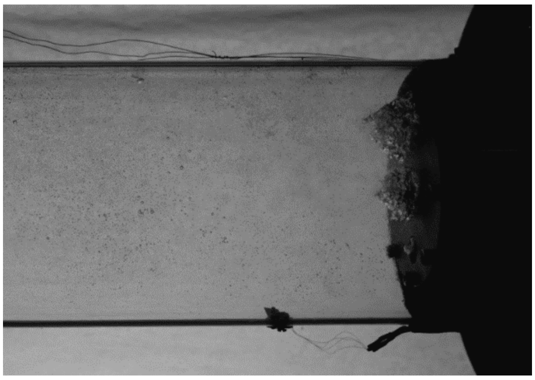

t = 210 ms

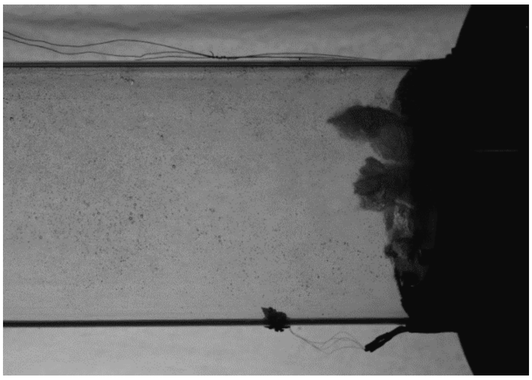

t = 221 ms

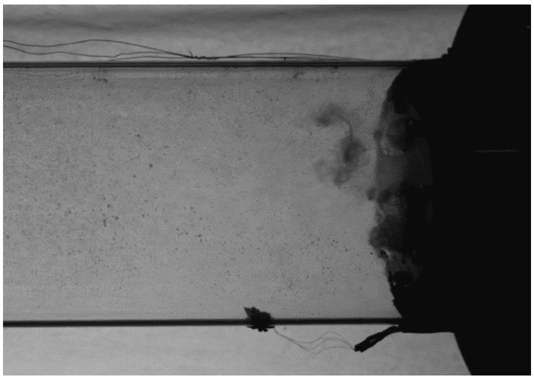

t = 226 ms

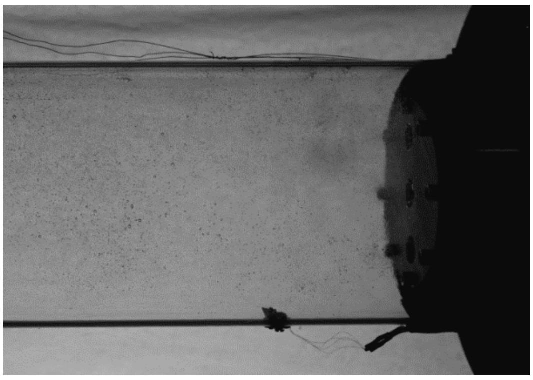

t = 234 ms

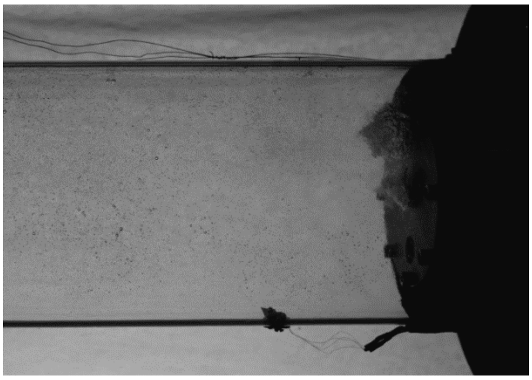

t = 259 ms

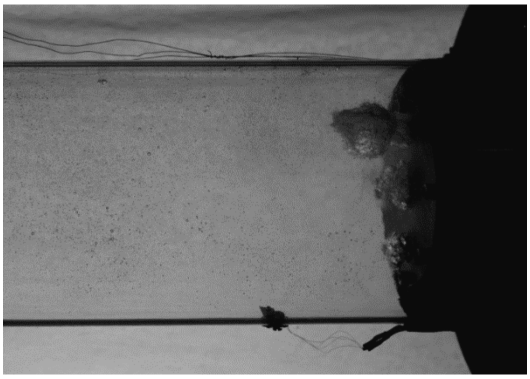

t = 270 ms

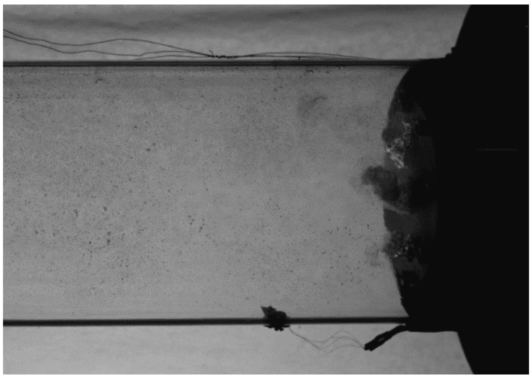

t = 281 ms

Figure 10. Frames of high speed video of the experiment SEF-T000 after time t = 350 s. Frames are shown, when the vapor bubbles have the maximum size, are contracting, have minimum size and are growing (continues on the following page). Data: Puustinen (2017).

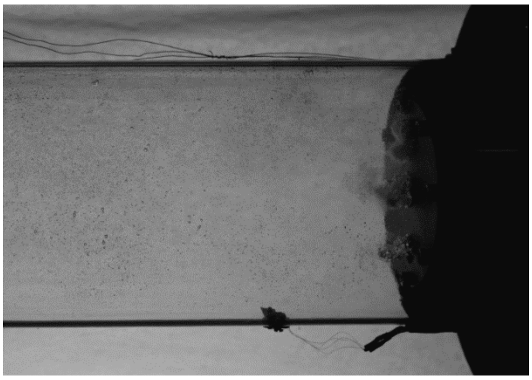

t = 287 ms

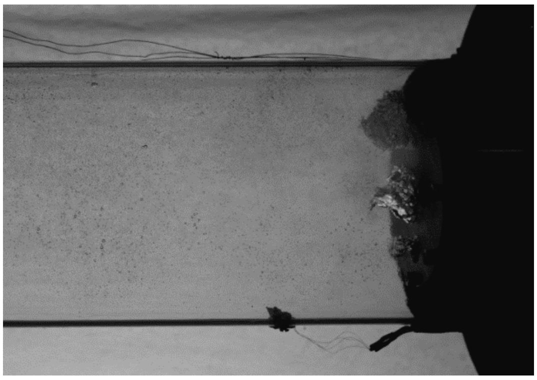

t = 301 ms

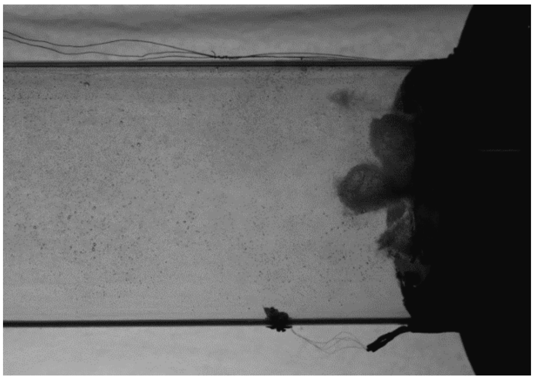

t = 311 ms

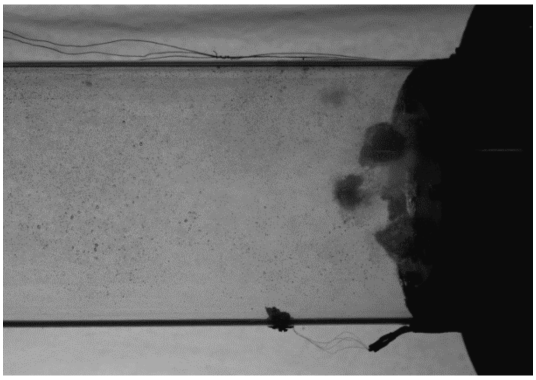

t = 314 ms

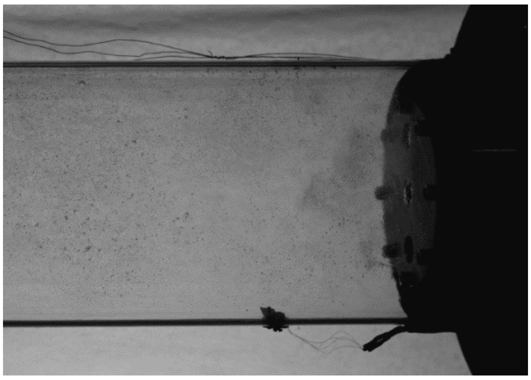

t = 323 ms

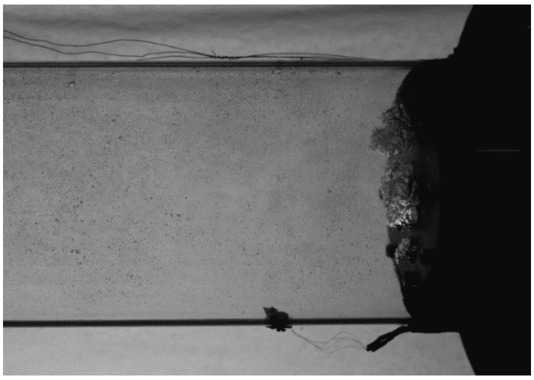

t = 344 ms

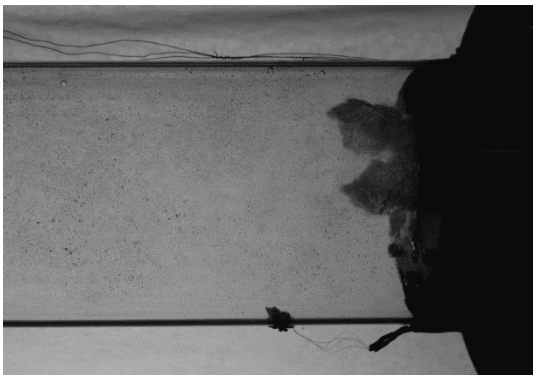

t = 357 ms

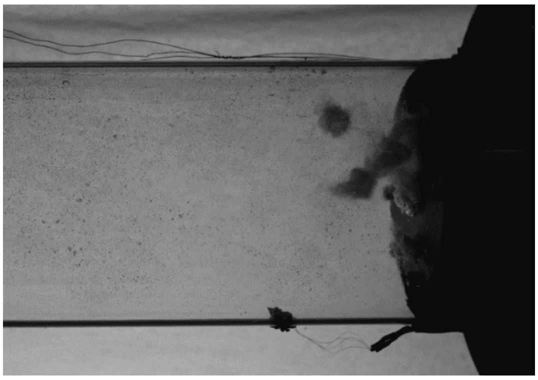

t = 361 ms

Figure 10. Frames of high speed video of the experiment SEF-T000 after time t = 350 s (continues from the previous page).

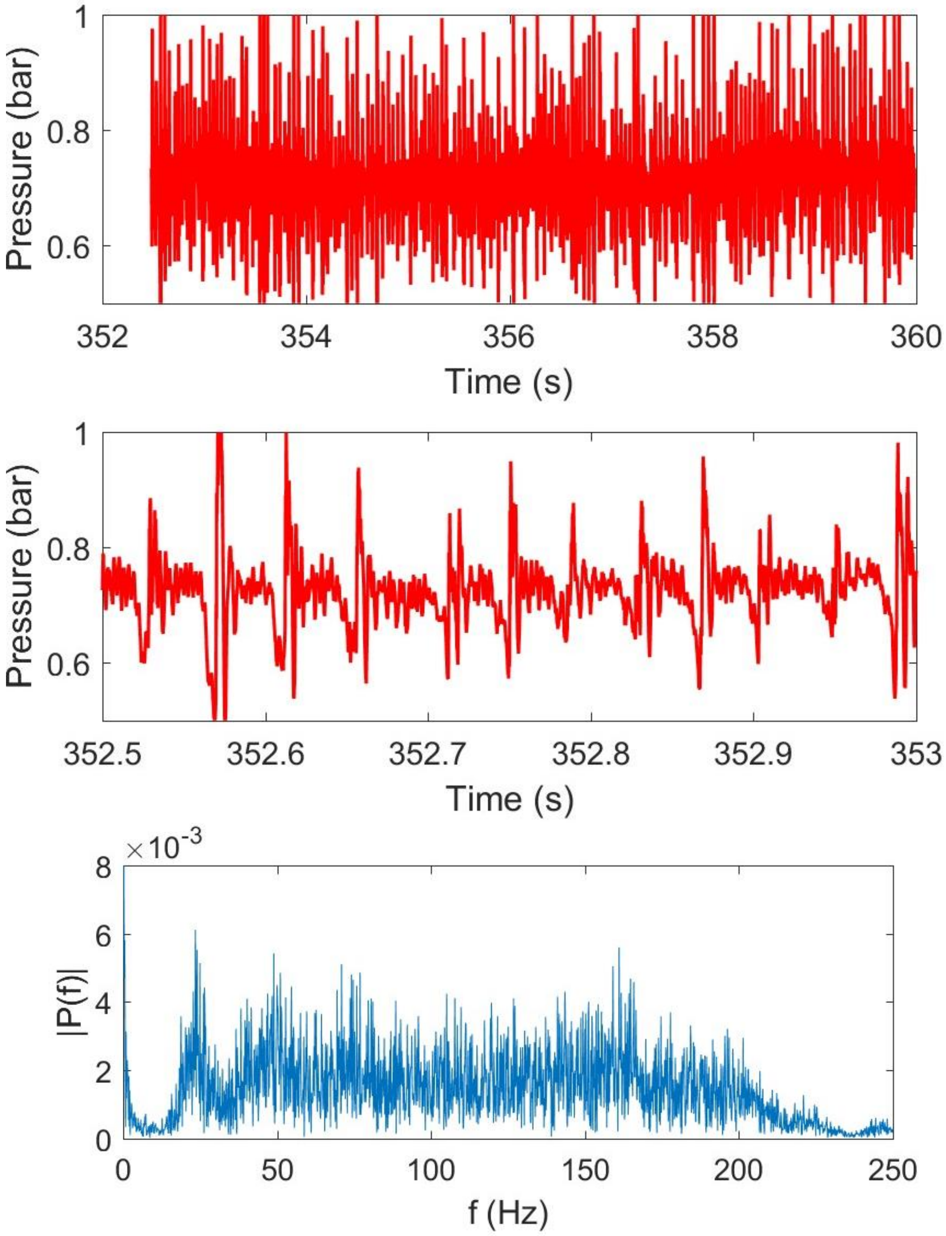

Figure 11. Pressure measured in front of the orifice plate in the plexiglass tube (top and middle frames) and the amplitude spectrum of the pressure (bottom frame) (data from Puustinen, 2017a).

6. Summary and conclusions

Pre-test SEF-T000 performed on direct-contact condensation by Puustinen et al. (2017) has been studied with Computational Fluid Dynamics (CFD) calculations. The pre-test was performed with the newly constructed separate effect test facility, where steam was injected into water pool. The mass flow rate of steam was small (14.8 g/s) and the temperature of the water was fairly high (67 °C) in the time interval chosen for the simulation. The steam was injected into water horizontally through three orifices having diameter of 16 mm, which corresponds to the mass flux of 24.5 kg/m^{2}s.

The oscillation patterns in direct-contact condensation experiments have previously been classified based on mass flux of steam and water temperature by several authors (Lahey and Moody, 1993; Nariai and Aya, 1986; Aya and Nariai, 1991). The classification maps suggest that the parameters of the experiment are close to the border line between condensation oscillation and chugging.

The simulation performed with the ANSYS Fluent version 18.2 contained several simplifying modelling assumptions, which affect the simulation results. Euler-Euler two-phase model was used, where the drag between vapor and water was modelled with "universal" drag model of Fluent. In the calculation, constant bubble diameter of one millimeter was assumed. These modelling choices affect the penetration length of the vapor jet into water.

The condensation was calculated by using the two-resistance model and the evaporation-condensation model of Fluent. In the two-resistance model, the Ranz-Marshall correlation for heat transfer was assumed on the liquid side. On the vapor side, zero resistance was assumed. Interfacial area of the phases was calculated with ia-symmetric model of Fluent. These modeling choices affect the condensation rate, which affects the penetration length of the vapor jet. The condensation rate also affects the growth time and collapse time of vapor bubble during the chugging oscillation.

In the simulation, the chugging oscillation was qualitatively very similar as in the experiment. The period of the oscillation was, however, in the simulation (83 ms) longer than in the experiment (43 ms). In particular, the collapse phase of the bubble was in the simulation (42 ms) considerably longer than in the experiment (11 ms). Visual observation from the high-speed video shows that during the collapse phase of the bubble, the surface of the bubble becomes unstable and the surface area between vapor and liquid-water increases rapidly. This phenomena is not included in the CFD model and it leads to much more rapid condensation of the bubbles in the experiment than in the simulation.

The growth phase of the vapor bubbles is also in the simulation (41 ms) somewhat longer than in the experiment (34 ms). The difference is probably due to the heat transfer and interfacial area models used in the simulation. In particular, the assumption of single bubble size with fixed diameter has room for improvement.

The penetration length of the vapor jet into water was larger in the simulation (73 mm) than in the experiment (46 mm). This is consistent with the discussion above, which suggests that the simulation underestimates the heat transfer coefficient and/or the interfacial surface area. The resulting underestimation of the condensation rate leads to too large penetration length of the vapor jet.

The pressure oscillations measured in the experiment (20…50 kPa) are most of the time larger than in the CFD simulation (10…20 kPa). The reason for this lies in the differences in the collapse speeds of the bubbles, which are shorter in the experiment than in the simulation, as was discussed above. The more rapid condensation of the bubbles in the experiments compared to simulation produces higher pressure oscillations.

In conclusion, the present CFD simulation produces qualitatively correct description of the chugging oscillation observed in the experiment. The period of the oscillation, the penetration of the vapor jet and the pressure oscillation are in the simulation reasonably close to the experimental observations. More accurate results could be achieved by improving the description of the interfacial area, in particular, in the collapse phase of the chugging oscillation.

References

Aya, I., and Nariai, H., 1991. Evaluation of heat transfer coefficient at direct-contact condensation of cold water and steam, Nuclear Engineering and Design **131**, 17–24.

Gallego-Marcos, I., Villanueva, W., and Kudinov, P., 2016. Thermal stratification and mixing in a large pool induced by operation of spargers, nozzles, and blowdown pipes, Nordic nuclear safety research, Report NKS-369, Roskilde, Denmark, 53 p.

Gallego-Marcos, I., Villanueva, W., and Kudinov, P., 2017. Modelling of a large water pool during operation of blowdown pipes, spargers, and nozzles, Nordic nuclear safety research, Report NKS-393, Roskilde, Denmark, 62 p.

Gulawani, S. S., Joshi, J. B., Shah, M. S., RamaPrasad, C. S., and Shukla, D. S., 2006. CFD analysis of flowpattern and heat transfer in direct contact steam condensation, Chemical Engineering Science **61**, 5204–5220.

Jo, B., Erkan, N., Takahashi, S., Song, D., Sagawa, W., and Okamoto, K., 2016. Thermal stratification in a scaled-down suppression pool of the Fukushima Daiichi nuclear power plants, Nuclear Engineering and Design **305**, 39–50.

Lahey, R. T., Moody, F. J., 1993. The thermal-hydraulics of a boiling water reactor, Chapter 11. American Nuclear Society, Illinois. 2nd edition.

Landram, C. S., McMaster, W. H., and Gong, E. Y., 1982. Steam chugging calculations with the PELE-IC code, Nuclear Engineering and Design **70**, 411–421.

Nariai, H., and Aya, I., 1986. Fluid and pressure oscillations occurring at direct contact condensation of steam flow with cold water, Nuclear Engineering and Design **95**, 35–45.

Patel, G., Tanskanen, V., Hujala, E., and Hyvärinen, J., 2017. Direct contact condensation modeling in pressure suppression pool system, Nuclear Engineering and Design **321**, 328–342.

Puustinen, M. and Kudinov, P., 2017. Design of the separate effect test facility for condensation studies. Private communication.

Puustinen, M., 2017. Construction of the separate effect test facility. Private communication.

Puustinen, M., Laine, J., Räsänen, A., Kotro, E., and Tielinen, K., 2017. Characterizing tests in SEF-POOL facility, Technical Report Lappeenranta University of Technology, Nuclear Engineering, INSTAB 3/2017.

Timperi, A., Chauhan, M., Pättikangas, T., and Niemi, J., 2013. Modelling of pressure loads in a pressure suppression pool, Nordic nuclear safety research, Report NKS-283, Roskilde, Denmark, 54 p.

Appendix F

Modelling of a Large Water Pool during Operation of Blowdown Pipes and Spargers

Modelling of a Large Water Pool during Operation of Blowdown Pipes and Spargers

Final Report from the NKS-R COPSAR activity (Contract: NKS_R_2015_114)

Ignacio Gallego-Marcos[a], Samanta Estévez-Albuja[b], Walter Villanueva[c], Pavel Kudinov[a]

[a] Royal Institute of Technology (KTH), Division of Nuclear Engineering, Stockholm, Sweden
[b] Universidad Politécnica de Madrid (UPM), Madrid, Spain
[c] Royal Institute of Technology (KTH), Division of Nuclear Power Safety, Stockholm, Sweden
E-mails: igm@kth.se, samanta.estevez.albuja@alumnos.upm.es, walterv@kth.se, pkudinov@kth.se

June 2018
Stockholm

Table of contents

EXECUTIVE SUMMARY 5
1. INTRODUCTION 6
2. GOALS AND TASKS 7
3. STATE OF THE ART REVIEW 8
3.1. Experiments on direct contact condensation 8
3.2. Experiments on pool behaviour 9
3.3. Analytical and numerical modelling 10
4. EHS/EMS MODELS 12
5. BLOWDOWN PIPES 13
5.1. Effect of non-condensable gases in the chugging regime 15
5.2. Implementation in Nordic BWR models 17
6. SPARGERS 20
6.1. PPOOLEX and PANDA experiments with spargers 20
6.2. CFD modelling of the PPOOLEX experiments 21
6.3. Separate Effect Facility (SEF) 23
6.4. CFD modelling of the full-scale Pressure Suppression Pool (PSP) 26
SUMMARY & CONCLUSIONS 32
ACKNOWLEDGEMENTS 34
DISCLAIMER 35
REFERENCES 36

EXECUTIVE SUMMARY

The development of thermal stratification in the Pressure Suppression Pool (PSP) of Boiling Water Reactors (BWRs) is an issue of safety significance since it can (i) affect the operation of the spray and Emergency Core Cooling System (ECCS) and (ii) lead to higher containment pressures than in completely mixed conditions. In a BWR, steam can be injected into the PSP through large diameter blowdown pipes connected to the drywell (in case of loss of coolant accident), or small-dimeter multi-hole spargers used for controlled depressurization of the primary coolant circuit. In this work, we present the development and validation of the Effective Heat Source (EHS) and Effective Momentum Source (EMS) models for blowdown pipes and spargers. These models were developed to predict the time and space averaged effect of the small scale direct contact condensation phenomena on the large scale circulation and heat transfer in the pool.

For the blowdown pipes, correlations have been developed using PPOOLEX experimental data to predict the transition between condensation regimes, and to estimate the effective momentum of chugging. A new implementation of the EHS/EMS models in GOTHIC has been proposed to enable simulating the pool and containment behaviour during prototypic LOCA conditions. A time-averaging model has also been proposed to minimize the effect of the numerical oscillations of the flow in the pool. Validation against the PPOOLEX MIX-04 and 06 experiments shows very good agreement to the pool temperatures and containment pressure. The effect of non-condensable gases on chugging is begin analysed by using the data from the clearing phases of the PPOOLEX MIX experiments. Preliminary results show that the volume fraction at which chugging is supressed decreases with the blowdown pipe diameter.

EHS/EMS models for sparger have been developed and implemented in ANSYS Fluent. It has been shown that using the k-Omega BSL turbulence model with the SGDH and a $C_{3\varepsilon}$ varying between 0 and 1 allows a good prediction of the stable stratification and erosion regimes. The effective momentum was calibrated using the PANDA HP5-1 to 3 experiments and the PPOOLEX SPA-T3 to T6 experiments. A Separate Effect Facility (SEF) has been built in cooperation with LUT to measure the effective momentum induced by the oscillatory bubble regime. The results show that the effective momentum is very similar to the steam momentum at the injection holes. The latter was observed to be a function of the cyclic bubble oscillations, and thus to deviate from standard estimations based on a constant steam mass flow rate. Comparison with the effective momentum estimated in the Fluent simulations shows a similar trend with respect to the subcooling, but a shift on absolute values.

The EHS/EMS models for spargers are under development. An experimental setup to measure the effective momentum induced by the oscillatory bubble regime during a steam injection through spargers has been designed by KTH and LUT. Preliminary experiments are expected to be performed before the end of the year, and continued through 2018. The EHS/EMS models for spargers have been implemented in ANSYS Fluent. It has been shown that using the k-Omega BSL turbulence model with the SGDH and a $C_{3\varepsilon}$ varying between 0 and 1 allows a good prediction of the stable stratification and erosion regimes. Validation of the EHS/EMS implementation in Fluent against the PANDA HP5-1, 2 experiments shows good agreement with the experimental data.

EHS/EMS for blowdown pipes have been implemented in a Nordic BWR model in GOTHIC for the analysis of the pool during a Small Break LOCA. EHS/EMS models for spargers have been validated against the full-scale PSP experiment performed in a Nordic BWR (where complete mixing was observed). Simulations of the PSP behavior for other steam injection conditions and sparger models has also been performed. The results show that the thermal stratification development in the pool can lead to larger pool surface temperatures than when assuming that all latent heat is homogeneously distributed in the pool volume above the injection holes.

1. INTRODUCTION

Steam condensation in a large water pool is used in some designs of light water reactors to prevent containment over-pressure [1, 2]. In Boiling Water Reactors (BWR) this pool is known as the Pressure Suppression Pool (PSP), whereas in Generation III reactors such as the AP1000 and APR1400 the pool is known as the In-containment Refuelling Water Storage Tank (IRWST). In a BWR, steam can be injected into the PSP through large diameter blowdown pipes connected to the drywell (in case of loss of coolant accident), or small-dimeter multi-hole spargers used for controlled depressurization of the primary coolant circuit.

Direct condensation of steam injected into a water pool is as a source of heat and momentum. Competition between these sources determines whether the pool is thermally stratified or mixed. For example, if steam is injected at low momentum, the latent heat is deposited in the water layer above the pipe outlet, while water below the pipe outlet remains cold [3]. Steam injections at higher momentum (e.g. chugging, oscillatory bubbles, and stable jets) can create larger momentum sources, and lead to development of a large scale circulation in the pool which can break or erode the stratified layer [4].

The development of thermal stratification in the PSP is an issue of safety significance. Higher surface temperatures of a stratified pool will lead to higher containment pressure compared to a completely mixed pool, at the same average pool temperature. An example of such behavior can be observed in the Fukushima Daiichi Unit 3 accident, during the operation of the Reactor Core Isolation Condenser (RCIC) [5, 6]. Lumped parameter codes under-estimated the maximum pressure by about 160 kPa assuming a mixed pool condition, while a much better agreement was obtained assuming that the pool was stratified.

Modelling the pool behaviour during a steam injection is a challenge due to the direct contact condensation phenomena. While CFD is too computationally expensive [7, 8, 9], lumped and 1D codes are inadequate for prediction of 3D, transient mixing phenomena. In general, state-of-the-art approaches cannot capture the effect of different condensation regimes due to the lack of the physical models.

To enable such prediction, Li & Kudinov developed in 2010 [10] the so called Effective Heat Source and Effective Momentum Source (EHS/EMS) models, which have been further developed in a series of publications [11, 12, 13, 14, 15, 16, 17]. The premise of these models is that the small-scale direct contact condensation phenomena determine the integral heat and momentum sources transferred to the pool, which in turn determine the large-scale pool circulation and temperature distribution. Due to the difference in scales, only the effect of direct contact condensation phenomena on the large scale phenomena should be modelled, not the details of the micro-scale condensation phenomena themselves.

In this work, we begin by presenting the goals and tasks of the project. Section 3 provides a state of the art review of the work done on direct contact condensation and pool behaviour. Sections 4 defines the EHS/EMS models, and Sections 5, 6, and the specific development for blowdown pipes, sparger, and mixing nozzles.

2. GOALS AND TASKS

The main goal of the project is to provide support to NORTHNET partners by development, validation and application of modelling capabilities for assessment of the PSP performance in Nordic BWR containments. In order to achieve the goal of the project, the main research objectives are: to develop and validate modelling capabilities of condensation, heat transfer and mixing in pressure suppression pools. In the Roadmap 3 for 2014-2018, developed by NORTHNET, following high priority tasks were identified as necessary to achieve the ultimate goal of the project:

- Task-1: To develop EHS/EMS models for the blowdown pipes in case of different steam condensation regimes and presence of non-condensable gases.
- Task-2: To develop EHS/EMS models for spargers and RHR nozzles.
- Task-3: To provide analytical support for PSP tests in the Nordic BWRs.
- Task-4: To validate the EHS/EMS models against OECD/HYMERES PANDA tests.
- Task-5: To provide analytical support to NORTHNET partners in addressing containment performance.
- Task-6: Analytical support for PPOOLEX tests and GOTHIC validation.

This document begins by presenting a literature review of previous works done in direct contact condensation and pool behaviour, Section 3. The status of the Effective Heat Source and Effective Momentum Source model (EHS/EMS) developed for blowdown pipes and spargers are presented in Sections 5 and 6 respectively. A summary of the status of each Task is presented at the end, in the Summary and Conclusions section.

3. STATE OF THE ART REVIEW

The pool behaviour during a steam injection is governed by a large number of parameters. For example, direct contact condensation determines the heat and momentum sources injected into the pool, single phase flow the transport of these sources across the pool, and density interfaces the transport between the stratified layer and the rest of the pool. Experimental data allows us to identify the most important variables affecting these phenomena. Based on these variables, analytical and numerical models can be developed to predict the pool behaviour.

This section we will begin by analysing the experiments performed on direct contact condensation and pool behaviour, sections 3.1 and 3.2 respectively, and conclude by presenting the numerical approaches used to model these phenomena, section 3.3.

3.1. Experiments on direct contact condensation

The steam condensation regimes which occur during an injection into a subcooled pool can be divided into two main groups: sonic, and sub-sonic. Sonic regimes occur when the injection pressure is about 0.53 times higher than the ambient. The large shear between vapour and liquid induces instabilities which entrain liquid droplets into the vapour core, leading to a highly diffused interface which gradually turns into a bubbly flow and eventually to single-phase liquid. Despite the unstable nature of the instabilities, sonic regimes are usually referred as “stable regimes”. This because the macroscopic jet parameters of penetration length, expansion ratio, heat transfer coefficient etc., remain relatively constant in time. Experiments performed in [18] show that the main variables affecting the aforementioned parameters are the steam mass flux, pool subcooling (steam minus pool temperature), and injection hole diameter. Thus, correlations of the jet parameters have been proposed as a function of these variables [18, 19, 20]. The shockwave pattern in sonic jets was studied by Wu et al. [21], where it is shown that high pressures after a shockwave cause an expansion of the jet when released into the pool. Since steam condensation is negligible during the expansion, the steam jet is confined to a divergent section which can accelerate the flow to super-sonic conditions, leading to another shockwave. Successive contraction-expansion waves can occur depending on the pressure inside the sparger and in the pool.

The liquid jet induced by the steam condensation was analysed by Choo et al. [22] using Particle Image Velocimetry (PIV). It was concluded that the liquid turbulent jet becomes self-similar after a certain distance from the injection. Coefficients were also proposed to model the turbulent profile as a function of the injection conditions. Van Wissen et al. [23] measured the turbulent intensities induced in the liquid, which were observed to reach maximum values of 30 %.

In the sub-sonic regimes, the heat transfer between steam and liquid becomes lower than in sonic conditions [24]. Thus, jets are able to expand and generate bubbles which eventually detach and condense through a collapse [25, 26], giving the name of oscillatory bubble regime. The frequency of the bubble growth-detach-collapse cycle was analysed by Fukuda [27], Hong et al. [28] and Cho et al. [29] for single and multi-hole injection respectively. The frequency was observed to vary between 50-600 Hz, and to depend mainly on the pool subcooling and injection hole diameter. For this regime, Tang et al. [30] analysed the collapse mechanism of the detached bubbles and stablished a regime map for the different modes. At lower steam mass fluxes, the flow enters into the chugging regime, where the collapse of large bubbles induces a sudden pressure drop which pushes liquid from the pool inside the injection pipe [31]. The transition between the oscillatory bubble and chugging regimes is characterized by a monotonic decrease of the detaching frequency along the steam mass flux range of 20-60 kg/(m^{2}s) [32], after which the frequency settles in stable values of 1-2 Hz [14]. Experiments performed by Aust & Seeliger [33] showed that chugging can be completely suppressed by designing a blowdown pipe outlet cut at 45^o. This effect was attributed to the counter-flow and high shear developing at the outlet section, which prevented large bubbles from forming for steam mass fluxes up to 100 kg/(m^{2}s). At very low steam mass fluxes chugging is supressed and all steam is condensed inside the blowdown pipe.

Single-hole condensation regime maps for sub-sonic regimes have been proposed by Aya & Nariai [34] Chan & Lee [25], Liang & Griffith [35], and Cho et al. [36]. In all of these works, the steam mass flux, pool and steam temperature were identified as the most important parameters determining the condensation regime. Petrovic de With et al. [37] combined the some of the previous maps into a 3D regime map which took into account the injection hole diameter. Condensation regime maps for the different modes of chugging regime were also proposed by Gregu et al. [38]. Multi-hole condensation regime maps for sonic and sub-sonic flow were proposed by [39], where it was observed that the transition between sonic and sub-sonic occurs at approximately 330 kg/(m^{2}s).

In a BWR, the pressure difference between the drywell and wetwell is determined by the submergence of the blowdown pipes, which can be between 1-6 m [1]. This hydro-static difference is usually not enough to trigger sonic flow. On the other hand, the large pressure difference between the primary circuit and the wetwell pool makes spargers more prone to develop shock waves. This can occur during the intermittent operation of the Safety Relief Valves (SRVs), or at the initial stages of the Automatic Depressurization System (ADS). For LOCA, long-term ADS operations, or exhaust of safety systems such as the Reactor Core Isolation Condenser (RCIC), sub-sonic regimes are expected to dominate the transient.

3.2. Experiments on pool behaviour

The transport of the heat and momentum sources generated during a steam injection is affected by the geometry of the pool. The main variables are the total pool depth, which determines the strength of natural circulation; the submergence depth of the pipes, which determines the location of the stratified layer; and the cross section area, which determines the interaction of radial jets with the walls. Due to the large-scale of the pool in a BWR, experiments are usually performed in smaller scale facilities. In this case, adequate scaling becomes an essential ingredient for the interpretation of the results [40].

The full-scale Marviken-FCSB tests performed in Sweden [41] showed that chugging occurs during prototypic LOCA transients in a BWR Mark II. Thermal stratification was also observed to develop once chugging was supressed due to the reduction in the steam mass flux. Extensive experimental campaigns were carried out by General Electric in a 1:130 reduced scale facility to analyse the pool swelling, pressure increase, pool temperature, etc. during a LOCA in a BWR Mark I [42], Mark II [43, 44], and Mark III [45, 46, 47]. Unfortunately, these reports are not public and could not be analysed by the authors. LOCA experiments were also performed in Japan by JAERI [48, 49] using a full scale 20^o sector of a BWR. Similar to Marviken, chugging was again present in most of the tests. However, since the duration of the JAERI experiments was limited to a few hundred seconds, no development of thermal stratification was observed.

The LINX facility [50] at Paul Scherrer Institut (PSI), Switzerland, was built to analyse the development of thermal stratification and mixing during the late stages (+1h) of a LOCA in a ESBWR. Steam was injected directly into the pool through a single-hole 40 mm vertical sparger. Air concentrations above 5% in mass were observed to cause a complete mixing of the pool; whereas pure steam led to a substantial thermal stratification development below the injection line, reaching temperature differences up to 30 ^{o}C [51]. Experiments performed by Moon et al. [52] focused on the high steam mass flux sonic regimes using prototypic multi-hole spargers of an APR1400. Due to the high jet momentum, complete mixing of the pool was observed in all of the tests. Experiments performed by Zhang et al. [53] with a scaled down models of the AP1000 quencher and IRWST showed that prototypic steam injection conditions can cause significant thermal stratification, specially due to the low submergence of the quenchers. Extensive experimental campaigns were performed in the POOLEX/PPOOLEX facility in Lappeenranta University of Technology (LUT), Finland, using blowdown pipes [54, 55, 56, 57, 58, 59]. Here, separate effect experiments were carried out to analyse the individual effect of parameters such as the drywell volume, pipe diameter, submergence, number of blowdown pipes, steam injection conditions, etc. Thermal stratification was observer during prototypic steam injection conditions of a BWR, even during weak chugging regimes.

Experiments in small scale facilities were performed by Solomon et al. [60], where it was observed that thermal stratification can develop during prototypic steam injections of the RCIC system. Experiments performed by Song et al. [61] showed that the pool Richardson number has capabilities on predicting the transition between thermal stratification and mixing.

Though some of the previous works were focused on the study of thermal stratification and mixing, little attention was given to the physical mechanisms which cause mixing and erosion of the stratified layer. In the field of atmospheric and oceanic research, Fernando [62] shows that the erosion regimes of stable stratified layer can be predicted by the bulk Richardson number. A detailed analysis done in by Fernando et al. [63, 64] further shows that low Richardson number flows are able to break down the stratified layer by penetrating into it. As the Richardson number increases, the turbulent eddies are only able to penetrate into the stratified layer, but only to impinge on it and splash some heavy liquid upwards. At very high Richardson numbers, turbulent eddies can only induce waves in the pool whose sporadic break up leads to local mixing. It has also been shown in [62] that the erosion velocity can be predicted as a function of the Richardson number and pool geometry.

3.3. Analytical and numerical modelling

Based on the experimental data presented in sections 3.1 and 3.2, a large number of works have been done in the modelling of direct contact condensation and pool behaviour.

Analytical models to predict the bubble diameters and detachment frequency during the oscillatory bubble regime were developed in [65, 66] using the Rayleigh-Plesset equation and momentum balances across the bubble. Chugging models were also developed by Aya & Nariai [31] and Pitts [67] using the conservation equations. These works were later extended by [68] to include the presence of non-condensable gases. Comparison to experimental data showed a good prediction of the frequency and amplitude of the oscillations. Stability analysis performed by Brennen [69] showed that chugging is usually sustained in the natural, manometer type, oscillation of the system.

CFD modelling of the chugging regime during the PPOOLEX experiments was carried out by Pättikangas et al. [70] using ANSYS Fluent. The Euler-Euler model was used model direct contact condensation. The heat transfer between steam and water was modelled using a Reynolds and Prandtl based Nusselt number correlation. Due to the high computational cost, the simulations were run in 2D-axisymmetric models. The results showed a qualitative agreement on the chugging oscillation and collapse. However, the Nusselt correlation was observed to under-estimate the condensation rate since it allowed small steam bubbles escape from the main chugging collapsing bubble. Tanskanen et al. [71] and Patel [72] used NEPTUNE_CFD and ANSYS Fluent respectively with the cell-based Hughes and Duffey correlation for the Nusselt number and obtained a better prediction for the heat transfer, which again showed quantitative good agreement with the PPOOLEX data in terms of bubble radius and frequency of collapse. Using the same Eulerian-Eulerian models, Pellegrini et al. [73] used a Rayleigh-Taylor instability model to simulate the direct contact condensation heat transfer during chugging.

Work done by KAERI [74, 75, 52] introduced the Steam Condensation Region Model (SCRM), based on previous work done by Gamble et al. [76]. The SCRM solves equations of mass, momentum, and energy in a control volume where steam condensed completely, and imposes single-phase liquid entrainment and condensate boundary conditions of the jet. Implementations of the SCRM were done in Star CCM+ and

ANSYS Fluent showed good agreement to complete mixing transients. Applicability to thermal stratification and mixing transients was not provided.

EHS/EMS models were introduced by Li & Kudinov (2010) [10] to develop predictive capabilities for long-term thermal stratification and mixing transients induced by a steam injection through blowdown pipes. The models were implemented in GOTHIC, and successfully validated against the PPOOLEX STB and MIX experiments [55, 58, 59], which were performed with different steam mass fluxes, pool temperatures, blowdown pipe diameters, etc.

Lumped parameter correlations for modelling of PSP stratification were developed in [77] based on 3D analysis results with GOTHIC. However, no evidence of the GOTHIC validity for prediction of pool mixing were demonstrated.

4. EHS/EMS models

Modeling of direct contact condensation is a challenge for contemporary codes. The small length and time scale of steam condensation phenomena requires very low mesh and time step when using CFD [7, 8, 9], making it unaffordable for long-term transients in a PSP. Lumped and 1D codes are inadequate for prediction of 3D, transient mixing phenomena. Moreover, containment codes such as GOTHIC [78], and other thermal hydraulic codes (e.g. RELAP5 [79]), do not have a model for prediction of the effect of steam blowdown into a pool. Available condensation models are mostly designed for pipe flow regimes such as bubbly, churn, film, etc.

To develop predictive capabilities for long-term thermal stratification and mixing transients, Li & Kudinov (2010) [10] introduced the concept of Effective Heat Source (EHS) and Effective Momentum Source (EMS) models. The main idea of the effective models is that, to predict the global pool behaviour, direct contact condensation phenomena occurring at the small temporal and spatial scales do not need to be resolved. Instead, it is the time-averaged Effective Heat (EHS) and Momentum (EMS) Sources transferred from the steam to the large scale pool circulation what needs to be modelled. The effective heat Q_{eff} and momentum M_{eff} sources are computed using equations (1) and (2) respectively [11],

$$Q_{eff}(t) = \frac{1}{\Delta t} \int_{t-\Delta t}^{t} Q(\tau) d\tau \tag{1}$$

$$M_{eff}(t) = \frac{1}{\Delta t} \int_{t-\Delta t}^{t} M(\tau) d\tau \tag{2}$$

where the integrals represent the time-average of the instantaneous variations of the sources over a period Δt of time. These variations are due to the oscillatory nature of direct contact condensation. For example, the large scale motions of the liquid inside the pipe during the chugging regime, the small scale oscillatory bubble behavior, etc.

The ultimate goal of the EHS/EMS models is to provide the effective heat and momentum sources through the chart shown in Figure 1. That is, they should be able to predict the condensation regime given the current steam and pool conditions, and derive its corresponding heat and momentum sources.

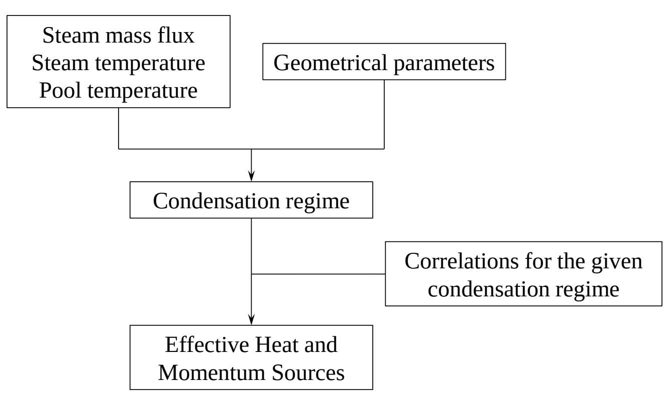

Figure 1: Calculation diagram of the EHS/EMS models

5. BLOWDOWN PIPES

The pool behaviour during a steam injection through blowdown pipes was extensively studied in a series of experimental campaigns performed in the PPOOLEX facility (LUT, Finland). In this section, we will focus on the PPOOLEX-MIX experiments, performed with blowdown pipe diameters of 214 mm and 109 mm.

Work done by Li et al. [11, 12] showed that the effective momentum M_{eff} induced by the chugging regime appearing in blowdown pipes is a function of the frequency f and amplitude A of the liquid level oscillations inside the pipe, equation (3).

$$M_{eff} = \rho_L A\left(\sqrt{2} f A\right)^2 \tag{3}$$

Villanueva et al. [14] showed that the frequency and amplitude of the oscillations were well correlated with the Froude number, equation (4). Non-dimensional forms of the amplitude and frequency were also proposed in [14] as a function of the drywell volume V, pipe diameter d, submergence l_s, total pipe length l_p, and number of blowdown pipes n. The results showed good agreement with Aya & Nariai data [81]. However, some deviations between the MIX experiments was observed in the frequency scaling.

$$Fr = \frac{G/\rho_s}{\sqrt{g l_s}} \tag{4}$$

Further development of the scaling was done in [15], where the total pipe length l_p was changed to the submergence depth l_s, and the scaling factor for the frequency was derived from the manometer-type relation of $f \propto \sqrt{g/A}$. This scaling showed a good agreement between all MIX experiments and with Aya & Nariai data. The non-dimensional parameters were then fitted to a Gaussian distribution to enable the prediction of the frequency, amplitude, and effective velocity for any geometrical configuration and injection conditions. The results for the Amplitude are show in Figure 2.

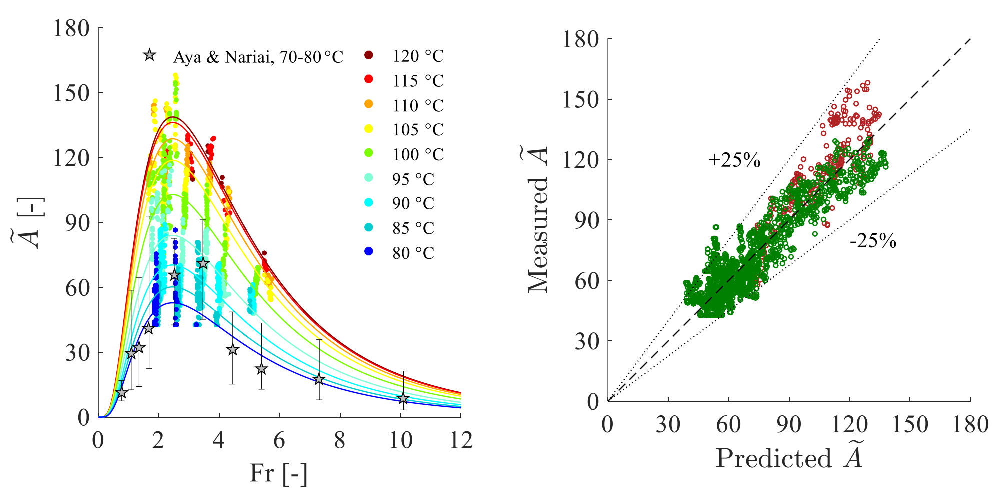

(a) (b)

Figure 2: Scaling of the non-dimensional amplitude of the chugging oscillations. Symbols (○) corresponds to the MIX 01-12 experiments, (⋆) to Aya & Nariai data [81], and solid lines to the analytical correlations given in [15]. The color band represents the subcooling ($\Delta T = T_s - T_p$).

The correlations for chugging proposed in [15] where implemented in GOTHIC using Dynamically Linked Libraries (DLL). Previous work done by the authors has shown that simulating direct contact condensation in GOTHIC leads to large amplitude numerical oscillations of the flow inside the blowdown pipe. To minimize their effect, and to enable us to control the momentum injected into the pool, a so called EHS/EMS containment model was developed. The main difference compared to a standard GOTHIC approach is that the blowdown pipe outlet is connected to a pressure boundary condition rather than to the wetwell pool. This prevents GOTHIC from injecting a numerically oscillating flow into the pool and induce artificial mixing. The flow injected into the pressure boundary condition was time-averaged, and then, based on the mass flow and temperatures, the condensation regime was selected. If chugging was predicted, the EMS pump is activated to induce the effective momentum predicted by the chugging correlations proposed in [15].

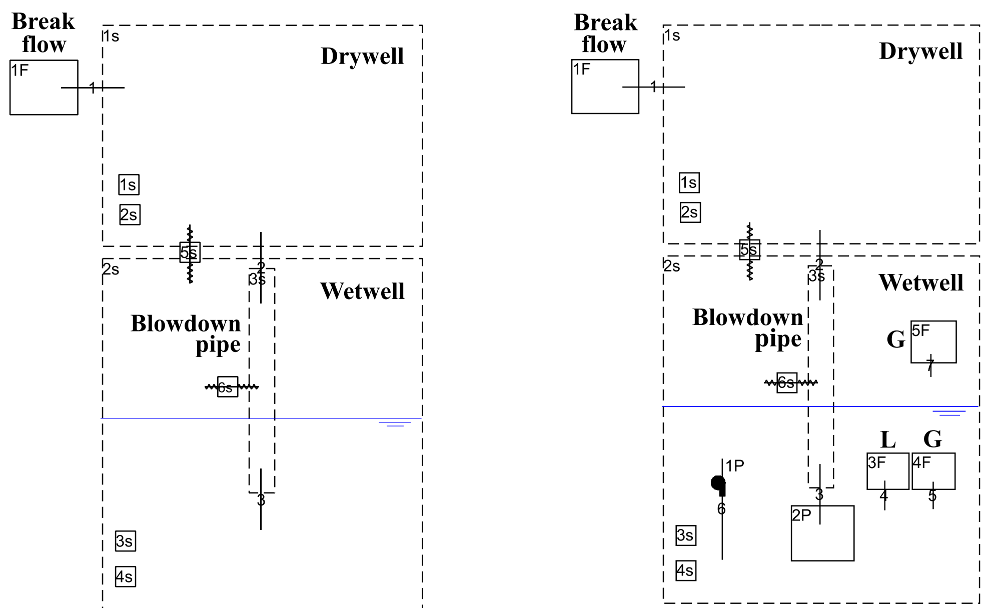

(a) (b)

Figure 3: GOTHIC models of a simplified containment using the (a) direct steam injection approach and (b) EHS/EMS containment model proposed in this work.

Validation of the EHS/EMS containment model and chugging correlations was done in [15] against the PPOOLEX MIX-04 and MIX-06 experiments [58]. In these experiments, the wetwell was initially filled with a 2.13 m pool, and a 214 mm diameter blowdown pipe was submerged 1.7 m into the pool and connected to the drywell floor. The gas spaces of the drywell and wetwell were initially filled with air. Similar to a LOCA scenario in a BWR, steam was injected into the drywell. The experiment consisted on an initial clearing phase where a high steam injection pushed all the non-condensable gases into the wetwell gas space; a stratification phase at lower steam flow rates, and a mixing phase where the steam flow was increased to induce chugging.

During the stratifications phase the pool surface temperature measured in PPOOLEX was very well predicted when using the EHS/EMS containment model, Figure 4. This is due to the time-averaging model, which prevented the numerical oscillations at the blowdown pipe outlet from entering into the pool; and to the gas flow boundary condition in the wetwell gas space, which prevented small gas volume fractions to enter into the pool and induce artificial mixing. In the mixing phase, transition to chugging was observed and the EMS model provided the effective momentum given the analytical correlations. We can see in Figure 4 that the mixing trend was very well predicted, leading to a mixing time of 350 s, similar to the 400 s obtained in the PPOOLEX experiment.

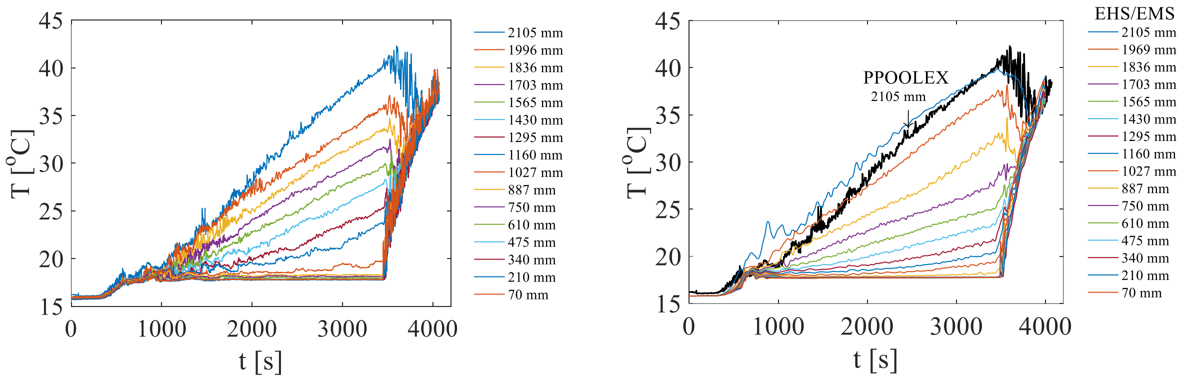

(a) (b)

Figure 4: Pool temperature distribution obtained in with the (a) PPOOLEX MIX-04 experiment, and (b) EHS/EMS containment model.

The pressures predicted with the EHS/EMS containment model and the direct steam injection simulation were quite similar (Figure 5). This is due to a short stratification phase and relatively low pool surface temperatures.

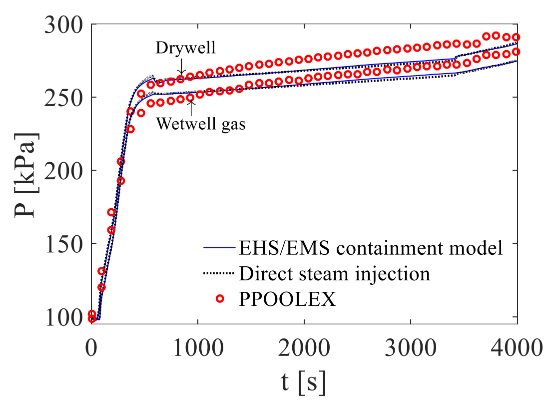

Figure 5: Pressure in the drywell and wetwell gas spaces obtained in the simulations and measured in the PPOOLEX MIX-04 experiment.

5.1. Effect of non-condensable gases in the chugging regime

Experiments performed by Kukita et al. in [83] estimated that chugging is completely suppressed when the injected flow has an air volume fraction over 3%. A theoretical analysis performed by [84] estimated that chugging is suppressed at air volume fractions over 3% for small scale installations and 7% for large scale installations.

In this section we use the PPOOLEX MIX data to estimate the amplitude and frequency of chugging as a function of the air volume fraction. In the clearing phase of the MIX experiments, a mixture of steam and air was pushed from the drywell into the wetwell through the blowdown pipes. Chugging was observed during all the clearing phases, meaning that certain flow rates of non-condensable gases were not enough to suppress it. Unfortunately, the air volume fraction was not measured in the experiments. However, it was estimated using the GOTHIC model presented in Figure 6. The sensitivity study performed for the drywell mesh is presented in Figure 6. The cell size of 150 mm was selected to estimate the air volume fractions during all the MIX experiments.

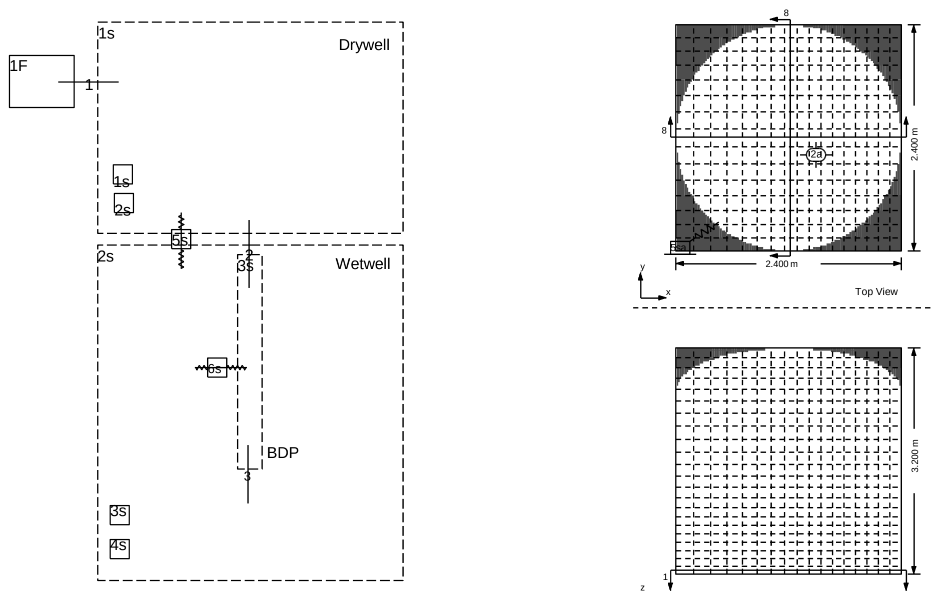

Figure 6. GOTHIC MIX-04 model. (a) Control volumes GOTHIC and (b) drywell mesh

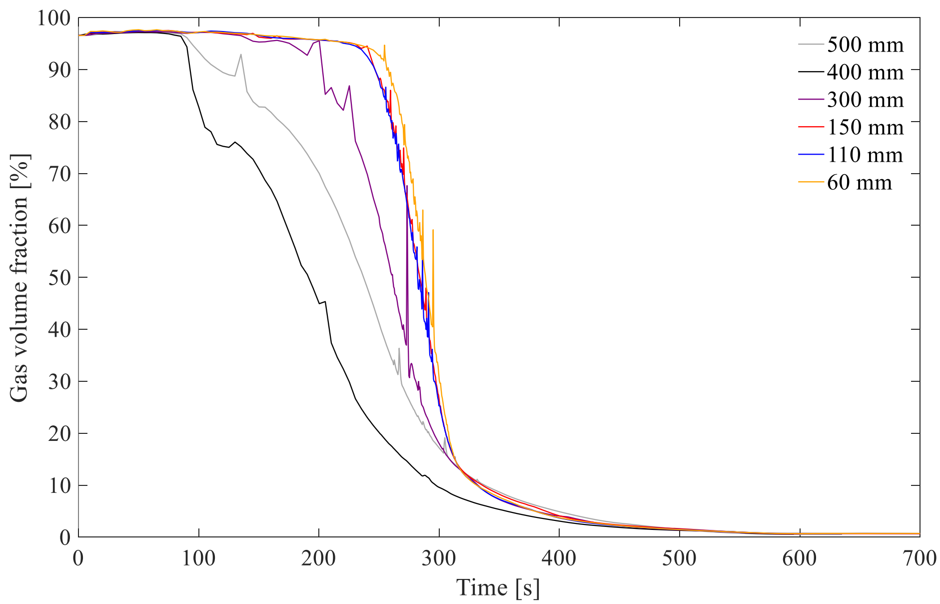

Figure 7. Sensitivity study of the drywell mesh. Gas volume fraction at the blowdown pipe during the MIX-04 experiment.

The volume fraction at which chugging is supressed was observed to decrease with the pipe diameter, being about 6% for 214 mm (MIX-01 to 06) and larger for 109 mm (MIX-07 to 12), Figure 8. The smooth changes in the amplitude shows that there is no threshold after which the regime radically changes. The behaviour at low volume fractions is still not well understood. In principle, the oscillations should be larger as the volume fraction decreases (reaching pure-steam conditions), rather than dropping down. Further analysis needs to be done to clarify this.

The scaling proposed in [15] for pure-steam conditions was observed to increase the difference between the MIX groups shown in Figure 8. This suggests that a different scaling approach is required for the case of air.

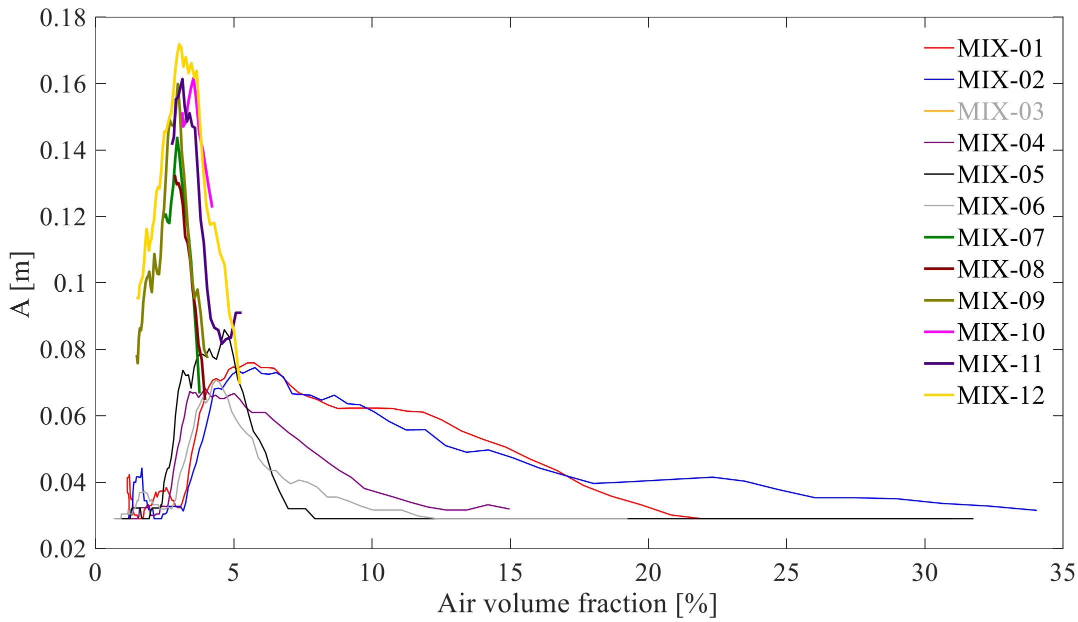

Figure 8. Amplitude of the chugging oscillations as a function of the estimated air volume fraction during the PPOOLEX MIX experiments.

5.2. Implementation in Nordic BWR models

The EHS/EMS models presented at the beginning of Section 5 are currently being implemented for a Nordic BWR containment for the analysis of LOCA transients. A sketch of the GOTHIC model is presented in Figure 9, where the EHS/EMS boundary conditions are similar to those in Figure 3. The annular shape of the upper drywell and wetwell was approximated to a rectangular volume with a 3D connector at both sides. This approach minimizes the number of un-used cells compared to using blocks to represent the annular geometry. The 40 blowdown pipes present in a full-scale containment were simplified to a single one. The same approach was used with the 64 spargers of the ADS system.

In the mesh, the cell size of the wetwell pool was set to 50 mm in the vertical direction, at the region below the injection points. In the axial direction, the size was increased to 1 to 2 m.

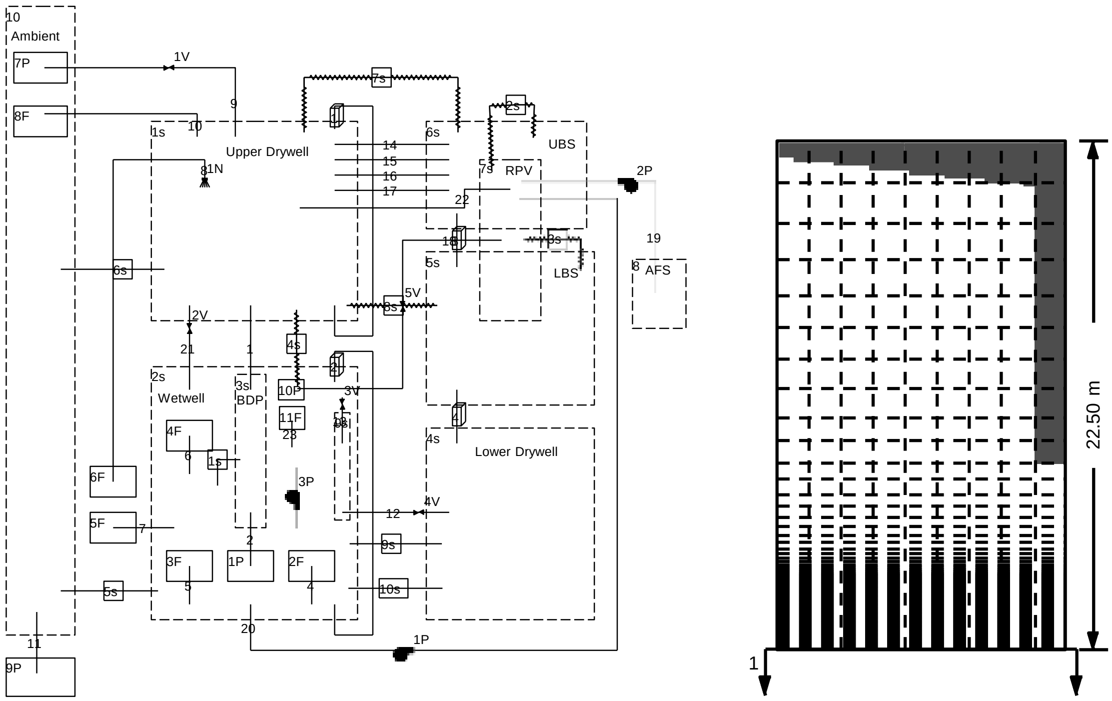

(a) (b)

Figure 9. GOTHIC model for a Nordic BWR (a) Over-view and (b) detail of the wetwell mesh.

The decay heat from the core is modelled using the American National Standards (ANS) 5.1 curve. This decay heat was given as a forcing function to a series of heaters located in the RPV volume. The SB LOCA scenario studied has a break size area of 0.00159 m^2 with a minimum section of 45 mm, located in the upper drywell. Station Black Out (SBO) is also assumed, and the safety systems of AFS, ECCS, spray and RHR are not activated, except the Rupture disks (361/362), which would open when the pressure inside the upper drywell reaches 450/550 kPa.

The initial condition in the containment is a Nitrogen atmosphere at 101.35 kPa. The gas temperatures are 45 °C in the UDW, 35 °C in the WW, and 80 °C in the biological shield. A pool of 10.3 m depth and 20 °C was set in the WW. The initial conditions in the RPV are water at saturation conditions of 7000 kPa with a liquid level 4 m above the core.

Preliminary results are shown in Figure 10, where we can see that thermal stratification begins to develop in the pool from the beginning of the transient. The mass flow rate is still too large to induce chugging, and thus its mixing capability has not yet been addressed. More analysis will be presented in further publications.

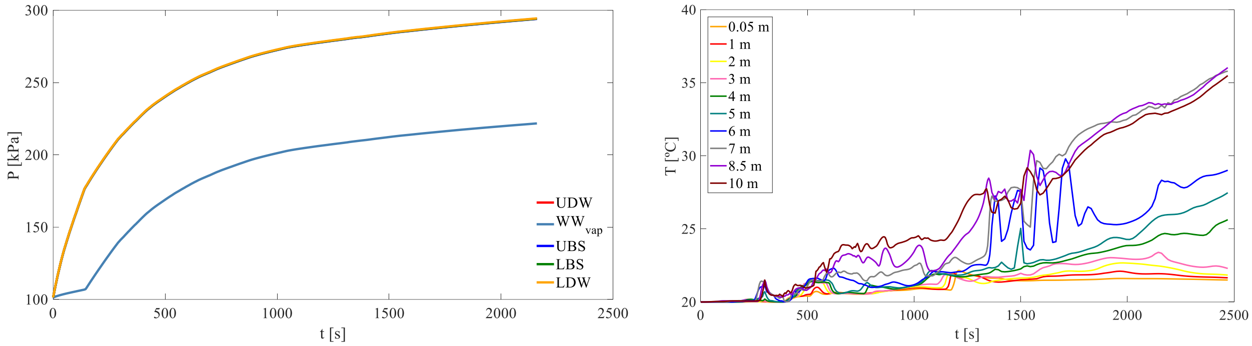

Figure 10. GOTHIC simulation of a SB LOCA with SBO (a) containment pressures (DW: DryWell, WW: WetWell, BS: Biological Shield, U: Upper, L: Lower) and (b) temperature along a vertical line in the pressure suppression pool.

6. SPARGERS

6.1. PPOOLEX and PANDA experiments with spargers

Details of the scaling methodology and analysis of the PPOOLEX and PANDA experiments with spargers are presented in [16]. In this section, we will present a brief summary of the main results.

The scaling was performed based on the roadmap to scaling proposed by D'Auria & Galassi [80] to preserve ranges of parameters and regimes that determine most important physical phenomena appearing in plant scale. The experimental data is then used for code validation and analysis of the physical phenomena. Once the code has been validated, it can be applied to predict plant phenomena. The experiments were designed to cover the sub-sonic condensation regimes occurring below 300 kg/(m^{2}s), which are expected to dominant during prototypic steam injections through spargers.

Analysis of the experiments showed that during the low steam injection phases the flow was driven upwards by buoyancy forces and stablished a high temperature layer, separated by a sharp thermocline from the cold layer below. In the high steam injection phase, the larger momentum induced by the steam jets caused a faster erosion of the cold layer. Nevertheless, the sharp temperature gradient across the thermocline was maintained. Transition between mixing and erosion was predicted based on the bulk Richardson number [62, 63, 64], equation (5),

$$Ri = \frac{\Delta b\ D}{U^2} \tag{5}$$

where Δb it the buoyancy jump across the thermocline, U the flow velocity above the thermocline, and D the distance between the sparger injection to the thermocline. The results were also compared to the so called Entrainment Law [62], equation (6),

$$\frac{U_E}{U} = CRi^{-n} \tag{6}$$

which relates vertical velocity at which the thermocline is pushed down U_E to the Richardson. The results were observed to follow well the relation proposed by equation (6), and the coefficients were calibrated to be C = 0.07 and n = 1.2.

Analysis of temperature and velocity fields in front of the sparger injection showed that jets oriented in the same direction merged to a single jet. This jet was observed to be self-similar, and correlations were proposed to model its spread based on time-averaged PIV data. The correlations were then used to assess possible interactions between the jets in the azimuthal direction.

It was also observed that the steam jets had a downwards inclination of about 15^o right at the injection holes. This effect was attributed to the downwards velocity component inside the sparger, which cannot be re-directed through the sharp injection holes. An analytical correlation was proposed to predict this angle in other sparger designs.

Analysis of the PIV data showed that the turbulence intensity in front of the injection holes reached values of up to 90%, which are much larger than previous intensities measured in a condensing steam jet [23]. Nevertheless, the oscillatory bubble regime, combined with a multi-hole injection, could have contributed to a significant increase of the intensity compared to the single-hole stable jet presented in [23]. Over-estimations of the turbulence levels caused by the PIV system were also addressed.

6.2. CFD modelling of the PPOOLEX experiments

The PPOOLEX and PANDA experiments with spargers presented in Section 6.1 were designed to analyze the large-scale pool behavior induced by the steam injection. Small-scale phenomena of direct contact condensation could not be measured. The simulations presented in this section were performed to provide an estimate of the effective momentum induced by the steam condensation regimes. The estimates were assumed to be adequate if they could successfully reproduce the ThermoCouples (TC) and Particle Image Velocimetry (PIV) data obtained in the experiments. All details of the simulation setup and results can be found in [17].

The simulations were performed with the CFD code of ANSYS Fluent 17.0. Calibration of the different modelling approaches showed that the capturing body forces in the liquid requires using a single-phase solver. Simulations performed with the Volume of Fluid (VOF) approach, typically used for pool analysis, showed a large sensitivity to the reference density, causing a partial mixing of the pool when using the air density, and a complete de-stabilization of the gas space when using the liquid one. Thus, only the liquid pool was modelled, and dynamic layering was used for the rising liquid level (caused by inflow and density changes).

Body forces in the mean flow were captured by defining a temperature dependent density. The Boussinesq approximation, valid for the temperature ranges of the sparger experiments, was observed to be inadequate due to the incapability to define a variable thermal expansion coefficient in Fluent.

Buoyancy effect on turbulence were also taken into account by adding through a UDF the Standard Gradient Diffusion Hypothesis (SGDH) in the k-Omega BSL model. A new correlation was proposed to model the $C_{3\varepsilon}$ parameter, which is a multiplier of the buoyancy term in the dissipation equation, using the gradient Richardson number. The results obtained with such modelling approach enabled the prediction stable stratification, not possible when using Fluent default two-equation models (which caused a large diffusion due to over-predictions of the turbulent viscosity at the thermocline).

Domain and mesh sensitivity studies were also performed. A full 3D modelling of the pool was observed to be necessary to capture flow asymmetries. The mesh was built using a multi-block hexa approach in ICEM CFD. Sensitivity studies showed that a cell size of 25 mm in the vertical direction and 128 cells in the azimuthal direction around the sparger was appropriate since it converged to finer mesh results. The resulting meshes for PPOOLEX and PANDA were about 500 thousand cells.

6.2.1. Calibration of the momentum sources

The injection angle, momentum profile and turbulent sources induced by the steam injection were discussed and estimated at the beginning of Section 6.2. Simulations performed with different values within their uncertainty ranges showed a large effect on the erosion velocity. For example, a larger downwards injection angle of 20^{o} led to a larger fraction of momentum directed towards the cold layer, and thus to a faster erosion of the cold layer. On the other hand, smaller angles such as 10^{o} led to a slower erosion. Calibration of the momentum sources was done by fixing these parameters to the estimates from the experiments for all PPOOLEX and PANDA simulations.

Comparison between two of the PPOOLEX experiments and simulation results is presented in Figure 11 and Figure 12. Comparison to all simulated PPOOLEX and PANDA experiments can be found in [17]. In general, it was concluded that the modelling approach from Sections 6.2 can successfully reproduce the pool behavior for a broad range of injection conditions. All the low steam injection phases were well captured in terms of the location of the cold layer and the sharp gradient across the thermocline. In addition, the gradient across the thermocline was maintained during the erosion transients of the high steam injection phases.

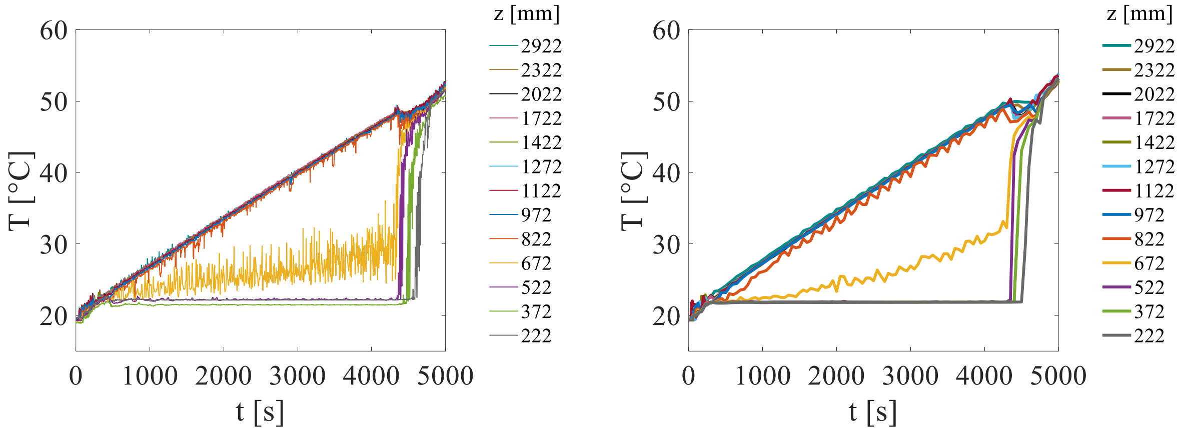

(a) (b)

Figure 11: PPOOLEX SPA-T3 (a) experiment and (b) Fluent simulation using the EHS/EMS models with the C coefficients from Figure 13. Temperature evolution along a vertical line of TCs in the pool.

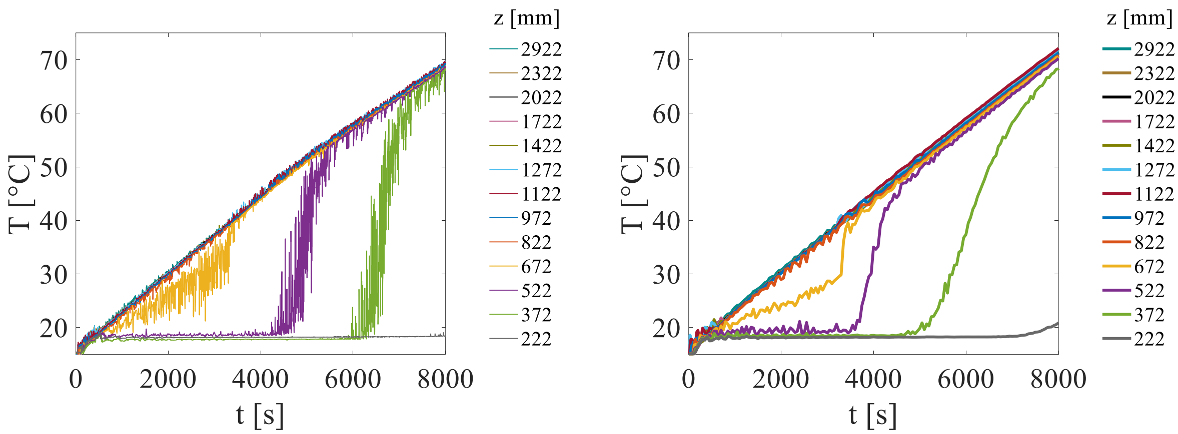

(a) (b)

Figure 12: PPOOLEX SPA-T6 (a) experiment and (b) Fluent simulation using the EHS/EMS models with the C coefficients from Figure 13. Temperature evolution along a vertical line of TCs in the pool.

The effective momentum M_{eff} calibrated for the PPOOLEX and PANDA experiments is presented in Figure 13. The results are shown as a function the condensation regime coefficient, equation (7),

$$C = \frac{M_{eff}}{\rho_s A_i U_s^2} \tag{7}$$

where $\rho_s A_i U_s^2$ is the theoretical estimate of the steam momentum at the injection holes. The differences between PPOOLEX and PANDA could be attributed to the uncertainty introduced by the modelling options and boundary conditions. Nevertheless, all of them show the same behaviour with respect to the subcooling. Comparison between the estimated C coefficients is done in Section 6.3 against experimental data.

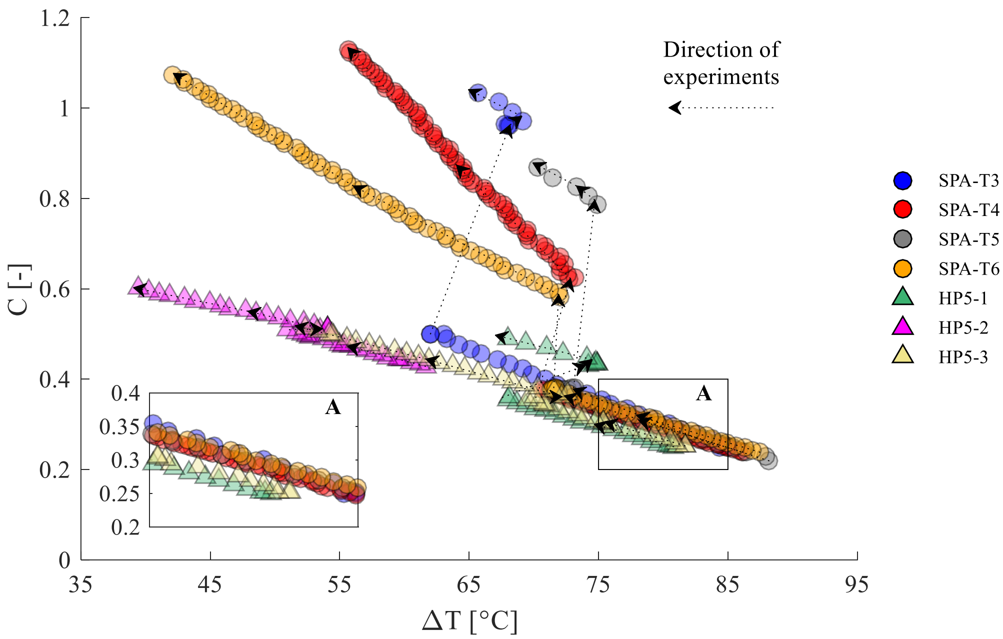

Figure 13: Condensation regime coefficient C estimated in the simulations as a function of the sub-cooling $\Delta T = T_s$-T_p. Symbols correspond to ▲ PANDA and ● PPOOLEX.

6.3. Separate Effect Facility (SEF)

In this section we present the results obtained in the Separate Effect Facility (SEF) built in Lappeenranta University of Technology (LUT), Finland. The goal of this facility is to measure all the details of direct contact condensation which could not be observed in large-scale PPOOLEX and PANDA experiments (Section 6.1), and to provide a direct measurement of the effective momentum.

An over-view of the SEF facility is presented in Figure 14. The dimensions of the water tank are 1500×300×600 mm. Steam is generated using a 1.5 MW heater and injected into the pool through a perforated plate located at the end of the sparger pipe, which is insulated to minimize steam condensation. The condensed flow is then guided through the PolyCarbonate (PC) pipe to impinge on the disk stack. The support rods of the sparger and PC pipes are allowed to rotate around their axis. Therefore, the steam force at the injection hole and the liquid force carried by the condensate liquid were measured independently using force sensors connecting the pipes to two support rod fixed to the ground.

Details of the steam condensation were recorded using a Phantom MIRO M310 camera, recording frequency of 2800 Hz; a pressure transducer of 7000 Hz; and thermocouples and a pressure measurements were also added obtain the steam injection conditions inside the sparger and pool temperatures.

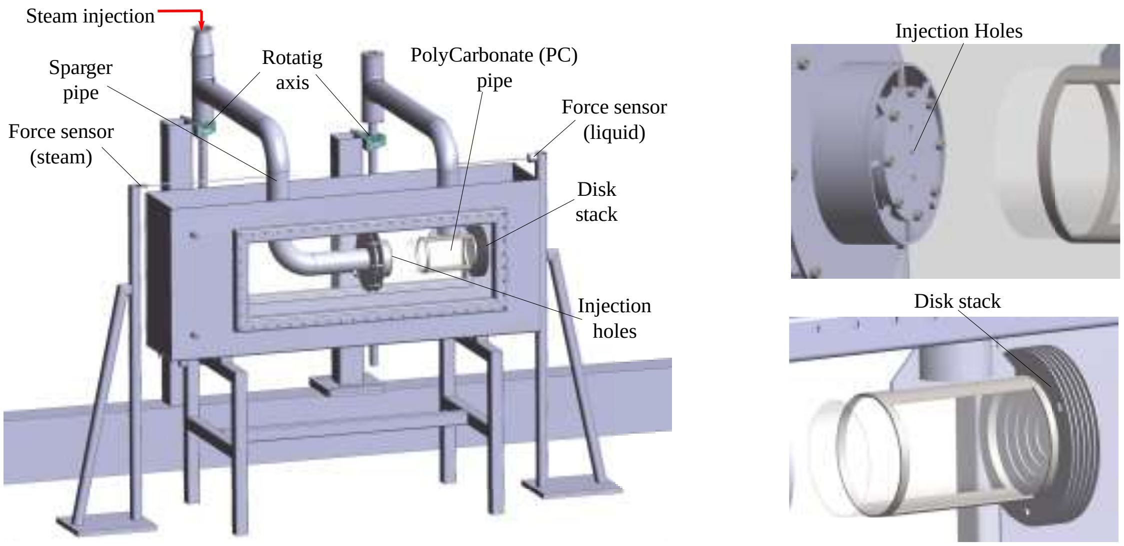

Figure 14: Separate Effect Facility (SEF). Over-view and details of the injection holes and disk stack.

6.3.1. Experimental results

The experimental campaign was divided into two main sets (Table 1). First, experiments were run without PC pipe to obtain data on the steam condensation without any possible disturbance. After this, the PC pipe was added to enabling measuring the effective momentum.

Table 1: Test matrix used in the SEF experiments. Pool temperatures were between 20 to 80 °C for all of the experiments. Steam temperatures about 105 °C.

Experiment identifier	Injection plate (#holes × diameter)	G [kg/(m^{2}s)]
Without PC pipe		
S10	1×16 mm	75
S6		125
S11		175
S7		225
S5		325
S12	1×12 mm	125
S13		175
S3	3×8 mm	125
S4		325
With PC pipe		
S14	1×16 mm	75
S15		125
S16	1×12 mm	125
S17	2×8 mm	125

The forces measured during the SEF-S16 experiment are shown in Figure 15a. Comparison with the pressure transducer and video images showed that the oscillations are due to the cyclic growth, necking and collapse of the steam bubbles. Negative forces suggest a fast deceleration of the flow injected into the pool, and positive peaks an acceleration. From this result, we can conclude that the steam flow rate at the injection hole is *not* constant.

The I-V points shown in Figure 15b are the mean values over the 12.5 s steps at which the force sensors were set to record. Although the steam mass flux was maintained constant for the whole experiment, the force was observed to increase with the pool temperature. This increase is probably due to the larger size of steam bubbles allowed to form at low subcoolings, which could lead to larger forces during the collapse.

The steam force at the injection hole induced by an injection into a water pool can be estimated with equation (8).

$$F_{th} = \frac{\dot{m}_s}{\rho_s A_i} + A_i(P_s - P_\infty) \tag{8}$$

Unfortunately, all the variables from equation (8) are subject to uncertainty. The steam flow rate $\dot{m}_s$ is not constant. The injection hole area A_i should be corrected by the contraction coefficient, occurring when injecting flow through a sharp orifice (an effect which was observed in the water-to-water experiments). The steam density ρ_s is also dependent on the instantaneous flow velocity and pressure differences. Lastly, the steam pressure P_s can be assumed to be equal to the hydro-static pressure of the pool P_∞ for a sub-conic regime (such as the oscillatory bubble regime).

In [17], the authors estimated equation (8) assuming that $\dot{m}_s$ is constant, A_i equal to the injection hole area, ρ_s a function of the steam temperature inside the sparger T_s and the hydro-static pressure in the pool P_∞, and $P_s = P_\infty$. We can see in Figure 15b that these assumptions lead to a good estimation of the order of magnitude, but cannot capture the dependency with the subcooling.

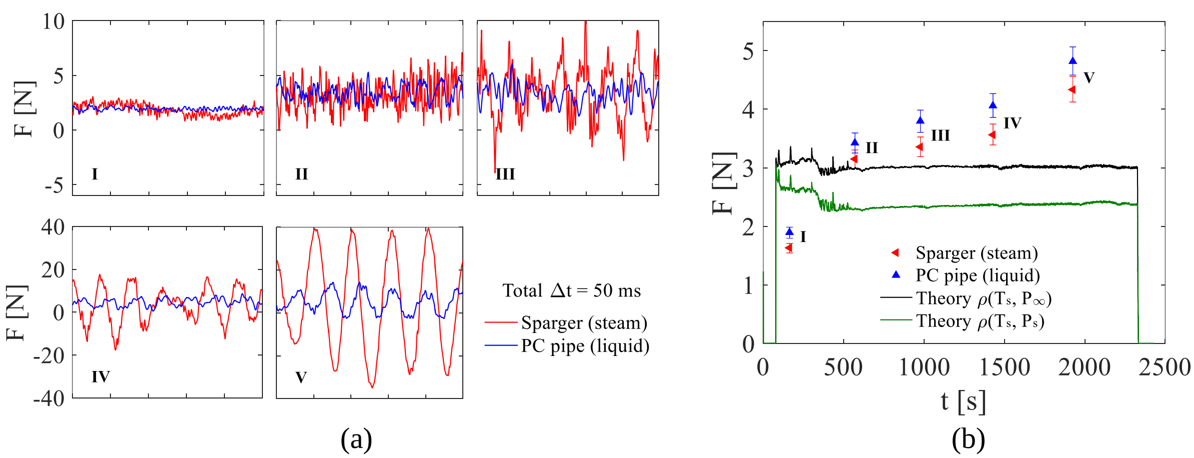

Figure 15: Forces measured in the SEF-S16 experiment: 1×12 mm, G = 125 kg/(m^{2}s). (a) Time-dependent forces, and (b) mean values compared with the theoretical estimates given by equation (8).

The C coefficients defined in equation (7) were determined using the force measurements obtained in SEF. We can see in Figure 16 that the calibrated and measured C vales show a similar trend with respect to the subcooling ΔT, but also a significant shift. The reason for this shift is probably due to the uncertainty in parameters defined in Fluent regarding the sparger injection. Mainly the injection angle, momentum profile and induced turbulence sources. Although these parameters were estimated based on the experimental data, small variations within the uncertainty ranges were observed to induce large changes in the results. The better agreement in some phases of the PPOOLEX experiments suggest that the assumptions done on the injection parameters was adequate.

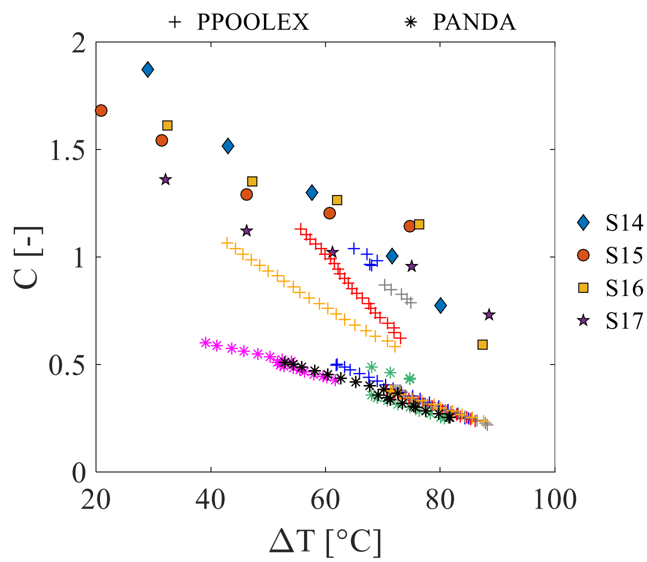

Figure 16: Condensation regime coefficients C obtained in the SEF facility and estimated in the Fluent simulations of the PPOOLEX and PANDA experiments with sparger (see Figure 13).

6.4. CFD modelling of the full-scale Pressure Suppression Pool (PSP)

6.4.1. Validation against Nordic BWR experiment on PSP

An experiment was performed in a Nordic BWR by injecting steam through a single sparger into the PSP. This sparger is not part of the ADS system, but a separate one used during the start-up of the reactor to clear water from the main steam lines by blowing it into the pool. The geometry of the sparger is similar to what was used in the PPOOLEX and PANDA experiments. Therefore, the models developed in [17] are expected to be applicable to the BWR sparger geometry. Similarities are the chamfered injection holes of 10 mm diameter, the pitch to diameter ratio of 5 in the vertical direction, and the area ratio between sparger pipe and injection hole area of 0.38. Differences are the total number of holes, which in the BWR sparger was 9 rings of 7 holes each (compared to 4×8 arrangement of PPOOLEX and PANDA).

The available data measured during the BWR transient was the steam temperature inside the sparger T_0, which varied between 200-250 ºC, and the total mass flow rate $\dot{m}_s$, which was maintained constant at 3.5 kg/s. These conditions lead to a sonic flow with a mass flux of about 800 kg/(m^{2}s). The effective momentum equation for a sparger was derived in [17] as equation (9),

$$M_{eff} = \rho_s A_i U_s^2 + (P_s - P_\infty) A_s \tag{9}$$

Where ρ is density, A cross section area, U mean flow velocity, and P pressure. For a sonic flow, the pressure P_s can be computed as a function of the pressure inside the sparger P_0 using equation (10).

$$\frac{P_s}{P_0} = \left(\frac{2}{\gamma + 1}\right)^{\frac{\gamma}{\gamma - 1}} \approx 0.53 \tag{10}$$

Since P_0 was not measured during the experiments, it was estimated based on the measured steam mass flow using equation (11).

$$\dot{m}_s = C_d A \sqrt{\gamma \rho_0 P_0 \left(\frac{2}{\gamma + 1}\right)^{\frac{\gamma+1}{\gamma-1}}} \tag{11}$$

Experimental values for the discharge coefficient C_d can be found in [16], where it will be assumed that it takes a value of 0.6. Solving equations (10) and (11) allowed us to estimate P_s to be at a quasi-constant value of 290 kPa. Since the hydrostatic pressure P_∞ was about 165 kPa, we can see that the pressure head accounts for a significant fraction of the momentum.

The case setup for the CFD model used to simulate the PSP transient was the same as presented in Section 6.2 [17]. That is, single-phase RANS approach using the k-Omega BSL model with added buoyancy terms. The effective heat and momentum boundary conditions were also assumed to be non-homogeneous, with a jet profile given by K = 40 and a downwards injection angle α = 10º.

An over-view of the PSP geometry is presented in Figure 17a. The total water volume was about 3300 m^3 and the pool depth 9.8 m. The tunnel for access to the lower drywell (central cylindrical volume in Figure 17a) was included in the model. This tunnel is 4.3 m tall and is expected to induce symmetry breaking effects which could affect the development of thermal stratification. The sparger was located at about 140º from the tunnel, submerged 6.9 m into the pool and located 600 mm from the wall. The size of the EHS/EMS region was estimated by maintaining the contraction ratio of length of rings/EMS region = 2.6 observed in the PANDA experiments, leading to a box of of 130x50 mm in the plant sparger (height of 6 cells of 25 mm each). Mid-point of the injection is located at 3.15 m.

The mesh dimensions were determined by the mesh sensitivity study done in [17]. The vertical cell size below the sparger was kept to 25 mm in all the pool to capture the sharp temperature gradients across the thermocline. The number of cells in the azimuthal direction of the sparger was set to 128 to minimize the diffusion of the sparger jets. The mesh was done independently for two separate volumes: a 1.2×1.2×9.8 m volume around the sparger and another one for the rest of the pool. The interfaces between these two volumes was non-conformal, allowing a reduction of the number of cells in the azimuthal direction as shown in (Figure 17b). The non-conformal interfaces were treated with the Matching option, which corresponds to completely overlapping faces.

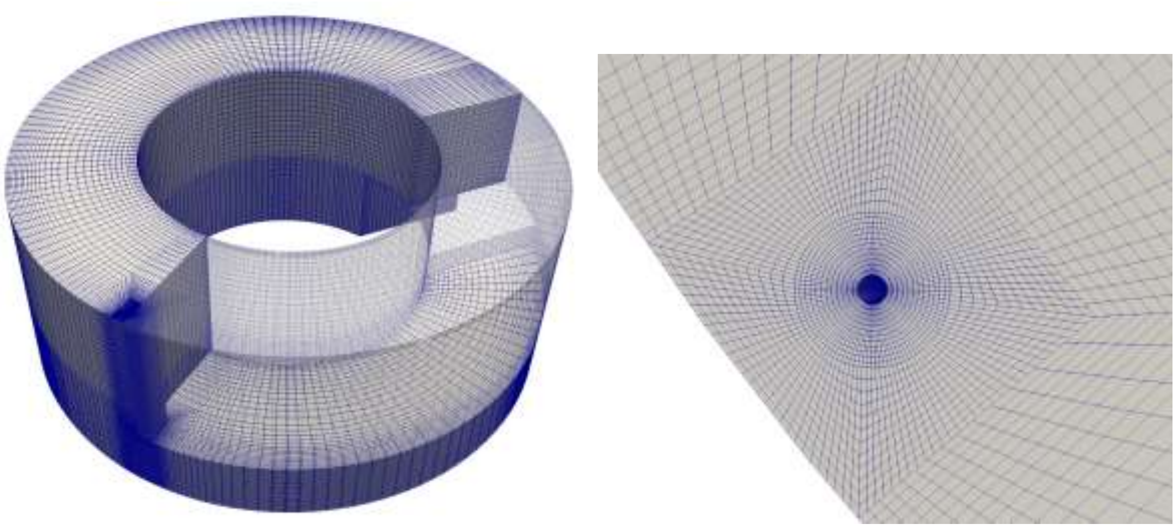

Figure 17: Mesh used for the BWR PSP transient. (a) Over-view and (b) detail of the sparger mesh and the non-conformal transition to the rest of the pool.

In the experiment, the lowest TC measuring the PSP temperature was located 4.3 m above the floor. Therefore, it was unclear whether the bottom part of the pool could present some degree of stratification. Comparison between experiment and simulation is presented in Figure 18a. Good agreement was obtained in terms of mean temperature and mixed conditions above 4.3 m. Below this level, homogeneous temperature was also observed, with only a minor stratification profile at the KD sector, which is the region close to the lower drywell tunnel (Figure 18b). Based on these results, we can conclude that a large enough single-source of momentum can induce mixing of a large PSP. Stratification is not observed in the azimuthal direction. This is due to the tendency of the flow to reach stable stratification conditions, in which temperature gradients align with the gravity vector.

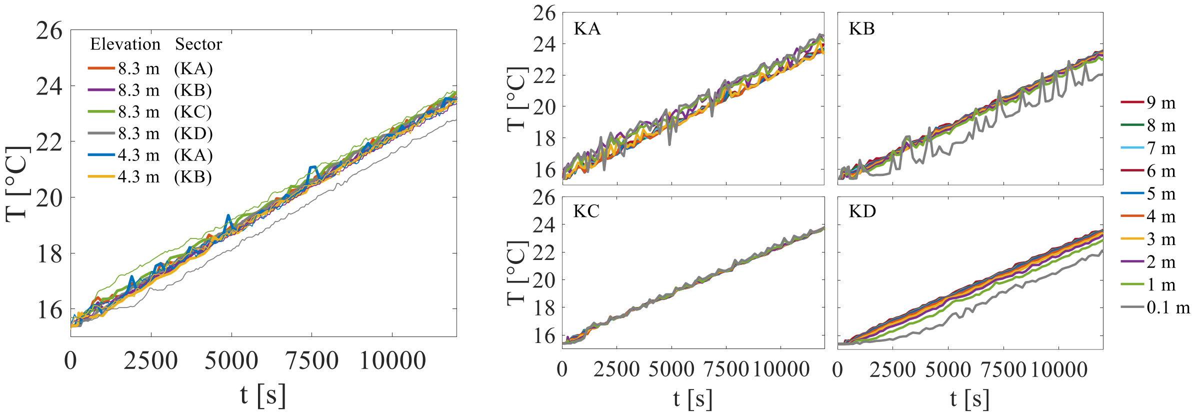

(a) (b)

Figure 18: Pool temperature evolution measured in the PSP experiment (—) and predicted with Fluent (▬) at the (a) locations where TCs are located in the PSP and (b) at different sectors and elevations of the PSP.

6.4.2. Pool behaviour at lower flow rate

We have seen in Section 6.4.1 that the high steam mass fluxes of 800 kg/(m2s) used in the PSP experiment led to sufficient momentum to mix the pool. This result does not imply that pool stratification is not a threat for plant safety. It only shows that, for certain injection conditions, mixing can occur. In this section, we will show that for other, less conservative, conditions, thermal stratification can also develop.

We assumed a steam injection of 0.3 kg/s through the same sparger as the one used in the PSP experiment of Section 6.4.1, leading to a steam mass flux of 70 kg/(m^{2}s). In the simulations performed for the PPOOLEX and PANDA experiments, it was estimated that the effective momentum for this regime has a C coefficient between 0.2-0.4 (Figure 13). Nevertheless, we chose to use $C = 1$ for the PSP simulation as a conservative assumption in terms of pool mixing. Moreover, the $C = 1$ assumption seems to agree better with the recent experiments performed in SEF (Figure 16).

The pool behaviour obtained with the aforementioned conditions is presented in Figure 19. Since the lowest thermocouples at the PSP are located 4.3 m above the floor, the operator could assume that the pool is completely mixed at this conditions (Figure 19a). However, plotting the results from the base of the pool reveals a cold layer of about 2 m. From this results, we can conclude that adding more thermocouples in the PSP is essential for operator’s decisions, and that thermal stratification can occur in a full-scale PSP.

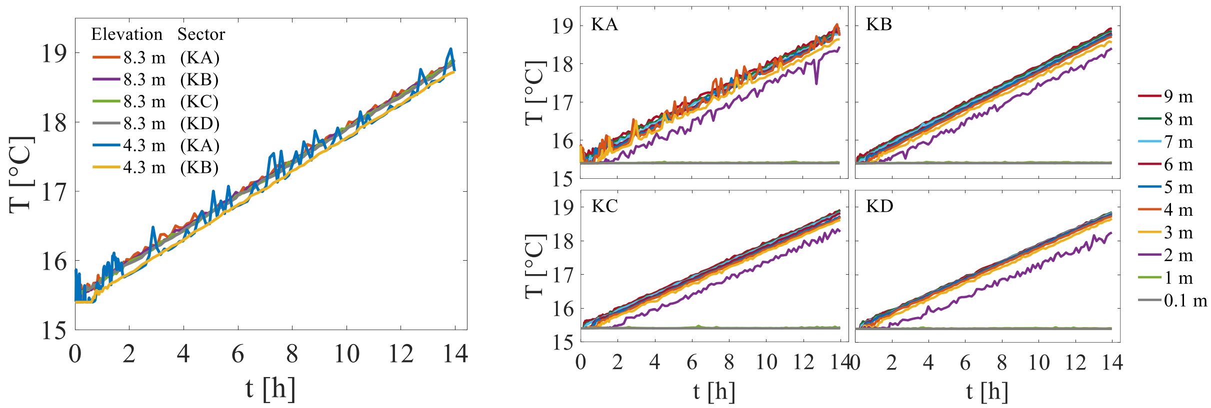

(a) (b)

Figure 19: Pool temperature evolution predicted with Fluent at the (a) locations where TCs are located in the PSP and (b) at different sectors and elevations of the PSP.

Another important observation from the simulations is that, despite steam was injected through a single sparger at low flow rates, no stratification was observed in the azimuthal direction. This result is physically reasonable, since buoyancy forces always tend to align stratification perpendicular the gravity vector. Nevertheless, it can be seen in [82] that several authors who addressed the PSP behaviour in Fukushima Unit 3 assumed azimuthal stratification in their analysis.

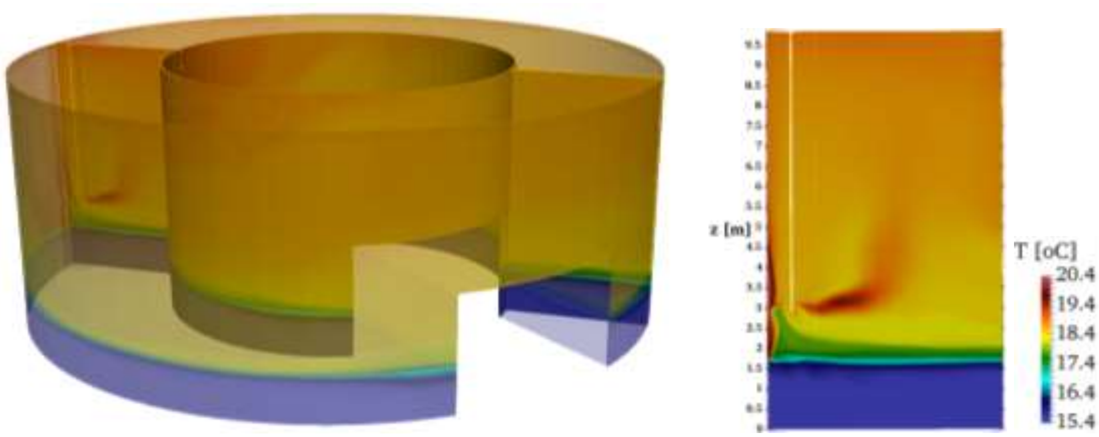

(a) (b)

Figure 20: Pool temperature field at t = 14 h in the (a) pool and (b) slice section where the sparger injects steam.

6.4.3. Injection through 314 spargers

The sparger used in the PSP experiment presented in Section 6.4.1 was not part of the ADS system 314. The 314 spargers have a much larger injection hole area and are arranged in 16 groups of 4, giving a total of 64. This numbers show that injecting the 3.5 kg/s used in the PSP experiment would have led to a substantial reduction of the steam mass flux, increasing the risk of thermal stratification.

In this section, we simulate the transient in which 3.5 kg/s are injected through all the spargers of the 314 system. Since no azimuthal stratification was observed in the transient from Section 6.4.2, symmetry boundary conditions were used to reduce the computational cost of the simulations, allowing us to reduce the PSP domain to 11.25º slice (Figure 21a). The flow distribution between the Load Reduction Ring (LRR) and sparger head was assessed the GOTHIC model presented in Figure 21b. For the given steam injection conditions, the model predicted that all steam is condensed inside the first 2.6 m of the submerged section, meaning that only condensed liquid flows out of the LRR holes.

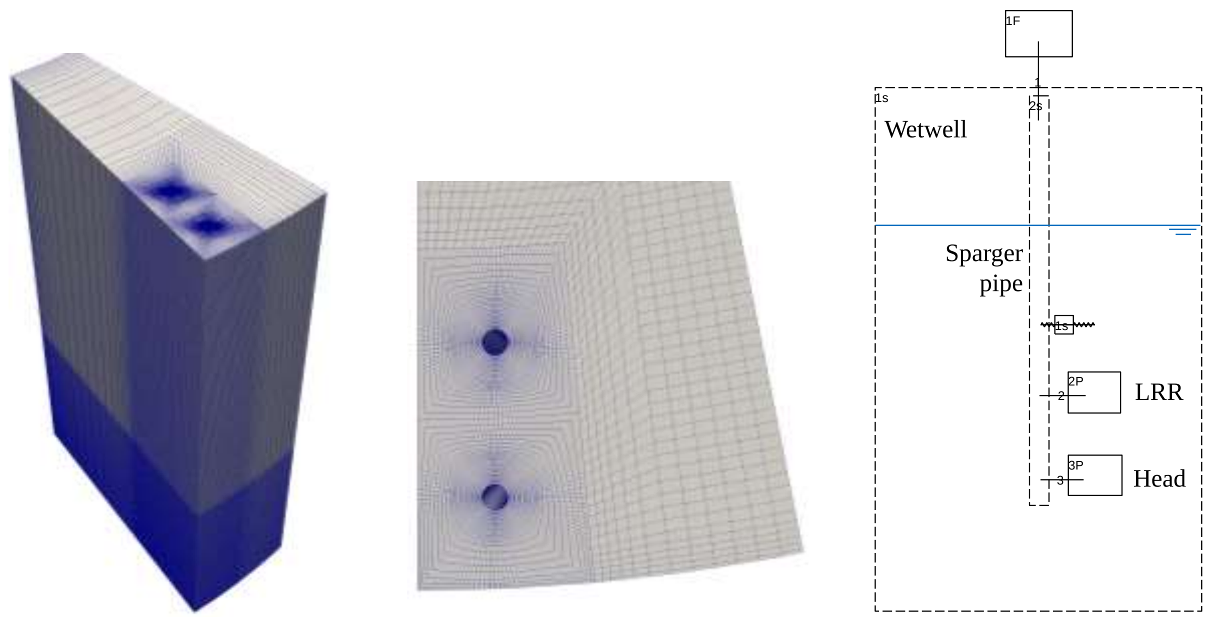

(a) (b)

Figure 21: Spargers of the 314 system. (a) Mesh used for the Fluent simulations and (b) GOTIC model used to estimate the flow distribution between the LRR and sparger head.

The uniform latent heat distribution along the sparger pipe led to a constant temperature gradient in the hot layer (Figure 22a). This profile is different from the one observed in Figure 19 and Figure 20, where the hot layer appears homogeneously heated. The linear temperature profiles observed in Figure 22b are similar to those observed in the PPOOLEX experiments with blowdown pipes when steam was condensing completely inside them.

A conservative assumption done in PSP analysis is that, due to the possibility of developing thermal stratification, only the pool volume above the injection point is considered for storing the latent heat. This volume is assumed to be homogeneously heated, leading to a certain pool surface temperature. The results presented in Figure 22 show that this assumption is not conservative enough due to the following reasons: **(1)** Steam can condense inside the pipe before reaching the injection holes and **(2)** if this occurs, a linear temperature profile develops, leading to larger pool surface temperatures than with the homogeneous temperature assumption.

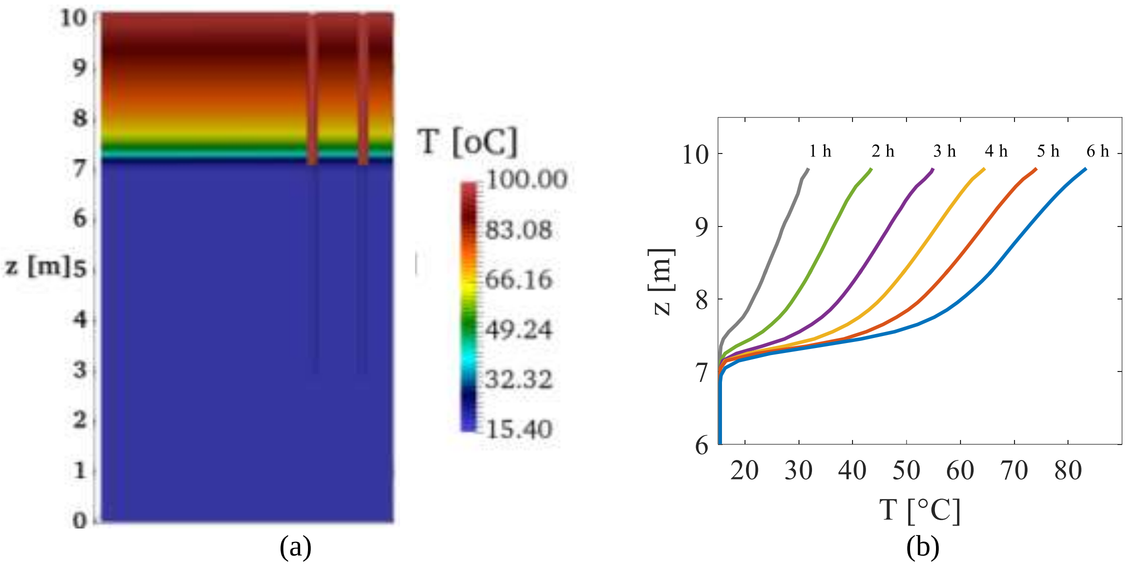

Figure 22: Simulation of a steam injection at 3.5 kg/s through the 64 spargers of the 314 system. (a) Pool temperature contours at 6 h and (b) vertical temperature profiles as a function of time. Note that in (b) the lowest vertical location of the plot is 6 m, not floor level.

SUMMARY & CONCLUSIONS

The development of thermal stratification in the pressure suppression pool of BWRs and o the In-containment Refuelling Water Storage Tank of advanced PWRs is a safety issue since it can lead to higher containment pressures than in completely mixed conditions, and affect the operation of the spray and Emergency Core Cooling System (ECCS). The main systems responsible for inducing thermal stratification or mixing of the pool are the spargers, mixing nozzles, blowdown pipes, and sprays. In this work, we have presented the development and validation of Effective Heat Source and Effective Momentum Source (EHS/EMS) models for blowdown pipes and spargers, which enable the prediction of the pool behaviour during long term-transients. A summary of the current status on the development and validation of the EHS/EMS models (according to the NORTNET-RM3 tasks) is shown below.

Task-1: To develop EHS/EMS models for the blowdown pipes in case of different steam condensation regimes and presence of non-condensable gases.

New correlations have been developed to predict the transition between condensation regimes, and to estimate the effective momentum of chugging. These correlations are function of the steam mas flux, pool sub-cooling, and geometry of the injection system. They were built using the PPOOLEX and all other all available experimental data. A new implementation of the EHS/EMS models in GOTHIC has been proposed to enable simulating the pool and containment behaviour during prototypic LOCA conditions. A time-averaging model has also been proposed to minimize the effect of the numerical oscillations of the flow in the pool. Validation against the PPOOLEX MIX-04 and MIX-06 experiments shows very good agreement to the pool temperatures and containment pressure.

The effect of non-condensable gases on chugging is begin analysed by using the data from the clearing phases of the PPOOLEX MIX experiments. Preliminary results show that the volume fraction at which chugging is supressed decreases with the blowdown pipe diameter.

Task-2: To develop EHS/EMS models for spargers and RHR nozzles.

A Separate Effect Facility (SEF) has been built in cooperation with LUT to measure the effective momentum induced by the oscillatory bubble regime. The results show that the effective momentum is very similar to the steam momentum at the injection holes. The latter was observed to be a function of the cyclic bubble oscillations, and thus to deviate from standard estimations based on a constant steam mass flow rate. Comparison with the effective momentum estimated in the Fluent simulations shows a similar trend with respect to the subcooling, but a shift on absolute values.

Task-3: To provide analytical support for PSP tests in the Nordic BWRs.

A scaling methodology has been developed and applied to the sparger and mixing nozzle experiments performed in PPOOLEX and PANDA. The goal was to preserve prototypical ranges of injection conditions and pool regimes occurring during prototypical BWR transients. The data obtained with the scaled experiments was used for analysis of the physical phenomena and code validation. Important physical phenomena to be considered in the CFD modelling has been identified: for example, the erosion and mixing mechanisms of the stratified layer, the oscillations at the thermocline, the self-similarity of the liquid jets induced by the sparger, and the downwards inclination of the jets. Codes and EHS/EMS models validated for these conditions can be then used to predict plant behaviour.

Task-4: To validate the EHS/EMS models against PANDA tests

The EHS/EMS models for sparger have been implemented in ANSYS Fluent. It has been shown that using the k-Omega BSL turbulence model with the SGDH and a $C_{3\varepsilon}$ varying between 0 and 1 allows a good prediction of the stable stratification and erosion regimes. The effective momentum was calibrated using the PANDA HP5-1 to 3 experiments and the PPOOLEX SPA-T3 to T6 experiments. The estimates have been compared to the experimental measures obtained in the Separate Effect Facility (SEF), see Task 2.

Task-5: To provide analytical support to NORTHNET partners in addressing containment performance

EHS/EMS for blowdown pipes have been implemented in a Nordic BWR model in GOTHIC for the analysis of the pool during a Small Break LOCA. EHS/EMS models for spargers have been validated against the full-scale PSP experiment performed in a Nordic BWR (where complete mixing was observed). Simulations of the PSP behavior for other steam injection conditions and sparger models has also been performed. The results show that the thermal stratification development in the pool can lead to larger pool surface temperatures than when assuming that all latent heat is homogeneously distributed in the pool volume above the injection holes.

Task-6: Analytical support for PPOOLEX tests and GOTHIC validation

Analytical support has been provided to the PPOOLEX and PANDA experiments with spargers and mixing nozzles. Pre-test simulations were run using GOTHIC. In the mixing nozzle experiments, the experimental results were observed to be very similar to the pre-test predictions. Analytical support will also be given for the separate effect facility to be built in LUT. Post-test analysis of the EHS/EMS models implemented GOTHIC showed good agreement to the pool behavior during the sparger tests SPA T1, T3, T4, T7. However, limitations of the code, mainly the Cartesian mesh, suggested that ANSYS Fluent, where the radial injection of the sparger can be better represented, would be more adequate for this purposes. Therefore, ANSYS Fluent was selected as the computational platform to validate the EHS/EMS models for spargers against the PPOOLEX and PANDA tests (see Task 4).

ACKNOWLEDGEMENTS

Financial support from the NORTHNET-RM3 and Nordic Nuclear Safety Program (NKS) is greatly acknowledged. The authors are grateful to Markku Puustinen (LUT) and co-workers for very fruitful discussions and unique experimental data which helped a lot in understanding, development and validation of the models. The authors are grateful to all the countries participating in the OECD/NEA HYMERES project. The authors would like to thank the secretariat and all the members of the Management Board and the Programme Review Group of the HYMERES project for their help in defining the test programme and evaluating the test results.

GOTHIC is developed and maintained by the Numerical Applications Division of Zachry Nuclear Engineering under EPRI sponsorship. We would like to acknowledge NAI for providing access to the program for educational and research purposes.

The ANSYS Fluent simulations were performed on resources provided by the Swedish National Infrastructure for Computing (SNIC) at PDC Centre for High Performance Computing (PDC-HPC). The authors are grateful to the PDC-HPC staff for assistance concerning the implementation aspects in making the code run on the PDC-HPC resources.

NKS conveys its gratitude to all organizations and persons who by means of financial support or contributions in kind have made the work presented in this report possible.

DISCLAIMER

REFERENCES

1. B. Pershagen, 1994. Light Water Reactor Safety. Pergamon Press.
2. R.T. Lahey, F.J. Moody. The Thermal Hydraulics of a Boiling Water Nuclear Reactor, 2nd edition, American Nuclear Society, La Grange Park, Ill, USA, 1993.
3. J. Laine, M. Puustinen, A. Räsänen. PPOOLEX experiments on the dynamics of free water surface in the blowdown pipe. Nordic Nuclear Safety Research, 2013, NKS-281.
4. J. Laine, M. Puustinen, A. Räsänen, PPOOLEX Experiments with a Sparger, Nordic Nuclear Safety Research, 2015, NKS-334.
5. S. Mizokami, D. Yamada, T. Honda, D. Yamauchi, Y. Yamanaka. Unsolved issues related to thermal-hydraulics in the suppression chamber during Fukushima Daiichi accident progressions. Journal of Nuclear Science and Technology, 53 (2016) 630-638.
6. S. Mizokami, Y. Yamanaka, M. Watanabe, T. Honda, T. Fuji, Y. Kojima, C.Y. PAIK, F. Rahn. State of the art MAAP analysis and future improvements on TEPCO Fukushima-Daiichi NPP accident. NURETH-15: The 15th International Topical Meeting on Nuclear Reactor Thermal Hydraulics, Pisa, Italy, May 12-17, paper number 536, 2013.
7. V. Tanskanen, A. Jordan, M. Puustinen, R. Kyrki-Rajamäki. CFD simulation and pattern recognition analysis of the chugging condensation regime. Annals of Nuclear Energy, 66 (2014) 133-143.
8. G. Patel, V. Tanskanen, E. Hujala, J. Hyvärinen. Direct contact condensation modeling in pressure suppression pool system. Nuclear Engineering and Design 321 (2017) 328-342.
9. M. Pellegrini, M. Naitoh. Application of two-phase flow DFC to the phenomena expected in Fukushima Daiichi S/C. OECD/NEA & IAEA Workshop CFD4NRS-6, 2016.
10. H. Li, P. Kudinov. Effective Approaches to Simulation of Thermal Stratification and Mixing in a Pressure Suppression Pool. OECD/NEA & IAEA Workshop CFD4NRS-3, Bethesda, MD, USA, September 14-16, 2010.
11. H. Li, W. Villanueva, P. Kudinov. Approach and Development of Effective Models for Simulation of Thermal Stratification and Mixing Induced by Steam Injection into a Large Pool of Water. Science and Technology of Nuclear Installations, 2014, Article ID 108782, 11 pages.
12. H. Li, W. Villanueva, M. Puustinen, J. Laine, P. Kudinov. Validation of Effective Models for Simulation of Thermal Stratification and Mixing Induced by Steam Injection into a Large Pool of Water. Science and Technology of Nuclear Installations, 2014, Article ID 752597, 18 pages.
13. H. Li, W. Villanueva, M. Puustinen, J. Laine, P. Kudinov. Thermal stratification and mixing in a suppression pool induced by direct steam injection. Annals of Nuclear Energy, 111 (2018) 487-498.
14. W. Villanueva, H. Li, M. Puustinen, P. Kudinov. Generalization of experimental data on amplitude and frequency of oscillations induced by steam injection into a subcooled pool. Nuclear Engineering and Design 295 (2015) 155-161.
15. I. Gallego-Marcos, W. Villanueva, P. Kudinov. Modelling of Pool Stratification and Mixing Induced by Steam Injection through Blowdown Pipes. Annals of Nuclear Energy, 112 (2018) 624-639.
16. I. Gallego-Marcos, P. Kudinov, W. Villanueva, R. Kapulla, S. Paranjape, D. Paladino, J. Laine, M. Puustinen, A. Räsänen, L. Pyy, E. Kotro. Pool Stratification and Mixing during a Steam Injection through Spargers: Analysis of the PPOOLEX and PANDA experiments. Submitted to Nuclear Engineering and Design, NED_2018_17.
17. I. Gallego-Marcos, P. Kudinov, W. Villanueva, R. Kapulla, S. Paranjape, D. Paladino, J. Laine, M. Puustinen, A. Räsänen, L. Pyy, E. Kotro. Pool Stratification and Mixing during a Steam Injection through Spargers: CFD modelling of the PPOOLEX and PANDA experiments. Submitted to Nuclear Engineering and Design, NED_2018_344.

18. C.H. Song, S. Cho, H.Y. Him, Y.Y. Bae, M.K. Chung, Characterization of direct contact condensation of steam jets discharging into a subcooled water, Proceedings of IAEA Technical Committee Meeting, PSI, Villigen, 1998.
19. J. Kerney, G.M. Feath, D.R. Olson. Penetration characteristics of a sub-merged steam jet. AIChE Journal 18(3) (1972) 584-553.
20. S.S. Gulawani, S.K. Dahikar, C.S. Mathpati, J.B. Joshi, M.S. Shah, C.S. RamaPrasad, D.S. Shukla. Analysis of flow pattern and heat transfer in direct contact condensation. Chemical Engineering Science, 64 (2009) 1719-1738.
21. X.Z Wu, J.J. Yan, W.J. Li, D.D. Pan, D.T. Chong, 2009. Experimental study on sonic steam jet condensation in quiescent subcooled water. Chemical Engineering Science, 64 (23), 5002-5012.
22. Y.J. Choo, C.H. Song, PIV measurements of turbulent jet and pool mixing produced by a steam jet discharge in a subcooled pool, Nuclear Engineering and Design 240 (9) (2010) 2215-2224.
23. R.J.E. Van Wissen, K.R.A.M. Schreel, C.W.M Van Der Geld, Particle image velocimetry measurements of a steam-driven confined turbulent water jet, Journal of Fluid Mechanics 530 (2005) 353-368.
24. S.H. Ju, H.C. No, F. Mayinger. Measurement of heat transfer coefficients for direct contact condensation in core makeup tanks using holographic interferometer. Nuclear Engineering and Design 199 (2000) 75-83.
25. Chan, C.K., Lee, C.K.B., 1982. A regime map for direct contact condensation. International Journal of Multiphase Flow, 8, 11-20.
26. M.E. Simpson, C.K. Chan, 1982. Hydrodynamics of a subsonic vapor jet in subcooled liquid. Journal of Heat Transfer, 104 (2), 271-278.
27. S. Fukuda, 1982. Pressure Variations due to Vapor Condensation in Liquid, (II). Journal of the Atomic Energy Society of Japan, 24 (6), 466-474.
28. J. Hong, G.C. Park, S. Cho, C.H. Song. Condensation dynamics of submerged steam jet in subcooled water. International Journal of Multiphase Flow 39 (2012) 66-77.
29. S. Cho, S.Y. Chun, W.P. Baek, Y. Kim, 2004. Effect of multiple holes on the performance of sparger during direct contact condensation. Experimental Thermal and Fluid Science, 28 (6), 629-638.
30. J. Tang, C. Yan, L. Sun, 2015. A study visualizing the collapse of vapor bubbles in a subcooled pool. International Journal of Heat and Mass Transfer, 88, 597-608.
31. I. Aya, H. Nariai, M. Kobayashi, 1980. Pressure and Fluid Oscillations in Vent System due to Steam Condensation, (II) High-Frequency Component of Pressure Oscillations in Vent Tubes under at Chugging and Condensation Oscillation. Journal of Nuclear Science and Technology, 20(3), 213-227.
32. D.H. Youn, K.B Ko, Y.Y. Lee, M.H. Kim, Y.Y. Bae, J.K. Park. The Direct Contact Condensation of Steam in a Pool at Low Mass Flux. Nuclear Science and Technology 40(10) (2003) 881-885.
33. E. Aust, D. Seeliger. Pool dynamics and dynamic loads in pressure suppression containment systems. Transactions of the American Nuclear Society 41 (1982) 696-699.
34. I. Aya, H. Nariai, 1987. Boundaries between regimes of pressure oscillations induced by steam condensation in pressure suppression containment. Nuclear Engineering and Design, 99, 31-40.
35. K.S. Liang, P. Griffith, 1994. Experimental and analytical study of direct contact condensation of steam in water, Nuclear Engineering and Design, 147 (3), 425-435.
36. S. Cho, C.H. Song, C.K. Park, S.K. Yang, M.K. Chung. Experimental study on dynamic pressure pulse in direct contact condensation of steam jets discharging into subcooled water. Proceedings of NTHAS98. Korea-Japan symposium on nuclear thermal hydraulics and safety; Pusan (Korea, Republic of), 21-24 Oct 1998, 291-298.
37. A. Petrovic de With, R.K. Calay, G. de With, 2007. Three dimensional condensation regime diagram for direct contact condensation of steam injected into water. International Journal of Heat and Mass Transfer, 50 (9-10), 1762-1770.

38. G. Gregu, M. Takahashi, M. Pellegrini, R. Mereu, Experimental study on steam chugging phenomenon in a vertical sparger, International Journal of Multiphase Flow 88 (2017) 87-98.
39. X.Z. Wu, J.J. Yan, W.J. Li, D.D. Pan, G.Y. Liu, W.J. Li, Condensation regime diagram for supersonic/sonic steam jet in subcooled water, Nuclear Engineering and Design 239 (12) (2009) 3142-3150.
40. F. D'Auria, G.M. Galassi, Scaling of nuclear reactor system thermal-hydraulics, Nuclear Engineering and Design 240 (10) (2010) 3267-3293.
41. MARVIKEN-FSCB-I, Marviken Full Scale Containment Blowdown Experiments Series I (1973).
42. W. Kennedy, D. McGovern, R. Maraschin, K. Wolfe. Rigid and flexible vent header testing in the quarter scale test facility. Mark I containment program, task 5.3.3. Technical report, General Electric Co., San Jose, CA (USA), 1978. Alternate Energy Division.
43. T.R. McIntyre, M.A. Ross, L.L. Myers. Mark II pressure suppression test program: Phase I tests. Technical report, General Electric Co., San Jose, CA (USA), 1976. Boiling Water Reactor Systems Dept.
44. W.A. Grafton, T.R. McIntyre, M.A. Ross. Mark II pressure suppression test program: Phase II and III tests. Technical report, General Electric Co., San Jose, CA (USA),1977. Boiling Water Reactor Projects Dept.
45. T.R. McIntyre, L.L. Myers, J.E. Torbeck, R.J. Booker. Mark III confirmatory test program: one third scale, three vent air tests. Technical report, General Electric Co., San Jose, Calif. (USA), 1975. Boiling Water Reactor Systems Dept.
46. A.M. Varzaly, W.A. Grafton, H. Chang, M.K. Mitchell. Mark III confirmatory test program: 1/root 3 scale condensation and stratification phenomena, test series 5807. Technical report, General Electric Co., San Jose, Calif. (USA), 1977. Boiling Water Reactor Systems Dept.
47. T.H. Chuang. Mark III one-third area scale submerged structure tests. Technical report, General Electric Co., San Jose, CA (USA), 1977. Boiling Water Reactor Systems Dept.
48. K. Namatame, Y. Kukita, I. Takeshita, Evaluation of primary blowdown flow rate and vent pipe steam mass flux (Tests 00002, 0003, 0004, 1101, 2101, 3101, 3102) - Full-Scale Mark II CRT program Test Evaluation Report No 1, JAERI-M 83-185 (1983).
49. Y. Kukita, I. Takeshita, K. Namatame, M. Kato, K. Moriya, M. Shiba, Statistical evaluation of steam condensation loads in pressure suppression pool (1) – Full-Scale Mark II CRT program. Test Evaluation Report No. 2, JAERI-M 9665 (1981).
50. J. Hart, W.J.M. Slegers, S.L. de Boer, M. Huggenberger, J. Lopez Jimenez, J.L. Munoz-Cobo Gonzalez, F. Reventos Puigjaner. TEPSS-Technology enhancement for passive safety systems. Nuclear Engineering and Design 209 (2001) 243-252.
51. C.D. Walsche, F.D. Cachard. Experimental investigation of condensation and mixing during venting of a steam/non-condensable gas mixture into a pressure suppression pool. Technical report, IAEA Report (1996) 53-61.
52. Y.T. Moon, H.D. Lee, G.C. Park, CFD simulation of a steam jet-induced thermal mixing into a subcooled water pool, Nuclear Engineering and Design 239 (2009) 2849-2863.
53. Y. Zhang, D. Lu, Z. Wang, X. Fu, Q. Cao, Y. Yang, G. Wu, Experimental research on the thermal stratification criteria and heat transfer model for the multi-holes steam ejection in IRWST of AP1000 plant, Applied Thermal Engineering 107 (2106) 1046-1056.
54. J. Laine, M. Puustinen, Condensation Pool Experiments with Steam Using DN200 Blowdown Pipe, Nordic Nuclear Safety Research (2005) NKS-111.
55. J. Laine, M. Puustinen, Thermal stratification experiments with the condensation pool test rig, Nordic Nuclear Safety Research (2006) NKS-117.

56. J. Laine, M. Puustinen, A. Räsänen, PPOOLEX Experiments on Thermal Stratification and Mixing, Nordic Nuclear Safety Research (2009) NKS-198.
57. M. Puustinen, J. Laine, A. Räsänen, Multiple blowdown pipe experiments with the PPOOLEX facility, Nordic Nuclear Safety Research (2011) NKS-241.
58. J. Laine, M. Puustinen, A. Räsänen, PPOOLEX experiments on the dynamics of free water surface in the blowdown pipe, Nordic Nuclear Safety Research (2013) NKS-281.
59. J. Laine, M. Puustinen, A. Räsänen, PPOOLEX Mixing Experiments, Nordic Nuclear Safety Research, (2014) NKS-309.
60. M. Solom, K.V. Kirkland, Experimental investigation of BWR Suppression Pool stratification during RCIC system operation, Nuclear Engineering and Design 310 (2016) 564-569.
61. D. Song, N. Erkan, B. Jo, K. Okamoto, Dimensional analysis of thermal stratification in a suppression pool, International Journal of Multiphase Flow 66 (2104) 92-100.
62. H.J.S. Fernando, Turbulent mixing in stratified fluids, Annual Review of Fluid Mechanics 23 (1991) 455-93.
63. H.J.S. Fernando, J.C.R. Hunt, Turbulence, waves and mixing at shear-free density interfaces. Part 1. A theoretical model, Journal of Fluid Mechanics 347 (1997) 197-234.
64. J.L. McGrath, H.J.S. Fernando, J.C.R Hunt, Turbulence, waves and mixing at shear-free density interfaces. Part 2. Laboratory experiments, Journal of Fluid Mechanics 347 (1997) 235-261.
65. C.H. Chen, V.K. Dhir. Hydrodynamics of a bubble formed at vent pipe exit. International Journal of Multiphase Flow 8(2) (1982) 147-163.
66. F. Yuan, D. Chong, Q. Zhao, W. Chen, J. Yan, Pressure oscillation of submerged steam condensation in condensation oscillation regime, International Journal of Heat and Mass Transfer 98 (2016) 193-203.
67. J.H. Pitts, Steam chugging in a boiling water reactor pressure-suppression system, International Journal of Multiphase Flow 6 (1980) 329-344.
68. M. Ali, V. Verma, A.K. Ghosh, Analytical thermal hydraulic model for steam chugging phenomenon, Nuclear Engineering and Design 237(19) (2007) 2025-2039.
69. C. Brennen, A Linear Dynamic Analysis of Vent Condensation Stability, Annual Meeting of the American Society of Mechanical Engineers, Chicago, Illinois, November 16-21, 1980.
70. T.J.H. Pättikangas, J. Niemi, J. Laine, M. Puustinen, H. Purhonen. CFD modelling of condensation of vapor in the pressurized PPOOLEX facility. CFD4NRS-3, 14-16 September 2010, Washington D.C., USA.
71. V. Tanskanen, A. Jordan, M. Puustinen, R. Kyrki-Rajamäki. CFD simulation and pattern recognition analysis of the chugging condensation regime. Annals of Nuclear Energy 66 (2014) 133-143.
72. G. Patel. Computational fluid dynamics analysis of steam condensation in nuclear power plant applications. Doctoral dissertation at Lappeenranta University of Technology, Finland, 2017.
73. M. Pellegrini, M. Naitoh, Application of two-phase flow DFC to the phenomena expected in Fukushima Daiichi S/C. OECD/NEA & IAEA Workshop CFD4NRS-6, 2016.
74. H.S. Kang, C.H. Song, CFD analysis for thermal mixing in a subcooled water tank under a high steam mass flux discharge condition", Nuclear Engineering and Design, 238 (2008) 492-501.
75. H.S. Kang, C.H. Song, CFD analysis of a turbulent jet behavior induced by a steam jet discharge through a single hole in a subcooled water tank, Nuclear Engineering and Design, 240 (2010) 2160-2168.
76. R.E. Gamble, T.T. Nguyen, B.S. Shiralkar, P.F. Peterson, R. Greifc, H. Tabatad, Pressure suppression pool mixing in passive advanced BWR plants, Nuclear Engineering and Design 204 (1-3) (2001) 321-336).
77. Ozdemir, O.E., George, T.L., 2015. BWR MARK I pressure suppression pool mixing and stratification analysis using GOTHIC lumped parameter modeling methodology. Annals of Nuclear Energy, 85, 532-543.
78. GOTHIC Thermal Hydraulic Analysis Package, Version 8.1(QA). EPRI, Palo Alto, CA: 2014.

79. RELAP5/MOD3.3 Code Manual Volume IV. US Nuclear Regulatory Commission, Washington DC, 2006.
80. F. D'Auria, G.M. Galassi, Scaling of nuclear reactor system thermal-hydraulics, Nuclear Engineering and Design 240 (10) (2010) 3267-3293.
81. I. Aya, H. Nariai. Chugging Phenomenon Induced by Steam condensation into pool water (amplitude and frequency of fluid oscillation). Translated from: Transactions of the Japan Society of Mechanical-Engineers 50 (1984) 2427-2435.
82. M., Pellegrini et al., 2016. Benchmark study of the accident at the Fukushima Daiichi NPS: best-estimate case comparison. Nuclear Technology 196, 198-210.
83. Y. Kukita, K. Namatame, I. Takeshita, and M. Shiba, 1983. The Non condensable Gas Effects on Loss-of-Coolant Accident Steam Condensation Loads in Boiling Water Reactor Pressure Suppression Pool. Nuclear Technology, 63, 2, 337-346.
84. S. M. Ali, V. Verma, and A. K. Ghosh, 2007. Analytical thermal hydraulic model for oscillatory condensation of steam in presence of air. Nuclear Engineering and Design, 237, 19, 2025-2039.

Bibliographic Data Sheet	**NKS-409**

Title	COPSAR-NKS Project; Summary report 2017
Author(s)	Markku Puustinen[a], Timo Pättikangas[b], Pavel Kudinov[c]
Affiliation(s)	[a] Lappeenranta University of Technology, School of Energy Systems, Nuclear Engineering [b] VTT Technical Research Centre of Finland Ltd [c] Royal Institute of Technology (KTH), Division of Nuclear Engineering, Stockholm, Sweden
ISBN	978-87-7893-498-7
Date	September 2018
Project	NKS-R / COPSAR
No. of pages	201
No. of tables	16
No. of illustrations	110
No. of references	152
Abstract max. 2000 characters	The COPSAR-NKS project has consisted of the combined effort by LUT, VTT and KTH to implement the ideas outlined in the NORTHNET Roadmap 3 document. To achieve the project objectives, a combined experimental/analytical/computational program has been carried out. LUT has been responsible for developing an experimental database on pool operation related phenomena in the PPOOLEX integral test facility and in the small-scale separate effect test facility. VTT and KTH have used the gathered experimental database for the development, improvement and validation of numerical simulation models. A small-scale separate effect test facility, SEF-POOL, has been designed and constructed at LUT based on a proposal from KTH with the aim to evaluate effective momentum for different condensation regimes. The facility allows the direct measurement of effective momentum induced by steam injection. Analysis of the preliminary steam injection tests by KTH showed that the steam momentum can be roughly predicted by the theoretical estimate and the frequencies obtained with the fast pressure transducer correlate well with the correlations proposed in the literature. Pre-test SEF-T000 performed on the SEF-POOL facility at LUT has been studied with Computational Fluid Dynamics (CFD) calculations at VTT. The simulation produced qualitatively correct description of the chugging oscillation observed in the experiment.
Key words	Steam injection, Direct-contact condensation, Thermal stratification, Mixing, Pressure suppression pool, Containment, Sparger, Spray, Effective momentum, BWR, CFD, GOTHIC

Available on request from the NKS Secretariat, P.O.Box 49, DK-4000 Roskilde, Denmark.
Phone (+45) 4677 4041, e-mail nks@nks.org, www.nks.org